

# Development of a touch stimulator for functional magnetic-resonance imaging

Submitted by Amer Qassim Mallah Alhussain to the University of  
Exeter as a thesis for the degree of Doctor of Philosophy in Physics,  
August 2013

This thesis is available for Library use on the understanding that it is copyright material and that no quotation from the thesis may be published without proper acknowledgement.

I certify that all material in this thesis which is not my own work has been identified and that no material has previously been submitted and approved for the award of a degree by this or any other University.

(Signature) .....

## Abstract

A tactile display system has been built with 25 contactors in a  $5 \times 5$  array with 2mm spacing, designed to stimulate the fingertip. The drive mechanism for each contactor is a piezoelectric bimorph, allowing the display to use in functional magnetic resonance imaging experiments (fMRI). The amplitude and frequency of stimulation can be pre-set, and each contactor can be activated separately using a personal computer. The tactile produce a wide variety of time-varying spatial patterns of touch stimulation. The sensation is “natural” and the participants do not find the experience unpleasant.

The psychophysics experiment and the first fMRI experiment involved identification of various patterns on the display: the tactile stimulus was stationary or moved in a circle or in a “random” trajectory with no obvious shape. Response was by push buttons. The second fMRI experiment focused on the relationship between the speed of tactile motion and the corresponding activation in the brain, using stimuli moving in a circular trajectory on the tactile display at various speeds in the range 2.9 to 77.9 mm s<sup>-1</sup>.

In the psychophysics experiment, the mean identification score was 80% after only a few minutes’ practice. The results of the first fMRI experiment showed highly significant activations in primary and secondary somatosensory cortices for contrasts of circle or random stimuli with the rest condition; low significant activations in SI and SII were observed for the contrast of stationary stimuli with rest. Broca's area was found to be activated for circle and random stimulation but not for stationary stimulation. Results from the second fMRI experiment showed small speed-sensitive activations in the left side of the brain, mostly in the primary somatosensory cortex.

The conclusion in present study was our tactile system can produce different types of tactile patterns and it works inside MRI scanner.

## Acknowledgements

Gratitude is the simplest thing one can say to the people who helped me during my study. Starting the acknowledgement with my supervisor Dr Ian Summers who gave me his guidance, support and encouragement throughout my research; without his help and support this study would not have seen see the light.

Also I want to thank the Ministry of Higher Education and Scientific Research in Iraq (MOHESR) for financial support that allowed the project to be carried out.

I would like to give many thanks to Dr Abdelmalek Benattayallah and Dr Jon Fulford for their assistance in running the fMRI scans and analysing the fMRI data.

Also very special thanks to Dr Adel Albadran and his family for their hospitality throughout my study as they became a second family to me.

Finally, many thanks to my family and friends who have supported and encouraged me throughout my study.

## The outline of the thesis

The thesis has ten chapters. Chapters one, two, three and four contain the theoretical background of the thesis. The processing and analysis steps of the data are presented in chapter five. Chapter six includes the practical part of the thesis, which is building the tactile display system. Chapters seven, eight and nine describe experiments using the tactile display – a psychophysics experiment and two fMRI experiments. Finally, chapter ten includes a summary and suggestions for future work. Below is a brief summary of each chapter.

CH.1: The first chapter is the introduction of the thesis which contains the main points in the thesis. Also this chapter reviewed the main experiments which run during the present study.

CH. 2: The second chapter starts with a description of the touch receptors that includes their structure, location and response characteristics. Information about the nervous system is also included in this chapter, and the process of producing the signal that encodes the information in the nervous system. A brief review of brain structure is also given in this chapter, focusing on the brain areas that show activation due to tactile stimulation.

CH. 3: Chapter three gives a brief review of the different kinds of tactile stimulator that have been developed to run various sorts of psychophysical or functional experiments.

CH. 4: Functional Magnetic Resonance Imaging (fMRI) is the imaging technique used in this research. Chapter four contains the theory of MRI and how the contrast between tissues in the image is formed by the MRI scanner. The Blood-Oxygenation-Level-Dependent (BOLD) effect is described in this chapter, as it is the tool used to investigate the active regions in the brain. The chapter ends with a description of the MRI scanner used during this research.

CH. 5: In this chapter the Statistical Parametric Mapping (SPM) software is described, which is the tool used in this study to analyse the fMRI data. This description contains the main steps of data analysis to determine the active areas in the brain by examining the relationship between the stimulation and the neural activity, and explains how the results are presented.

CH. 6: The tactile display system which was built during the study is characterized in detail in this chapter, which covers each part of the system: the tactile stimulator, the electronic

hardware and the computer interface. In addition there is an overview of the software program used to produce the tactile patterns.

CH. 7: Chapter seven describes a psychophysics experiment, designed to test the tactile display system. The performance of the system is found to be good. This chapter also includes a preliminary experiment to check that the system will work in an MRI scanner, and that operation of the system does not interfere with the MRI process.

CH. 8: The first fMRI study is described in this chapter. Participants are asked to identify different types of moving tactile stimulus and respond by push buttons. Activations are observed in brain areas including the primary and secondary somatosensory cortices. A discussion of results is included.

CH. 9: The relationship between the speed of tactile motion and activation in the brain is the focus of the second fMRI study, presented in chapter nine. Participants were asked to concentrate on stimuli moving in a circular trajectory on the tactile display at various speeds in the range 2.9 to 77.9 mm s<sup>-1</sup>. A discussion of results is included.

CH. 10: Chapter ten provides a summary of the results from the various experiments and a brief evaluation of the tactile display system. Some suggestions for future work are given.

## List of figures

1.1 Mechanoreceptors .....	4
1.2 Neuron .....	6
1.3 Signal in the neuron .....	7
1.4 Somatosensory pathway .....	9
1.5 Cytoarchitectonics of SI and SII .....	11
1.6 Topographic of SI .....	11
2.1 Precession of the proton .....	16
2.2 Zeeman Effect .....	16
2.3 BOLD signal .....	22
2.4 BOLD hemodynamic response .....	22
2.5 Diagram of EPI .....	24
2.6 fMRI experimental designs .....	26
2.7 MRI scanner .....	27
2.8 1.5 T scanner .....	29
3.1 Piezoceramic wafer .....	32
3.2 Contactors with tubes .....	32
3.3 Dense array stimulator .....	33
3.4 The 100-contactor tactile array .....	34
3.5 Electrode array .....	35
3.6 Dimensions of a letter .....	36
3.7 Rotating drum stimulator .....	37
3.8 2D geometric shapes .....	38
3.9 Broca's area .....	39
3.10 TOR and NOP conditions .....	40
3.11 TOR-NOP contrast .....	40
3.12 Activation due to tactile motion .....	41

4.1 MRicro program .....	44
4.2 Talairach space .....	46
5.1 Tactile simulator .....	54
5.2 Tactile array .....	54
5.3 Oscillator principle and circuit diagram .....	55
5.4 Sinusoidal output waveform .....	56
5.5 Diagram of the amplifier .....	57
5.6 UBW32 card .....	58
5.7 Connection circuit .....	59
5.8 Tactile system .....	60
5.9 Complete tactile system .....	61
5.10 Chart of software program .....	62
6.1 Three stimulus .....	66
6.2 Time sequence .....	66
6.3 The response box .....	68
6.4 Percentage-correct answers .....	68
6.5 The confusion matrix .....	69
6.6 The MR image of the phantom .....	71
6.7 Time variation of intensity .....	72
7.1 The E-prime display .....	76
7.2 The sequence of the first fMRI experiment .....	76
7.3 Conditions in the first fMRI experiment .....	78
7.4 Percentage correct responses .....	80
7.5 The confusion matrix .....	80
7.6 Glass-brain views (Circle and Rest) .....	81
7.7 Glass-brain views (Random and Rest) .....	84
7.8 Glass-brain views (Stationary and Rest) .....	87



7.9 Rendered-brain views (Circle and Rest) .....	91
7.10 Rendered-brain views (Circle and Rest) .....	92
7.11 Rendered-brain views (Stationary and Rest) .....	93
7.12 Rendered brain-Circle and Stationary (BA 4) .....	94
7.13 Rendered brain-Random and Stationary (BA 4).....	95
7.14 Rendered brain-(Circle + Random) and Stationary (BA 4) .....	96
7.15 Rendered brain-Circle and Rest (BA44) .....	97
7.16 Rendered brain-Random and Rest (BA44) .....	97
7.17 Rendered brain-Stationary and Rest (BA44) .....	97
8.1 The circular movement of the stimulus .....	101
8.2 Time sequence of the second fMRI .....	102
8.3 The design matrices for analysis in the second fMRI .....	104
8.4 Activations in SI and SII-sub 1 (all speed) .....	105
8.5 Activations in SI and SII-second level (all speed) .....	107

## List of tables

6.1 Details of the volunteers (Tactile experiment) .....	67
6.2 The components of the fluid phantom .....	70
7.1 Details of the participants (First fMRI experiment) .....	79
7.2 Coordinates activation-Circle vs. Rest (SI) .....	82
7.3 Coordinates activation-Circle vs. Rest (SII) .....	83
7.4 Coordinates activation-Random vs. Rest (SI) .....	85
7.5 Coordinates activation-Random vs. Rest (SII) .....	86
7.6 Coordinates activation-Stationary vs. Rest (SI) .....	88
7.7 Coordinates activation-Stationary vs. Rest (SII) .....	89
7.8 Coordinates activation-Circle vs. Rest (SI) second level .....	91
7.9 Coordinates activation-Circle vs. Rest (SII) second level .....	91
7.10 Coordinates activation-Random vs. Rest (SI) second level .....	92
7.11 Coordinates activation-Random vs. Rest (SII) second level .....	92
7.12 Coordinates activation-Stationary vs. Rest (SI) second level .....	93
7.13 Coordinates activation-Stationary vs. Rest (SII) second level .....	93
7.14 Coordinates activation-Circle and Stationary (BA4) .....	95
7.15 Coordinates activation- Random and Stationary (BA4) .....	95
7.16 Coordinates activation (Circle + Random) and Stationary (BA4) .....	96
7.17 Coordinates activations in left side Broca's area .....	98
7.18 Coordinates activations in Right side Broca's area .....	99
8.1 The four speeds of tactile movement .....	102
8.2 Details of participants (second fMRI) experiment .....	103
8.3 Coordinates activations in SI and SII (left side) all speed .....	106
8.4 Coordinates activations in SI and SII (Right side) all speed .....	106
8.5 Coordinates activations in SI and SII-second level .....	107
8.6 Coordinates of areas in SI and SII-linear relation .....	108

## Abbreviations and Symbols

MC: Meissner Corpuscles

RAI: Rapidly Adapting type I

SAI: Slowly Adapting I

SAII: Slowly adapting type II

RAII: Rapidly Adapting type II

CNS: Central Nervous System

PNS: Peripheral Nervous System

Hz: Hertz

lb: Pound

cm: centimetre

SI: Primary Somatosensory Cortex

VP: Ventroposterior nucleus

SII: Secondary Somatosensory Cortex

PPC: Posterior Parietal Cortex

(LIP): Lateral Intraparietal area,

MST: Medial Superior Temporal area

VIP: Ventral Intraparietal area

VPL: Ventral Posterior Nucleus

NMR: Nuclear Magnetic Resonance

MRI: Magnetic Resonance Imaging

fMRI: Functional magnetic resonance Imaging

T: Tesla

$\vec{J}$  : Angular momentum

$\vec{I}$  : Spin

$\hbar$  : Planck's constant

$\vec{\mu}$  : Magnetic moment

$\gamma$  : Gyromagnetic ratio  
L: torque  
 $B_0$  : External magnetic field  
RF: Radio frequency  
 $\omega_0$  : Larmor frequency  
K: Boltzmann constant  
T: Absolute temperature  
M: Total magnetic moment  
 $T_1$ : Spin-lattice relaxation Time  
 $T_2$ : Spin-spin relaxation Time  
 $T_2^*$ : Time decay of MRI signal  
TR: Repetition Times  
TE: Echo Time  
EEG: Electroencephalography  
CBV: Cerebral blood volume  
CBF: Cerebral blood flow  
Gd-DTPA: Gadolinium diethylene-triamine-pentaacetic acid  
BOLD: Blood Oxygenation Level-Dependent  
HR: Hemodynamic Response  
CMRO<sub>2</sub>: Cerebral metabolic rate of oxygen  
SE: Spin Echo  
GE: Gradient Echo  
EPI: Echo-planar imaging  
SNR: Signal-to-Noise Ratio  
DC: Direct current  
MEG: Magnetoencephalography  
PET: Positron emission tomography

hMT+ /V5: middle temporal complex

SPM: Statistical Parametric Mapping

AFNI: Analysis of Functional NeuroImages

BV: Brain Voyager QX

DICOM: Digital Imaging and Communications in Medicine

MNI: Montreal Neurological Institute

AC: anterior commissure

PC: posterior commissure

FWHM: half its maximum height

GLM: General Linear Model

OLS: ordinary least squares

FEW: Family wise error

GRF: Gaussian Random Fields

FET: Filed Effect-type Transistor

op-amp: operational amplifier

$f$ : linear frequency

$R$ : Resister

$C$ : Capacitor

USB: Universal Serial Bus port

MCU: Microcontroller unite

FOV: Field of view

ROI: Region-of-interest

SD: standard deviation

# Contents

Abstract .....	I
Acknowledgements .....	II
Outline of the thesis .....	III
List of figures .....	V
List of tables .....	VIII
Abbreviations and Symbols .....	IX

## Introduction

Introduction .....	1
--------------------	---

## The somatosensory system

2.1 Introduction .....	5
2.2 Meissner Corpuscles (MCs) .....	5
2.3 Merkel cells .....	5
2.4 Ruffini receptors .....	6
2.5 Pacinian corpuscles (PCs) .....	6
2.6 Receptive fields .....	6
2.7 The nervous system .....	7
2.8 Nerve Cells .....	7
2.9 Generation of signals in the PNS .....	8
2.10 Somatosensory Pathways .....	10
2.11 The human brain .....	11
2.12 Brain mapping .....	11
2.13 Somatosensory cortical regions .....	13
2.13.1 Primary somatosensory (SI) cortex .....	13
2.13.2 Secondary Somatosensory (SII) cortex .....	13

2.13.3 Posterior parietal cortex (PPC) .....	15
2.14 Summary .....	15

## Previous studies involving tactile displays

3.1 Overview .....	17
3.2 Design and development of tactile displays .....	17
3.3 Psychophysics experiments with tactile displays .....	22
3.4 fMRI studies using a tactile display .....	24
3.5 Summary .....	28

## Magnetic Resonance Imaging

4.1 Introduction .....	30
4.2 The Theory of MRI .....	30
4.3 Image Formation .....	34
4.4 Image weighting .....	35
4.5 Functional Magnetic Resonance Imaging (fMRI) .....	36
4.5.1 Blood Oxygenation Level Dependent effect .....	36
4.6 Pulse sequences .....	38
4.6.1 Echo planar imaging .....	39
4.7 Functional MR Experiment Design .....	40
4.7.1 Block fMRI Design .....	40
4.7.2 Event-Related fMRI Design .....	40
4.7.3 Mixed Design .....	40
4.8 The Components of the MR Scanner .....	41
4.9 Artefacts in MRI images .....	43
4.10 Magnetic Resonance Imaging Noise .....	44

4.11 Summary .....	44
--------------------	----

## Analysis of the fMRI data

5.1 Introduction .....	47
5.3 Pre-processing Stage .....	47
5.3.1 Slice Time correction .....	47
5.3.2 Realignment .....	48
5.3.3 Normalization .....	48
5.3.3.1 The Talairach Atlas .....	49
5.3.3.2 The MNI template .....	49
5.3.4 Smoothing .....	51
5.4 The statistical Model .....	51
5.5 <i>Modulation parameters</i> .....	53
5.5 Functional Data Processing .....	53
5.6 Summary .....	54

## The Tactile Display System

6.1 Overview .....	56
6.2 The Tactile Stimulator .....	56
6.2.1 The Piezoelectric Effect .....	56
6.2.2 The Tactile Array .....	57
6.3 The Drive Electronics .....	59
6.4 The Control System .....	61
6.4.1 The Hardware .....	61
6.4.2 The Software .....	66



6.5 Summary .....	67
-------------------	----

## Preliminary experiments with the tactile display

7.1 Introduction .....	69
7.2 Design of the Psychophysics Experiment .....	69
7.3 Procedure for the Psychophysics Experiment .....	72
7.4 Results from the Psychophysics Experiment .....	72
7.5 Discussion and Conclusion for the Psychophysics Experiment .....	74
7.6 Image Artefacts .....	74
7.7 Summary .....	77

## The First fMRI Experiment

8.1 Introduction .....	79
8.2 Experiment Protocol .....	79
8.3 Acquisition of fMRI data .....	82
8.4 Analysis of fMRI data .....	82
8.5 Results .....	84
8.6 Individual fMRI Analysis for SI and SII .....	87
8.6.1 Contrast of Circle vs. Rest .....	87
8.6.2 Contrast of Random vs. Rest .....	91
8.6.3 Contrast of Stationary vs. Rest .....	94
8.7 Group fMRI Analysis .....	97
8.7.1 Group analysis for SI and SII .....	97

8.7.2 Group analysis for the primary motor cortex .....	101
8.7.3 Group analysis for Broca's region .....	103
8.8 Conclusion and Summary .....	107
<b>The second fMRI Experiment</b>	
9.1 Introduction .....	109
9.2 Procedure .....	110
9.3 Data analysis .....	111
9.4 Results and Discussion .....	114
9.5 Summary .....	117
<b>Conclusions and Future work</b>	
10.1 Introduction .....	119
10.2 Psychophysics experiment .....	119
10.3 First fMRI experiment .....	120
10.3.1 Primary and secondary somatosensory cortex .....	120
10.3.2 Primary motor region (M1) and Broca's Region .....	121
10.4 Second fMRI experiment .....	121
10.5 Evaluation of the tactile display .....	122
10.6 Future work .....	123
Bibliography .....	125

# **Chapter one**

## **Introduction**

## 1.1 Introduction

The sense of touch in humans and animals is used to obtain information about the shape, mechanical properties and state (stationary or moving) of tangible objects. Many researchers have investigated the structure and function of organs involved in the sense of touch.

The motivation of the present study was to build a tactile display that could be used to run different kinds of tactile experiment (psychophysics or fMRI experiments). The review of former studies (chapter two) shows some of the limitations of previous designs of tactile display. Some of these designs are very simple and can produce only a small range of tactile stimuli while others cannot be used in a high magnetic field to carry out fMRI experiments. The present work tried to overcome these limitations as much as possible, and produced a significant improvement on previously available designs, combining versatility, ease of use, ease of interfacing, portability and MRI compatibility.

The first section of the present study contained the work of building and developing the tactile system as follows: the first part of this work included the repair of existing 25-contactor tactile arrays. The second part included development of the drive electronics and the control system. This work aimed to make these components small and easy to transport (so they could be utilized in different laboratories and with different MRI systems) while providing drive voltages with a wide range of amplitudes (0 to 23.5 volt peak to peak) and frequencies (25 Hz to 2 kHz).

The control system involved both hardware and software. Both of these components were designed to provide separate control of each contactor in the tactile array, so that a variety of different tactile patterns could be specified and delivered relatively easily. All the programs for the present study were written by the author. The hardware was built in such way that connection between the tactile array and the drive electronics was optical. This method of connection prevented electrical noise from the digital electronics from entering the MRI scanner and so avoided noise in the MRI images. The drive electronics and control system were built by the author. The whole system (drive electronics and control system) was placed in one box, covered by copper sheet to provide radio-frequency screening.

The second section in present study covered some psychophysics experiments – primary studies that aimed to test the tactile system, and the main psychophysics experiment involving the discrimination of moving patterns on the array. Results demonstrated that the system was able to deliver an appropriate range of distinguishable stimuli.

The third section in the present study contained two fMRI experiments. One purpose of the first experiment was to demonstrate that the system could work inside an MRI scanner without producing any artefacts or noise in the images, using the same protocol as the main psychophysics experiment. A second purpose was to investigate brain activation in relation to tactile shape perception, using contrasted trajectories of moving touch stimulation. The aim of the second fMRI study was to investigate brain activation as a function of speed on the tactile array, for movement with a circular trajectory. Both experiments took advantage of the capability of the tactile display to deliver stimuli which are novel in the context of fMRI – spatiotemporal patterns of tactile sensation that allow an investigation of the brain's response to shape and movement.

During the present work two identical tactile systems were constructed, each providing the opportunity to run more advanced experiments (psychophysics or fMRI experiments) than with previously available designs.

## **Chapter two**

# The somatosensory system

## 2.1 Introduction

The human body is equipped with capabilities to communicate with the world. Amongst these capabilities are the senses that either exist in one part of the body, like vision and hearing, or are spread over different parts of the body, like touch. The mechanoreceptors or touch receptors are the first stage in touch perception and are distributed in the glabrous (hairless) skin and in the hairy skin. There are four main types of tactile receptors; below is a brief description of these receptors.

## 2.2 Meissner Corpuscles (MCs)

Meissner corpuscles are partially unmyelinated nerve endings, either encapsulated or unencapsulated. They are classified as rapidly adapting type I (RAI) receptors [1, 2]. They respond particularly to vibration at low frequency (light touch). Their optimum response frequency is between 30–40 Hz [3, 4]. MCs are found in the dermis, just below the epidermis, in glabrous skin. The size of MCs varies with skin site: MCs in the fingertips and lips are larger than those in dorsum of the hand and dorsum of the foot. The shape of MCs varies between oval, oblong or cylindrical [5, 6]. They were first described by Wagner and Meissner in 1852 [7].

## 2.3 Merkel cells

The receptor known as the Merkel cell is different from other receptors because it is a specialized single cell. Merkel cells were described in the mammalian epidermis by Friedrich Merkel in 1875, and named by him as Tastzellen or touch cells [8, 9]. The cells usually exhibit an oval shape and measure about 10-15  $\mu\text{m}$  along their longest diameter [10, 11]. Merkel cells are located in the basal layer of the epidermis in both hairy and glabrous skin, with particularly high density beneath the ridges on the fingertip [12]. Merkel cells are classified as slowly adapting mechanoreceptors type I (SAI) and respond particularly to frequencies in the range 5–15 Hz [13, 14].

## 2.4 Ruffini receptors

Ruffini receptors (Ruffini endings), first reported by Angelo Ruffini in 1894, are classified as slowly adapting mechanoreceptors type II (SAII), responding to stretch in the connective tissue in the frequency range 15–200 Hz [15-18]. They are spindle shaped with diameter approximately 50  $\mu\text{m}$  [19]. They are located in the reticular layer of the dermis in both glabrous and hairy skin [20].

## 2.5 Pacinian corpuscles (PCs)

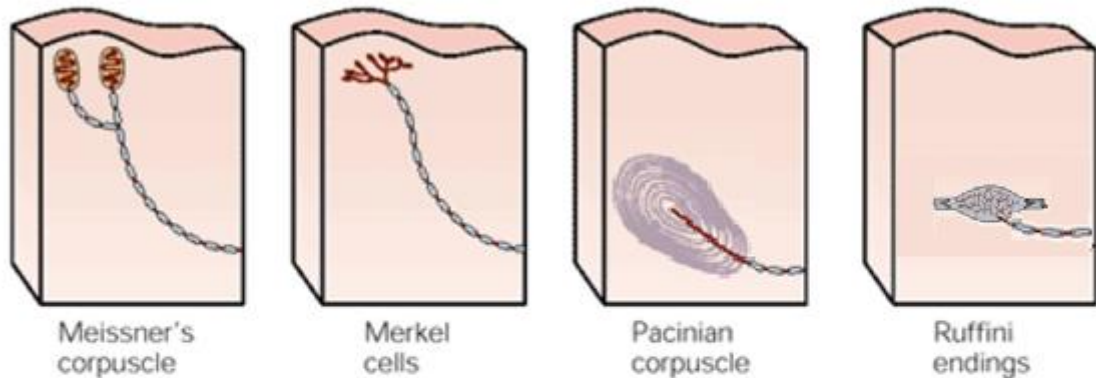
Discovered by Italian anatomist Filippo Pacini in 1831, the size (up to 1 mm diameter) and the easy accessibility of pacinian corpuscles make them the most widely investigated receptor at ultrastructural and electrophysiological levels [21-23]. PCs are encapsulating nerve endings having non-neural accessory structures known lamellae surrounding the neural component [24]. The size of PCs depends on their location; the deeper in the skin the more lamellae and so the larger the size [25]. Generally PCs have an ovoid shape although some have more complex shapes [26]. Pacinian corpuscles are found in various parts of the mammalian body, including tendons and joints. In human skin, they are localized in the deeper part of the dermis. They are common in glabrous skin while very rare in hairy skin. The maximum density of PCs is found in the index finger [27]. The function of the PC is to detect pressure changes over a wide range of frequencies between 40–800 Hz, with a peak response at around 250 Hz. PCs are classified as rapidly adapting type II (RAII) receptors [28, 29].

## 2.6 Receptive fields

In addition to the differences between tactile receptors in terms of location, frequency and adaptation rate, there are also differences in receptive field, i.e., the area on the skin within which a stimulus can excite the receptor. Merkel cells (SAI) and Meissner corpuscles (RAI) have smaller receptive fields while pacinian corpuscles (RAII) and Ruffini receptors (SAII) have larger fields [30]. Figure 2.1 shows the relative positions and receptive fields for the four populations of touch receptors in human skin.



### Receptor location



### Receptive field



Fig. 2.1: The relative positions and receptive fields for the four populations of mechanoreceptors in human skin [31].

## 2.7 The nervous system

The nervous system is an organ containing a network of specialized cells that are responsible for sending, receiving and processing nerve impulses throughout the body. The nervous system is divided into two major divisions: the central nervous system (CNS) which is contained within bony cases, in particular the skull and spine (the brain and spinal cord), and the peripheral nervous system (PNS) which spreads through the rest of the body. The CNS consists of four main parts: cerebral cortex, cerebellum, brain stem and spinal cord [32].

## 2.8 Nerve Cells

Neurons (nerve cells) and glial (neuroglial) cells are the basic units of the nervous system. Neurons come in different shapes and sizes; each has four morphologically specialized regions with particular functions (figure 2.2). Firstly, the dendrites with diverging

branches, forming a “dendrite tree” which may cover a large area. Secondly, the soma or perikaryon, the body of the nerve cell and the centre of metabolic activity, containing the nucleus. Thirdly, the axon which runs from the body of the neuron with a length varying from a fraction of a millimetre to a metre (in the human). The axon connects to the fourth of the functional regions – the axon terminals [33]. Typically the dendrites work as the input interface of the neuron while the axon provides the output, conducting electrical impulses from the cell body to other neurons.

Glial cells are the supportive cells that surround the cell bodies, dendrites, and axons of neurons in both the CNS and PNS. For a long time the main function of the glial cells was thought to be physically supporting and protecting the neurons, but recently they have been found to play a role in nervous activity [34].

## 2.9 Generation of signals in the PNS

The peripheral nervous system (PNS) works as a communications network in the body. Electrical signals or potentials are utilized to encode information at various locations in the nervous system, e.g., membrane resting potential, action potential, receptor potential, and synaptic potential. All these kinds of electrical potential are produced by the same basic mechanism. This mechanism can be understood by examining the structure of the nerve cell: the plasma membrane of the neuron is made up of a double layer (bilayer) of molecules that forms a diffusion barrier between the inside and outside of the cell. This bilayer is based on fatty molecules, and includes proteins that form pores or channels that let certain ions enter or leave the cell. Some of these channels are normally open while others stay closed unless they receive an electrical or mechanical signal [35].

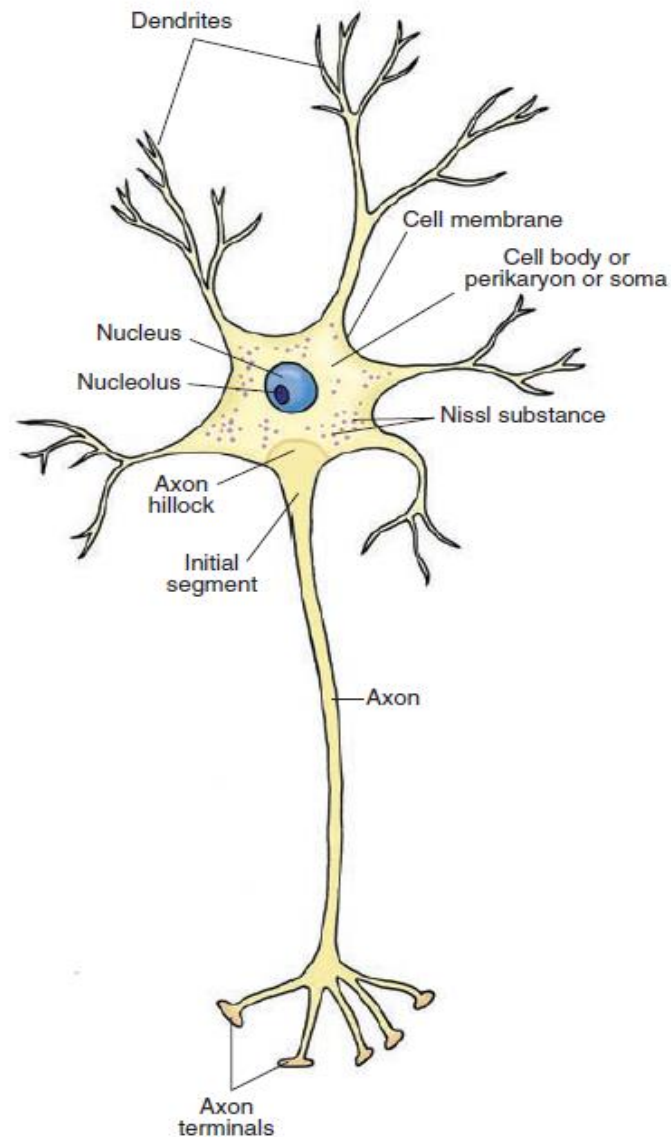


Fig. 2.2: The structure of the neuron [32].

In the absence of an external stimulus (resting state), the inside of the cell has a higher concentration of positive ions whereas the outside has a higher concentration of negative ions. Therefore, the potential inside the cell is more negative than the potential outside the cell. The difference in potential across the cell membrane, known as the “cell potential”, is about  $-70$  mV (resting state, see figure 2.3). If the neuron receives a specific stimulus which is able to open an ion channel, and enough ions flow into the cell to bring down the cell potential by about 20 mV (threshold potential), the interior voltage will continue to rise until

the cell potential is around +30 mV. This sudden reversal of cell potential is known as an action potential, and the process of generating the action potential forms the basis of neural signalling. Subsequently, the positive cell potential leads positive ions to leave the cell, causing a sudden reversal of the cell potential, back to a level that is slightly more negative than the resting state [36].

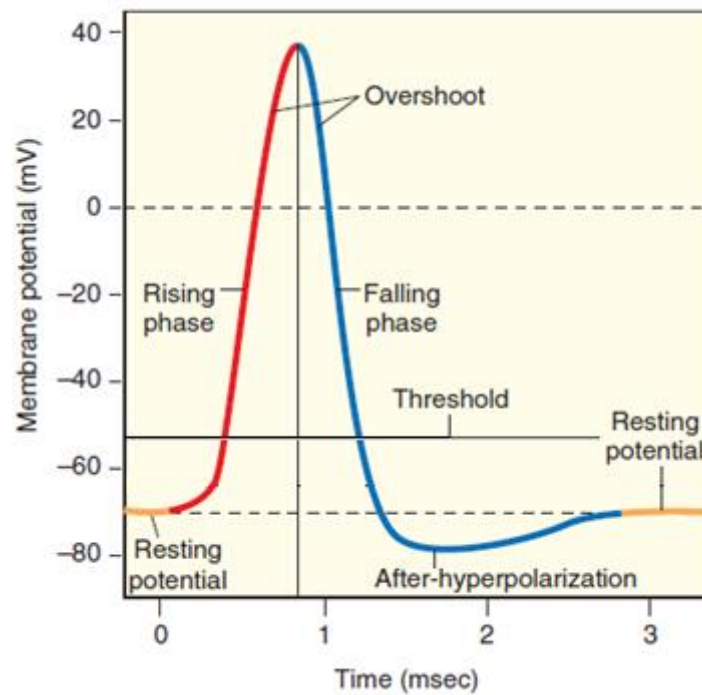


Fig. 2.3: The process of produce signal in the neuron [32].

## 2.10 Somatosensory Pathways

The information produced by different types of mechanoreceptor is transmitted by afferent sensory axons to enter the ipsilateral dorsal column, which is one of the grey matter columns in spinal cord, see figure 2.4. The neuronal cell bodies that give rise to these afferent axons are located in the dorsal root ganglia. These neurons are also called the first-order neurons because they initiate the sensory process. The grey matter of the spinal cord is surrounded by white matter and has a cross-section in the shape of the letter H, with two dorsal (posterior) parts and two ventral (anterior) parts. Afferent sensory axons ascend in the spinal cord to the medulla without crossing to the contralateral column. The axons in the

dorsal column are organized in such a way that the fibres carrying information from the lower limbs are located in the medial subdivision of the dorsal column (called the gracile tract) while the cuneate tract (the lateral subdivision of the dorsal column) carries information from the upper limbs. The axons in the gracile and cuneate tracts are known as the second-order neurons. Neurons from both the gracile and cuneate tracts give rise to axons which cross to the other side of the brain and ascend to the thalamus in a long fibre bundle named the medial lemniscus. The axons of the medial lemniscus reach a specific place in the thalamus called the ventral posterior nucleus (VPL). The axons in the ventral posterior region of the thalamus are named the third-order neurons [31, 37].

## 2.11 The human brain

The human brain is the most complicated structure in the human body. In the adult human it weighs on average 1.5 kg with a size of around 1130 cm<sup>3</sup> in women and 1260 cm<sup>3</sup> in men [38]. The main parts of the brain are: the cerebrum, diencephalon, brainstem and cerebellum (little brain). The cerebrum is the major division of the brain, associated with higher brain function. It is covered by the cerebral cortex which is a thin layer of gray matter with thickness about 3 millimetres; the gray colour come from cell bodies and dendrites [39]. Underneath the cerebral cortex is a much thicker layer of fibre tracts called the white matter. Both halves of the cerebrum are divided into four lobes on each side by deep fissures. The diencephalon is the second part of the brain mainly composed of the thalamus and the hypothalamus and it is located beneath the cerebral hemispheres. The brain stem, which is below the cerebrum and in front of the cerebellum, connects the brain to the spinal cord. Finally, the cerebellum is much smaller than the cerebrum and sits at the back of the brain [40].

## 2.12 Brain mapping

The aim of brain mapping is to specify the location of structures and functional areas in the brain. One of the early attempts was published in 1858 by Rudolf Berlin, describing the classification of cells in the human cortex into six layers, depending on the variations of cell size and type in these layers. In 1874 Vladimir Betz published a study of localisation of cortical function, and many other studies were been published during the late 19<sup>th</sup> and early 20<sup>th</sup> century, using a range of approaches. Most of these studies were concerned with cortical structure rather than function. However, in 1909 the German physician Korbinian Brodmann

published *Localisation in the Cerebral Cortex* and presented a functional map of the brain that is still used today [41, 42]. Brodmann's map divides the human cortex into forty-six numbered areas, some with subdivisions. In the years since Brodmann's map was published, new techniques for brain imaging have provided more details about cortical organisation.

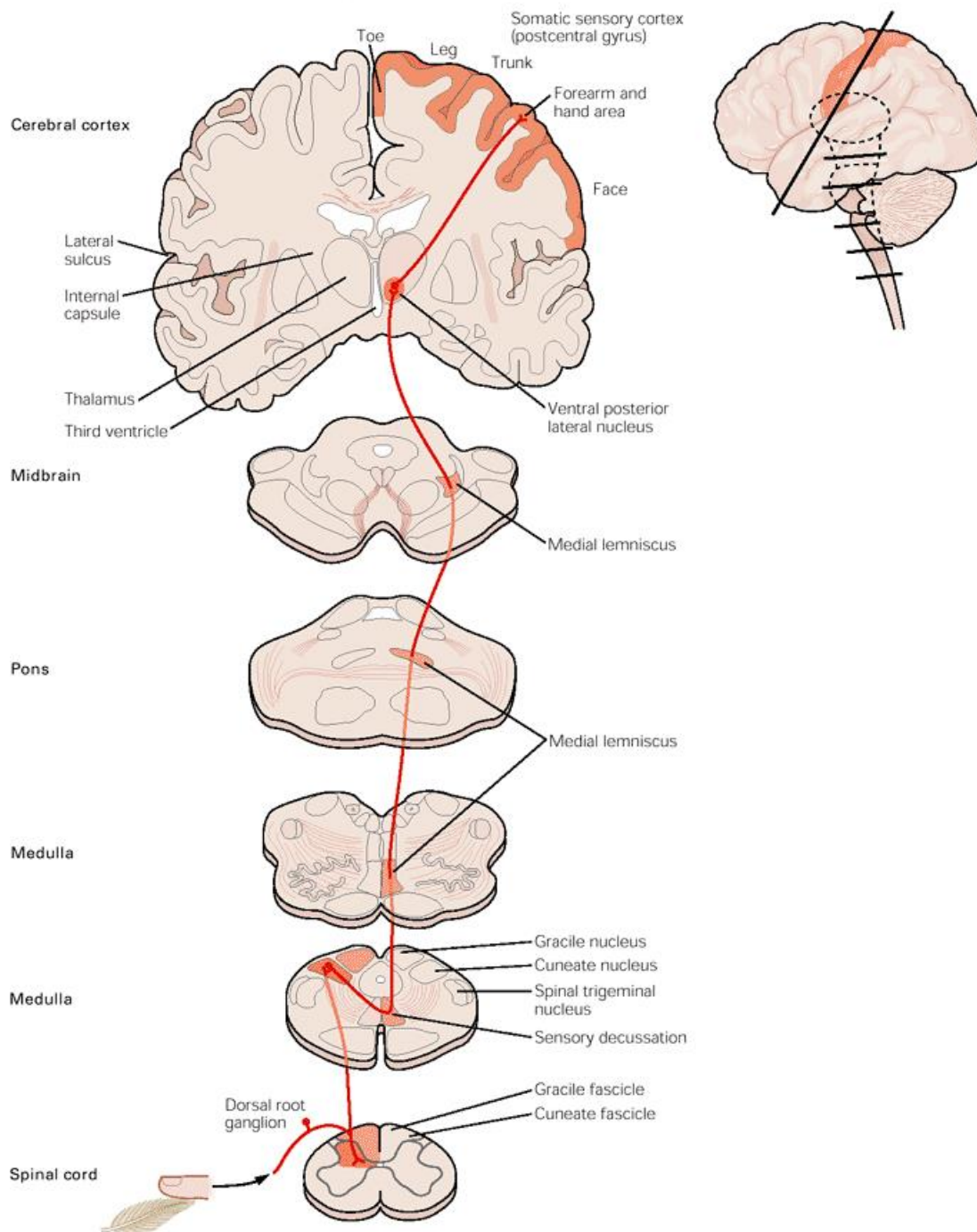


Fig. 2.4: The somatosensory pathway [31].

## 2.13 Somatosensory cortical regions

Results from studies on somatosensory perception suggest that more than one area in the brain is involved in the various aspects of somatic sensation, such as localization of tactile stimuli on the body surface and tactile pattern recognition. Below is a brief review of some cortical regions involved in somatosensory perception.

### 2.13.1 Primary somatosensory (SI) cortex

SI is the main cortical region in the brain related to somatic sensation. In humans it is situated in a region in the posterior bank of the central sulcus, which extends across the surface of the postcentral gyrus. Cytoarchitectonic investigation of SI suggests four subdivisions that receive most of their subcortical afferent fibres from the ventroposterior nucleus (VP) of the thalamus. The SI area receives the information from the contralateral side of the body and both sides of the face and scalp, in addition to the information from the thoracic and abdominal viscera and the vestibular system [43]. The subdivision areas of SI are Brodmann areas 1, 2, 3a and 3b. Area 3a occupies the fundus of the central sulcus, area 3b the anterior wall of the postcentral gyrus, area 1 its crown and area 2 its posterior wall (figure 2.5). The columns of neurons in these four cortical areas of SI are coordinated in such way that there is a complete topographic representation of the body, representing the foot, leg, trunk, forelimbs and the face, from medial to lateral [44], as shown in figure 2.6.

### 2.13.2 Secondary Somatosensory (SII) cortex

The term secondary somatosensory cortex (SII) was first used to describe a second somatotopic representation of cat's feet, close to the previously described SI cortex [45]. Several type of brain mapping techniques have identified SII in the human brain on the parietal operculum, just below the head representation in SI and covering parts of Brodmann areas 40 and 43. The cytoarchitectonics showed that the human SII region consists of four different cytoarchitectonic areas. The functionality of SII relates to many kinds of stimulation, such as light touch, visceral sensations and tactile attention [46, 47].

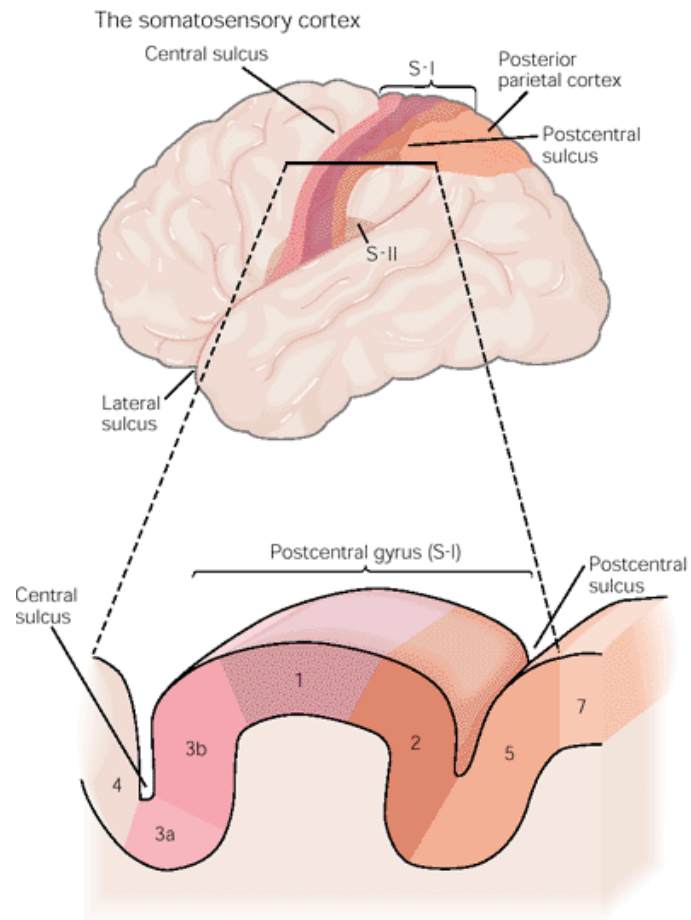


Fig. 2.5: The cytoarchitectonics of the primary somatosensory cortex [31].

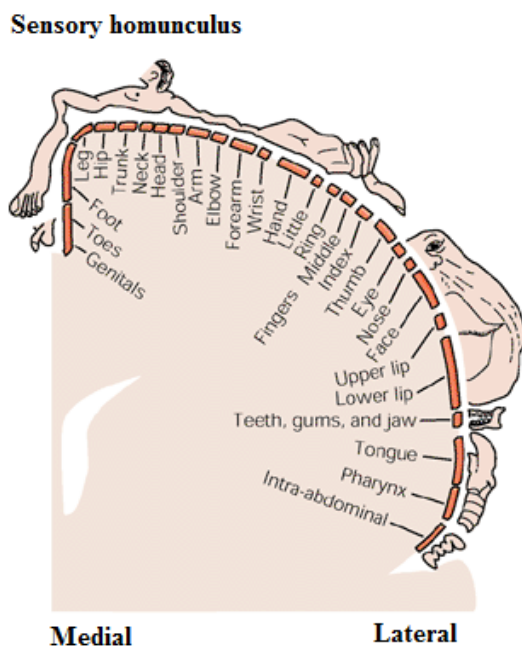


Fig. 2.6: The topographic representation of the body in the somatosensory cortex SI [31].



### 2.13.3 Posterior parietal cortex (PPC)

The posterior parietal cortex (PPC) has traditionally been considered as a sensory area which has higher-level sensory functions, associated with different sensory modalities. It is also involved in the earliest stages of movement planning [48]. The PPC contains several distinct cortical areas within Brodmann's areas 5, 7a and 7b; these are the lateral intraparietal area (LIP), the medial superior temporal area (MST), and the ventral intraparietal area (VIP) [49, 50].

## 2.14 Summary

This chapter has described the tactile system in brief. It has reviewed the properties of the main tactile receptors, discussed the process of generating a signal in the peripheral nervous system, and outlined the pathway used to send signals from the touch receptors to the brain. The chapter concludes with a description of the brain areas which show activation in response to tactile stimulation.

The next chapter reviews previous studies which have made use of tactile displays to investigate the process of touch perception.

## **Chapter Three**

# Previous studies involving tactile displays

## 3.1 Overview

There are two directions of research that relate to tactile displays. The first direction includes work by researchers whose main interest is to build and develop a versatile tactile display for general applications (for example, in the context of virtual reality); the second direction includes work by researchers whose main interest is to experiment on the sense of touch using controlled tactile stimuli from a purpose-built device (for example, in the context of psychophysics or fMRI studies). This review of previous studies concentrates mainly on the second direction but includes some coverage of the first direction.

## 3.2 Design and development of tactile displays

Today, more than eighty years after the building of the first tactile display, there are many designs and prototypes of tactile displays, and their development is ongoing. The variety includes simple and complex structures and also a wide range of different drive mechanisms [51, 52]. Desire of the researchers to cover many properties of tactile sensation is the motivation to build and develop these tactile displays. It is difficult to cover so many devices in a short review; therefore the following paragraphs will concentrate on some typical examples, with different design strategies and different uses.

Harrington et al [53] used a simple device: a piezoceramic wafer driven by an alternating voltage to produce a mechanical vibration; stimulation was provided directly to the fingertips by the circular wafer (see figure 3.1). Simplicity and ease of use are the main advantages of this design, and the piezoceramic drive mechanism was able to function inside an MRI scanner, unaffected by the static magnetic field and without producing any image artefacts. A disadvantage is that the stimulator needs more than one finger to hold it, and a further disadvantage is the humming noise produced during stimulation. This stimulator was used in an fMRI study, and results showed activation in the expected areas (the primary somatosensory cortex, Brodmann areas 1, 2, and 3, and Brodmann area 40).

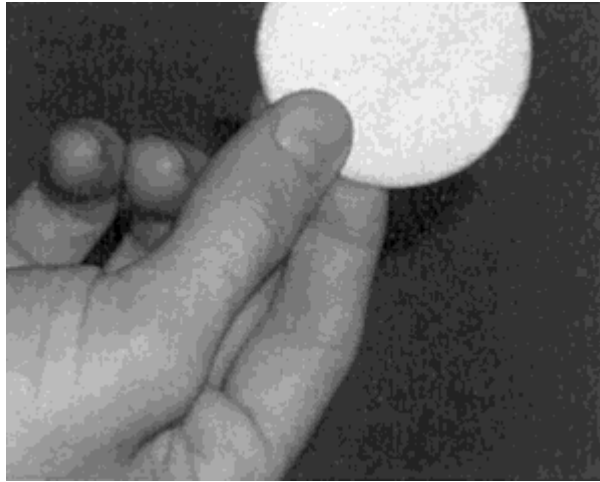


Fig. 3.1: The piezoceramic wafer, held between the thumb, index and middle finger [53].

Briggs et al [54] designed a vibrotactile stimulator that was driven pneumatically. The vibration was produced by distensible contactors, made from latex rubber, each fixed on a rectangular flat plastic holder (see figure 3.2). Each contactor was connected to a tube that delivered pulses of pressurized air from a control box. The intensity and frequency of these pulses (and hence the intensity and frequency of the vibrotactile stimulus) was determined electrically, using either manual or computer control. Although this system is suitable for an fMRI experiment, the latex rubber contactors were found to have a short lifetime and the system is not able to stimulate a small area on the skin.

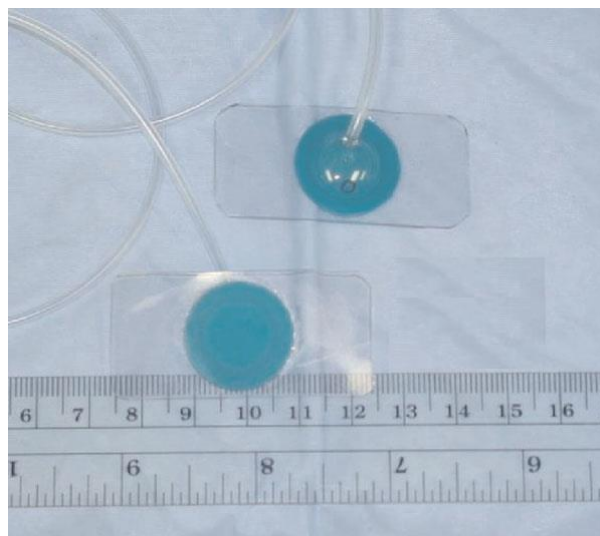


Fig. 3.2: The contactors with tubes to deliver the pulses of pressurized air [54].

A “dense array stimulator” with 400 contactors was built by Killebrew et al [55]. It is driven electromagnetically by linear motors, arranged in four planes of 100 motors each, one on top of another. It stimulates a skin area of 1 cm<sup>2</sup> (figure 3.3). The range of stimulation frequency is from DC (0 Hz) to over 250 Hz, with displacements up to 100 μm. Each of the contactors is controlled separately: each linear motor drives a shaft whose end delivers stimulation to the skin. The electronic hardware consists of digital-signal-processing boards, driver boards, sensor boards, etc. The software which is used to control the stimulator and to produce different types of pattern is written in C++. The dense array has the ability to produce complex spatial-temporal patterns, which is one of its main advantages. The complexity of the design is a major disadvantage (it is not clear if the system has ever been fully operational). A further disadvantage of the device is its large size – it is only suitable for psychophysics experiments in a single location and it is certainly not fMRI compatible.

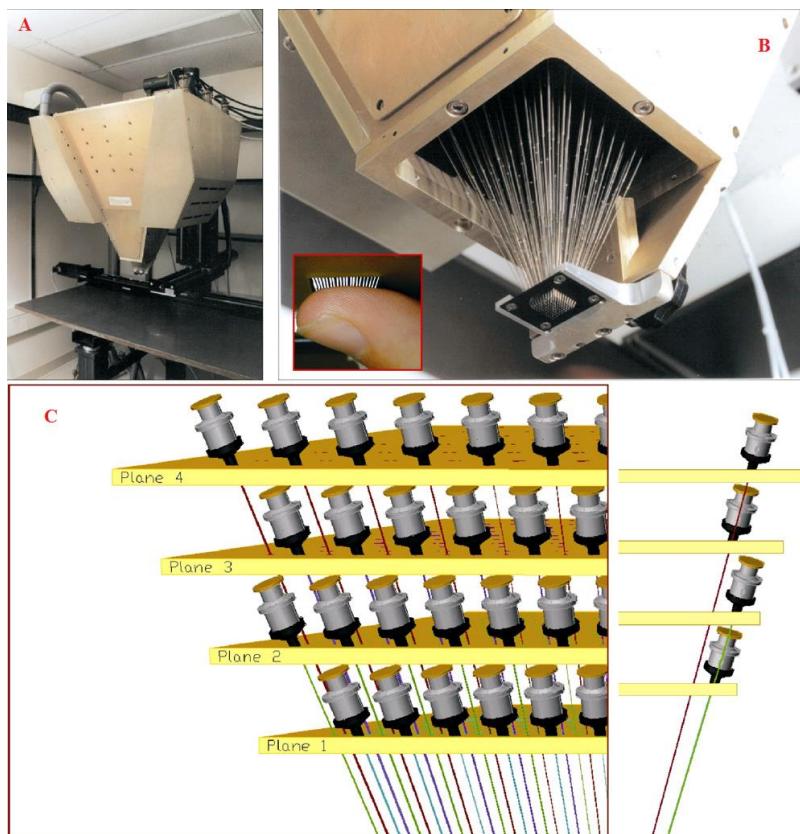


Fig. 3.3: (A) The dense array stimulator; (B) the contactor surface on the fingertip; (C) the arrangement of the linear motors in four layers [55].

Summers and Chanter built one of the several tactile displays that use piezoelectric drive mechanisms [56]. Their tactile array uses 100 piezoelectric bimorphs (for more details about piezoelectric bimorphs see 6.2.1), each connected by a brass wire link to the contactor surface (see figure 3.4). The contactors (0.6 mm diameter) are arranged in a square matrix ( $10 \times 10$ ) covering an area of  $1 \text{ cm}^2$ . The  $10 \times 10$  moving contactors are surrounded by 44 fixed contactors, giving a  $12 \times 12$  array overall. The device works over a range of frequencies between 20 to 400 Hz; the piezoelectric bimorphs are driven with a maximum voltage of 85 V peak-to-peak. The maximum displacement of the array depends on frequency – at 40 Hz it is around  $50 \mu\text{m}$  peak-to-peak and around  $6 \mu\text{m}$  peak-to-peak at 320 Hz. (This compensates for the increased sensitivity of the skin at higher frequencies.) Each of the contactors is driven independently, which leads to a wide range of output possibilities.

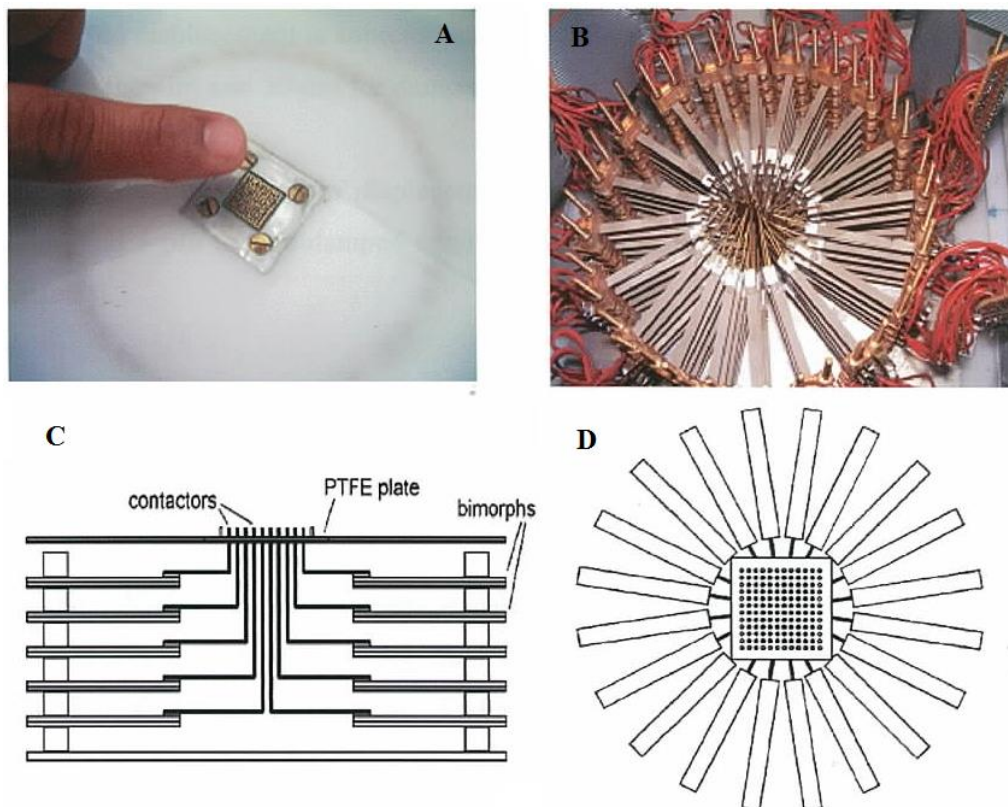


Fig. 3.4: The 100-contactor tactile array. (A) The contactor area; (B) the arrangement of the 100 piezoelectric bimorphs; (C) side view of the drive mechanism; (D) the bimorphs are arranged in 5 planes, with 20 in each plane [57].

The problem with this design, and all tactile displays driven by piezoelectric effect, is that the piezoelectric effect is weak and therefore high voltage is needed to produce strong stimulation. However because piezoelectric ceramic is not affected by magnetic field this type of tactile display is fMRI compatible. This device, developed in Exeter, has been used in psychophysics and fMRI experiments [57, 58]. It is the basis of the stimulator used in the present study.

Electrical (electrocutaneous) stimulation involves direct stimulation of the nerves which run from the touch receptors, using electrodes on the skin; this is different from the mechanical stimulation considered in the previous paragraphs, in which nerve signals are generated “naturally” by the touch receptors in the skin [59]. The sensation produced by electrical stimulation is rather different from normal touch sensation – some persons find it unpleasant. An advantage of electrical stimulation is that fixing the stimulator to the skin is very easy, and there is no mechanism involved. Kajimoto et al [60] used electrical stimulation in their “augmented reality” system. It utilizes a 4×4 matrix of stainless steel electrodes; the diameter of each electrode is 1.0 mm and each electrode delivers current pulses of 1.0 to 3.0 mA (100 to 300 V) with 0.2 ms duration (figure 3.5).

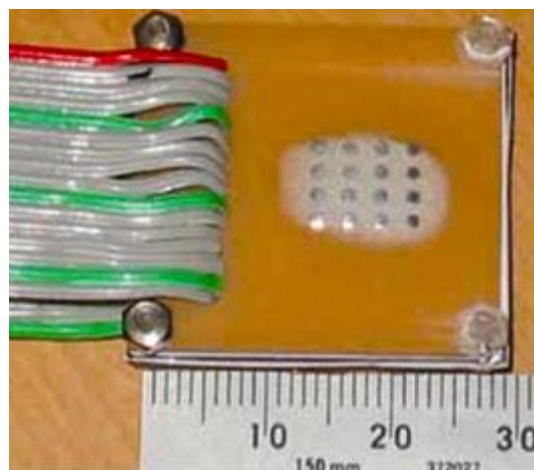


Fig. 3.5: Electrode array for electrical stimulation [60].

### 3.3 Psychophysics experiments with tactile displays

Psychophysics experiments on tactile perception have studied many aspects of touch, such as the spatial and temporal resolution of the skin and the capability of pattern recognition. For these purposes the researcher has utilized either real objects or a tactile display to provide controlled stimuli. Craig has reported numerous studies using the Optacton, a stimulator array designed as a reading aid for the blind [61], Some studies using novel stimulators are outlined below.

Master et al [62] examined the effect of age (youth, young adults and seniors) on tactile pattern recognition; also the effect of gender and handedness was tested. The tactile patterns consisted of ten embossed capital letters (see figure 3.6). The letters were made of flexible nylon sheet. Each was glued on top of a peg of diameter 1.0 cm, and a stepper motor was used to present the required sequence of individual pegs/letters for exploration by the finger. Master et al found the greatest effect on pattern-recognition ability was from age, with marginal effects from gender and handedness. This type of tactile display has the advantage that it is easy to design and construct, but the limited range of possible experiments is a major disadvantage.

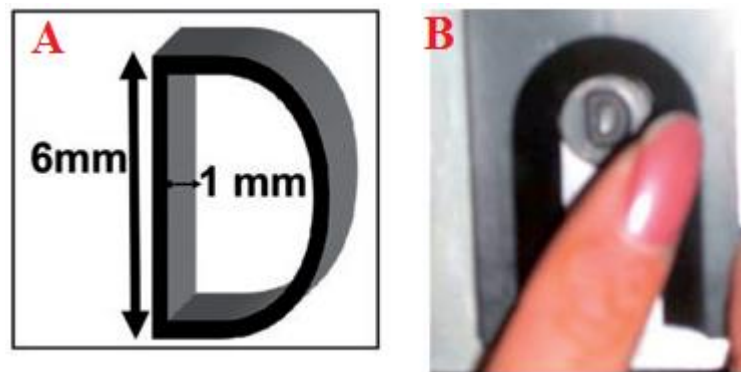


Fig. 3.6: (A) The dimensions of a letter; (B) a selected letter is presented to the finger.

Johnson and Philips also used a motor-driven device to present a tactile pattern to the finger, but in their system (figure 3.7) the finger is fixed and a rotating drum is used to move a textured surface tangentially across the skin [63]. Drum rotation moves the surface in the X



direction, axial displacement of the drum moves the surface in the  $Y$  direction, and a torque motor controls the contact force between the surface and the finger in the  $Z$  direction. There is also an assembly for overall positioning and orientation of the stimulator on the skin.

The main advantage of this design is the accuracy of control of the position in three axes. On the other hand there are some disadvantages: the size of the drum limits the type of patterns that can be presented, and it is necessary to change the drum if a different set of patterns is required [55].

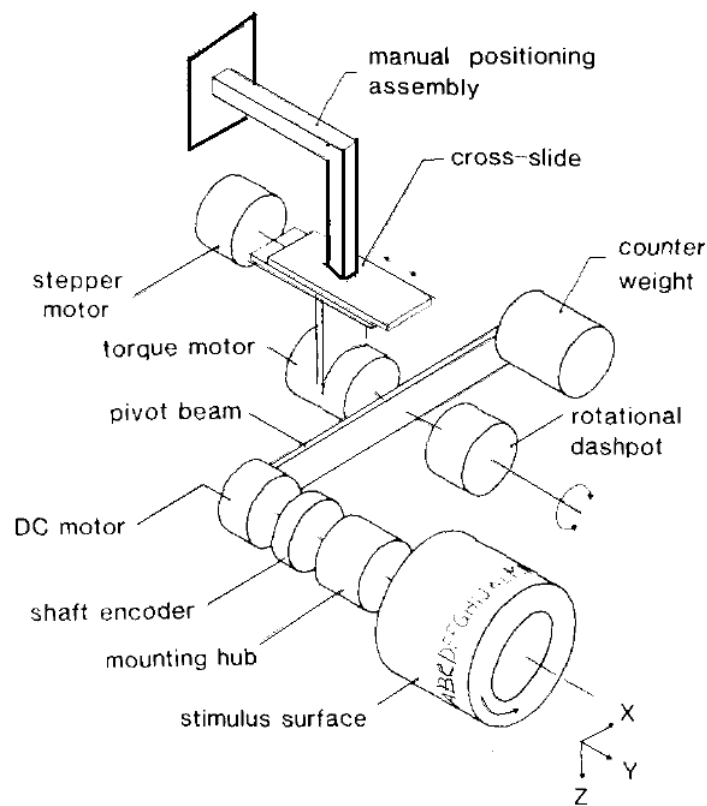


Fig. 3.7: Schematic diagram of the parts of the rotating drum stimulator [63].

### 3.4 fMRI studies using a tactile display

While psychophysics experiments are interested in studying the different types of *perception* that may be caused by the interaction of the touch receptors with the surrounding environment, fMRI research is focussed on mapping the *brain activity* produced by tactile stimulation. The difficulty of the fMRI technique is the interaction between the high magnetic field of the MRI scanner and any tactile display that uses an electromagnetic mechanism. Therefore most tactile displays used in fMRI research are driven pneumatically or piezoelectrically to deliver a static pressure or vibration which produces a mechanical displacement of the skin. Ferromagnetic materials must be avoided in the construction; large pieces of electrically conducting material must also be avoided, because eddy currents will flow in them when magnetic-field gradients are switched, causing them to move within the magnet. Savini et al [64] investigated the tactile recognition of 2D geometrical shapes with passive presentation (no exploratory movements) . The shapes were square, circle, ellipse and triangle, see figure 3.8, and made of wood. Each shape was presented with the same force (4N) by using a flexible-bar device.

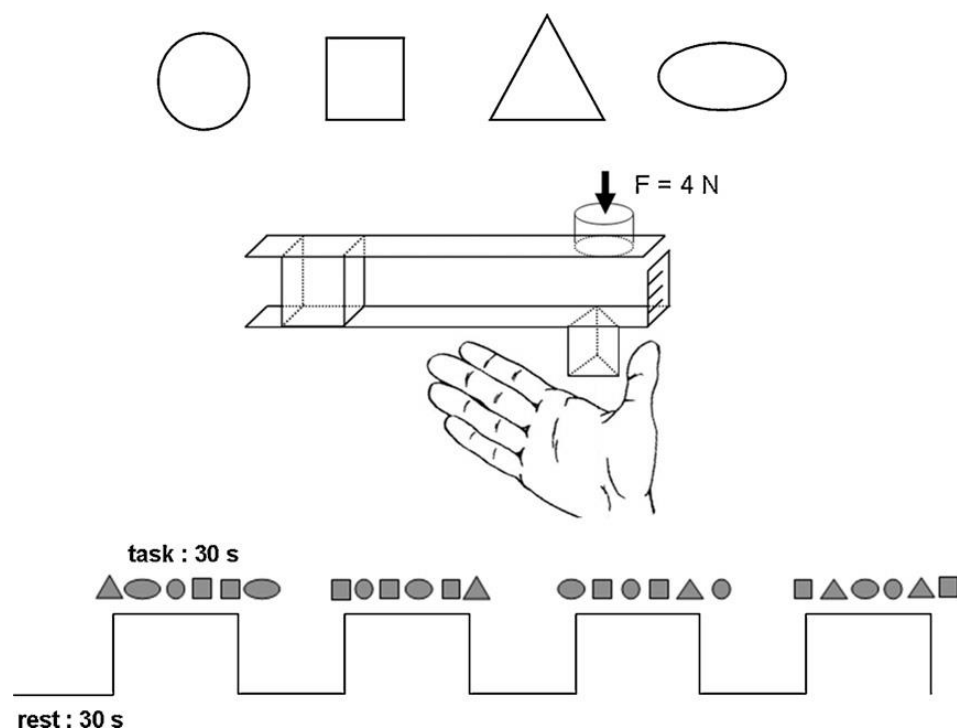


Fig. 3.8: (Top) the 2D geometric shapes used by Savini et al; (centre) the flexible-bar device used to present the shapes; (bottom) the fMRI block design [64].

Their fMRI experiment used a block paradigm of 30 seconds stimulation and 30 seconds rest. There were three different stimulation conditions: attending to the shape without being asked to identify it, identifying the shape without being asked to give a response, and a “recognition” condition (response to the identified shape with four buttons). For all three conditions there was significant activation (BOLD signal) in SI, SII and insula. Prefrontal, premotor, and parietal areas of the brain were activated, together with Broca’s area, in the two conditions involving identification (figure 3.9). In the “recognition” condition the activation in Broca’s area increased with correct responses. Savini et al proposed that Broca’s area may be involved in the successful selection of the correct response.

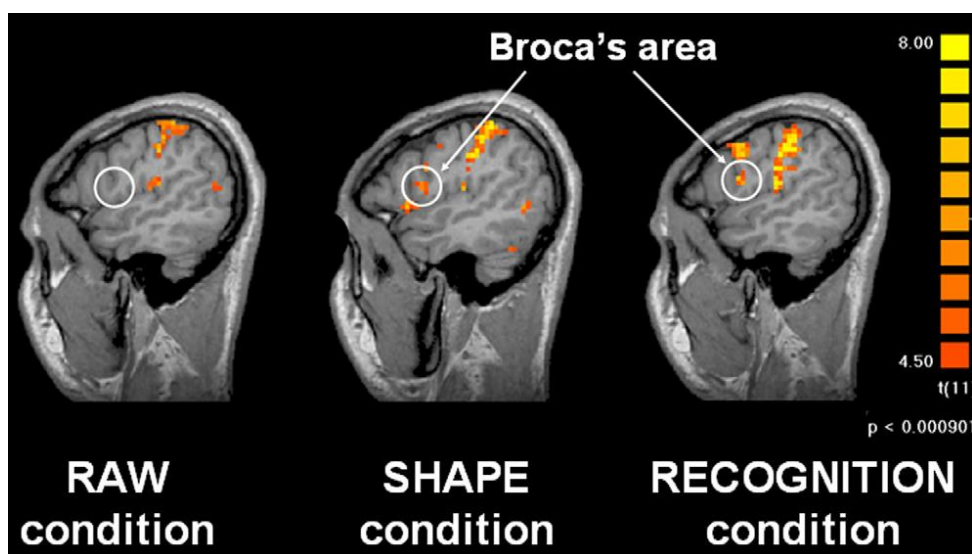


Fig. 3.9: There is activation in SI and SII for all three conditions, while Broca’s area shows activation for the two conditions involving identification [64].

Reed et al [65] used naturalistic objects to study tactile object recognition in the brain. They utilized 16 “nonsense” objects built from balsa wood and 120 real objects (found in the environment of every day, i.e., house, office and garage), made from nonmagnetic material. The fMRI experiment ran in a block design with two conditions: real tactile object recognition (TOR) with rest periods, and real tactile object recognition (TOR) with nonsense object palpation (NOP), see Figure 3.10.

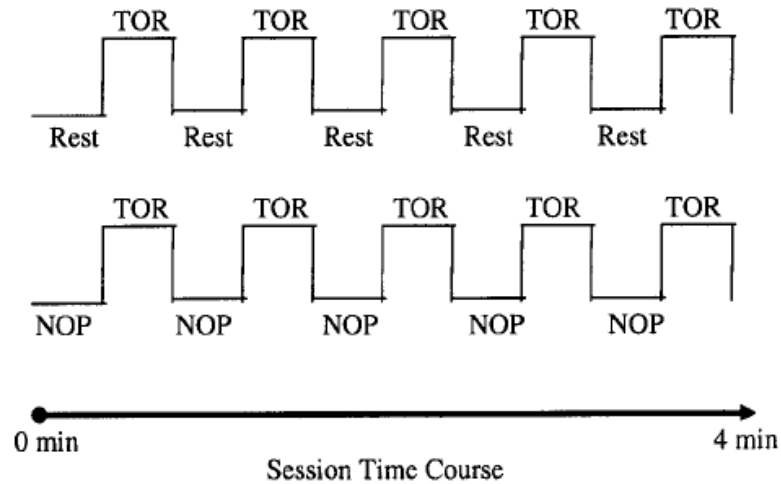


Fig.3.10: Blocks with tactile object recognition (TOR) and nonsense object palpation (NOP) [14].

In the TOR and NOP conditions, subjects explored the object with the right hand, using grasping and rubbing, and with closed eyes. The TOR-NOP contrast, relating to higher-level object recognition, showed activation in the secondary somatosensory area (SII) and insula (see figure 3.11), also in the medial and lateral secondary motor cortices (but not in the primary motor areas).

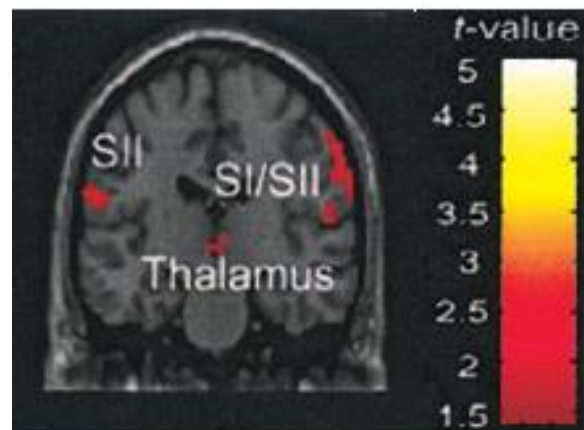


Fig. 3.11: Activation relating to the TOR-NOP contrast; SI and SII label the first and second somatosensory areas respectively; adapted from ref. [65].

Summers et al used the tactile display described in [56] and shown in figure 2.4 to study the regions of the brain that are activated by a moving vibrotactile stimulus [58]. The tactile stimuli consisted of two types: stationary and moving. The stationary tactile stimulus was based on vibration of one of the ten lines of the tactile display for 1000 ms, at a frequency of 40 Hz and with amplitude of 50  $\mu\text{m}$ . The moving stimulus was based on the ten lines of the display vibrating in sequence, each for 100 ms, again at a frequency of 40 Hz and with amplitude of 50  $\mu\text{m}$ . The stimulation was on the fingertip of digit 2 of the right hand. There were also equivalent visual stimuli: stationary and moving. The experiment was run in a block design, contrasting moving with stationary tactile stimuli, and moving with stationary visual stimuli. The most interesting results in this study show the middle temporal complex (hMT+ /V5) and the intraparietal area of the posterior parietal cortex are involved in processing both tactile and visual motion (see figure 3.12).

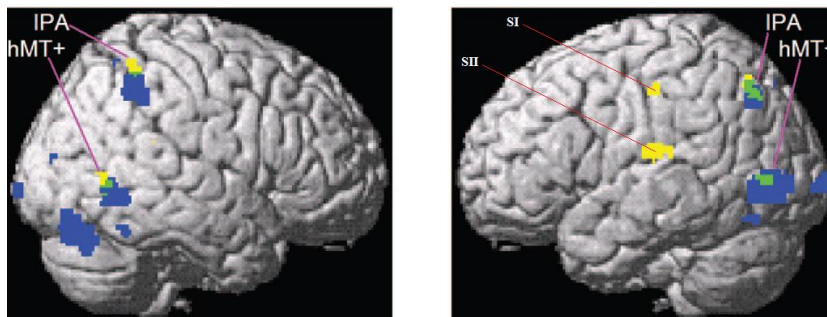


Fig. 3.12: The activation due to tactile motion (yellow) and visual motion (blue); hMT+ = middle temporal complex; IPA= intraparietal area [58].

This review concentrates on tactile displays that are designed to stimulate the fingertip, because the tactile device used in the present study is one of those types; however, the literature includes studies in which other parts of the body are stimulated, e.g., the foot [66], tongue [67] and face. Other kinds of brain mapping technique are available, e.g., positron emission tomography (PET) [68], electro-encephalography (EEG) and magneto encephalography (MEG) [69], but fMRI is one of the most common techniques and is used in the present study.

### 3.5 Summary

This chapter has reviewed previous attempts to build tactile stimulators and use them in psychophysics or fMRI studies. The review has focused on tactile stimulation at the fingertip, because the present study involved stimulation of this part of body, and on studies that used fMRI as tool to record brain activity (although studies that utilized other techniques such as EEG, PET and MEG are also mentioned).

The next chapter includes a description of the system for magnetic resonance imaging (MRI).

## **Chapter Four**

# Magnetic Resonance Imaging

## 4.1 Introduction

Historically, the roots of magnetic resonance imaging (MRI) can be traced back to the middle of the twentieth century when Bloch and Purcell separately discovered the phenomenon of nuclear magnetic resonance (NMR) in 1946 [70, 71]. The early application of NMR in physics and chemistry was focused on studying the composition and movement of molecules. In biology most of the early use of magnetic resonance was confined to the determination of spatial maps of the distribution of  $^1\text{H}$ ,  $^{13}\text{C}$  and  $^{31}\text{P}$  in living tissue using NMR spectroscopy [72]. In terms of NMR imaging techniques, the first two-dimensional (2D) image was produced when Lauterbur succeeded in obtaining an image of two glass tubes filled with water in 1973 [73]. This was followed by the significant anatomical/physiological NMR development in 1976 when Mansfield and Maudsley published the first in-vivo cross-sectional image of a finger [74] and the first image of a human thorax in 1977 [75]. At that time, as a result of the poor public perception of “nuclear” devices, the term NMR was generally replaced by MRI. The first commercial MRI system became available in 1983, built by Toshiba with field strength of 0.15 T. Nowadays the MRI machine is considered a basic tool in many research facilities or hospitals as a result of the high spatial resolution and lack of ionizing radiation.

## 4.2 The Theory of MRI

The process which leads to the production of images in MRI scanners is complex and contains many intricate steps. To understand these steps a basic understanding of the underlying physical principals is required. If atoms are considered initially, they are made up of a nucleus around which negative electrons move around in specific orbitals. Inside the nucleus are nucleons, subdivided into protons and neutrons. Without going into sufficient detail to describe the all of the components of atoms, two specific traits are important to explain MRI phenomena. These are nuclear angular momentum and nuclear magnetic moment, which are best examined by adopting a quantum physics approach.

Both protons and neutrons have an angular momentum  $\vec{J}$  as a result of possessing an intrinsic property called spin  $\vec{I}$  where:

$$\vec{J} = \hbar \vec{I} \dots\dots\dots 4.1$$

where  $\hbar = \frac{h}{2\pi}$  ;  $\hbar$  is Planck’s constant (  $1.054 \times 10^{-34}$  J s).



The value of the total angular momentum of the nucleus is the vector sum over the protons and neutrons. In units of  $\hbar$  it can be zero, a half integer or an integer; only nuclei with non-zero angular momentum (i.e., half integer or integer spin numbers) are active in MRI experiments.

The nuclear angular momentum  $\vec{J}$  is associated with a magnetic moment  $\vec{\mu}$  given by [76]:

$$\vec{\mu} = \gamma \vec{J} \dots\dots\dots 4.2$$

where  $\gamma$  is the gyromagnetic ratio.

The nucleus of hydrogen,  $^1\text{H}$  (one proton) is the principal nucleus that generates signal in biological MRI, the isotope having a high natural abundance (99.98%) and there being a high prevalence within the human body (which is approximately 70% water).

The hydrogen nucleus (spin number =  $1/2$ ) has angular momentum  $1/2\hbar$  and an associated magnetic moment  $\gamma 1/2\hbar$ , and so behaves like a tiny and very weak bar magnet [77]. In the absence of an external magnetic field, the directions of the tiny magnetic fields from each proton are randomly distributed in space, the magnetic moments cancel each other out, and thus the net magnetic vector is zero. Applying an external static field acts to align the direction of the magnetic field of the hydrogen with the direction of the external field. The torque  $L$  from the external field is given by

$$L = \mu \times B_0 \dots\dots\dots 4.3$$

where  $\mu$  is the magnetic moment and  $B_0$  is the external magnetic field. It causes the proton to precess around the external field (see figure 4.1). The frequency of precession, also known as the Larmor frequency  $\omega_0$ , is given by:

$$\omega_0 = -\gamma B_0 \dots\dots\dots 4.4$$

where the negative sign indicates the direction of the spin precession around the applied field. The external static magnetic field also works to split the energy level of the proton (figure 4.2) into two levels according to the Zeeman effect with the energy  $E$  of these levels given by [78]:

$$E_+ = -\gamma\hbar B_0/2 \dots\dots\dots 4.5$$

and

$$E_- = +\gamma\hbar B_0/2 \dots\dots\dots 4.6$$

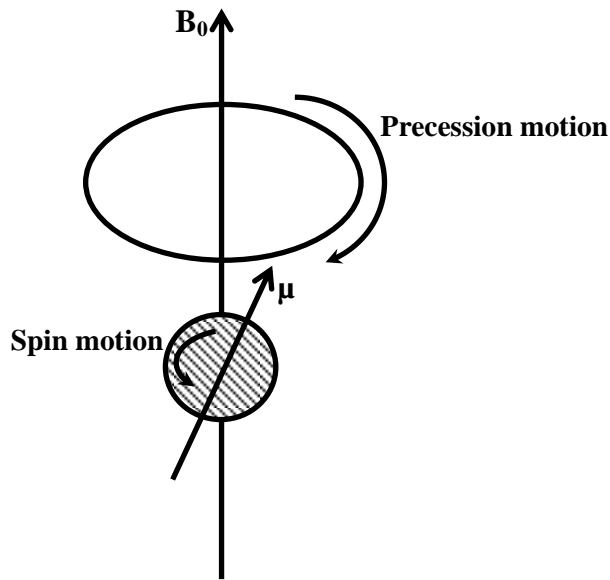


Fig. 4.1: Precession of the proton magnetic moment  $\mu$  around the magnetic field  $B_0$ .

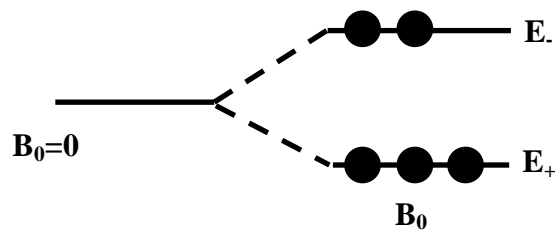


Fig. 4.2: Zeeman effect to split the proton energy level.

At room temperature the energy distribution of protons follows Boltzmann statistics, where a very small majority of the protons ( $N_+$ ) align with the external field relative to those protons ( $N_-$ ) which align against the field. The relative population distribution is given by[79]:

$$\frac{N_+}{N_-} = e^{\hbar\omega_0/KT} \dots\dots\dots 4.7$$

where  $\omega_0$  is the Larmor frequency ; k is the Boltzmann constant and  $T$  is the absolute temperature.

A basic image sequence requires the net magnetic vector to be flipped away from the direction of the external static magnetic field. In order for this to occur, a radio frequency (RF) pulse (represented by a magnetic field  $B_1$ ) must be applied at the Larmor frequency - the resonance condition.

The Bloch equation provides a description of the time  $t$  evolution of the net magnetic vector during and after the application of an RF pulse [80] and is given by:

$$\frac{dM}{dt} = \gamma M \times B_{\text{tot}} - \frac{M_x}{T_2} \vec{i} - \frac{M_y}{T_2} \vec{j} - \frac{M_z + M_0}{T_1} \vec{k} \dots\dots\dots 4.8$$

where  $M$  is the net magnetic vector with components  $M_x$ ,  $M_y$  and  $M_z$ ;  $M_0$  is the equilibrium magnetization,  $B_{\text{tot}}$  is the total applied magnetic field (static field  $B_0$  plus RF field  $B_1$ ), and  $T_1$  and  $T_2$  are the spin-lattice and spin-spin relaxation time constants respectively.

During the application of the RF pulse at the Larmor frequency, some protons move from the lower energy level to the higher energy level. After turning off the RF pulse, these protons lose their energy as a result of two relaxation processes which occur simultaneously and independently. The first is spin-lattice relaxation or longitudinal recovery which is the process whereby the proton loses its energy to the surrounding environment. This process is assumed to be exponential and is represented by the following relationship:

$$M_z(t) = M_0(1 - e^{-t/T_1}) \dots\dots\dots 4.9$$

where  $M_z(t)$  is the magnetization at time  $t$ ,  $M_0$  is the equilibrium magnetization, and  $T_1$  is determined by the rate of recovery.

The second form of relaxation is called spin-spin relaxation, where the nuclei exchange energy with neighbouring nuclei and become out of phase with each other. This is also known as transverse decay and is described by:

$$M_{xy}(t) = M_0 e^{-t/T_2} \dots\dots\dots 4.10$$

where  $M_{xy}(t)$  is the magnetization in the  $xy$  plane at time  $t$ , and  $T_2$  is determined by the rate of decay.

The contrast seen in MR imaging between tissues depends on a combination of the tissues' proton density,  $T_1$  value and  $T_2$  value [81-83]. Some imaging sequences are sensitive to  $T_2^*$

rather than  $T_2$ .  $T_2^*$  is dependent upon  $T_2$  but also has contributions resulting from inhomogeneities in the local static magnetic field. It is given by the equation:

$$\frac{1}{T_2^*} = \frac{1}{T_2} + \frac{1}{T_{2inhomo}} + \frac{1}{T_{2ms}} \dots\dots\dots 4.11$$

where  $1/T_{2inhomo}$  describes local static-field differences and  $1/T_{2ms}$  the differences in magnetic susceptibility of the tissue [84].

### 4.3 Image Formation

If only an RF pulse is applied to a sample the resulting signal does not contain any spatial information, and it is therefore not possible to discriminate the relative signal contribution from different locations within the tissue. To overcome this limitation and to be able to subsequently produce an image, three magnetic-field gradients are required: one in each of the  $x$ ,  $y$ , and  $z$  directions. These give rise to processes known as slice selection, readout or frequency encoding, and phase encoding.

The slice-select gradient (for example, applied in the  $z$ -direction) is an additional temporary magnetic field, varying linearly with position that is applied in addition to the constant static field. This means that the magnetic field will no longer be uniform in the  $z$  direction. According to equation 3.4 the precession frequency is directly proportional to the strength of magnetic field. Thus, after applying the additional magnetic-field gradient, the precessional frequency will vary along the  $z$  axis. Hence, if an RF pulse is subsequently applied with a limited bandwidth (about 1–2 kHz); only those protons at specific locations will be excited, thereby leading to signal being generated from only a certain slice within the tissue. The bandwidth  $\Delta\omega$  of the radio frequency pulse and the amplitude  $G_z$  of the gradient field determine the thickness  $\Delta z$  of this slice[85]:

$$\Delta z = \frac{\Delta\omega}{\gamma G_z} \dots\dots\dots 4.12$$

Each proton resonates at a frequency  $\omega_i$  dependent on its position  $r_i$  such that:

$$\omega_i = \gamma(B_0 + G \cdot r_i) \dots\dots\dots 4.13$$

At this point the signal contains information from the entire slice without any indication of the contribution of each point (pixel) within the slice. Localization within the slice is achieved by means of two more gradients, each orthogonal to the slice-select gradient: a phase-encoding gradient (for example, applied in the  $y$  direction) and a frequency-encoding

gradient (for example, applied in the  $x$  direction). These gradients allow acquisition of data by scanning  $k$ -space in two dimensions; the two-dimensional image may be calculated from these data by using an inverse Fourier transform. The frequency-encoding gradient is applied across the slice during readout (i.e., data acquisition), so the range of frequencies  $\Delta\omega_{RO}$  in the readout signal is determined by the amplitude  $G_{FE}$  of this gradient and the field of view  $FOV$  of the tissue that is imaged [84, 86]:

$$\Delta\omega_{RO} = 2 \times \omega_{NQ} = \gamma(G_{FE} \times FOV) \dots\dots\dots 4.14$$

where  $\omega_{NQ}$  is the minimum Nyquist frequency, i.e., half the minimum frequency at which the readout signal should be sampled. (The Nyquist theorem explains that the sampling frequency should be at least twice the highest frequency contained in the signal from the tissue [82].

#### 4.4 Image weighting

The characteristic that makes MRI particularly useful in clinic applications is the signal contrast between different areas of the tissue and between normal and abnormal tissue. The main processes used to obtain contrast in MR imaging are based on differences in relaxation times  $T_1$  and  $T_2$  and proton density in different tissues.

$T_1$  weighted images use differences in spin-lattice relaxation time to distinguish between different tissues. Water and fat, which are the main components of human tissue, have different value of  $T_1$ . Thus, for example, for imaging sequences which utilise short repetition times (200-700 ms), fat will appear bright relative to water due to its shorter  $T_1$  value. (The repetition time  $TR$  is the time between consecutive RF excitation pulses).

$T_2$  weighted images use differences in the spin-spin relaxation time to obtain contrast between tissues. Using long echo times (80-100 ms) leads to higher signal intensity in water relative to fat due to its longer  $T_2$  value. (The echo time  $TE$  is the time between the excitation pulse and the peak of the subsequently acquired signal.) Generally for optimizing anatomical detail  $T_1$  weighting is utilized while  $T_2$  weighting is found to be generally superior for the visualization of pathological conditions [86, 87].

$T_2^*$  weighted images have a contrast dependent both on  $T_2$  and the local magnetic inhomogeneities within the tissue. In functional MRI (fMRI)  $T_2^*$  contrast is typically used, specifically to allow differences in tissue oxygenation state to be identified. The best Blood Oxygenation Level Dependent (BOLD) contrast is seen with a  $TE$  equal to  $2/3$  of  $T_2^*$  [88].

## 4.5 Functional Magnetic Resonance Imaging (fMRI)

The early historical applications of MRI in medicine were focused on producing structural images of organs. However, with the development of both higher temporal and spatial resolutions, more functional based assessments become possible. Generally within medical imaging there are both direct and indirect ways to examine functional activity within the brain.

An example of a direct method is a technique such as Electroencephalography (EEG) which detects the electrical signal produced by an active neuron in the brain, thereby revealing functional areas in the brain. In contrast, functional magnetic resonance imaging (fMRI) is a technique that generates images of activated brain regions via the indirect measurement of regional cerebral blood volume (CBV), cerebral blood flow (CBF), and blood oxygenation, which are modified by neural activity.

fMRI techniques can utilize three methods to observe the brain's function. The first approach uses an injected contrast agent such as gadolinium diethylene-triamine-pentaacetic acid (Gd-DTPA) to track the changes in blood volume during activation tasks. The first application of this method was in animals by Villringer et al and it was subsequently used in human studies by Belliveau et al [89, 90]. The second method uses blood oxygenation as a naturally present contrast agent via the BOLD effect. Both of these techniques rely on variations in magnetic susceptibility either due to the presence of gadolinium or alterations in blood oxygenation leading to modifications in the homogeneity of the local magnetic field. The third technique measures quantitative perfusion thereby linking local blood flow changes with brain activation [18, 91].

### 4.5.1 Blood Oxygenation Level Dependent effect

Functional magnetic resonance imaging of the brain depends on both the physiological changes that accompany the neural activity in the brain and the contrast that originates from the BOLD signal due to the blood acting as a naturally present contrast agent. The basis of this contrast depends on haemoglobin having magnetic properties which are dependent upon its oxygenation state. Oxyhaemoglobin is weakly diamagnetic while deoxyhaemoglobin is paramagnetic as a result of four unpaired electrons. These differences in magnetic properties mean any alteration in the amount of oxygenated and deoxygenated blood will lead to associated alterations in local magnetic susceptibility within the blood and hence variations in MRI signal intensity. Alterations in blood composition within the brain

depend upon the Hemodynamic Response (HR) in the brain following activation; this hemodynamic response includes changes in CBF, CBV and cerebral metabolic rate of oxygen (CMRO<sub>2</sub>) [92].

Although the discovery of the characteristics of the magnetic state of haemoglobin took place before the discovery of MRI itself [27] and the magnetic susceptibility effects of blood on the relaxation time  $T_2^*$  were demonstrated in 1982 [93] the first functional images were not undertaken until 1990. The early use of BOLD contrast in functional MR imaging was in animals by Ogawa et al, where it was shown veins became noticeably darker when the oxygen content inside them was reduced. In 1992 BOLD contrast was first applied to the study of the functional brain in humans [40, 94].

Stimulating the brain through any type of task will lead to an increase in CBF to match the energy demands of the brain associated with the task. However, the increase in the CBF surpasses the increase in CMRO<sub>2</sub>. This disproportionate change in CBF compared to CMRO<sub>2</sub> may be because extraction of oxygen from the blood is less efficient at higher flow rates [95] or the CBF increase occurs over a larger volume than for the increase in CMRO<sub>2</sub> [96]. The increase in CBF does not occur in the stimulated area of the brain immediately. Instead, there is a delay of approximately two seconds as the blood travels from the arteries to capillaries and draining veins. This delay results in an initial dip in the BOLD signal in functional MR due to the increased CMRO<sub>2</sub> not being immediately compensated by an increased CBF [87, 97, 98]. Subsequently, the BOLD signal increases rapidly as a result of increased the oxyhemoglobin in the blood vessels, to reach a peak 6 to 9 seconds from the start of the stimulation [89]. Figure 4.3 shows the time course for the BOLD signal. The shape of the peak and the length of the plateau periods depend on the properties and length of the stimulation, as shown in figure 4.4.

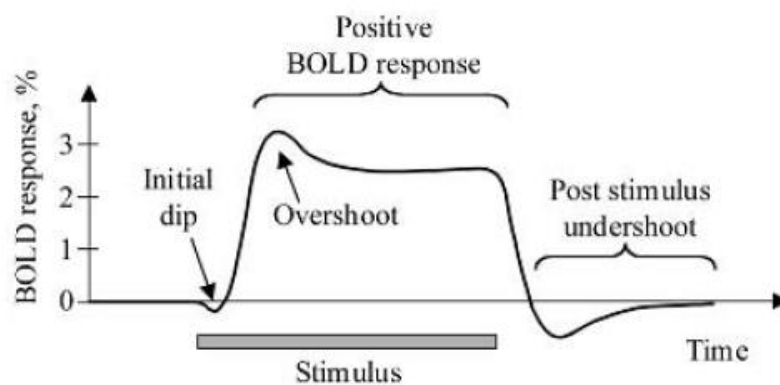


Fig. 4.3: Schematic representation of the common features of the fMRI BOLD response [99].

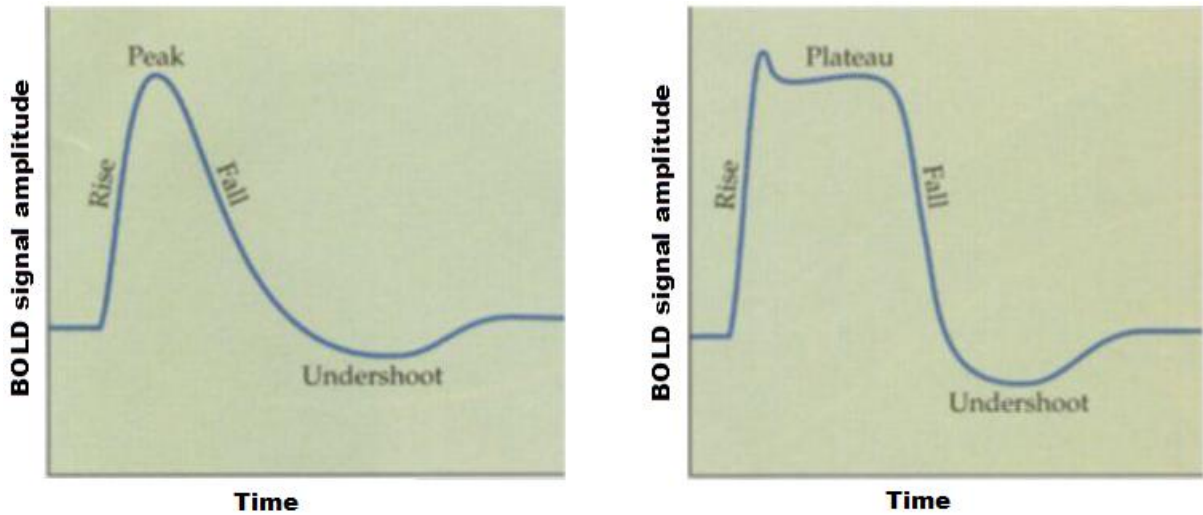


Fig. 4.4: The BOLD hemodynamic response. (A) single event;(B) block of multiple events [90].

Following the cessation of the stimulus the amplitude of the BOLD signal decreases, dropping below the baseline level and continuing to be below the baseline for a few seconds, a feature known as the post-stimulus undershoot. According to the balloon model by Buxton and colleagues, this effect occurs as a result of the blood flow after stimulus onset being greater into the venous compartment than the blood flow out, so the (venous) blood volume increases, but at the end of the stimulation the blood flow decreases more rapidly than blood volume, leading to an increase in deoxyhemoglobin and a reduction of the fMRI signal [100, 101]. Although the increase in signal from the BOLD effect is only about 1% at 1.5 T, which is small compared with technique that use contrast agents, it has the great advantage of being non-invasive and is still capable of producing an in-plane spatial resolution of about 3-4 mm.

## 4.6 Pulse sequences

There are many parameters that control the contrast in magnetic resonance images and to control these parameters a range of a pulse sequences is used. Generally the pulse sequences can be categorized as Spin Echo (SE) or Gradient Echo (GE) pulse sequences. In the spin echo at least two RF-pulses are used, a  $90^\circ$  excitation pulse followed by a  $180^\circ$  rephasing pulse to generate a spin echo (sometimes more than one rephasing pulse is utilized). Two kinds of spin echo are ordinarily used: single echo and multi-echo (echo-train spin echo is a variant of the latter). In GE sequences, the echo is generated by switching



magnetic-field gradients. When using a short  $TR$  to reduce overall imaging time, the excitation pulse in GE sequences is often less than  $90^\circ$  to avoid excessive  $T_1$  weighting [84].

#### 4.6.1 Echo planar imaging

For fMRI, in order to obtain the high temporal resolution necessary to see the stimulus-induced signal-intensity changes, a very rapid MRI pulse sequence is required. In addition, the sequence must have large  $T_2^*$  weighting in order for the BOLD contrast to be apparent. As a result the method that is most typically used in fMRI experiments is echo-planar imaging (EPI) [102]. In EPI multiple gradients are used to generate echoes to allow the production of an image with a single RF excitation. Figure 4.5 illustrates the time scheme of the gradient-echo EPI sequence.

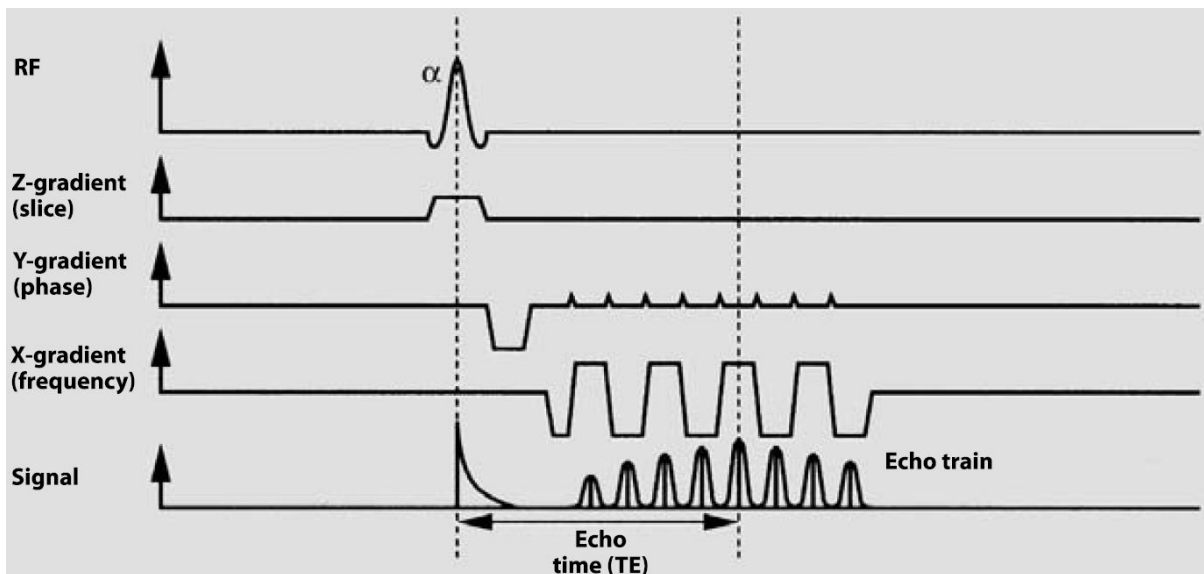


Fig. 4.5: Diagram of the time course of a single-shot echo-planar sequence [103].

## 4.7 Functional MR Experiment Design

The aim of an fMRI experiment is to determine the regions of the brain that are active during specific tasks. Because the changes in BOLD signal are very small during brain activation, fMRI experiments need to be carefully designed in order to obtain sufficient signal to noise to generate statistically significant results. Generally there are two approaches to the design of functional MR experiments: block and event-related [104].

### 4.7.1 Block fMRI Design

In a block design, a series of stimulus blocks are presented each lasting between a few seconds or up to several minutes. Within each block the participants are performing the same task, or ‘experimental condition’. Between blocks are periods of rest, representing a baseline condition. The block design has high statistical power and hence it is the most popular experimental design within fMRI. An example of a block design is shown in Figure 4.6.

### 4.7.2 Event-Related fMRI Design

In an event-related design very short and discrete stimuli are presented with the length of each event being short compared to the time between events. Even though the statistical power of event related designs is low, this design is more representative of the type of real world transient events that human brains deal with every day. An example of an event-related design is shown in Figure 4.6.

### 4.7.3 Mixed Design

As an option to utilize the high statistical power of the block design and the relevance of event-related designs it is possible to combine the two methods. Figure 4.6 illustrates an example of a mixed design.

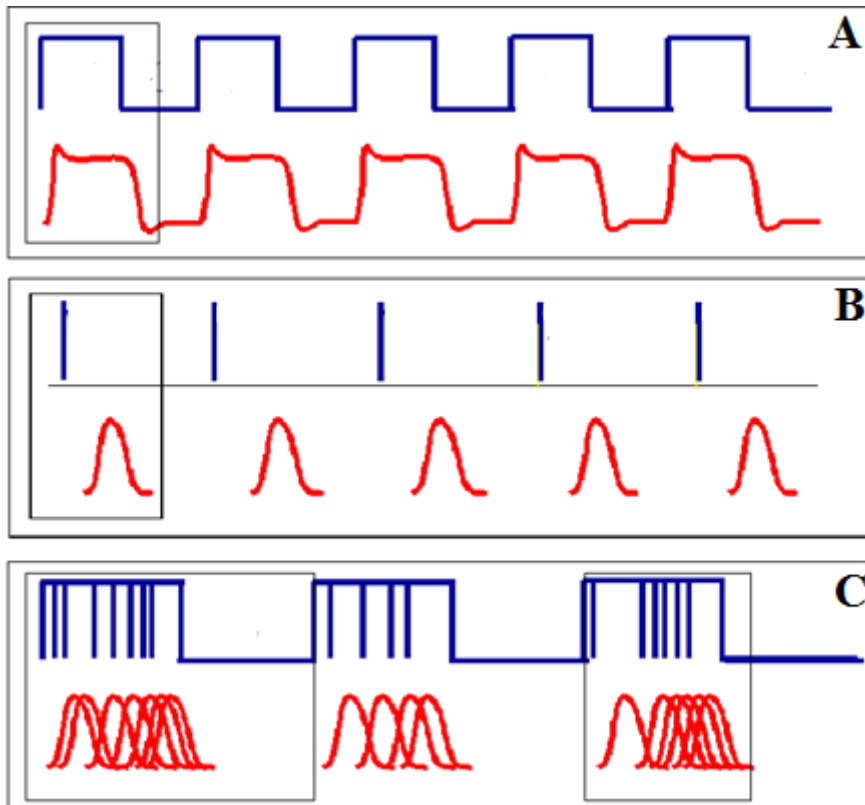


Fig 4.6: The different types of fMRI experimental designs. (A) Block design with a cycle of one or more conditions, each block lasting for a few seconds. (B) Event-related design with short-duration events, and (C) a mixed design with blocks of short-duration events. The blue lines represent the time course of the stimuli and the red lines show the BOLD hemodynamic response [105].

## 4.8 The Components of the MR Scanner

The MRI scanner is one of the most important pieces of diagnostic equipment in hospitals worldwide. Because of this there is continual development of MRI scanners, both the hardware and software components. The following paragraph describes the main parts of the MRI scanner, as shown in figure 4.7.

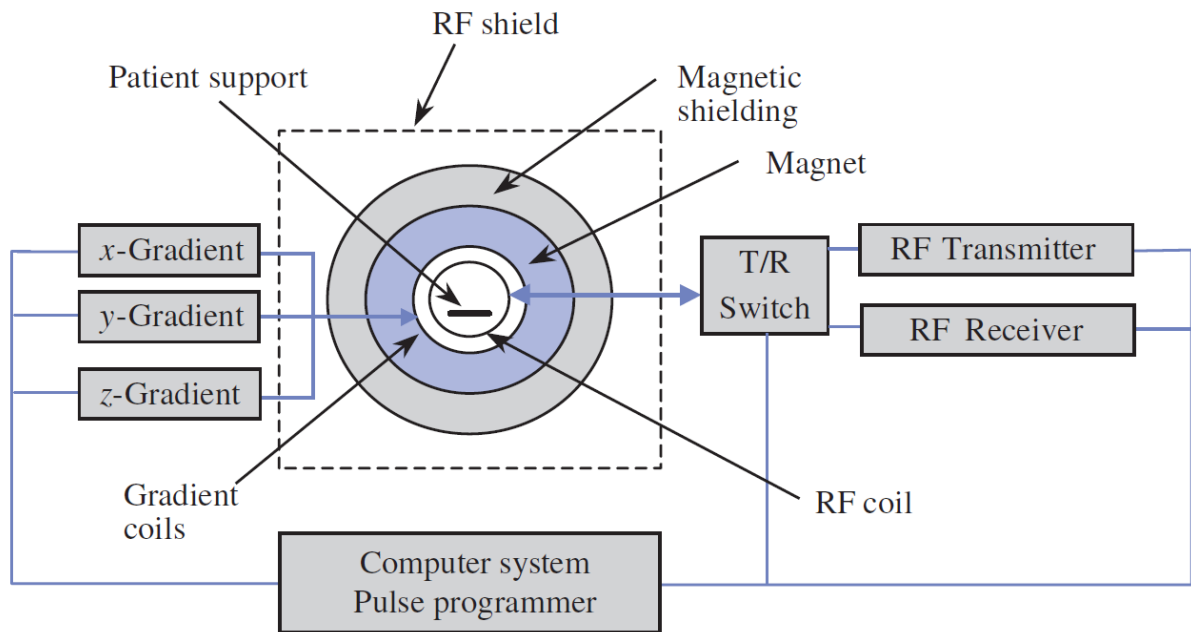


Fig 4.7: The major parts of the MRI scanner [82].

The first and the most important consideration is the static magnetic field – many sorts of magnet are used to produce the static magnetic field: permanent magnets can be used to produce fields up to 0.3 T; these days most MRI scanners utilize superconducting magnets, using materials that have zero resistance at temperatures near absolute zero, which can produce fields up to around 10 T. The majority of clinical machines have field strength of 1.5T, although 3 T machines are becoming more common. The homogeneity and strength of the magnetic field are the most important features for any MRI scanner. Some of the inhomogeneity can be removed by shimming: additional electromagnetic coils generating compensatory magnetic fields.

The second part of the MRI scanner is the radiofrequency system which is used to produce a radiofrequency pulse at the Larmor frequency to excite nuclei in a specific part of the imaged object, and also to receive the signal from the object. Because distance between the receiver coil and the object affects the strength of the received signal, the coil used to receive the signal is generally designed to be positioned close to the volume that is imaged. Many receiver coils are in the form of a phased array: multiple coils whose receptive fields are arranged in an overlapping pattern.

The third part of the MRI scanner is the gradients, as described in section 2.3, which are used to provide spatial information for the 2D or 3D image, i.e., to separate the signal contribution from each part of the object. In the MRI scanner there are three orthogonal linear magnetic-field gradients, created by three sets of electromagnetic coils.

To produce a magnetic resonance image, all these parts must work together to implement the appropriate sequence of operations; this requires highly accurate timing control from a computer system, composed of multiple microprocessors which control each subsystem of the MRI scanner and take commands from a main computer [82].

All the imaging processes in the present research were done using the 1.5 T Philips Intera MR imager at the Exeter MR Research Centre, see figure 10. The diameter of the scanner bore is 54 cm with a maximum gradient strength of  $60 \text{ mT m}^{-1}$ . During the functional and structural scans a SENSE coil was used, composed of 8 elements.

## 4.9 Artefacts in MRI images

During magnetic resonance imaging, features may appear in the image that does not exist in the object which has been imaged; these features are called artefacts. The source of the artefacts comes either from the object or from the magnetic resonance machine. Object motion often causes artefacts – if the motion is periodic (like pulsatile heart or respiratory motions) the artefact will appear as a “ghost”, while if the motion is not periodic (such as head motion and coughing) it will causes diffuse image noise [106]. Another artefact coming from the object shows as bright or dark outlines at fat-water interfaces; this is known as a chemical shift artefact. This artefact is due to protons having a slightly different resonance frequency in water and fat (as a result of their micromagnetic environment) – the frequency difference is interpreted in the image as a displacement of fat with respect to water [107].

The hardware of the MR machine can also produce some artefacts in the images. Inhomogeneity in the static magnetic field can lead to spatial and intensity distortions. Similarly, spatial distortions can be caused by non-linearity in the magnetic-field gradients: some parts of the imaged volume have more gradient than others [82]. In addition to the above, many other image artefacts can be observed (generated by the imaging hardware or the object that has been scanned).

## 4.10 Magnetic Resonance Imaging Noise

The magnetic resonance signal that is received in the detector coil contains some non-meaningful components, together with the main signal of interest; this unwanted signal is called noise. Understanding the sources of the noise will lead to improved MR images. Noise in MRI is measured using the quantity called signal-to-Noise Ratio (SNR); high SNR allows high-quality images to be obtained in both structural and functional applications of MRI. The two main sources of noise in magnetic resonance imaging are thermal and physiological – thermal noise is the unavoidable noise in most implementations of the MRI; physiological noise can be a major source of noise in dynamic applications such as fMRI.

Thermal noise in MR images is due to thermal electron motion within both the scanned object and the hardware of the MR machine. It increases with the strength of the static magnetic field of the scanner (but signal amplitude increases faster, so SNR increases with field strength). Physiological noise has similar origins to the physiological artefacts described above, e.g., tissue fluctuations related to the heart or respiratory cycle [108].

## 4.11 Summary

Chapter three has described the MRI technique, including a review of the theoretical background and the basis of image contrast between tissues. The chapter has also described functional imaging (fMRI).

The next chapter reviews the analysis of fMRI data using SPM software.



Fig. 4.8: the 1.5 T Philips Intera MR imager at the Exeter MR Research Centre. The SENSE head coil of 8 elements is fixed to the moveable table of the scanner.

## **Chapter five**

# *Analysis of the fMRI data*



## 5.1 Introduction

The objective of an fMRI experiment is the determination of which areas of the brain are active when a specific task is undertaken. However, in order to reach this conclusion the fMRI data must undergo many analysis stages. These stages consist of an initial data conversion step so the data is in the appropriate format for subsequent analysis, pre-processing to ensure the data is free of movement and is presented in standard brain space to allow inter-subject comparisons and post-processing to examine the statistical correlations between signal intensity changes within the brain and the stimulus paradigm.

There is a wide range of fMRI data analysis software available, such as Statistical Parametric Mapping (SPM) (<http://www.fil.ion.ucl.ac.uk/spm/>), Analysis of Functional NeuroImages (AFNI) (<http://www.afni.nimh.nih.gov/>) and Brain Voyager QX (BV) (<http://www.brainvoyager.com/>).

In the present study all analysis was undertaken in SPM, specifically the 2008 release: version SPM8. SPM (SPM8) is a package of MATLAB functions and routines with some compiled C-language code. It was written by the Wellcome Trust Centre for Neuroimaging at University College London and was originally released in 1991 as the SPM91 version, followed by regular updates every two to three years [109].

## 5.2 Pre-processing Stage

The primary steps in pre-processing comprise slice-time correction, realignment, normalization and smoothing. The order of these steps is somewhat flexible depending upon the exact nature of the protocol. For the current study, the analysis order was slice time correction, realignment, normalization and finally smoothing. A brief explanation of each stage is presented below.

### 5.2.1 Slice Time correction

Functional images of the brain are collected in slices. However, the slices are collected sequentially rather than simultaneously. This can result in differences of up to a few seconds in acquisition times between slices, with the sensitivity of the data to these differences being dependent upon the exact order that the slices are acquired in and the type of fMRI protocol – event-related designs being more sensitive than block designs. In the present study slices are collected in an interleaved fashion such that initially slices with an odd number (1, 3, 5 ...) are collected, followed by slices with an even number (2, 4, 6 ...).

Because the SPM model examining the correlation between voxel signal intensity changes and stimulus time course assumes all slices are acquired simultaneously, a correction process is required. Two such methods are the Fourier shift procedure, where each voxel's intensity is time shifted to match the reference slice, or the interpolation method which uses a linear, sinc or spline function to correct for the slice-time differences – sinc interpolation is used in SPM [110]. Following correction, SPM creates another version of functional data file which has the same name but with a prefix 'a' added to signify the slice timing process has been undertaken.

### 5.2.2 Realignment

The movement of the subject's head during the functional scan is a significant problem, as the fMRI analysis procedure requires assessing the time course of signal change on a voxel by voxel basis. It is therefore necessary to correct for any movement such that the subject's head can be assumed to occupy the same spatial coordinate location throughout the experiment. This is done by assuming the movement does not change the shape and the size of the brain, allowing it to be treated as a rigid body. The position of any voxel in the brain can be identified by three coordinate values ( $x, y, z$ ) [111] with the movement of a rigid body characterized by six parameters – three translations along  $x, y, z$  and three rotations about  $x, y, z$ . The output of the realignment procedure from SPM is a set of image files with the prefix 'r'. In the present study the translational movements along the  $x, y$ , or  $z$  directions were always less than 3 mm and the rotations about the  $x, y$ , or  $z$  axes were always less than 1.5 degrees.

### 5.2.3 Normalization

There is a huge variation in the shape and the size of the brain across individuals. These differences would lead to a mismatching of active regions between individuals for any kind of group analysis if such variations were ignored. Therefore, in advance of group analysis it is necessary to register each individual's functional images to a standard brain template via a procedure known as spatial normalization. The most commonly used brain template was created by the Montreal Neurological Institute (MNI). In order to identify different brain regions, a number of atlases have been created based on specific anatomical landmarks [112, 113]. The Talairach Atlas was created by Jean Talairach in 1967 and further developed in 1988 by Talairach and Tournoux.

Two stages are used by SPM to transform MRI images to the MNI template – linear transformation (affine transformation) and non-linear transformation. In the linear step SPM uses 12 parameters to correct the differences in head shape and position between functional images and the template. The subsequent non-linear transformation is more flexible in the registration of images than the affine transformation, resulting in more accurate corrections for smaller-scale anatomical differences. Following normalization SPM creates images files with a prefix ‘w’.

### 5.2.3.1 The Talairach Atlas

The coordinate system of the Talairach atlas is defined by a specific set of anatomical landmarks located within the brain. These landmarks comprise the anterior commissure (AC), posterior commissure (PC), the midline sagittal plane and the exterior boundaries of the brain at each edge (figure 5.1). The line that passes through the AC point and orthogonal to the AC-PC line is defined as the  $x$ -axis; the line connecting the most superior part of the AC and the most inferior part of the PC is defined as the  $y$ -axis, while the  $z$ -axis is the line that passes through the interhemispheric fissure and the AC [114, 115]. The Talairach atlas has been widely used for fMRI analysis but, as it is based on the anatomy of the brain of a single 60-year-old woman, it has faced criticism for not representing average neuroanatomy.

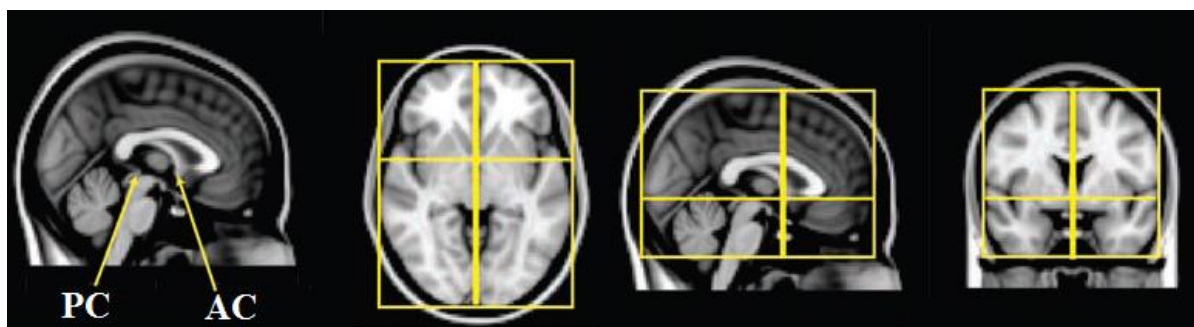


Fig. 5.1: The anatomical landmarks used to define Talairach space [116].

### 5.2.3.2 The MNI template

The MNI template is the brain template that is most widely used for spatial normalization. It was created at the Montreal Neurological Institute. Their first template,

MNI305, was constructed by aligning 305 separate brains manually to the Talairach brain; the second MNI template, MNI105, was based on 152 brains that were registered to MNI305. There is some discrepancy between the Talairach atlas and the MNI templates due to the MNI brain being larger than the Talairach brain by about 10 mm and due to a significant difference in the shape of the two brains.

There are two ways to convert MNI to Talairach coordinates [117].

The first method is to use the affine transform:

$$\hat{X} = 0.88X - 0.8$$

$$\hat{Y} = 0.97Y - 3.32$$

$$\hat{Z} = 0.05Y + 0.88Z - 0.44$$

where  $\hat{X}$ ,  $\hat{Y}$  and  $\hat{Z}$  are the coordinates in the MNI template;  $X$ ,  $Y$  and  $Z$  are the coordinates in the Talairach atlas.

The second approach is to use the non-linear transform as follows [118]:

Superior to the AC ( $Z \geq 0$ )  $\hat{X} = 0.9900X$

$$\hat{Y} = 0.9688Y + 0.0460Z$$

$$\hat{Z} = -0.0485Y + 0.9189Z$$

Inferior to the AC ( $Z < 0$ )  $\hat{X} = 0.9900X$

$$\hat{Y} = 0.9688Y + 0.0420Z$$

$$\hat{Z} = -0.0485Y + 0.8390Z$$

For both fMRI experiments in the present study, the coordinates of activated brain areas are specified using the MNI templates – Talairach co-ordinates are not explicitly stated.

## 5.2.4 Smoothing

Smoothing is carried out in order to minimize the noise in fMRI data and so increase the signal-to-noise ratio (SNR). Smoothing involves the convolution of the three-dimensional image with a three-dimensional Gaussian filter (Gaussian kernel) often described by the full width of the kernel at half its maximum height (FWHM) [119]. The smoothing acts to blur the functional images leading to the signal intensity of a voxel being given by the initial intensity of the voxel and those surrounding, weighted by the Gaussian. Smoothing reduces the spatial resolution of the data and extends the extent of activated volumes [116]. It can be advantageous for group analysis because the spatial blurring reduces individual anatomical differences. Following smoothing SPM creates image files with a prefix 's'.

## 5.3 The statistical Model

After the completion of pre-processing, the next step is to design the model that is used to assess how the data responds to an external stimulus. The General Linear Model (GLM) is the tool used to examine the changes in signal intensity resulting from the BOLD effect in every voxel within the brain. During functional imaging, each voxel is scanned repeatedly during the time course of the experiment. The GLM treats each voxel signal as a linear combination of individual signals plus noise and is written as [120]:

$$y_n = x_{n1}\beta_1 + x_{n2}\beta_2 + \dots + x_{np}\beta_p + \varepsilon_n \dots \dots \dots 5.1$$

where  $y_n$  is the measure of the MR signal (BOLD signal) of a voxel;  $x_{n1 \rightarrow np}$  are the explanatory variables (predictor variables) which are related to the conditions of the experiment;  $\beta_{n \rightarrow p}$  are the contributory amplitudes of the explanatory variables in the MR signal and  $\varepsilon_n$  is the error term.

Most fMRI experiments repeat the signal collection from each voxel many times, so therefore, equation 4.1 can be rewritten as:

$$Y = X\beta + \varepsilon \dots \dots \dots 5.2$$

where  $Y$  is a matrix with  $n$  rows and one column displaying the times series of fMRI measurements;  $X$  is the so called 'design matrix' with  $n$  rows and  $p$  columns;  $\beta$  is the  $p \times 1$  vector of unknown amplitude contributions of the explanatory variables;  $\varepsilon$  is a matrix of  $n$  rows and one column.

As most fMRI experiments have multiple subjects the analysis is run in stages; the first stage (first level or fixed effect) contains the analysis of the data for each individual subject. The objective in the first level is to measure the value of  $\beta$ , i.e., how much each predictor variable contributes to the observed MR signal. This is achieved by fitting the model (GLM) independently to the signal time course of each voxel and using ordinary least squares (OLS) minimisation to estimate the value  $\beta$  [121]:

$$\hat{\beta} = (X^T X)^{-1} X^T Y \dots\dots\dots 5.3$$

where  $\hat{\beta}$  is the estimated value or the maximum likelihood of  $\beta$ ; the superscript  $T$  indicates the transposed matrix of  $X$ .

After determining the amplitude or weight of each of the explanatory variables in the MR measurement, contrasts are run in SPM using  $t$ -tests or  $F$ -tests between the conditions of the experiment to determine whether the individual  $\beta$  values are statistically significant.

Both types of test examine the null hypothesis and assess whether the data from each voxel show a statistically significant activation during the different conditions of the experiment. The  $t$ -test (Student  $t$ -test) examines the direction of any signal changes, i.e., whether there is an increase or decrease associated with an experimental condition compared with baseline, while the  $F$ -test assesses the total effect of the condition on the MR signal of each voxel relative to baseline, irrespective of the direction of signal change.

The probability level ( $p$  value), expressing the statistical significance of any correspondence between signal intensity variation and experimental protocol, can be expressed as either uncorrected or corrected [corrected for family wise error (FWE)]. The default uncorrected threshold in SPM8 is 0.001 which means, with a brain volume typically consisting of about 100,000 voxels, 100 false-positive voxels would be anticipated. Alternatively, Bonferroni procedures with Gaussian Random Fields (GRF) theory can be used to calculate the corrected value of  $p$  (FWE) with a default value of 0.05. Additionally, cluster criteria can be applied that stipulate an individual voxel cannot be defined as activated unless it has a specified number of neighbours that also fulfil the  $p$ -value threshold.

As the aim of the majority of fMRI studies is to examine stimulus effects across individuals so as to make predictions about a wider population, first level or fixed effect analysis is followed by second level analysis looking at population statistics. SPM has the capability to do this, again testing the null hypothesis by using the  $t$ -test or  $F$ -test.

## 5.4 Parametric Modulation

The results that came from the analysis of functional MR imaging show the relationship between the stimulus and neural activity; this is the main aim in most fMRI studies, but the correlation between the study parameters (the stimulation types) and the fMRI signal can reveal more information about this relationship. The GLM (equations 4.1 and 4.2) is the model that is used to describe the change in the BOLD signal in the brain due to performing the task, where the contrast of the  $t$ -test or  $F$ -test after fitting the model represents the zero-order term of the relationship between the BOLD signal and the stimulation [122].

A polynomial expansion can be used to characterize the higher order terms of this relation, which includes the first order, the second order and so on. The polynomial expansion is an extension of the GLM [122, 123] where:

$$p(x) = p_1x^n + p_2x^{n-1} + \dots + p_nx + p_{n+1}, \dots \quad 5.4$$

where  $p(x)$  have the same meaning as  $y_n$ ;  $p_{1 \rightarrow n+1}$  as  $x_{n1 \rightarrow np}$  and  $x^n$  as  $\beta_{n \rightarrow p}$ .

Just as the design matrix  $X$  in the GLM contains one column for each explanatory variable, the design matrix in the polynomial expansion includes several columns, one for each order of each explanatory variable.

After building the design matrix for the polynomial expansion, the null hypothesis is tested to see those voxels that correlate with the different order terms in the model of the stimulation.

## 5.5 Further Details of Data Processing in the Present Study

The data from the first fMRI study (chapter 8), and from the first part of the second fMRI study (chapter 9), were analysed in the same way, using a linear model. Before starting the analyses the raw fMRI data were converted to Analyse format using MRICro software. This was followed by slice-time correction, realignment, normalization and smoothing, as described above. In the slice-time correction the image slices in each volume were registered to slice number 20; realignment was to a T1-weighted structural image (taken for each participant); parameters obtained for normalization of the T1-weighted structural image to an MNI template were then used to normalize the fMRI data set; smoothing involved a Gaussian kernel with FWHM of  $8 \times 8 \times 8$  mm for single-subject analyses and for group analyses.

Additionally, to remove any drift of signal baseline, a high-pass filter at 128 seconds period was applied to the data.

The first-level analyses were run by convolving the haemodynamic response function with boxcar functions based on the timings for the various experimental conditions; see 8.4 for more details of the first fMRI experiment and 9.3 for more details of the first part of the second fMRI experiment. Section 9.3 also includes analysis using a non-linear (quadratic) model).

## 5.6 Summary

Chapter four has outlined the processing and analysis steps for the functional MRI data and the model used to obtain the results. This chapter has also described the steps (slice-time correction, realignment, normalization and smoothing) that are applied to the fMRI data before using the model to determine the active areas in the brain. Modelling of a non-linear relation between stimulus magnitude and brain activation is described towards the end of the chapter.



## **Chapter six**

# The Tactile Display System

## 6.1 Overview

The main focus of this study is the development and validation of a novel tactile display system for use in fMRI. There is a need for new tactile displays – the study of touch and tactile receptors is less well developed than the study of vision or hearing; it has been held back by the insufficiency of tactile stimulators which can provide a wide range of controlled touch stimuli. Although the design of tactile displays began in the mid-1950s, their development is still ongoing [124]. According to the type of the mechanism which is used to stimulate the skin, two kinds of tactile display are found: vibrotactile and electrotactile. Among the vibrotactile class are displays that use pneumatic, electromagnetic or piezoelectric mechanisms [54, 56, 125] to apply mechanical stimuli to the skin, while electrotactile displays stimulate the nerves in the skin by applying a current (1–10 mA) via electrodes [126, 127]. Electrotactile displays have low cost and low power consumption but the unnatural sensation that they produce is unpleasant for some people. Vibrotactile displays can produce a more natural sensation over a wide range of amplitude and frequency, and so is a better choice for experiments using brain mapping techniques (fMRI, EEG, MEG) to study the processing of tactile sensation. The tactile display that has been built for the present study is a vibrotactile device with piezoelectric drive mechanisms. The different parts of the system – the display, the drive electronics (sine wave oscillator and amplifiers) and associated hardware/software – are described below.

## 6.2 The Tactile Stimulator

Before the details of the vibrotactile stimulator, below is a brief description of the piezoelectric effect.

### 6.2.1 The Piezoelectric Effect

The piezoelectric effect was discovered in 1880 by two French mineralogists René and Antoine. The piezoelectric effect occurs when non-conductive materials generate a voltage when exposed to mechanical stress. This effect is reversible which means that applying a voltage to the piezoelectric materials will change the shape of these materials by a small amount. This property makes it possible to use this type of material to build tactile actuators. The value of the displacement output depends on the piezoelectric constant of the material and on the applied voltage.

For a material with piezoelectric constant  $D$ , the mechanical stress  $S$  produced by an applied electric field  $E$  is:

$$S = D \times E \dots\dots\dots 6.1$$

Piezoelectric materials can be divided in two main groups: crystals and ceramics. Piezoceramics are easily available with a range of properties for different applications. The limitation of using piezoelectric drive for tactile actuators is that the piezoelectric effect is weak, i.e., the piezoelectric constant  $D$  is small, so a high drive voltage (high electric field) is required to produce a strong sensation.

Different shapes of piezoceramic material are available – the piezoelectric bimorph is one of them, designed with a geometry that “amplifies” the displacement output. The bimorph consists of two slabs of piezoceramic material placed on either side of a plate conductor. The polarities of the piezoceramic slabs are either in the same direction (parallel poled) or in the opposite direction [128, 129]. The piezoelectric bimorphs used in present study were parallel poled, with the two slabs of piezoceramic material placed on either side of a thin conducting plate; the drive voltage was applied in one sense to the first piezoelectric slab and in the other sense to the second, causing one side of the bimorph to contract and the other side to expand, producing an overall curvature of the structure.

### 6.2.2 The Tactile Array

Tactile simulators using a piezoelectric drive mechanism can have a wide variety of structures, from a single wafer of piezoceramic [53] to a complex structure a bimorphs arranged in an array of one or two dimensions [130].

The vibrotactile display used for the present study is based on a device (Figure 6.1) developed at Exeter for incorporation into a haptic interface [131] to deliver virtual touch sensations in the context of active exploration of a virtual environment. (The present study involves only passive stimulation.) The stimulator has 25 contactors arranged in a  $5 \times 5$  array (2 mm spacing) covering an area of  $1 \text{ cm}^2$  on the fingertip. Each of the 25 contactors is made from brass wire with diameter 0.6 mm, and driven by a piezoelectric bimorph which gives a working bandwidth of 25-200 Hz. The bimorph actuators are made from PZT-5H (lead zirconate titanate), made by APC International (American Piezo Company). At the start of this project, five of these devices were available in various states of repair – all five were reconditioned and tested. (Two complete display/hardware/software systems were eventually

built – one of these was evaluated in an fMRI context and the other will be made available for use in other laboratories.) For use in the MRI scanner the tactile array is placed inside a perspex box with dimensions 270 mm in length, 190 mm in width and 74 mm in height, see figure 6.2.

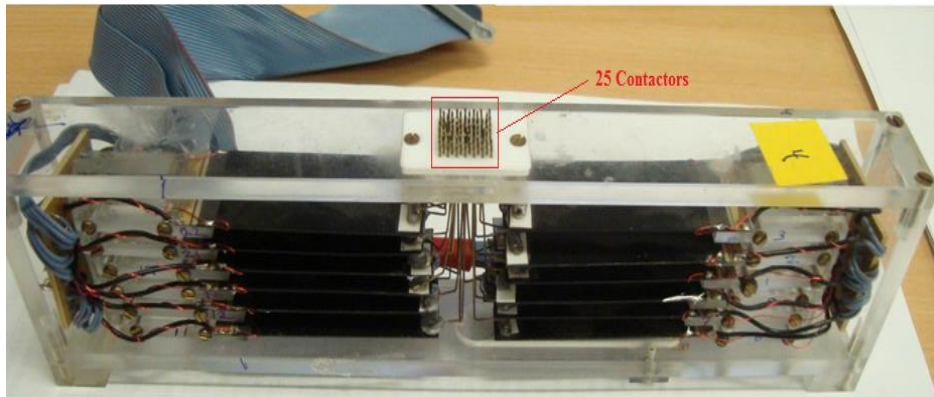


Fig. 6.1: The tactile simulator (the 25 contactors are shown in the red square).

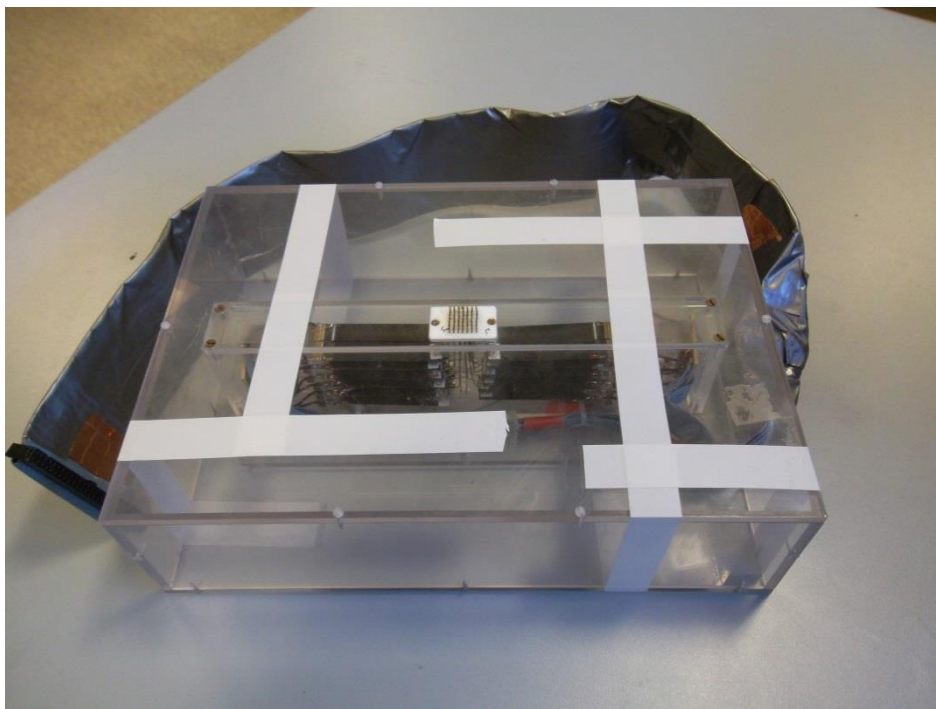


Fig. 6.2: The tactile array inside the perspex box.

## 6.3 The Drive Electronics

In principle, the tactile array can be driven with sine-waves or mixtures of sine-waves with variable amplitude and frequency, or with broadband signals of arbitrary waveform. For the present study, the decision was made to drive the 25 channels of the tactile array with sine-waves of fixed (preset) amplitude and frequency, switching the individual channels “on” and “off” to producing different spatial distributions of stimulation on the fingertip. This has the advantage that stimulation patterns are specified simply by 25 binary bits (“0” or “1”). A sine-wave oscillator was built to drive the actuators of the vibrotactile display, which require drive frequencies in the range 25 to 200 Hz. The oscillator circuit is composed of two parts, an amplifier and a feedback circuit (figure 6.3).

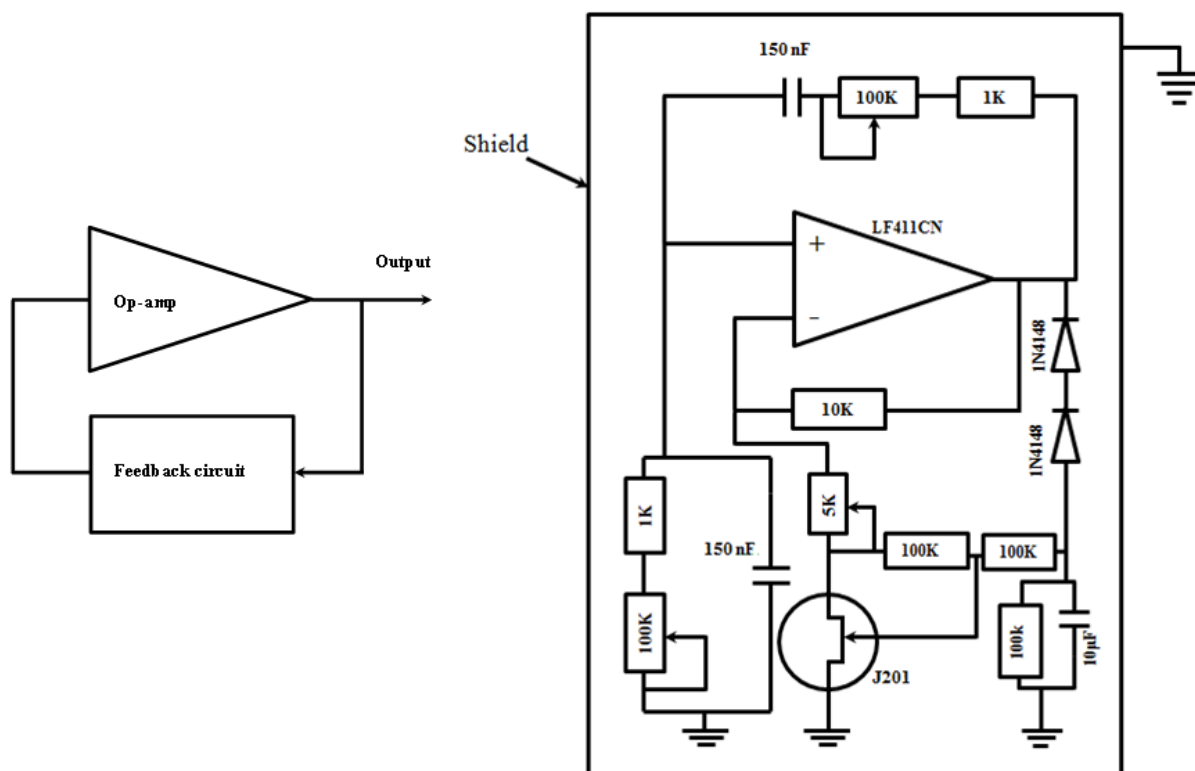


Fig. 6.3: (Left) the principle of the oscillator and (right) the full circuit diagram.

The sine-wave oscillator is of the Wien bridge type, in which the feedback is provided by a network with two equal resistors  $R$  and two equal capacitors  $C$ . In this case  $R$  is variable (1 to 101 k $\Omega$ ) and  $C$  is 100 nF (see figure 6.3). The gain of the amplifier, based on a type 411 operational amplifier, is controlled by a type J201 transistor (FET) which sets the output amplitude.

The feedback circuit works to control the oscillation frequency; the required condition to make the Wien bridge circuit oscillate is that the RC network should produce zero phase shift [132, 133]. This occurs at a frequency (see Appendix A) given by:

$$\omega = \frac{1}{RC} \quad \text{or} \quad f = \frac{1}{2\pi RC} \dots\dots\dots 6.5$$

The oscillator output was measured to be in the range 25 Hz to 2 kHz. The output amplitude was set at 4.3 V peak-to-peak. Figure 6.4 shows the waveform for two frequencies. As the amplitude of the sine-wave output is not enough to drive the piezoelectric bimorph actuators, an amplifier circuit was built to increase the amplitude of the sine-wave, based on a high-voltage operational amplifier, type OPA551PA (figure 6.5). The tactile stimulator has 25 actuators, requiring five amplifier circuits – each one driving five actuators. The circuit runs from a  $\pm 25$  V power supply. The sine-wave is fed from the oscillator to the drive amplifiers via an overall amplitude control.

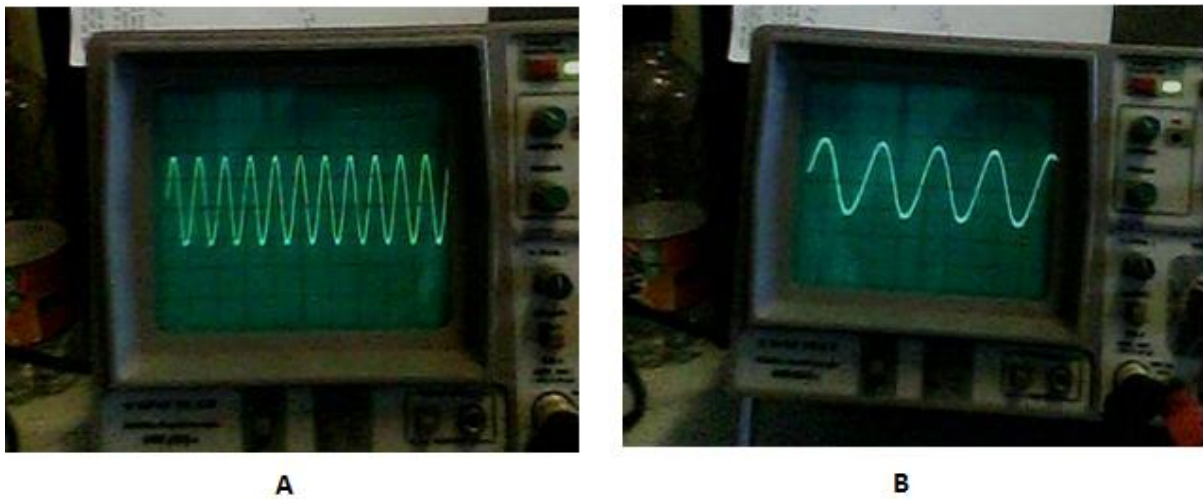


Fig. 6.4: The sinusoidal output waveform for two frequencies. A (1061 Hz) and B (15 Hz).

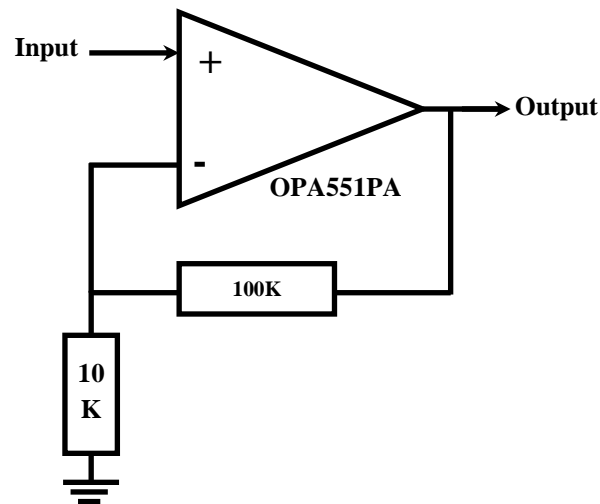


Fig. 6.5: Diagram of the amplifier circuit which drives the piezoelectric bimorph actuators.

## 6.4 The Control System

Most computer-controlled devices these days are run using the Universal Serial Bus (USB) port. The control system for the tactile display is built around a USB card, allowing it to be connected to a PC with any operating system. The control system must switch the drive signals to the 25 actuators separately (on or off), leading to the choice of a card with more than digital 25 outputs. The control system has two parts: the hardware part and the software part; below is a description of both of these parts.

The original intention was to run software to control the stimuli on a PC, and use the USB card to transfer the 25-bit control data to the drive electronics. However, in practice this strategy was simplified by running the control software on the USB card, so that the PC has no significant involvement when running experiments.

### 6.4.1 The Hardware

The hardware part consists of a USB card type UBW32 (figure 6.6), supplied by SparkFun Electronics, which is a small board that can be plugged into a computer (running Windows, MacOS or Linux) via USB. The UBW32 is based around the PIC32MX795 32-bit

CPU from Microchip, and includes all of the external circuitry needed to run this PIC device. Power can be provided over USB or from an external source. The UBW32 has 32 kBytes of RAM and 512 kBytes of Flash memory. It has 78 input/output pins and the CPU runs at 80MHz.



Fig. 6.6: The UBW32 card.

Twenty-five outputs of the UBW32 card are used to control a connection circuit (figure 6.7) which provides 25 digitally controlled links between the drive amplifiers and the actuators. This circuit also works to protect the UBW32 card from the high voltages coming from the drive amplifiers. The main part of this circuit is a set of 25 optically isolated voltage-controlled switches, type AQY210EH; there are also 25 LEDs to indicate which channels are active and so what pattern the tactile display produces. All the electronic components of the tactile system are shown in figure 6.8. In use for an fMRI experiment, the tactile display and the control electronics are placed in separate rooms (the MRI control room and the MRI scanner room) and connected by a 7-metre 25-channel cable. The optical isolation provided by the connection circuit prevents digital noise from the USB card and the control PC from entering the MRI scanner room. The electronic circuit box and the cable are covered by copper sheet and grounded to earth, see figure 6.9.



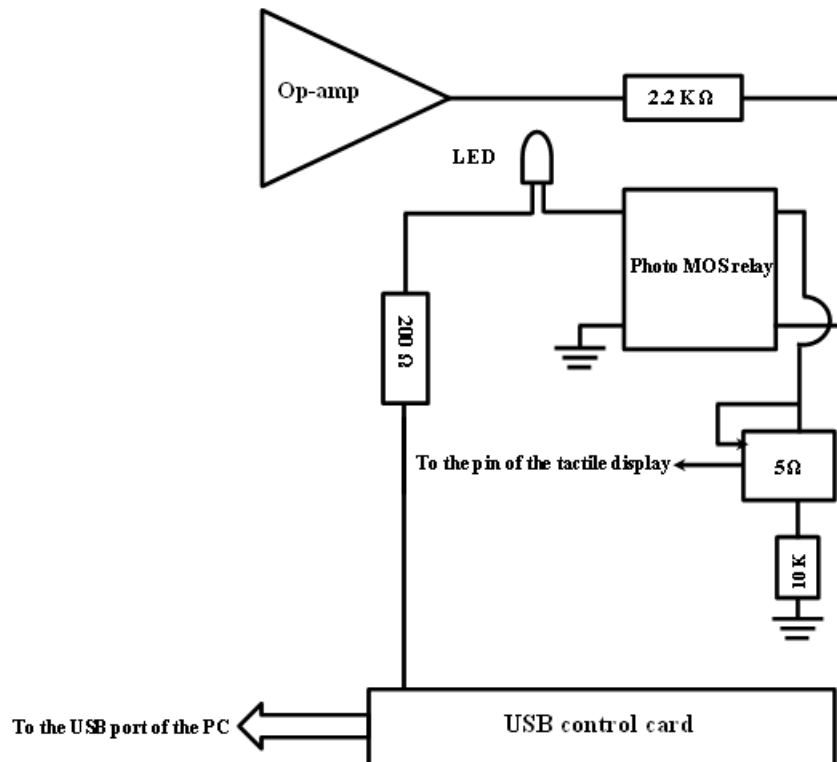


Fig. 6.7: The connection circuit (one of the 25 channels); the two earths are separate.

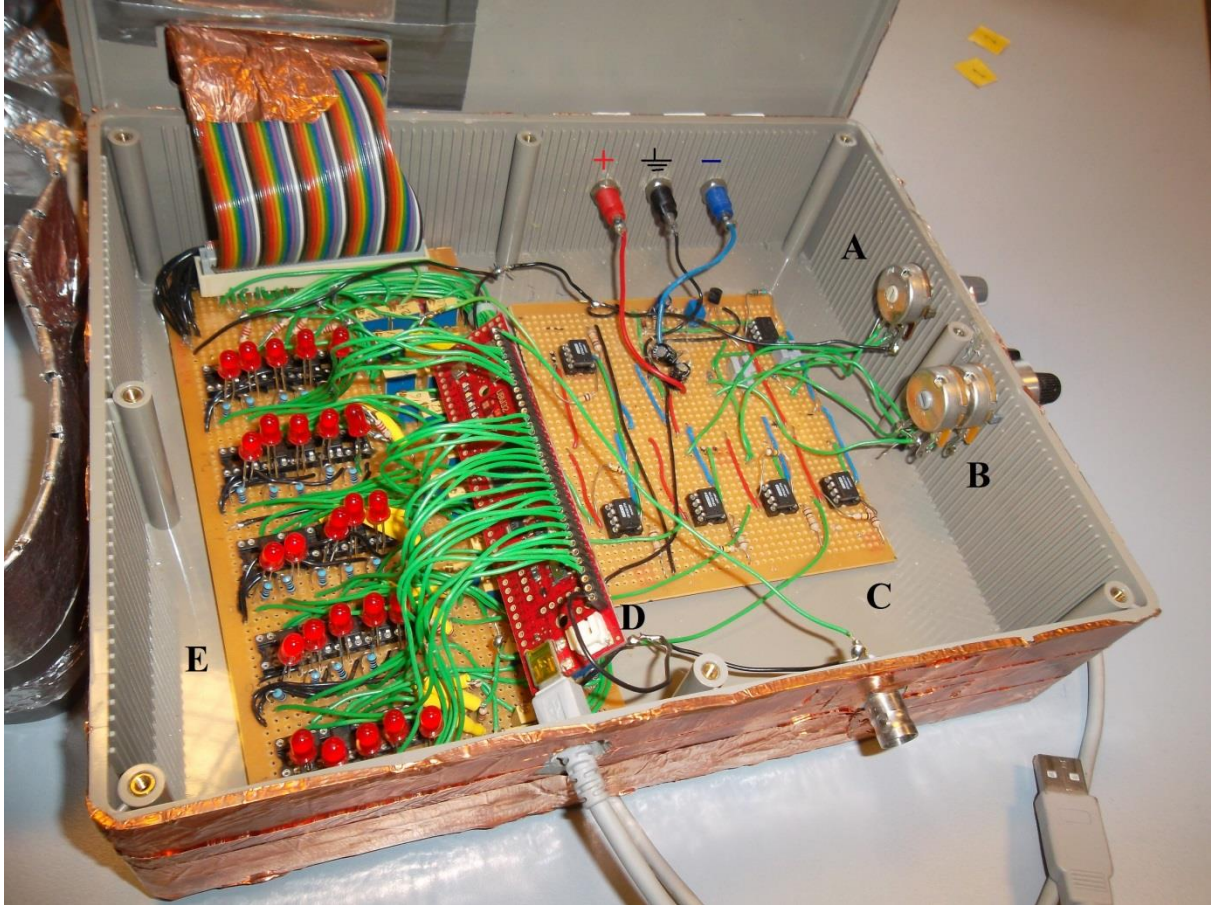


Fig. 6.8: The tactile system without the tactile array. (A) Amplitude control; (B) Frequency control; (C) The oscillator and the amplifiers; (D) The UBW32 card; (E) The connection circuit which connects the amplifier outputs to the tactile array.

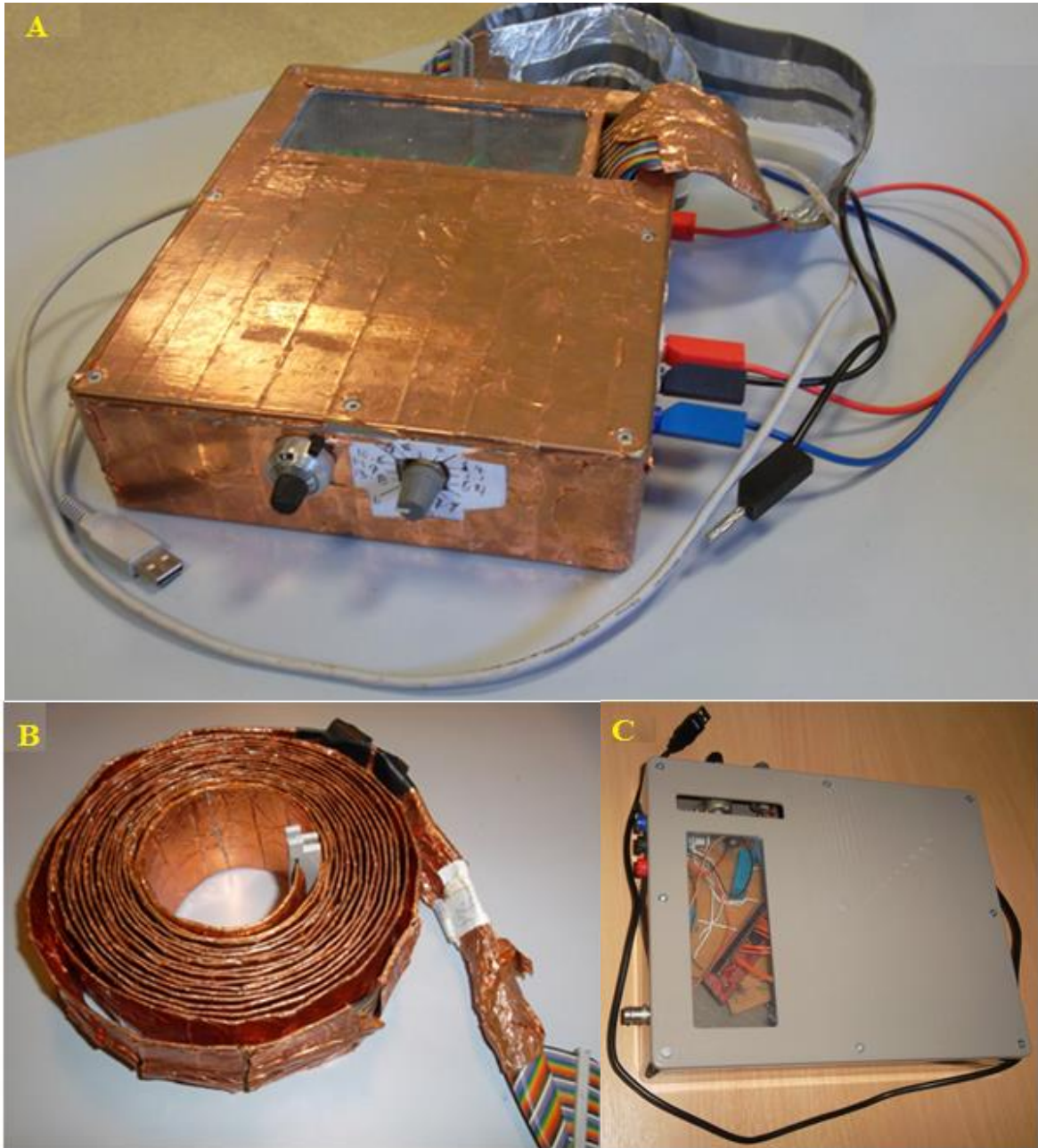


Fig. 6.9: (A) The complete tactile system; (B) the 25-channel cable to connect between the tactile array and the control system; (C) the second control system built in the present study.

## 6.4.2 The Software

The second part of the control system is the software program. The UBW32 can be programmed using StickOS™ BASIC, which provides a programming environment that includes an easy-to-use editor, transparent line-by-line compiler, interactive debugger, performance profiler, and flash file system, all running entirely within the microcontroller on the card, and controlled through an interactive command-line user interface.

The program runs entirely on the UBW32 card. It outputs a series of “frames” – spatial patterns of vibration of specified duration. During the development of the software, many programs were written to check the control of the card outputs and the timing of program steps. The flow chart in figure 6.10 shows the final program. The first step is to declare the 25 digital outputs of the USB control board. After setting the time of the stimulation the program will activate the contactors in the tactile display on the basis of the data that has been loaded. The data is in binary form: twenty-five 0s or 1s to represent each “frame” – a “one” allows the drive signal (voltage sine-wave) to reach a particular contactor; a “zero” blocks the drive signal.

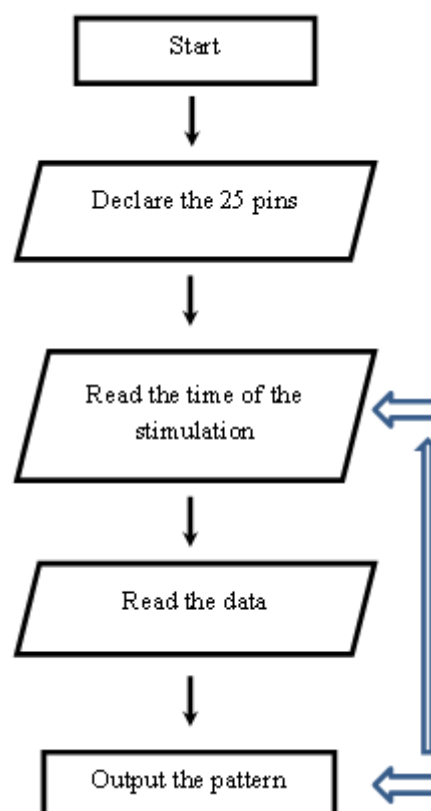


Fig. 6.10: The flow chart of the software program.

The binary number system is used to write the data which specifies the tactile patterns an alternative is to use the hexadecimal system, but this takes up more memory on card and limits the number of patterns that can be stored.

In the fMRI experiments in the present study, sequences of frames were designed to create a point of tactile stimulation which traces out a trajectory, e.g., a circle, on the fingertip. A full listing of the software is given in appendices B and C, (All programs used in the present study – for the various experiments, and also for numerous preparatory studies – were entirely written by the author

## 6.5 Summary

Chapter five has covered the various stages of designing and building the tactile system. These stages were: repairing the existing tactile arrays, constructing the drive electronics, and constructing the control system (hardware and software). Many versions of the control software were developed; the software used for the main experiments in the present study is given in appendices B and C.

## **Chapter seven**

# Preliminary experiments with the tactile display

## 7.1 Introduction

To make sure that the system worked well and could produce many different patterns of tactile sensation, numerous informal experiments were carried out. These were followed by further investigations to evaluate the display: (a) a psychophysics experiment to test the tactile display with subjects in a non-fMRI context, described in sections 6.2 to 6.5; (b) an investigation of the image artefacts produced by running the display in the MRI scanner, described in section 6.6.

## 7.2 Design of the Psychophysics Experiment

Although there have been many previous psychophysics experiments on tactile perception, these have been limited by the availability of suitable tactile stimulators. Many experiments remain to be done, and the tactile display developed in the present study has possibilities for various novel experiments on touch perception.

To take advantage of the capability of the system to produce different types of tactile patterns on the fingertip, and to investigate the ability of the subject to discriminate different patterns (trajectories) produced by the array, three contrasting classes of stimuli were designed (see figure 7.2) for use in an identification task. All stimuli involve a localised sensation on the fingertip, produced by vibration of a pair of adjacent contactors from the set of 25, with a particular stimulus specified in terms of a particular sequence of contactor pairs. For “circle” stimuli the contactor pair moves stepwise along an approximately circular trajectory, and the localised sensation appears to trace out a clockwise circle on the fingertip; for “random” stimuli the contactor pair moves randomly about the array, and the localised sensation appears to trace out a path with no obvious shape; for “stationary” stimuli the contactor pair alternates between the diagonals of a  $2 \times 2$  square, and the localised sensation appears to have no movement over the fingertip.

An informal experiment was run to establish the best way to produce the sensation of movement. Three alternatives were compared, using a circular trajectory: in the first, the trajectory was traced out by activation of a single pin from the 25 pins of the tactile array; in the second, the trajectory was traced out by adjacent pairs of pins; in the third, by four adjacent pins, see figure 7.1 and 7.2 (a). Each of the trajectories was formed from 12 frames, with frame duration of 83 ms (rotation rate of one cycle per second). The participants (three participants, each presented several times with the stimuli) were asked to specify which of the three alternatives gave the best representation of a circle – it was found to be the “two pin”

presentation. Consequently, this presentation was chosen for “circle” stimuli in subsequent experiments; it was also used to present “random” and “stationary” stimuli.

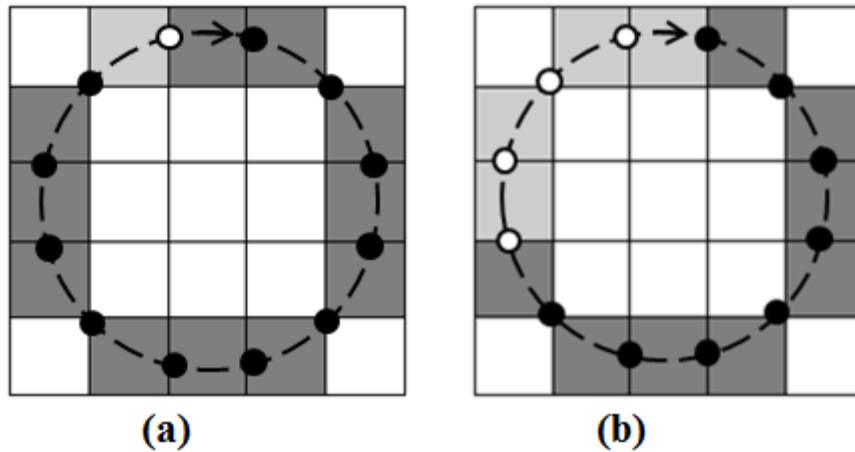


Fig. 7.1 Methods used to present a “circle” trajectory: (a) one pin, (b) four pins. A single frame is shown in light gray shading.

The “circle” stimuli have four possible starting points and each time frame has duration 83 ms, resulting in 9 rotations within the overall stimulus time of 9.0 s. The “random” stimuli also have four possible starting points and each time frame has duration 83 ms, with a random sequence of 36 stimulus locations repeated three times within the overall stimulus time of 9.0 s. (Different starting points are used so that the test subject cannot identify the type of stimulation from the starting point.) The “stationary” stimuli have 6 possible locations and each time frame has duration 215 ms, resulting in sufficient modulation of the stimulus to minimise adaptation. (Adaptation causes the subjective sensation from a single “still” frame to die away during the overall stimulus time of 9.0 s, as the perceptual system starts to ignore the steady sensation. Alternating between two frames – see figure 7.2(c) – means that the stimulus is not steady and so the subjective sensation is sustained.) For all stimuli, the frequency of vibratory stimulation was 40 Hz, as suggested by Carr [134] and the vibration amplitude was set to provide a comfortable sensation level. The pins were driven in phase – this may have helped the individual point stimuli to be perceived as a coherent whole, although there is little in the literature to suggest that relative phase is important in this context.



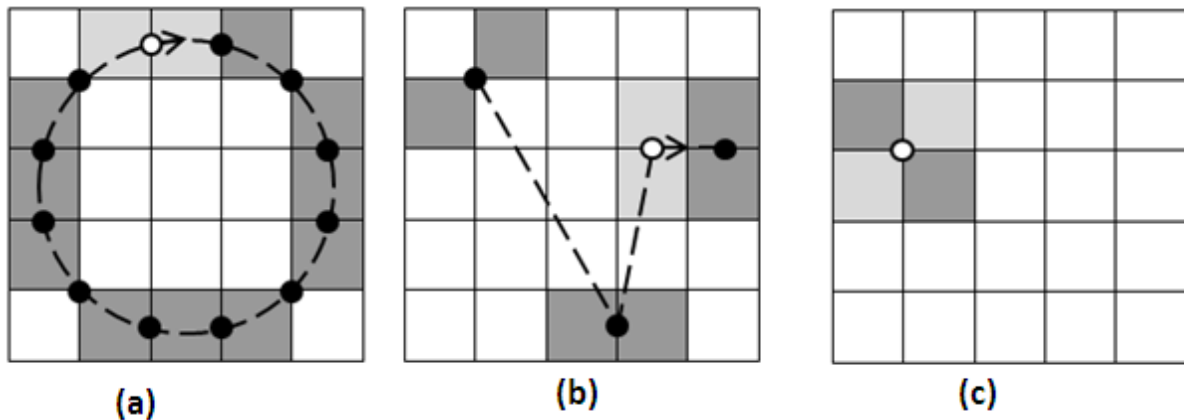


Fig. 7.2: The three stimulus types as a sequence of time frames (contactor pairs indicated by shaded squares; apparent stimulus location indicated by circular dots): (a) circle, (b) random – only part of the sequence is shown, (c) stationary. In each case a particular time frame is highlighted using light gray shading for the contactor pair and a white dot for the apparent stimulus location.

The sequence for the experiment (figure 7.3) is determined by software on the UBW32 card (see appendix B for a software listing). It runs as follows: the stimulus cycle starts with a trigger pulse that is sent by a function generator (Feedback type FG600); after the card has received the trigger pulse there is a period of rest with variable duration (0 to 6 seconds), after that 9 seconds of stimulation, then another variable period of no stimulation (rest) of duration 21 to 27 seconds until the next trigger pulse starts the next cycle (one pulse every 36 s). The advantage of the variable timing between stimulus cycles is to make the incidence of the stimulus unexpected. The participants are required to identify the type of stimulus, and give their answer in the rest period after the stimulation.

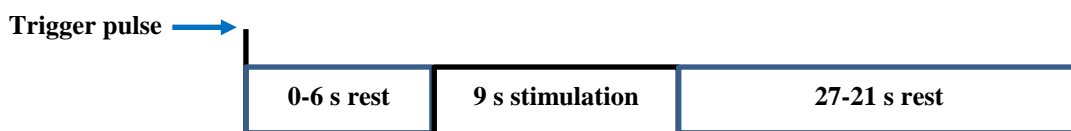


Fig. 7.3: The time sequence of the tactile experiment.

### 7.3 Procedure for the Psychophysics Experiment

Seven subjects took part in the study: details in Table 7.1. Each participant sat on a chair and was asked to gently rest the fingertip of the right index finger on the vibrating part of the tactile display and hold the response box with the left hand (see figure 7.4). They were given a short period (around 2 minutes) of familiarisation with the tactile array and demonstrations of the three types of stimuli. The intention was to provide sufficient preparation for subjects to undertake the task, rather than training to improve subjects' performance. The experiment involved identification of 27 stimuli in a single test run, with a rest period after each stimulus for subjects to respond via one of three push buttons which controlled three different-coloured LEDs; the researcher recorded the response of the participant according to the LED that lit up. Stimuli were presented in a random order: 9 "circle" (in 4 variations), 9 "random" (in 4 variations) and 9 "stationary" (in 6 variations).

Table 7.1: Details of the volunteers who participated in the tactile study.

No. Subject	age	Gender	Handedness
Sub 1	34	M	R
Sub 2	25	M	R
Sub 3	32	M	R
Sub 4	26	M	R
Sub 5	40	M	L
Sub 6	39	F	R
Sub 7	31	M	R

### 7.4 Results from the Psychophysics Experiment

Results from the seven subjects are shown in Figure 7.5. All subjects scored at above chance level (33%) for all stimulus types. Four subjects scored 100% for all stimulus types. The mean discrimination score was (82) %. Figure 7.6 shows a confusion matrix for subjects' responses and it is clear that errors are equally distributed between the stimulus types. The kappa statistic, indicating the degree to which subjects agreed when categorizing the stimuli [135], was 0.73.

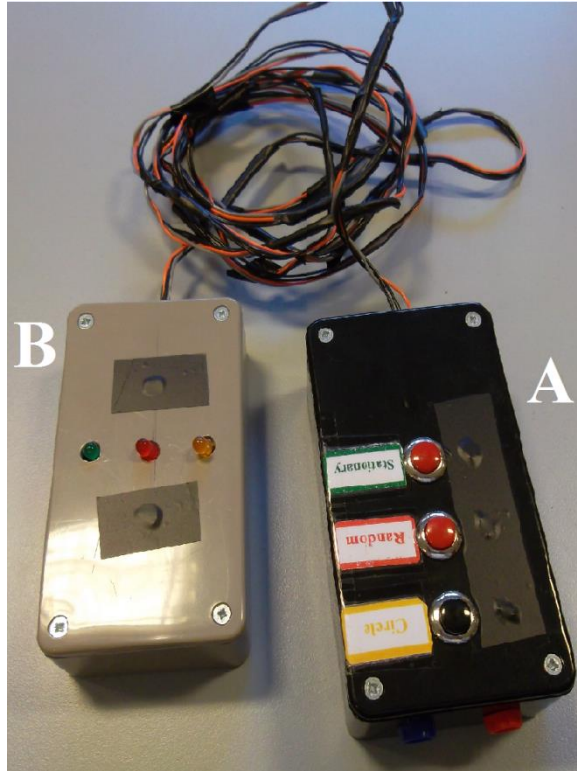


Fig. 7.4: The equipment used to record participants' responses; (A) button box; (B) LED box.

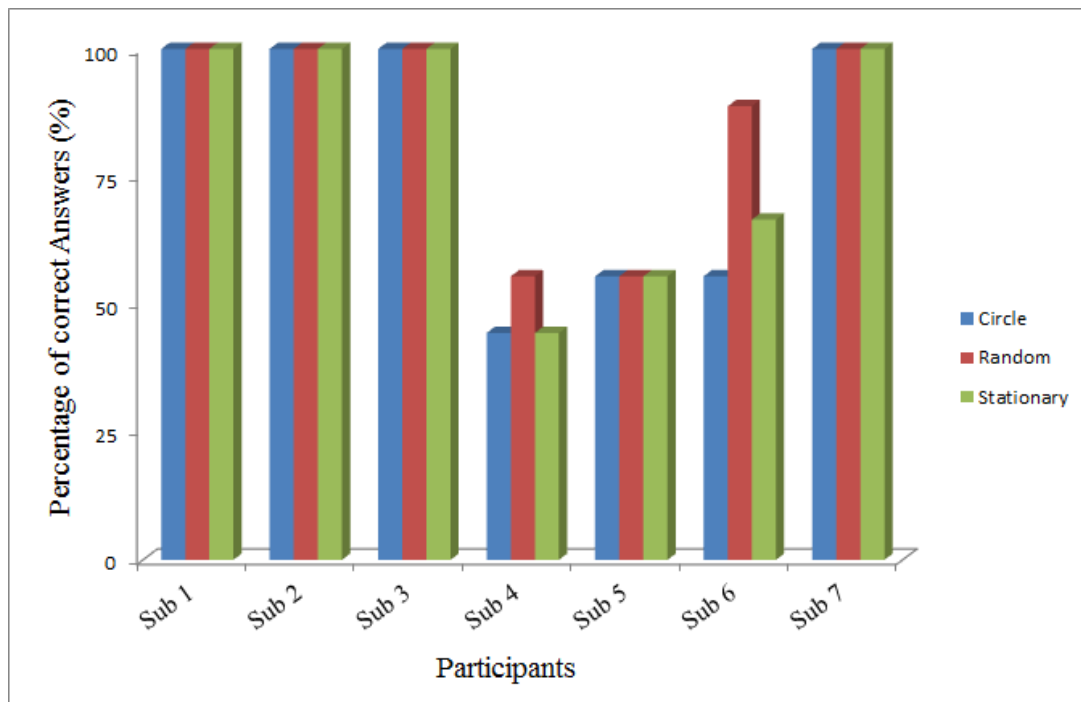


Fig.7.5: Percentage-correct answers for all seven subjects, arranged by stimulus type.

<b>Response</b> <b>Stimulation</b>	<b>Circle</b>	<b>Random</b>	<b>Stationary</b>
<b>Circle</b>	<b>50</b>	<b>6</b>	<b>7</b>
<b>Random</b>	<b>8</b>	<b>54</b>	<b>1</b>
<b>Stationary</b>	<b>6</b>	<b>6</b>	<b>51</b>

Fig.7.6: The confusion matrix for subjects' responses.

## 7.5 Discussion and Conclusion for the Psychophysics Experiment

Four of the seven subjects produced perfect identification scores, even with the limited familiarisation and demonstrated provided. A further one subject produced an average scores around 75% (i.e., well above chance) and it may be conjectured that subject might produce higher scores if given additional training. It is clear that a tactile display of this type has the capability of providing spatial information in a form that is easily assimilated, at least by some users. This experiment leads to an experiment (next chapter) which includes fMRI measurements of brain activation in subjects performing a similar identification task, with a view to identifying brain centres associated with the perception of tactile shape and movement. (In a different application, the results of this experiment suggest that a tactile display of this type can provide a useful enhancement to a haptic interface, providing the associated technical challenges can be overcome.)

## 7.6 Image Artefacts

The objective of this experiment is to clarify the tactile system does not produce noise or artefacts in the MR imaging that can affect the fMRI results, see 4.9 and 4.10 for more details about sources of noise and artefacts. Imaging is carried out on the 1.5 T Philips Inera MR imager at the Exeter MR Research Centre. The experiment runs using a fluid phantom of volume 3000 ml whose components (Table 7.2) are intended to reproduce the MR properties of human tissue.

Table 7.2: The components of the fluid phantom (per 1000 ml).

1000 ml demineralized water
770 mg $\text{CuSO}_4 \cdot 5\text{H}_2\text{O}$
2000 mg NaCl
0.15 ml $\text{H}_2\text{SO}_4$ (0.1M solution)
1 ml arquad (1% solution – to prevent growth of algae and bacteria)

The experiment runs in two sessions using the same imaging parameters; the scan in the first session is carried out using the phantom only while the second scan runs while the tactile display is installed in the scanner and working (producing the sequence of stimuli and rest periods described above).

The MR imaging uses gradient echo  $T_2^*$ -weighted EPI sequences with the following parameters: repetition time (TR) = 3 s, echo time (TE) = 45 ms, matrix size  $80 \times 80$ , field of view (FOV) =  $240 \times 117 \times 240$  mm, in-plane pixel size  $3 \times 3$  mm, flip angle  $90^\circ$ , slice thickness 3 mm (without gaps between the slices). These parameters are used for 100 dynamics in 39 slices. The scan time is 5.05 minutes.

A region of interest (ROI) of about  $6.9 \text{ cm}^2$  was analysed in the 39 slices in each of the two scans (see figure 6.7). Figure 6.8 shows the time variation of intensity (mean  $\pm$  SD) for the ROI in the 20<sup>th</sup> slice. The first 24 dynamics are shown, corresponding to the first 72 seconds of each scan. The difference between mean gray level in the “with” and “without” scans is not significant, and there is no sign in the “with” case that the images are affected by the 36-second operating cycle of the tactile display. There is some evidence that image non-uniformity (standard deviation (SD) of gray levels, shown by error bars in figure 7.7) is

slightly higher in the “with” case. No “ghosts” or other spatial artefacts could be associated with the stimulator (see figure 6.6) – it would have been possible to check for such localised artefacts using a comparison of corresponding line profiles in the two images, but this was not done due to the lack of evidence in the images.

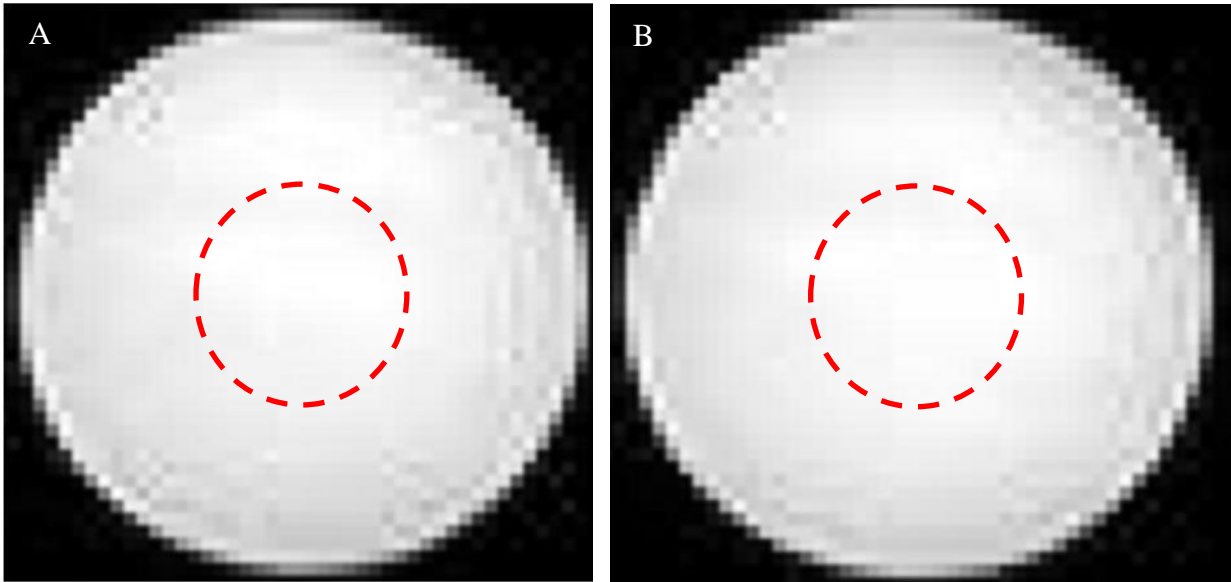


Fig. 7.7: The MR image of the phantom. Corresponding slices are shown for (A) when the tactile display is not present and (B) when the tactile display is present.

No artefact image features were observed in the “with” case, and we may conclude that the tactile display is suitable to use in fMRI experiments. With hindsight, it would have been useful to repeat this investigation when imaging a human subject; however, the phantom experiment described here, in which no artefacts were observed, involved the same imaging parameters (TE, TR and FOV) as those used in the subsequent fMRI experiments.

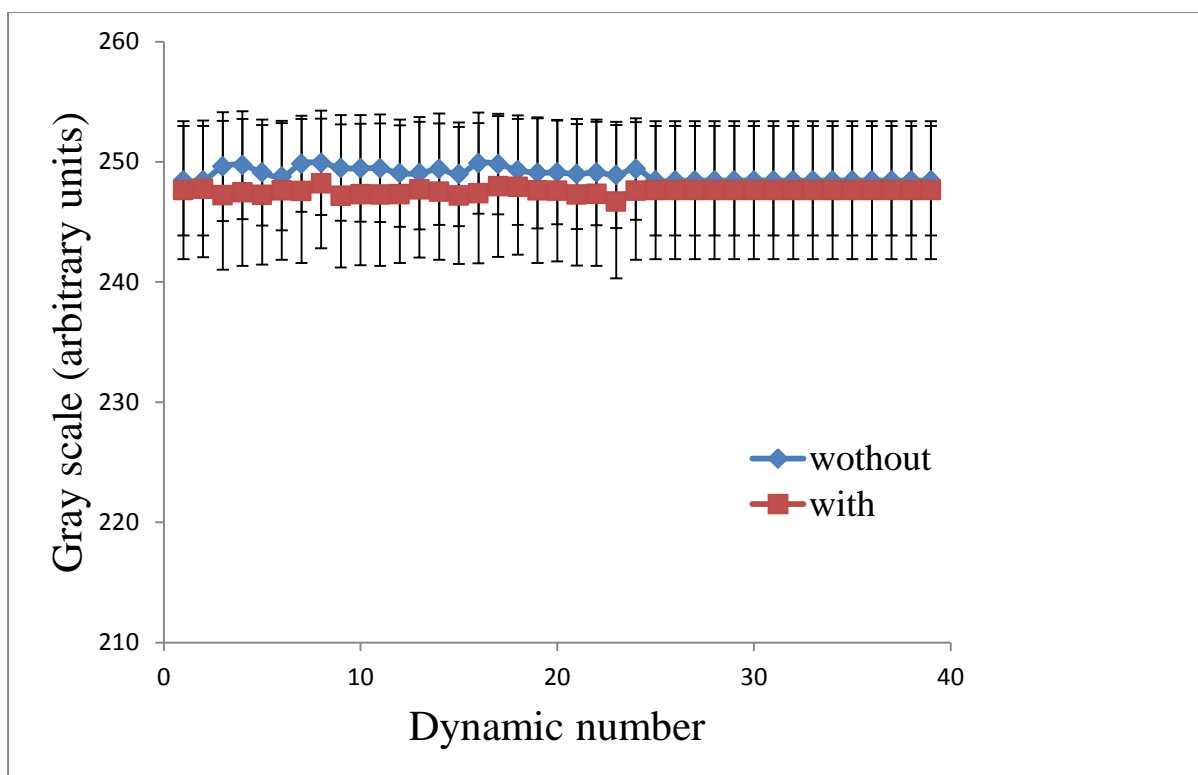


Fig.7.8: Time variation of intensity (mean  $\pm$  SD) for the ROI in the 20th slice. Data are shown for scans with the tactile display present and operating, and without the display present.

## 7.7 Summary

Chapter six has covered the preliminary experiment. The findings of this experiment showed that the display system was able to produce a range of distinguishable tactile stimuli. The overall accuracy for identification of “circle”, “random” and “stationary stimuli was 82%. Also in this chapter, an experiment has been described which shows the tactile display does not produce any significant artefacts in MRI images.

After these preliminary experiments, two fMRI experiments were done: the first to study the response of the brain to different patterns of touch stimulation on the fingertip, and the second to investigate the response of the brain to different speeds of tactile motion.

## **Chapter eight**

# The First fMRI Experiment



## 8.1. Introduction

This experiment is an fMRI version of the psychophysics experiment described in the chapter six. For the three main experiments in this study (the psychophysics experiment and the two fMRI experiments in this chapter and chapter 8), ethics approval has been obtained from the School of Physics Ethics Committee at the University of Exeter. All the participants in these experiments were healthy and each participant was given a leaflet of information which described the nature of the experiment and, for the fMRI experiments, each participant had to read and sign an MRI Safety Checklist before entering the MRI scanner room. The participants were given time to read the information about the experiment and ask questions before signing a consent form. Copies of the information leaflet, MRI Safety Checklist and the consent form can be found in appendix D.

## 8.2. Experiment Protocol

As well as providing novel information on brain activity during touch perception (for example, in relation to the circle/random contrast and the moving/stationary contrast), a major aim of this experiment is to check the ability of the tactile-display system to work in an MRI environment and produce brain activation in expected areas such as SI and SII. It is important that the display is not affected by the high magnetic field, and that there is no effect on the image quality from the presence or operation of the display.

In addition to the tactile display, participants in the fMRI experiment were provided with a visual display – a projection screen viewed via a mirror. The experiment uses the same protocol that was used to produce tactile stimulation in the psychophysics experiment, described in the chapter six, with the following changes:

- 1- The number of stimuli has been doubled to 54, 18 of each tactile pattern (circle, random and stationary).
- 2- The participants are given a visual cue to indicate when a response (push button) is required – three words (circle, random and stationary) appear on the projection screen. The response period begins 9 seconds after the finish the stimulation, and lasts 5 seconds. This specified response period was introduced so that brain activations related to finger movement are separated in time from activations relating to the stimulus.
- 3- During all times except the period of the participants' response the screen displays a blue circle.

As in the psychophysics experiment, described in the chapter six, the task is to recognise the tactile pattern that is present on the right index fingertip, and each participant is asked to follow the steps below:

- 1- The participant is asked to put the tip of the right index finger lightly on the tactile display, without applying any pressure.
- 2- To minimize the movement of the head/eyes the participant is asked to focus on the blue circle on the screen.

The participant is asked to not press a response button until he or she see the words (circle, random and stationary) on the screen, so the time between the stimulation and the response is at least 9 seconds.

The software in the control part of the tactile display was designed to run the stimulation patterns synchronously with the timing of the MRI dynamics – each dynamic lasts 3 seconds and the scanner sends a trigger pulse every 12 dynamics (every 36 seconds).

E-prime (Experimenter's Prime) software was used to present the visual response cue at the appropriate times, according to the unpredictable timing pattern of the stimuli (see section 7.2). It was also used to record the responses of the participant. Before the start of imaging, when the subject has been positioned in the MRI scanner, E-prime displays a brief description of the experiment, and during the imaging E-prime displays the blue circle or the response cue, see figure 8.1. The experiment contains one session of functional imaging (block design) with duration of 32.5 minutes followed by a structural scan of 3.5 minutes, see figure 8.2. For an fMRI experiment of a given overall duration, there is a trade-off between the number of stimuli and the time allocated for each stimulus and associated rest periods. According to the considerable experience of block-design fMRI experiments in Exeter, a relatively short stimulation time of 9 s was chosen; this allowed 54 stimulus-rest cycles to be included in the imaging time of around half an hour (first experiment), thus improving the statistical power of the analysis, and avoided adaptation or fatigue of the subject in response to an over-long tactile stimulus.

A

There are three different types of test items in the experiment:

- *Circle-moving* (clockwise) in a circular path;
- *Random-moving* in a path that has no obvious shape;
- *Stationary*-no movement over the fingertip.

The task is to specify which type of stimulation was displayed using the push buttons.

Top to Circle

Medial to Random

Bottom to stationary

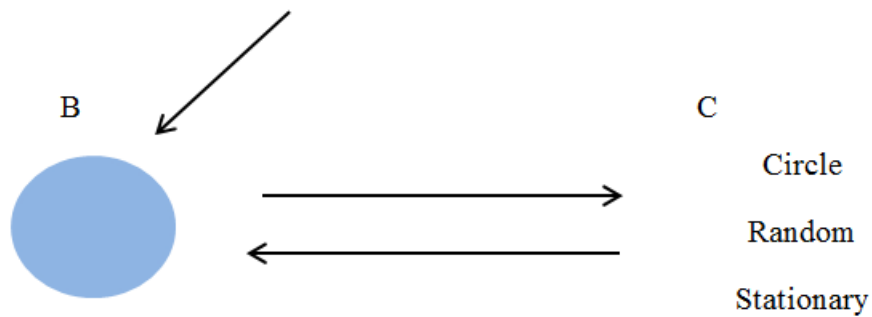


Fig. 8.1: The E-prime display in the first fMRI experiment. (A) the brief description of the experiment; (B) the blue circle which is displayed during the time of experiment except at response time; (C) the hunt word which is displayed during the response time; The arrows show the order or the display.

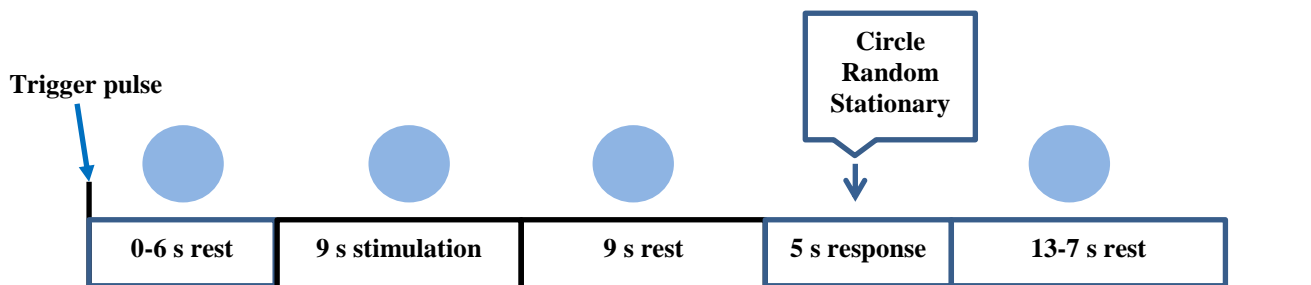


Fig. 8.2: The block design of the first fMRI experiment; a single stimulation cycle is shown.

### 8.3. Acquisition of fMRI data

Both functional and structural scans were run using the 1.5 T Philips Intera MR imager at the Exeter MR Research Centre. The acquisition of fMRI was performed using gradient echo  $T_2^*$ -weighted EPI sequences with BOLD contrast, with the following parameters: repetition time (TR) = 3 s, echo time (TE) = 45 ms, matrix size  $80 \times 80$ , field of view (FOV) =  $240 \times 117 \times 240$  mm., in-plane pixel size  $3 \times 3$  mm, flip angle  $90^\circ$ , slice thickness 3 mm (without gaps between the slices). These parameters are used for 650 dynamics with 39 slices. The scan time is 32.5 minutes. At the end of the functional scan a high-resolution structural volume was acquired using a series of  $T_1$ -weighted images according to following parameters: TR = 25 ms, TE = 4.18 ms, matrix size  $256 \times 204$ , FOV =  $230 \times 128 \times 183.6$  mm., in-plane pixel size  $0.9 \times 0.9$  mm, flip angle  $30^\circ$ , slice thickness 1.6 mm (with 0.8 mm overlap between slices). The number of slices is 160 and the duration of the scan is 3.4 minutes. An 8-element SENSE head coil was used for both acquisitions; multi-channel acquisition allows the duration of the structural scan to be reduced by a factor of four.

### 8.4. Analysis of fMRI data

Details of the analysis procedure have been given in Chapter 4. SPM8 software is used to analyze the fMRI data. Before starting this process, the raw fMRI data is converted to Analyze format using MRICro.

The pre-processing stage includes four steps. The slice time correction is the first step which runs on the fMRI data using the middle slice (slice number 20) as reference to register all other slices. The spatial realignment is the next step; the third step is to normalize all volumes to the standard MNI template, and finally all volumes are smoothed using an  $8 \times 8 \times 8$  mm gaussian. Further details of SPM analysis in general, and relating specifically to the present study, are given in Chapter 5.

The fMRI experiment used a block design. The time sequence of the experiment (figure 8.2) has different periods of rest (no stimulation) in different parts of the time sequence (before and after stimulation) – for analysis, data for the rest condition has been divided into three parts, one before the stimulation and two after the stimulation. The rest which follows the stimulation is labelled with the stimulus type so that, for the contrast between stimulus and rest conditions, the comparison was run between each type of stimulus and the corresponding

following rest. (This method will minimize the effect of the button push on the rest period that is selected for contrast with the stimulus.) The rest which precedes the stimulus is similarly labelled, giving a total of 11 experimental conditions: 3 types of stimulus, 7 types of rest, and the response period. The sequence of these 11 conditions is specified in SPM as a design matrix (see figure 8.3).

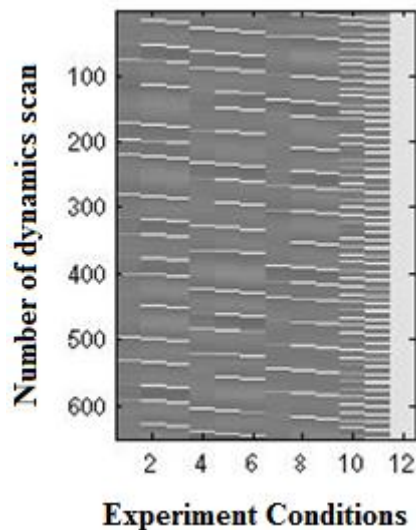


Fig. 8.3: Time course of the 11 conditions in the first fMRI experiment (3 types of stimulus, 7 types of rest, and response); time is represented vertically as the sequence of image dynamics; the light bands in columns 2, 5 and 8 show the timing of the 3 types of stimulus; the light bands in column 10 show the timing of the response periods; the light bands in the other 7 columns show the timing of the various rest periods.

A region of interest (ROI) is used to define the region of the brain in which SPM calculates each contrast. There are several advantages of using a ROI to determine the active area. First, it allows selected regions to be separately explored for activation during different sorts of stimulation. Secondly it increases the power of the statistical analysis by focusing the statistical tests on the ROI, instead of the whole brain. Definition of the ROI depends on the cytoarchitectonic structure or anatomical landmarks of the brain. In the present study, ROIs were defined using the WFU PickAtlas ([www.ansir.wfubmc.edu](http://www.ansir.wfubmc.edu)), software developed in the ANSIR Laboratory at the Wake Forest University School of Medicine.

Previous studies have investigated the brain regions that are active during tactile stimulation using different types of imaging technique such as PET [136-138], MEG [139, 140] and fMRI using different strengths of magnetic field [58, 141, 142]. Most of these studies confirm that the primary somatosensory cortex (SI) and the secondary somatosensory cortex (SII) [45] are the gateway to touch processing in the brain. In the experiment described in this chapter,

these areas were studied in detail for the contrast between stimulation and rest, and the contrast between the different kinds of stimuli (Circle, Random and Stationary). Results are displayed using two different p-value thresholds ( $p \leq 0.05$  corrected and  $p \leq 0.001$  uncorrected) – these are the most commonly used thresholds in similar studies [64, 143]. The  $p \leq 0.05$  (corrected) threshold is more rigorous, while the  $p \leq 0.001$  (uncorrected) threshold allows weaker activations to be tentatively identified. (In some cases, as detailed below, an uncorrected threshold of  $p \leq 0.009$  was used).

## 8.5. Results

There are advantages from asking the participants to give a response to the tactile patterns: it is possible to identify subjects who are not paying attention or are unable to perform the recognition task. Participants' attention is important for a successful fMRI study, and participants' behaviour is important when interpreting their brain activations. Before reviewing the findings of the experiment, the responses of the participants will be presented. Nineteen participants took part in the study, but equipment problems (fault with push buttons) caused responses from 4 subjects to be lost. From the remaining 15 participants, four were eliminated on the basis that they scored less than 66.7%; the purpose of this was to exclude participants who may not have been perceiving the stimuli as intended; the exclusion threshold was set mid-way between the chance score of 33.3% (3-way choice) and the perfect score of 100%. There were thus 11 participants whose data were fully analysed. All are male, ten right-handed and one left-handed, mean age of 28 years ( $SD = 6.1$ ). Table 8.1 shows the details for the volunteers.

Table 8.1: Details of the participants in first fMRI study.

Sub. No.	Gender	Age years	Handedness
Sub 1	M	32	R
Sub 2	M	26	R
Sub 3	M	24	R
Sub 4	M	34	R
Sub 5	M	32	R
Sub 6	M	23	L
Sub 7	M	31	R
Sub 8	M	40	R
Sub 9	M	22	R
Sub 10	M	22	R
Sub 11	M	20	R

Figure 8.4 shows the % correct responses for the eleven participants whilst figure 8.5 shows the confusion matrix. The confusion matrix and the response scores showed the participants can distinguish between the different kinds of stimuli, providing further validation of the tactile display. The overall accuracy was 83.3 % and the kappa statistic [135] was 0.75. These may be compared to the (very similar) corresponding figures of 82.0 % and 0.73 from the psychophysics experiment in Chapter 7. However, it must be remembered that the average score from the fMRI experiment has been elevated by removal of data from four low-scoring subjects – without this, the average score for the fMRI experiment would be lower, presumably reflecting the difficulty of concentrating on the task in the fMRI environment. (The error patterns in the two experiments, as indicated by the confusion matrices in figures 8.5 and 7.6 showed some minor differences).

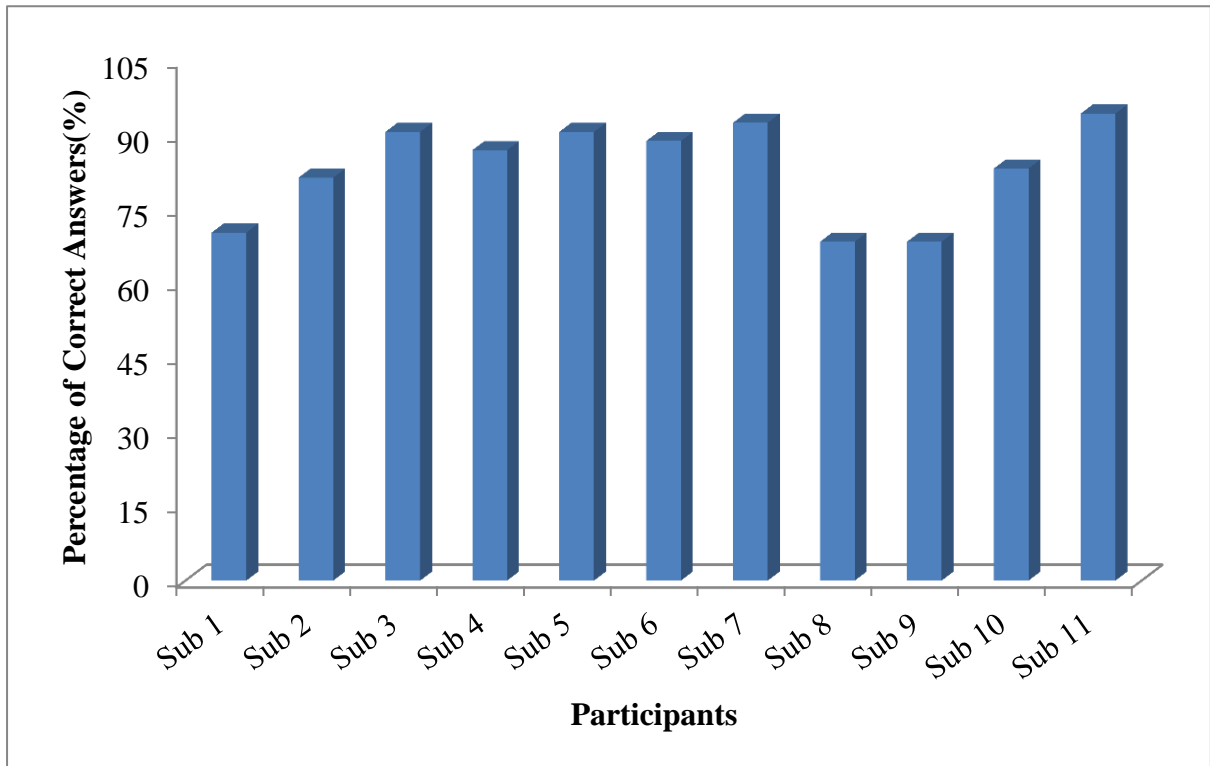


Fig. 8.4: The percentage correct responses for the 11 participants.

Response \ Stimulation	Circle	Random	Stationary
Circle	144	44	10
Random	38	158	2
Stationary		5	193

Fig. 8.5: The confusion matrix for the 11 participants.



## 8.6 Individual fMRI Analysis for SI and SII

### 8.6.1 Contrast of Circle vs. Rest

The Circle stimulus moves along a trajectory which traces out an obviously recognizable shape on the fingertip (see section 6.2). Figure 8.6 shows the activation in SI and SII for the contrast between Circle stimulation and Rest for Subject 1. Corresponding results for Subjects 2 to 11 are in Appendix E 1.1. The Circle stimulation showed a strong activation in both SI and SII regions, on both sides of the brain. Tables 8.2 and 8.3 show the coordinates of the centres of maximum activation in SI and SII, in addition to statistical measures ( $t$ -value,  $Z$ -score and  $K_E$  value). Tables 8.2 and 8.3 show the coordinates of the centres of maximum activation in SI and SII, in addition to statistical measures ( $t$ -value,  $Z$ -score and  $K_E$  value). The tables show results for a corrected threshold of  $p \leq 0.05$ , together with some weaker activations (asterisked) that are identified at an uncorrected threshold of  $p \leq 0.001$ .

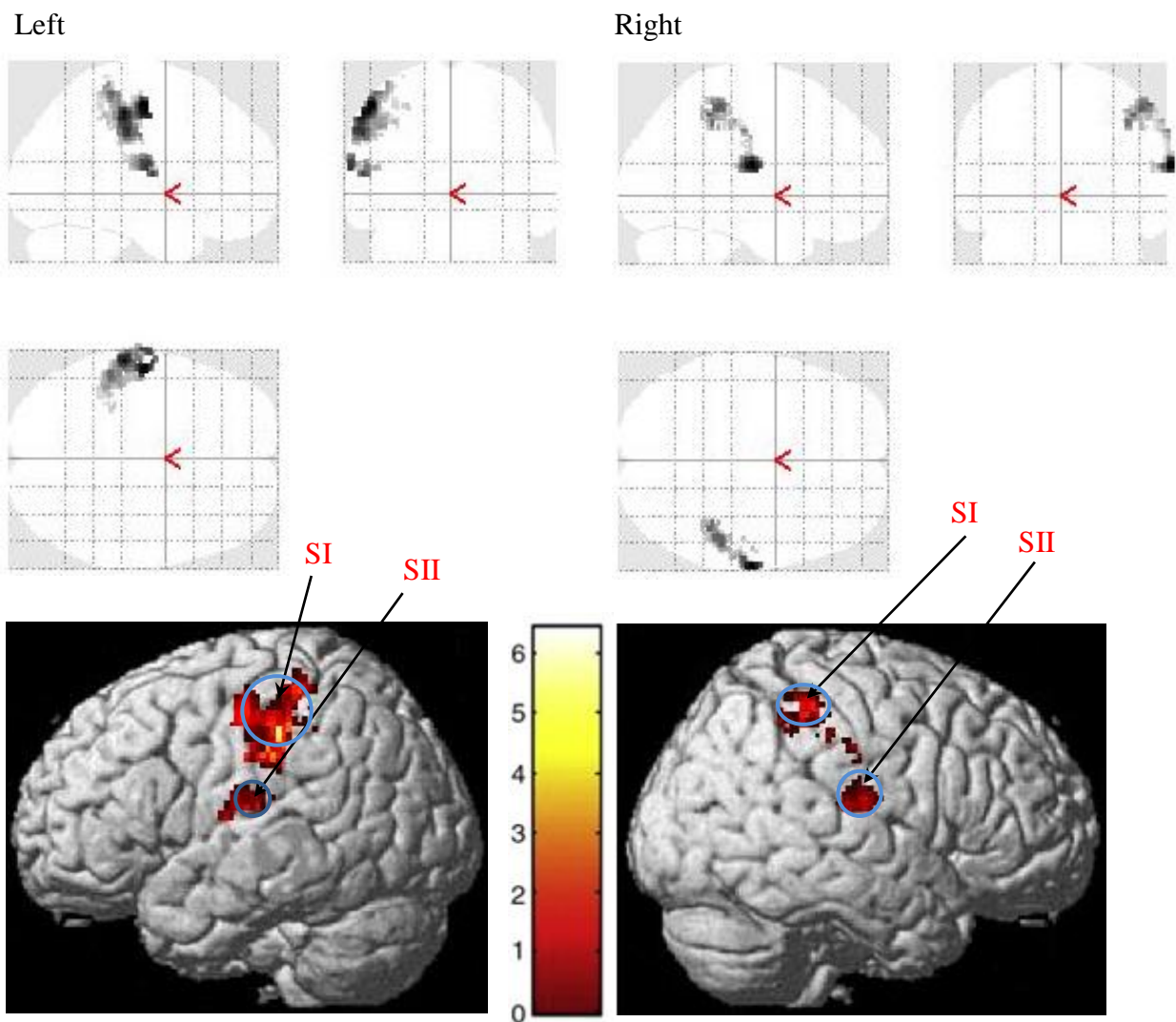


Fig. 8.6: Glass-brain views (upper panels) and rendered-brain views (lower panels) of activation for the contrast between Circle and Rest for subject 1 in areas SI and SII. Threshold corrected,  $p$  value of  $\leq 0.05$ . The  $t$ -value colour scale for the rendered images is shown at lower centre – the same scale is used for all rendered images in this chapter and the next.

Table 8.2: The coordinates of the activation in the primary somatosensory cortex with the maximum  $t$ -value and  $Z$ -score for the participants in first fMRI study for the contrast between Circle vs. Rest.

Participants	SI - left				SI - right			
	$t$ -value	Z- score	$K_E$	MNI coordinates (x, y, z)	$t$ -value	Z-score	$K_E$	MNI coordinates (x, y, z)
Sub 1	8.25	Inf	523	(-52, -16, 52) BA3	5.25	5.19	97	(66, -22, 38) BA1
Sub 2	6.11	6.01	111	(-58, -30, 50) BA2	4.92	4.87	20	(62, -18, 32) BA3
Sub 3	4.84	4.79	29	(-50, -26, 60) BA1	3.36*	3.34*	3*	(64, -20, 38)* BA3
Sub 4	5.94	5.85	210	(-54, -30, 54) BA2	3.99	3.85	2	(62, -28, 42) BA1
Sub 5	6.83	6.70	294	(-46, -32, 60) BA2	5.54	5.47	81	(52, -30 44) BA 2
Sub 6	5.92	5.83	24	(-32, -36, 70) BA1	4.23	4.20	3	(44, -38, 66) BA 2
Sub 7	6.17	6.07	148	(-62, -12, 24) BA3	7.06	6.92	67	(58, -22, 38) BA 3
Sub 8	7.57	7.40	371	(-54, -18, 54) BA3	6.38	6.27	344	(46, -34, 62) BA1
Sub 9	6.07	5.98	96	(-54, -22, 54) BA1	3.24*	3.23*	5*	(56, -28, 54)* BA2
Sub 10	7.19	7.04	110	(-60, -20, 38) BA3	6.23	6.13	241	(62, -28, 44) BA 1
Sub 11	----	----	---	----	----	---	---	---

(\*) threshold uncorrected,  $p$  value of  $\leq 0.001$ ; otherwise threshold corrected,  $p \leq 0.05$ ;  $K_E$  = number of voxels.

Table 8.3: The coordinates of the activation in the secondary somatosensory cortex with the maximum  $t$ -value and  $Z$ -score for the participants in first fMRI study for the contrast between Circle vs. Rest.

Participants	SII - left				SII - right			
	$t$ -value	$Z$ -score	$K_E$	MNI coordinates (x, y, z)	$t$ -value	$Z$ -score	$K_E$	MNI coordinates (x, y, z)
Sub 1	7.09	6.94	55	(-66, -14,14) BA 43	6.95	6.81	69	(68, -16, 16) BA 43
Sub 2	3.72*	3.70*	7*	(-66, -18,16)* BA43	----	----	--	----
Sub 3	3.36*	3.35*	5*	(-56, -30, 18)* BA40	4.28	4.25	7	(64, -34, 26) BA40
Sub 4	4.19	4.16	2	(-56, -12, 10) BA43	4.85	4.80	41	(62, -24, 16) BA40
Sub 5	5.22	5.16	13	(-50, -32, 22) BA 40	5.60	5.53	86	(66, -16, 14) BA43
Sub 6	3.56*	3.54*	2*	(-66, -20, 14)* BA40	3.53*	3.51*	46*	(66, -22, 20)* BA40
Sub 7	8.49	Inf	140	(-64, -20, 16) BA40	4.72	4.67	18	(56, -12,12) BA43
Sub 8	4.68	4.64	5	(-54, -14, 18) BA43	4.11	4.08	3	(62, -8, 20) BA43
Sub 9	----	----	---	----	----	----	--	----
Sub 10	5.89	5.81	30	(-56, -14, 18) BA43	6.72	6.60	114	(66, -16, 20)BA43
Sub 11	----	----	---	----	4.67	4.63	54	(68, -30,22) BA40

(\*) Threshold uncorrected with  $p$  value of  $\leq 0.001$ ; otherwise threshold corrected,  $p \leq 0.05$ ;  
 $K_E$  = number of voxels.

### 8.6.2 Contrast of Random vs. Rest

The Random stimulus moves along a trajectory which traces out no obvious shape on the fingertip (see section 7.2). Figure 8.7 shows activation due to the contrast between Random and Rest conditions for Subject 1. Corresponding results from Subjects 2 to 11 are in Appendix E 1.2. Tables 8.4 and 8.5 show the statistical measures ( $t$ -value,  $Z$ -score and  $K_E$  value) for the activations, and the coordinates of the centres of maximum activation in SI and SII. The tables show results for a corrected threshold of  $p \leq 0.05$ , together with some weaker activations (asterisked) that are identified at uncorrected thresholds of  $p \leq 0.001$  and (in SII)  $p \leq 0.009$ .

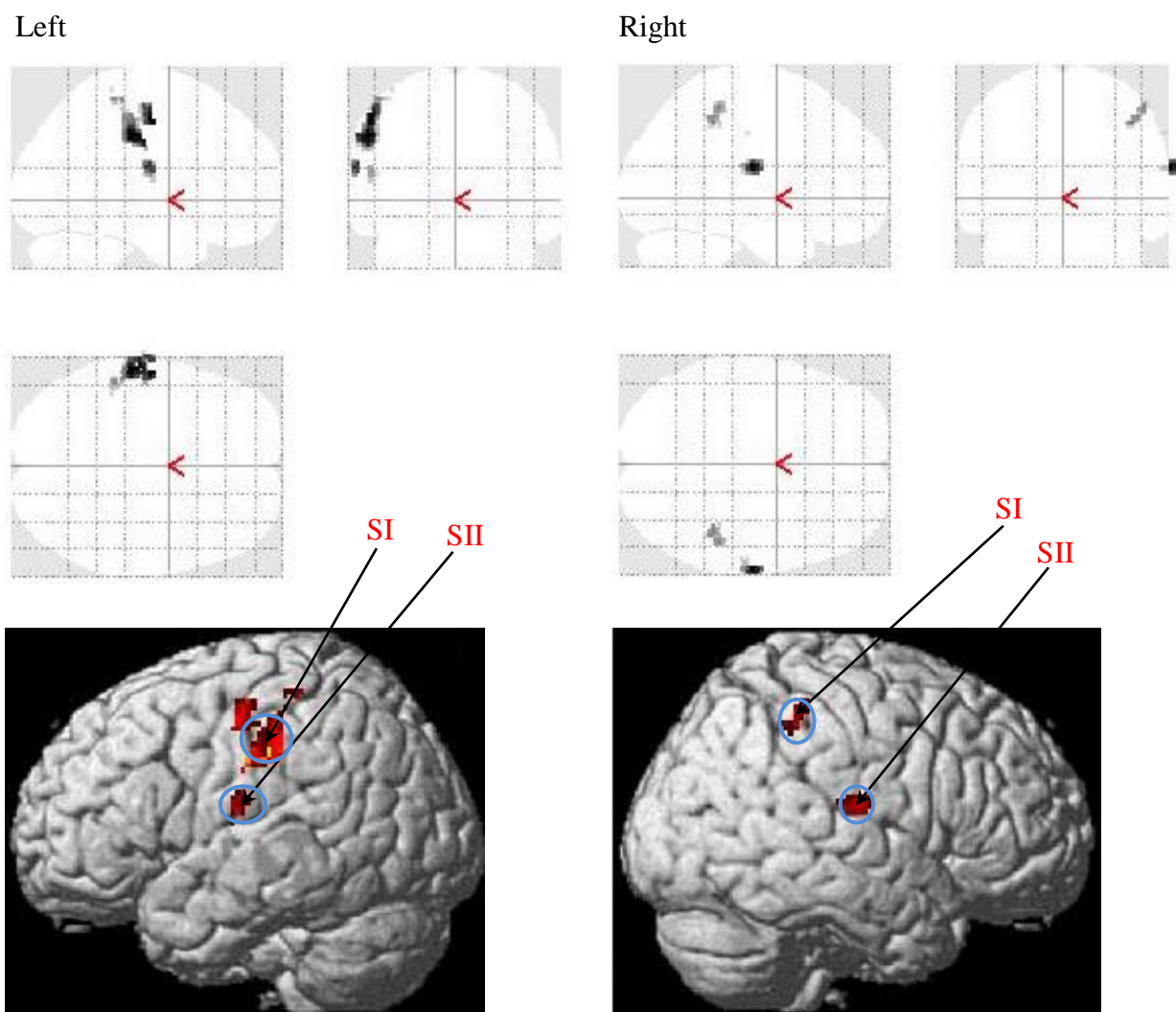


Fig. 8.7: Glass-brain views (upper panels) and rendered-brain views (lower panels) of activation for the contrast between Random and Rest for subject 1 in areas SI and SII. Threshold corrected,  $p$  value of  $\leq 0.05$ .

Table 8.4: The coordinates of the activations in the primary somatosensory cortex with the maximum  $t$ -value and  $Z$ -score for the participants in first fMRI study for the contrast between Random vs. Rest.

Participants	SI - left				SI - right			
	$t$ -value	$Z$ -score	$K_E$	MNI coordinates (x, y, z)	$t$ -value	$Z$ -score	$K_E$	MNI coordinates (x, y, z)
Sub 1	6.36	6.25	205	(-56, -12,46) BA3	4.15	4.12	4	(62, -20,38) BA3
Sub 2	5.16	5.10	110	(-56, -30, 46) BA2	4.68	4.64	18	(66, -22, 36) BA1
Sub 3	7.29	7.13	145	(-50, -28, 60) BA1	4.37	4.34	19	(68, -22, 26) BA2
Sub 4	7.18	7.04	127	(-48, -34, 60) BA2	4.49	4.45	3	(68, -18, 26) BA1
Sub 5	7.82	7.63	366	(-44, -30, 66) BA1	5.10	5.04	23	(48, -30, 44) BA2
Sub 6	3.88	3.86	2	(-32, -34, 70) BA3	4.14	4.11	5	(68, -22, 24) BA2
Sub 7	8.13	Inf	357	(-62, -12, 26) BA3	8.25	Inf	145	(58, -22, 36) BA3
Sub 8	7.28	7.12	250	(-54, -18, 54) BA3	5.37	5.30	20	(64, -16, 28) BA3
Sub 9	6.50	6.39	208	(-52, -26, 58) BA1	4.58	4.54	19	(66, -20, 34) BA1
Sub 10	7.32	7.17	214	(-54, -12, 52) BA3	5.29	5.23	17	(62, -28,44) BA1
Sub 11	3.05*	3.04*	15*	(-50, -18, 60)* BA3	3.59*	3.57*	9*	(66, -24, 24)* BA2

(\*) threshold uncorrected with  $p$  value of  $\leq 0.001$ ; otherwise threshold corrected,  $p \leq 0.05$ ;  
 $K_E$  = number of voxels

Table 8.5: The coordinates of the activations in the secondary somatosensory cortex with the maximum  $t$ -value and  $Z$ -score for the participants in first fMRI study for the contrast between Random vs. Rest.

Participants	SII - left				SII - right			
	$t$ -value	$Z$ -score	$K_E$	MNI coordinates (x, y, z)	$t$ -value	$Z$ -score	$K_E$	MNI coordinates (x, y, z)
Sub 1	5.74	5.66	23	(-66, -16, 18) BA43	5.88	5.80	45	(66, -18,18)BA43
Sub 2	3.75*	3.73*	13*	(-64, -20, 16)* BA40	----	----	----	----
Sub 3	4.53	4.49	5	(-56, -28, 20) BA40	4.38	4.35	49	(60, -34,22) BA40
Sub 4	3.17*	3.15*	1*	(-56, -12, 10)* BA43	----	----	----	----
Sub 5	5.04	4.98	6	(-64, -12, 22) BA43	4.90	4.85	23	(68, -16,14) BA43
Sub 6	3.25*	3.23*	5*	(-62, -28,22)* BA40	3.77*	3.75*	96*	(66, -16,14)* BA43
Sub 7	7.86	7.67	60	(-64, -20, 16) BA43	---	---	---	----
Sub 8	----	----	---	----	----	---	---	---
Sub 9	4.85	4.80	12	(-54, -16, 18) BA43	3.51*	3.49*	7*	(60, -8, 12)* BA43
Sub 10	---	---	---	---	4.96	4.91	42	(66, -22,20) BA40
Sub 11	----	----	---	---	4.90**	4.85**	127**	(68, -28, 20)** BA40

(\*) threshold uncorrected with  $p$  value of  $\leq 0.001$ ; (\*\*) threshold uncorrected with  $p$  value of  $\leq 0.009$ ;  $K_E$  = number of voxels.

### 8.6.3 Contrast of Stationary vs. Rest

The Stationary stimulus has no obvious movement over the fingertip. Stimulation switches between the diagonals of a 2×2 square on the stimulator array (see section 7.2). Figure 7.8 displays the activations for the contrast between the Stationary and Rest conditions for Subject 1. Corresponding results from Subject 2 and Subjects 4 to 10 are in Appendix E 1.3; Subjects 1, 3, 10 and 11 did not show any activation in SI or SII on either side of the brain ( $p \leq 0.009$ , uncorrected). The tables show results for a corrected threshold of  $p \leq 0.05$ , together with some weaker activations (asterisked) that are identified at uncorrected thresholds of  $p \leq 0.001$  and  $p \leq 0.009$ .

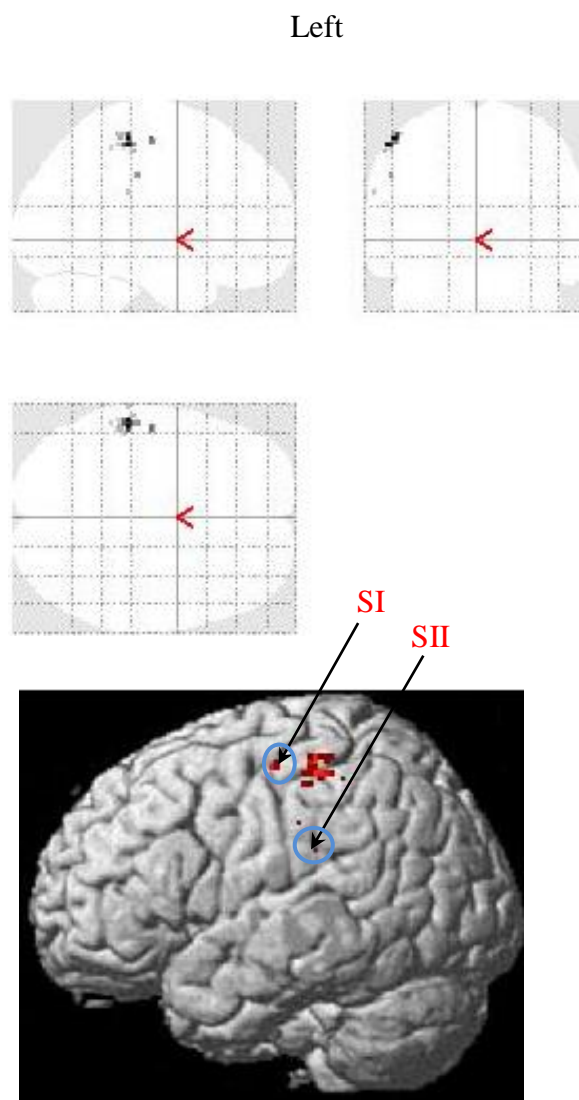


Fig. 8.8: Glass-brain views (upper panel) and rendered-brain views (lower panel) of activation for the contrast between Stationary and Rest for subject 1 in areas SI and SII. Threshold uncorrected,  $p$  value of  $\leq 0.009$ . No activations were observed on the right side of the brain ( $p \leq 0.009$ , uncorrected).



Table 8.6: The coordinates of the activations in the primary somatosensory cortex with the maximum  $t$ -value and  $Z$ -score for the participants in first fMRI study for the contrast between Stationary vs. Rest.

Participants	SI - left				SI - right			
	$t$ -value	$Z$ -score	$K_E$	MNI coordinates (x, y, z)	$t$ -value	$Z$ -score	$K_E$	MNI coordinates (x, y, z)
Sub 1	----	-----	----	-----	----	-----	----	-----
Sub 2	4.02*	3.99*	33*	(-62, -30, 34)* BA3	3.84*	3.82*	17*	(46, -24, 64)* BA 3
Sub 3	----	----	---	----	----	----	---	-----
Sub 4	3.02**	3.01**	3**	(-50, -18, 60)**BA3	3.45**	3.43**	85**	(58, -30, 50)**BA 2
Sub 5	2.87**	2.85**	36**	(-50, -30, 60)** BA2	----	----	----	----
Sub 6	---	---	---	----	4.21*	4.18*	26*	(66, -22, 38)* BA1
Sub 7	4.74	4.69	100	(-48, -32, 56) BA2	5.86	5.78	26	(44, -38, 64) BA2
Sub 8	5.85	5.77	83	(-52, -24, 56) BA1	5.49	5.42	23	(66, -14, 26) BA3
Sub 9	5.44	5.37	47	(-54, -20, 54) BA1	----	----	---	----
Sub 10	----	-----	----	-----	----	-----	---	-----
Sub 11	----	----	---	----	----	----	---	-----

(\*) threshold uncorrected with  $p$  value of  $\leq 0.001$ ; (\*\*) threshold uncorrected with  $p$  value of  $\leq 0.009$ ; otherwise threshold corrected,  $p \leq 0.05$ ;  $K_E$  = number of voxels.

Table 8.7: The coordinates of the activations in the secondary somatosensory cortex with the maximum  $t$ -value and  $Z$ -score for the participants in first fMRI study for the contrast between Stationary vs. Rest.

Participants	SII - left				SII - right			
	$t$ -value	Z- score	$K_E$	MNI coordinates (x, y, z)	$t$ -value	Z-score	$K_E$	MNI coordinates (x, y, z)
Sub 1	---	---	--	----	----	----	---	----
Sub 2	3.72*	3.69*	7*	(-66, -14, 14)* BA43	---	---	---	----
Sub 3	-----	----	--	-----	---	----	---	---
Sub 4	----	----	---	----	3.30*	3.29*	3*	(56, -10, 10)*BA43
Sub 5	2.93**	2.91**	4**	(-58, -8, 16)** BA43	----	----	----	----
Sub 6	3.90*	3.88*	68*	(-60, -30,20)* BA40	3.85*	3.82*	4*	(54, -30, 18)* BA40
Sub 7	5.19	5.14	27	(-66, -20,22) BA43	----	----	----	----
Sub 8	4.59	4.55	5	(-56, -14, 18) BA43	4.47*	4.43*	8*	(66, -16, 22)* BA43
Sub 9	2.84**	2.83**	4**	(-48, -16, 18)** BA43	----	----	---	----
Sub 10	----	---	---	-----	----	----	--	-----
Sub 11	----	----	---	----	----	----	---	----

(\*) threshold uncorrected with  $p$  value of  $\leq 0.001$ ; (\*\*) threshold uncorrected with  $p$  value of  $\leq 0.009$ ; otherwise threshold corrected,  $p \leq 0.05$ ;  $K_E$  = number of voxels.

The results from both types of moving stimulation (Circle and Random) are similar: significant SI activation in most almost all subjects (with a high number KE of voxels activated) and significant SII activation in around half the subjects with suggested SII activation in some of the remaining subjects (again with large cluster sizes). Activation caused by the Stationary stimulus is less, with smaller cluster sizes: only 3 subjects from 11 show significant SI activation, with suggested SI activation in a further one subject, and only 2 subjects from 11 show significant SII activation, with suggested SII activation in a further two subjects. These findings in the present study agree with the results of previous research [144, 145]. The primary somatosensory cortex has neurons involved in the first stages of motion processing [146, 147] and the active perception of surface curvature [137]. This provides a possible explanation for the stronger activations observed for moving stimuli. Another factor is that tactile sensitivity over the surface of the fingertip is not homogenous [148], affecting stationary stimuli in a different way to moving stimuli.

Generally, SI showed more activation than SII – stimuli are presented at 40 Hz, and low-frequency stimulation is known to produce less activation in SII than higher frequencies [149]. This may be because perception of 40 Hz stimuli involves Meissner corpuscles, and Meissner afferents have less connections to SII than the Pacinian afferents which respond to high-frequency stimuli [149, 150]. Similar comments apply to the results for SI and SII from the group analysis (next section). Part of this work was published in In Proceedings of the 29st Annual Scientific Meeting of the ESMRMB, Lisbon/PT, October 2012. See Appendix G.

## 8.7 Group fMRI Analysis

### 8.7.1 Group analysis for SI and SII

Figures 8.9, 8.10 and 8.11 show activations from a group analysis for contrasts between Circle stimuli and Rest, Random stimuli and Rest, and Stationary stimuli and Rest, respectively. Tables 8.8, 8.10 and 8.12 give the coordinates and statistical measures of the activated regions in SI, while tables 8.9, 8.11 and 8.13 show the coordinates and statistical measures of the activated regions in SII.

Following a similar pattern to the individual-subject analyses, results from the group analysis showed significant SI and SII activations due to Circle and Random stimulation (Tables 8.8 to 8.11) but no significant activations in SI or SII for Stationary stimulation (Tables 8.12 and 8.13), for which SI activation is only suggested ( $p \leq 0.001$ , uncorrected). Activations on the right side of the brain are similar to those on the left side – this is surprising because

stimulation on the right hand is expected to produce more left-side activations in SI and SII. From the individual-subject analyses it can be seen that the pattern of right-side activation is variable. It is likely that right-side activations are affected by participants moving their left-hand fingers over the response push buttons during the stimulation period.

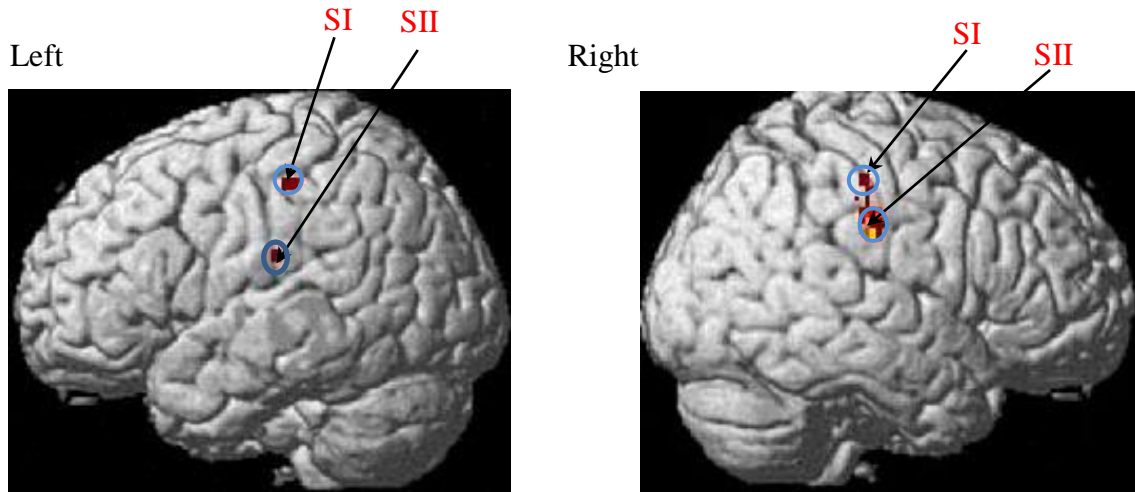


Fig. 8.9: Rendered-brain views of activation of the contrast between Circle and Rest for the group analysis (second-level) in areas SI and SII. Threshold corrected with  $p$  value of  $\leq 0.05$ .

Table 8.8: The coordinates of the activations in the primary somatosensory cortex, with the maximum  $t$ -values and  $Z$ -scores, for the contrast in the group analysis (second level) between Circle vs. Rest.  $K_E$  = number of voxels; threshold corrected,  $p \leq 0.05$ .

SI left				SI right			
$t$ -value	$Z$ -score	$K_E$	MNI coordinates	$t$ -value	$Z$ -score	$K_E$	MNI coordinates
8.92	4.59	5	(-66, -22, 24) BA2	12.58	5.21	101	(64, -24, 36) BA1

Table 8.9: The coordinates of the activations in the secondary somatosensory cortex, with the maximum  $t$ -values and  $Z$ -scores, for the contrast in the group analysis (second level) between Circle vs. Rest.  $K_E$  = number of voxels; threshold corrected,  $p \leq 0.05$ .

SII left				SII right			
$t$ -value	$Z$ -score	$K_E$	MNI coordinates	$t$ -value	$Z$ -score	$K_E$	MNI coordinates
----	-----	----	-----	11.70	5.08	15	(60, -24, 28)BA40

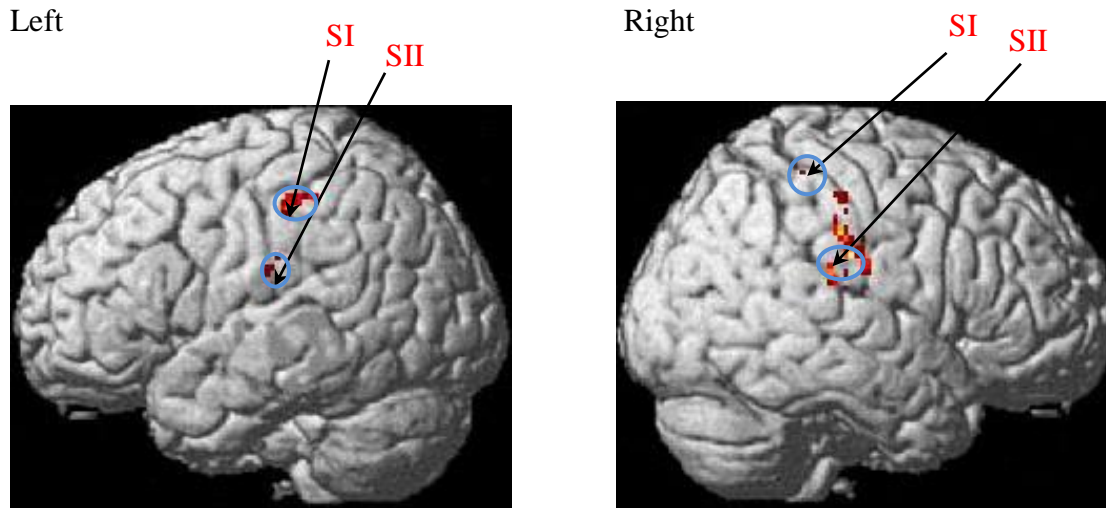


Fig. 8.10: Rendered-brain views of activation of the contrast between Random and Rest for the group analysis (second-level) in areas SI and SII. Threshold corrected with  $p$  value of  $\leq 0.05$ .

Table 8.10: The coordinates of the activations in the primary somatosensory cortex, with the maximum  $t$ -values and  $Z$ -scores, for the contrast in the group analysis (second level) between Random vs. Rest.  $K_E$  = number of voxels; threshold corrected,  $p \leq 0.05$ .

SI left				SI right			
$t$ -value	$Z$ -score	$K_E$	MNI coordinates	$t$ -value	$Z$ -score	$K_E$	MNI coordinates
9.11	4.63	42	(-54, -28, 48) BA2	12.16	5.15	119	(62, -22, 28) BA2

Table 8.11: The coordinates of the activations in the secondary somatosensory cortex, with the maximum  $t$ -values and  $Z$ -scores, for the contrast in the group analysis (second level) between Random vs. Rest.  $K_E$  = number of voxels; threshold corrected,  $p \leq 0.05$ .

SII left				SII right			
$t$ -value	$Z$ -score	$K_E$	MNI coordinates	$t$ -value	$Z$ -score	$K_E$	MNI coordinates
10.48	4.89	6	(-64, -24, 22) BA40	12.44	5.19	10	(60, -24, 28) BA40

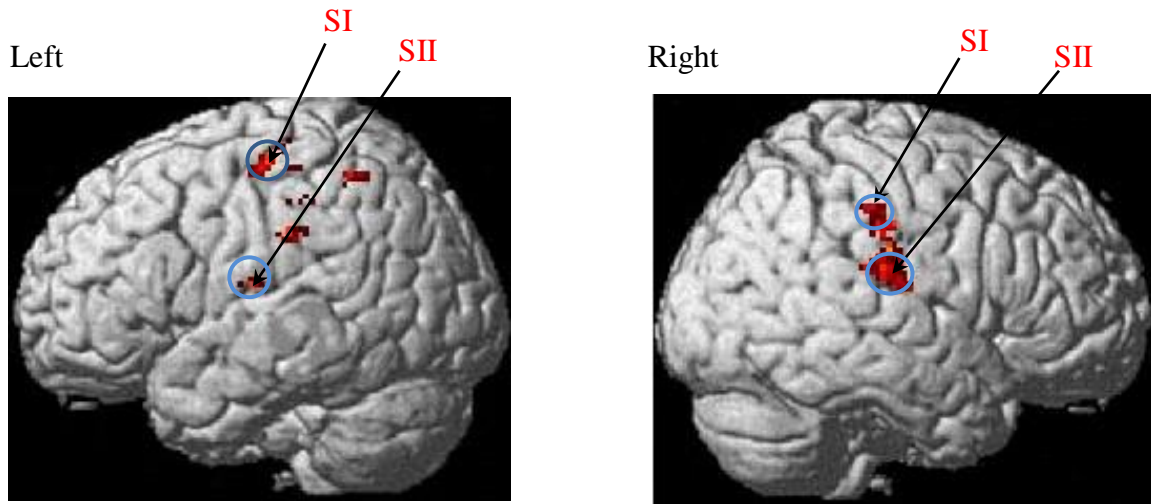


Fig. 8.11: Rendered-brain views of activation of the contrast between Stationary and Rest for the group analysis (second-level) in areas SI and SII. Threshold uncorrected with  $p$  value  $\leq 0.009$ .

Table 8.12: The coordinates of the activations in the primary somatosensory cortex, with the maximum  $t$ -values and  $Z$ -scores, for the contrast in the group analysis (second level) between Stationary vs. Rest. (\*)  $p$  value of  $\leq 0.001$ , uncorrected;  $K_E$  = number of voxels.

SI left				SI right			
$t$ -value	$Z$ -score	$K_E$	MNI coordinates	$t$ -value	$Z$ -score	$K_E$	MNI coordinates
4.42*	3.22*	3*	(-48, -18, 60)* BA3	4.99*	3.46*	4*	(62, -28, 44)* BA1

Table 8.13: The coordinates of the activations in the secondary somatosensory cortex, with the maximum  $t$ -values and  $Z$ -scores, for the contrast in the group analysis (second level) between Stationary vs. Rest. (\*\*)  $p$  value of  $\leq 0.009$ , uncorrected;  $K_E$  = number of voxels.

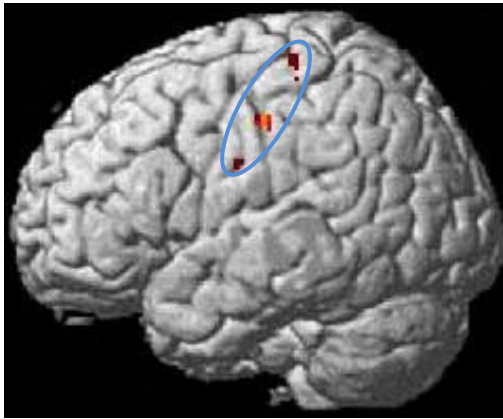
SII left				SII right			
$t$ -value	$Z$ -score	$K_E$	MNI coordinates	$t$ -value	$Z$ -score	$K_E$	MNI coordinates
3.34**	2.67**	10**	(-48, -16, 14)** BA43	4.61**	3.30**	47**	(66, -24, 22)** BA40

## 8.7.2 Group analysis for the primary motor cortex

Many areas of the brain are used in the process of touch perception, Some regions, such as SI and SII, are associated mainly with touch while others are also associated with other senses (e.g., kinesthesia, vision, hearing) [137, 151]. Group analysis of the first fMRI experiment explored the primary motor area (this section) and Broca's area (see section 8.7.3), in addition to SI and SII (above).

Previous studies in humans and animals have observed activations in the primary motor area (M1) of the brain due to active and passive movement of the hand [152-154]. Activations relating to passive movement are weak compared with activations caused by active movement [153, 155]. For the present study, figures 8.12 and 8.13 show results for the primary motor cortex (Brodmann area 4) from the group analysis for the following moving/stationary contrasts: Circle vs. Stationary and (Circle + Random) vs. stationary. Tables 8.14 and 8.15 show the coordinates of the centre of maximum activation and the statistical measures for these areas. The figures and tables showed the activation in primary motor area (M1) due to tactile motion is not significant at the level of  $p \leq 0.05$  (corrected). This is not surprising because tactile motion does not involve a physical motion of the finger (active or passive). The right side of the brain shows stronger activation than the left side – as mentioned before, it is likely that right-side activations are affected by participants moving their left-hand fingers over the response push buttons during the stimulation period.

Left



Right

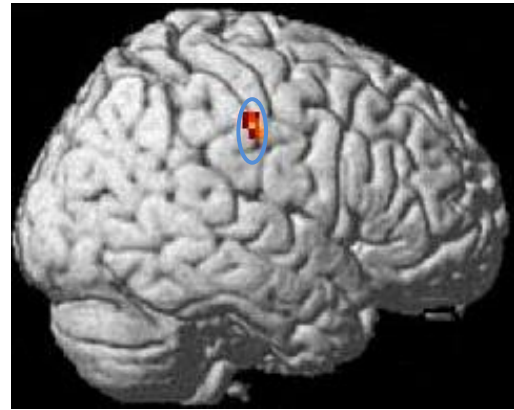


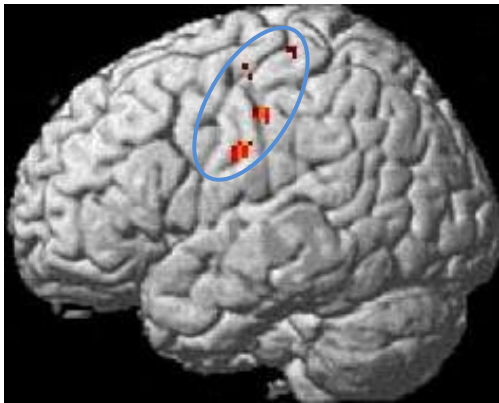
Fig. 8.12: Rendered brain showing (circled in blue) the activation in the primary motor area (Brodmann area 4) for the contrast between Circle and Stationary (group analysis); threshold uncorrected,  $p$  value  $\leq 0.009$ .

Table 8.14: The coordinates of activations in the primary motor cortex (Brodmann area 4), with maximum values of the  $t$ -value and  $Z$ -score, for the contrast between Circle and Stationary.  $K_E$  = number of voxels; (\*)  $p$  value  $\leq 0.001$ , uncorrected; (\*\*)  $p$  value  $\leq 0.009$ , uncorrected.

BA4 left				BA4 right			
$t$ -value	$Z$ -score	$K_E$	MNI coordinates	$t$ -value	$Z$ -score	$K_E$	MNI coordinates
3.98**	3.01**	15**	(-60, -22, 44)**	4.87*	3.41*	6*	(60, -18, 40)*



Left



Right

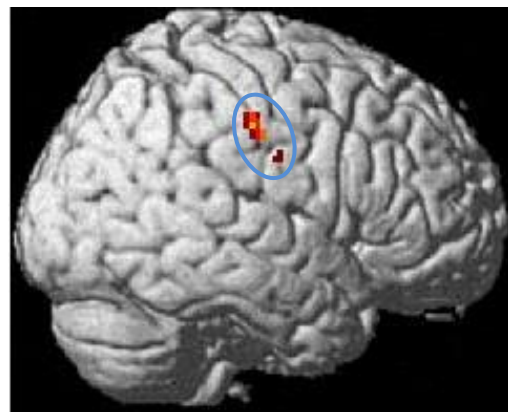


Fig. 8.13: Rendered brain showing (circled in blue) the activation in the primary motor area (Brodmann area 4) for the contrast between (Circle + Random) and Stationary (group analysis); threshold uncorrected,  $p$  value  $\leq 0.009$ .

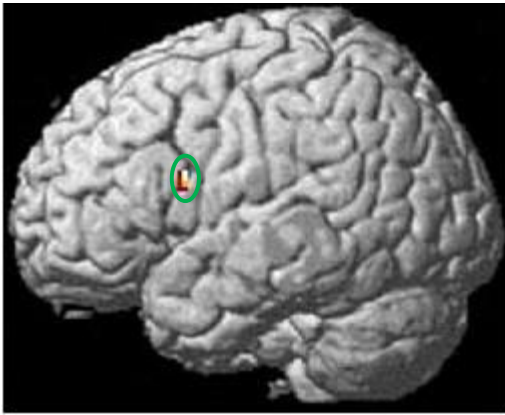
Table 8.15: The coordinates of activations in Brodmann area 4, with maximum values of the  $t$ -value and  $Z$ -score, for the contrast between (Circle + Random) and Stationary.  $K_E$  = number of voxels; (\*)  $p$  value  $\leq 0.001$ , uncorrected; (\*\*)  $p$  value  $\leq 0.009$ , uncorrected.

BA4 left				BA4 right			
$t$ -value	$Z$ -score	$K_E$	MNI coordinates	$t$ -value	$Z$ -score	$K_E$	MNI coordinates
3.94**	2.99**	15**	(-60, -22, 44)**	4.50*	3.25*	6*	(60, -22, 44)*

### 8.7.3 Group analysis for Broca's region

Broca's region is located in the inferior frontal gyrus. This area is composed from Brodmann area 44 or, according to some authors, from areas 44 and 45 [156-158]. It has been found that Broca's region is involved directly or indirectly in different functions such as speech production, language, motor preparation and shape recognition [64, 157, 159]. For the present study, figures 8.15 to 8.17 show results for Broca's area (Brodmann area 44) from the group analysis. Tables 8.16 and 8.17 show the statistical measures for various contrasts which relate to shape recognition.

Left



Right

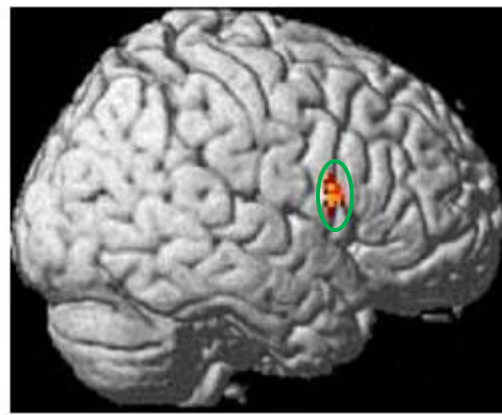
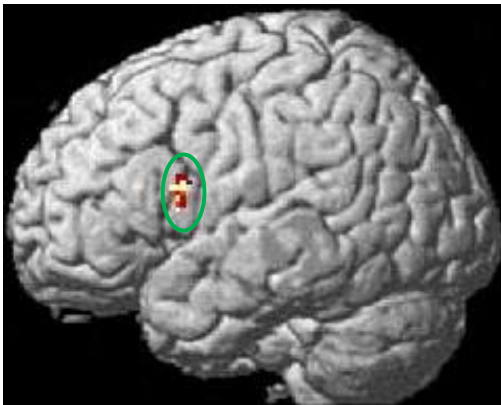


Fig. 8.14: Rendered brain showing (circled in green) the activation in Broca's region (Brodmann area 44) for the contrast between Circle and Rest (group analysis); threshold corrected,  $p$  value  $\leq 0.05$ .

Left



Right

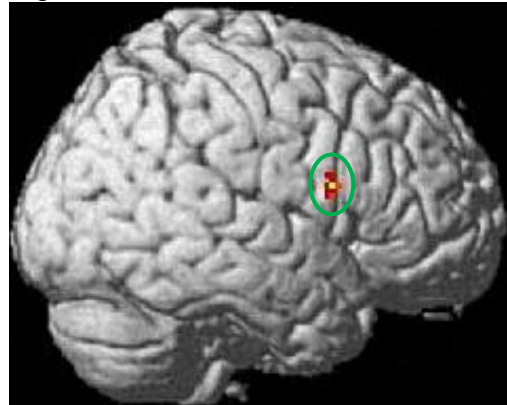


Fig. 8.15: Rendered brain (circled in green) the activation in Broca's region (Brodmann area 44) for the contrast between Random and Rest (group analysis); threshold corrected,  $p$  value  $\leq 0.05$ .

Right

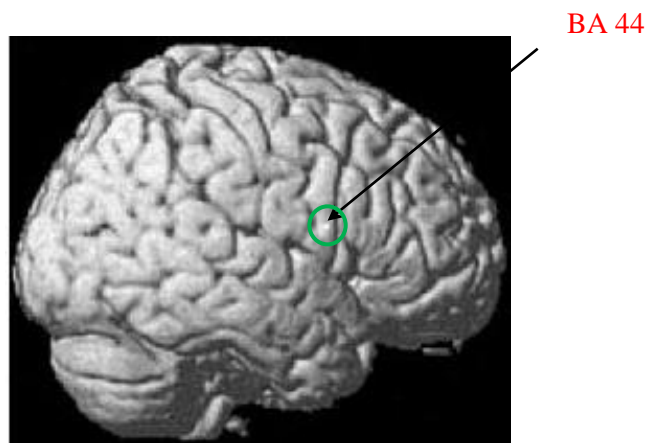


Fig. 8.16: Rendered brain showing (circled in green) the activation in Broca's region (Brodmann area 44) for the contrast between Stationary and Rest (group analysis); threshold uncorrected,  $p \leq 0.009$ . No activations were observed in left side BA44 ( $p \leq 0.009$ , uncorrected).

Table 8.16: The coordinates of the activations in left side Broca's area (Brodmann area 44) with  $t$ -values and  $Z$ -scores (group analysis);  $K_E$  = number of voxels; (\*) threshold uncorrected,  $p$  value  $\leq 0.001$ ; otherwise threshold corrected,  $p \leq 0.05$ .

Statistical Measure Contrast	$K_E$	$Z$ -score	$t$ -value	MNI coordinates
Circle vs. rest	26	4.46	8.33	(-56, 8, 22)
Random vs. rest	47	4.44	8.27	(-52, 10, 14)
Stationary vs. rest	----	-----	-----	-----
Circle vs. stationary (CS)	5	3.75	5.80	(-52, 10, 20)
Random vs. stationary (RS)	2*	3.30*	4.60*	(-52, 10, 20)*
Circle & Random vs. stationary (CRS)	4	3.77	5.86	(-52, 10, 20)

Table 8.17: The coordinates of the activations in right side Broca's area (Brodmann area 44) with  $t$ -values and  $Z$ -scores (group analysis);  $K_E$  = number of voxels; (\*) threshold uncorrected,  $p$  value  $\leq 0.001$ ; (\*\*) threshold uncorrected,  $p$  value  $\leq 0.009$ ; otherwise threshold corrected,  $p \leq 0.05$

Statistical Measure Contrast	$K_E$	Z-score	$t$ -value	MNI coordinates
Circle vs. rest	56	4.37	7.94	(54, 10, 22)
Random vs. rest	25	4.23	7.41	(54, 10, 22)
Stationary vs. rest	2**	2.58**	3.17**	(58, 8, 16)**
----	----	----	----	----
----	----	----	----	----
----	---	---	---	----

The figures (8.15 to 8.17) and tables (8.17 and 8.18) both suggest that Broca's region is activated significantly by Circle and Random stimuli, and not activated significantly by Stationary stimuli. This is in line with the idea that Broca's region takes part in geometric shape recognition [64].

In summary, the areas that showed significant activation in this experiment were SI, SII, Brodmann area 4 and Broca's region. Previous studies have found that the middle temporal complex (hMT/V5) is active during tactile motion [58, 142]. However, in the present experiment, activations in this area for the (Circle + Random) vs Stationary contrast were not significant, and below the lowest threshold used ( $p$  value  $\leq 0.009$ , uncorrected).

## 8.8 Summary and Conclusion

The results presented in this chapter demonstrate that the tactile display can deliver distinguishable stimuli in the high magnetic field of an MRI scanner. Subjects' average recognition score inside the MRI scanner room was 83.3%. The operation of the display did not prevent the acquisition of useful fMRI data. From the fMRI analysis, activations were observed in SI, SII, the primary motor cortex and Broca's area. Circle and Random stimuli showed more significant activation than Stationary stimuli.

# **Chapter nine**

## **The Second fMRI Experiment**

## 9.1. Introduction

The sense of touch can be utilized to provide different sorts of information about object movement, like direction, shape (e.g., linear or circular) and speed of motion. The tactile display in the present study has been designed to allow experiments on all of these aspects of the tactile stimulus. This chapter describes an fMRI experiment on the effect of speed. Some previous designs of tactile stimulator have provided moving stimuli at varying speeds, but only a few have been suitable for use in an MRI scanner [160-162]. The sense of tactile movement has been produced with a rotating brush over a fixed location on the skin, or by a rotating drum with raised patterns (usually patterns of dots) [136, 160, 163]. The way in which moving stimuli are presented has an effect on the “feel” of the motion and so will affect the participant’s response [161].

The second fMRI experiment in the present study aims to investigate the relationship between the active areas in the brain and the speed of motion. The tactile stimulus moves in a circle on the fingertip (figure 7.2 a) at four speeds, labelled Very Fast, Medium, Slow and Very Slow; table 8.1 shows the details of the speed parameters. As in the first experiment, a localised sensation on the fingertip is produced by vibration of a pair of adjacent contactors, the contactor pair moves stepwise along an approximately circular trajectory, and the speed is changed by changing the step time. The stimulus moves clockwise; only one starting point for the circle was used in this second experiment.

Table 9.1: The four speeds of tactile movement used in the second fMRI study.

	Time for one circle (s)	Total number of circles	Speed (mm.sec <sup>-1</sup> )
Very Slow	9.0	1	2.9
Slow	3.0	3	8.7
Medium	1.0	9	26.1
Very Fast	0.335	27	77.9

## 9.2. Procedure

In this experiment, participants are asked to identify the speed of the stimulus mentally (to themselves) but are not asked to respond by push button. The idea is to avoid the problems caused in the first experiment by movement of the left hand on the push buttons. The experiment runs in two sessions, each one lasting 16.2 minutes. During each session there are nine examples of each of the four speeds, at an average interval of 27 seconds. Figure 9.1 shows the time sequence of the experiment. The functional sessions were followed by a structural scan; MRI parameters were the same as in the first experiment, with fMRI volumes acquired every 3 seconds.

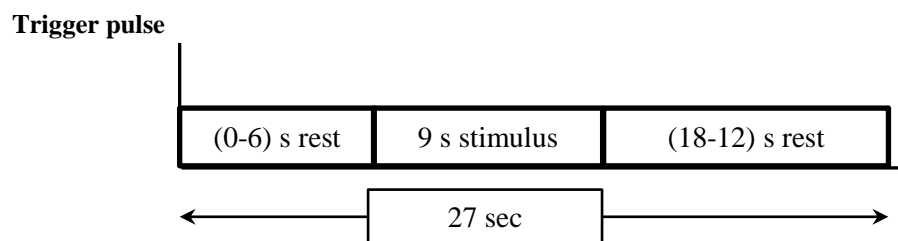


Fig. 9.1: The time sequence of the second fMRI experiment.

Before starting the experiment each participant practised for a few minutes with the tactile display, to learn to distinguish between the different speeds. After entering the MRI scanner, each participant was asked to gently put their fingertip (the index finger of the right hand) on the tactile display, and was asked to:

- 1- Concentrate on feeling the different speeds.
- 2- Focus on the blue circle on the screen.

(The visual display of a blue circle was used in a similar way to the first experiment, to minimise head/eye movement.)

Twelve participants (seven male) took part in the second fMRI experiment, age  $28.4 \pm 5.45$  years, all right handed. Table 9.2 show details of the participants.



Table 9.2: Details of participants in the second fMRI experiment.

Participants	Age	Gender	Handedness
Sub 1	25	F	R
Sub 2	25	M	R
Sub 3	24	F	R
Sub 4	30	M	R
Sub 5	24	M	R
Sub 6	28	F	R
Sub 7	20	F	R
Sub 8	31	F	R
Sub 9	41	M	R
Sub 10	30	M	R
Sub 11	30	M	R
Sub 12	33	M	R

### 9.3. Data analysis

The analysis of the data in the second fMRI experiment is run in two stages (see figure 8.2): the first stage aims to determine the activation areas due to stimuli of each speed, whereas the object of the second stage is to locate the areas that show a relationship (linear or quadratic) between the speed of tactile motion and the strength of activation. The analysis in the first stage followed the same procedure as in the first fMRI experiment.

The second stage of analysis runs to see the effect of increasing speed on the activation of the brain. Each of the predictor variables in the design matrix is weighted according to speed (the higher speed, the larger weighting), as follows: all the rest conditions = zero, Very Fast = 27, Medium = 9, Slow = 3 and Very Slow = 1. After finishing the design matrix, the null hypothesis is tested using a  $t$ -test with different thresholds, with both corrected and uncorrected  $p$  values. As in the first fMRI experiment, the second fMRI experiment utilized ROIs to focus on activity in specific regions in the brain.

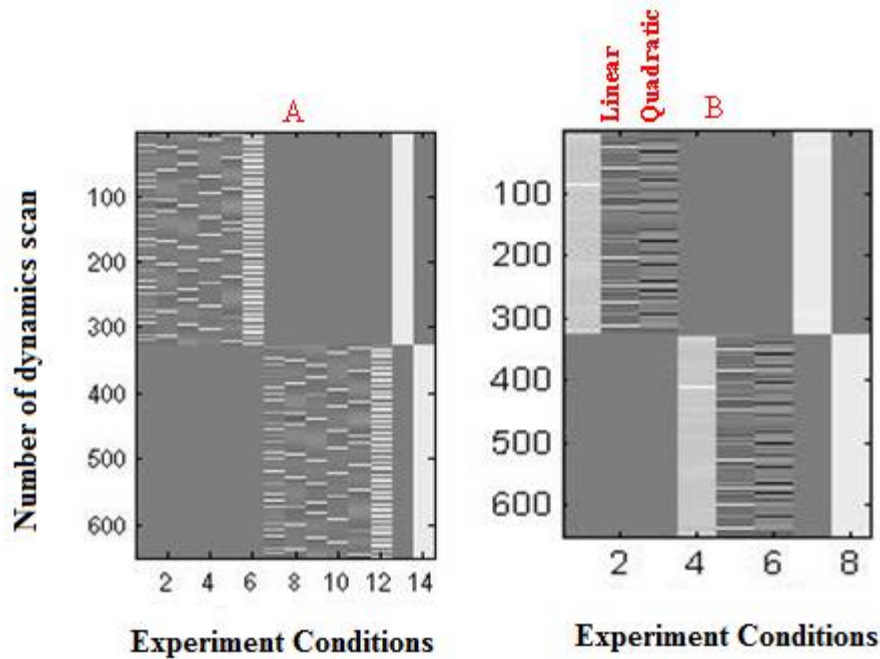


Fig.9.2: The design matrices for analysis in the second fMRI experiment; “A” specifies the experimental conditions; “B” is a design matrix of predictor variables for different speeds; time is represented vertically as the sequence of image dynamics; timings of the four types of stimulus in the first session are represented by the light bands in columns 2 to 5 at the top left of panel A; timing of the four types of stimulus in the second session are represented by the light bands in columns 8 to 11 at the bottom right of panel A; a linear representation of stimulus speed is shown by the grey scale in columns 2 and 5 of panel B; a quadratic representation of stimulus speed is shown by the grey scale in columns 3 and 6 of panel B.

## 9.4. Results and Discussion

Results from an individual-subject analysis for the contrast between stimulus (all speeds) and rest are shown for subject 1 in figure 9.3 (panels A and B), and for other subjects in Appendix F (panels A and B in all figures). Tables 8.3 and 8.4 show the coordinates of the maximum activations, together with statistical measures ( $t$ -value,  $Z$ -score and number of voxels), for all subjects. With tactile stimulation on the right hand, 6 subjects from 12 showed significant left-side activations in both SI and SII (with suggested activation in a further one subject); 4 subjects showed significant right-side activations in SI (with suggested activation in a further one subject); 3 subjects showed significant right-side activation in SII. Five subjects showed no activations in SI or SII for the stimulus (all speeds) vs. rest contrast, but these subjects all showed activation for the Very Fast vs. rest contrast (not shown).

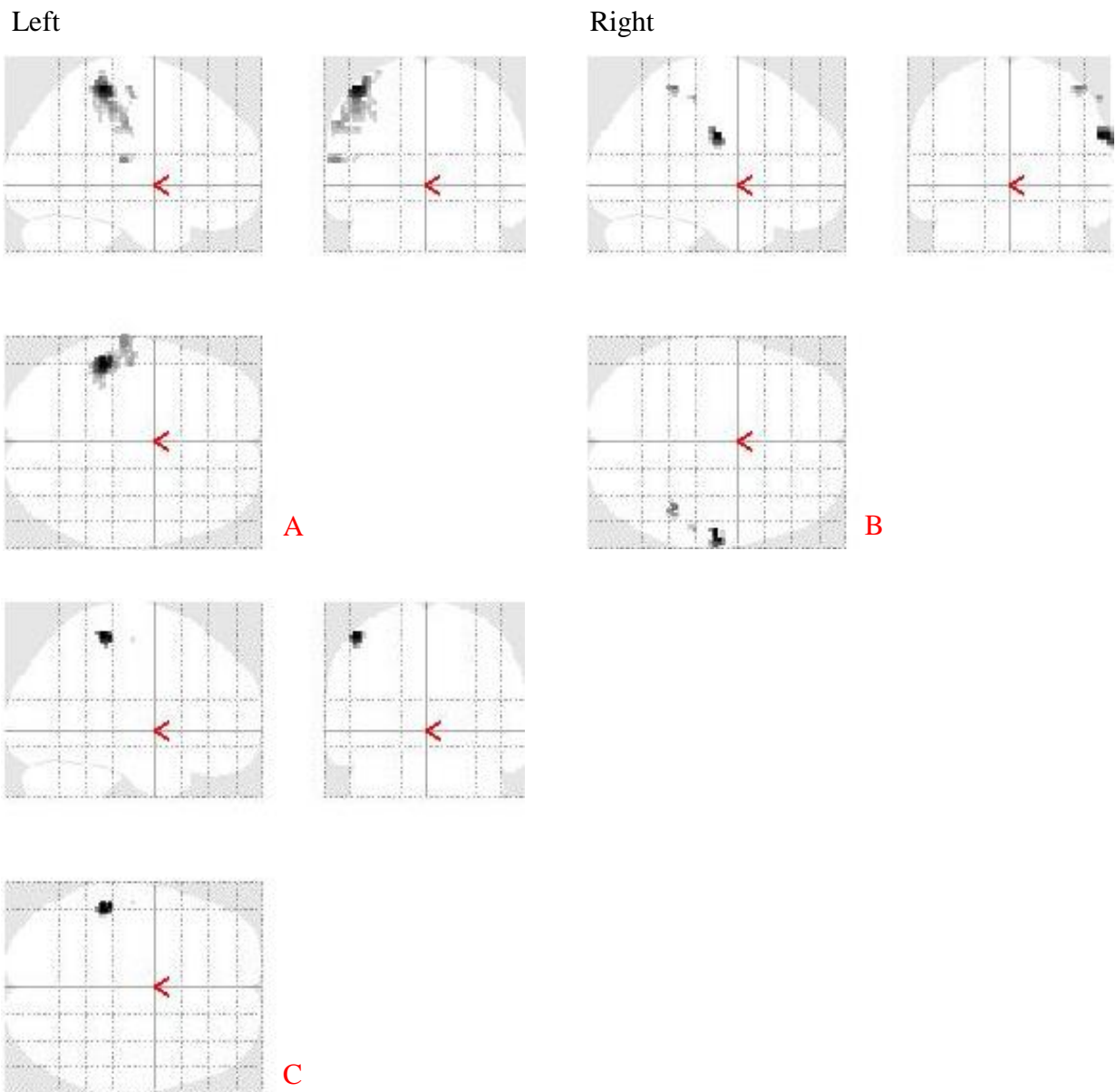


Fig. 9.3: (A, B) Activations in SI and SII for the contrast between stimulus (all speeds) and rest for subject 1 (A: left side, B: right side); threshold corrected with  $p$  value of  $\leq 0.05$ ; (C) brain area (left side) which showed a linear relation between activation and speed; threshold corrected with  $p$  value of  $\leq 0.05$ .

Table 9.3: The coordinates of activations in SI and SII (left side) for the contrast between stimulus (all speeds) and rest, with statistical measures for the active areas ( $t$ -value,  $Z$ -core and number of voxels  $K_E$ ) for all the participants; (\*)  $p \leq 0.001$ , uncorrected; otherwise threshold corrected,  $p \leq 0.05$ .

Statistical parameters Participants	$K_E$	$t$ -value	$Z$ score	MNI coordinates SI & SII
Sub 1	231	9.12	Inf	(-48, -34, 60) BA2
	19	5.97	5.89	(-62, -22, 14) BA40
Sub 2	11	5.34	5.28	(-56, -14, 46) BA3
	11	4.73	4.73	(-64, -20, 14) BA40
Sub 3	----	----	----	----
Sub 4	1205	16.14	Inf	(-54, -18, 50) BA1
	1205	11.04	Inf	(-66, -18, 16) BA43
Sub 5	953	10.76	Inf	(-52, -28, 58) BA1
	16	7.18	7.03	(-56, -14, 18) BA43
Sub 6	---	---	---	---
Sub 7	---	---	---	---
Sub 8	347	6.32	6.22	(-20, -32, 64) BA3
	88	6.47	6.36	(-66, -14, 18) BA43
Sub 9	---	---	---	----
Sub 10	3*	3.28*	3.27*	(-50, -26, 60)* BA1
	6*	3.53*	3.51*	(-64, -10, 16)* BA43
Sub 11	---	---	---	---
Sub 12	297	8.38	5.97	(-54, -26, 54) BA2
	38	5.48	5.42	(-66, -18, 16) BA43

Table 9.4: The coordinates of activations in SI and SII (right side) for the contrast between stimulus (all speeds) and rest, with statistical measures for the active areas ( $t$ - value,  $Z$ - core and number of voxels  $K_E$ ) for all the participants; (\*)  $p \leq 0.001$ , uncorrected.

Statistical parameters Participants	$K_E$	$t$ -value	$Z$ score	MNI coordinates SI & SII
Sub 1	49	6.83	6.70	(60, -16, 30) BA3
Sub 2	7*	3.36*	3.34*	(58, -20, 50)* BA1
Sub 3	---	---	---	---
Sub 4	1493	14.85	Inf	(56, -28, 54) BA2
	28	7.73	7.54	(58, -14, 18) BA43
Sub 5	131	4.52	4.48	(54, -26, 52) BA2
Sub 6	---	---	---	---
Sub 7	---	---	---	---
Sub 8	7	5.17	5.11	(58, -18, 46) BA1
	13	4.46	4.42	(56, -16, 18) BA43
Sub 9	---	---	---	---
Sub 10	---	---	---	---
Sub 11	---	---	---	---
Sub 12	14	5.03	4.97	(66,-46, 22) BA40

Seven participants showed significant left-side activation in SI and/or SII which represented a linear relationship with stimulus speed (with suggested linear SII activation in a further one subject). This is shown for subject 1 in figure 4 (panel C), and for other subjects in Appendix F (panel C in all figures). Table 8.5 shows the coordinates of the maximum activations, together with statistical measures ( $t$ -value,  $Z$ -score and number of voxels), for all subjects. One participant showed significant activation in both SI and SII, five in SI only and one in SII only. Generally, the areas that showed a linear relationship are smaller than the areas for the stimulus (all speeds) vs. rest contrast. The group analysis for both contrasts (all speeds vs. rest and linear relationship with stimulus speed) showed no significant activations (only one voxel at a  $p$ -value of  $\leq 0.001$ , uncorrected), indicating that there was no consistent pattern in the observed single-subject activations in SI and/or SII).

The quadratic relation between stimulus speed and activation was also tested for, but no significant activations were found in the group analysis, or in any of the single-subject analyses.

Table 9.5: The coordinates of areas in SI and SII which show a linear relation between activation and speed, together with statistical measures of the active areas ( $t$ -value,  $Z$ -score and number of voxels  $K_E$ ) for all the participants; (\*)  $p \leq 0.001$ , uncorrected.

Statistical parameters Participants	$K_E$	$t$ -value	$Z$ score	MNI coordinates SI & SII
Sub 1	45	5.01	4.96	(-50, -32, 58) BA2
Sub 2	6	4.49	4.45	(-66, -18, 14) BA43
	----	----	----	-----
Sub 3	----	---	----	-----
Sub 4	368	8.54	Inf	(-56, -14, 50) BA3
	54	6.12	6.03	(-50, -18, 16) BA43
Sub 5	53	5.66	5.59	(-52, -26, 58) BA1
Sub 6	----	----	----	----
Sub 7	----	----	----	----
Sub 8	19	5.27	5.21	(-40, -30, 56) BA3
Sub 9	164	5.57	5.50	(-52, -32, 56) BA2
Sub 10	----	----	----	-----
Sub 11	6*	3.66*	3.64*	(-54, -16, 18)* BA43
Sub 12	106	4.38	4.35	(-54, -26, 54) BA2

For all contrasts investigated, left side activations were generally stronger than right side activations, as expected for stimulation on the right hand. As discussed in chapter 7, this was not the case for the results from the first fMRI experiment, where left-hand push buttons were used. The decision not to use push buttons in the second experiment is probably the reason for the difference.

Results on the effect of stimulus speed are difficult to interpret in relation to previous studies – as mentioned in the introduction to this chapter; the type of stimulator has an effect on the “feel” of the motion and so may affect the observed activations. The present findings showed a linear relationship between the speed and the strength of activation, mostly in the left side primary somatosensory cortex (SI); activations in SI were in different locations (BA1, BA2 and BA3) in different subjects, causing a weak activation in the group analysis. DiCarlo et al, found that the firing rates of neurons in BA3b of SI increase with increase in rotation speed of a drum stimulator [164]. Sinclair and Burton, in a study on monkeys, found small area in

SI which in which some cells had a significant correlation with speed [165]. In both studies, the motion-sensitive area was small – as observed in the present study. The quadratic relation between stimulus speed and activation was also tested for, but the analysis did not show any significant activations.

## 9.5 Summary

The experiment described in this chapter has demonstrated the ability of the tactile display to produce stimulation with different speeds. An fMRI analysis was run to study the brain response to tactile simulation with different speeds. In 7 of the 12 subjects, small regions in SI and/or SII demonstrated a linear relation between the activation in the brain and the speed of tactile motion.

## **Chapter ten**

# Conclusions and Future work



## 10.1 Introduction

The main focus of the present research was to build and evaluate a novel tactile display system with a wide range of possible applications. Features of the system include 25 contactors at 2 mm spacing, stimulation with variable amplitudes and frequencies, in addition to easy control and programming using any personal computer (PC). The present research includes three experiments, one psychophysics experiment and two fMRI experiments; a general discussion of these studies is in the following sections.

The tactile-display system developed in the present study has the ability to produce a wide range of tactile patterns, in contrast to some other systems [53, 54, 166] which are limited in this respect. The tactile patterns each consist of a sequence of “frames” on the 25-element array, which has 2-mm resolution. There are no constraints on the spatial distribution of stimulation within a frame, or on the relation between one frame and next. The display is thus particularly suitable for representing different types of stimulus movement – an aspect which is not available from some previous designs [167]. No magnetic materials are used in the design of the tactile array, so the system can be used to study the function of the brain using the fMRI technique – some tactile displays [55] do not allow this. Perhaps the closest relation to the present device is the system [56] developed in Exeter over ten years ago – the present device represents a considerable advance in terms of ease of programming, ease of interfacing, portability and MRI compatibility.

## 10.2 Psychophysics experiment

The main purpose of this experiment is to examine the ability of the tactile display system to produce different sort of tactile patterns, and investigate whether these patterns can be recognised by a test subject. The results showed that the tactile display system is successful and can be used for a psychophysics experiment. The confusion matrix for subjects’ responses (Chapter 7, figure 7.6) shows around 82% correct for the three types of stimulation (Circle, Random and Stationary) after only a few minutes’ practice. More than half of the participants (four from seven) scored 100% correct response; the other three participants averaged around 55% correct and it is likely that they would produce higher scores if given additional training. The overall recognition score for the tactile stimuli was 82% and the kappa statistic (subject agreement) was 0.73. These two figures can be improved, as mentioned above, by giving the participants more time to practice – for most of them this was the first time they had experienced this type of perception. Ability to produce

different types of tactile patterns. Nevertheless, this experiment successfully validated the tactile display in terms of its capability to produce a range of distinguishable, moving tactile patterns.

### 10.3 First fMRI experiment

The good performance of the tactile display in the psychophysics experiment gave confidence to run the first fMRI experiment. The difficulty of performing tactile fMRI studies comes from the interaction between the tactile system and the high magnetic field of the scanner – the tactile display which was built in present study uses piezoelectric bimorphs which are largely unaffected by the magnetic field and do not interfere with the uniformity of the field or the radio frequency signals that are used during imaging.

Before running the first fMRI experiment, a preliminary experiment was run to check the above statement (see Chapter 7, figures 7.7 and 7.8). No image artefacts or noise problems were observed when using the tactile display in the MRI scanner, and it was concluded that the tactile display is suitable to use in fMRI experiments. Using the same protocol as that used in the psychophysics experiment, with some minor modifications, the first fMRI experiment was run. The author is not aware of an equivalent study in the existing literature. Figures 8.4 and 8.5 (Chapter 8) show the percentage correct responses and confusion matrix, respectively, proving that the tactile display is capable of generating stimulus patterns and participants can recognise these patterns with good accuracy, even inside the MRI scanner.

#### 10.3.1 Primary and secondary somatosensory cortex

Both SI and SII take part in first stages of tactile perception [167]; therefore these regions were studied in detail. The results for the contrast between the two types of moving stimulation (Circle or Random) and the Rest condition show significant activations in SI and SII (right and left side) at a corrected  $p$  value of  $\leq 0.05$  (Chapter 8, Tables 8.2 to 8.5). Generally, SI shows more activation than SII – stimuli are presented at 40 Hz, and low-frequency stimulation is known to produce less activation in SII than higher frequencies [149, 150, 168]. The Stationary stimulation produces less activation in SI and SII than the two types of moving stimulation, even at an uncorrected  $p$  value of  $\leq 0.001$  or  $\leq 0.009$ , see Tables 8.6 and 8.7 (Chapter 8). This may indicate sensitivity to movement, but results may also be affected by the small area that is stimulated for the Stationary stimuli (only 4/25 of the contactors are used).

The above discussion reviews the results of the individual-subject analysis – the group analysis (Chapter 8, Tables 8.8 to 8.13) is compatible with individual results. Activations on the right side of the brain are similar to those on the left side – this is surprising because stimulation on the right hand is expected to produce more left-side activations in SI and SII. It is likely that right-side activations are affected by participants moving their left-hand fingers over the response push buttons during the stimulation period. Push-button response was not used in the second fMRI experiment.

### 10.3.2 Primary motor region (M1) and Broca's Region

Although there is no physical movement of the participant's finger during the experiment, a sensation of movement on the fingertip is produced by the Circle and Random stimuli. The primary motor cortex was investigated for the contrast between Circle, Random and Stationary stimuli. Some weak activations were observed (at uncorrected  $p$  values of  $\leq 0.001$  or  $0.009$ ), see Tables 8.14 to 8.16 (Chapter 8). It seems that Random stimuli produce more activations than Circle stimuli, possibly because the speed of movement over the tactile display is faster for the Random stimuli.

Brodman area 44, which is called Broca's region, is involved in several brain functions including shape recognition [64]. Broca's region was more active in the Circle vs. Stationary contrast than in the Random vs. Stationary contrast (Chapter 8, Tables 8.17 and 8.18); this may be because the Circle stimuli provide a well-defined shape.

## 10.4 Second fMRI experiment

The first fMRI study proved the tactile stimulator can produce various types of tactile patterns which can be used in fMRI research – the tactile stimuli are easily controlled and well specified. These results encouraged us to run the second fMRI study. The aim of the second fMRI experiment was to study the relation between the speed of tactile motion and brain activation. The author is not aware of an equivalent study in the existing literature. Circle stimuli were used, with the stimulus moving over the display at four different speeds in the range  $2.9$  to  $77.9 \text{ mm s}^{-1}$ . The first stage of data analysis (Chapter 9, Tables 9.3 and 9.4) showed that 8 participants (from 12) had activations in SI and/or SII (left side) for the contrast between stimulus and rest (threshold corrected with  $p$  value of  $\leq 0.05$ ); in the second stage of data analysis (Chapter 9, Table 9.6), ten participants showed a linear relation

between speed and brain activation in SI and/or SII. The motion-sensitive areas were small, less than the areas activated for the stimulus vs. rest contrast.

The above discussion reviews the results of the individual-subject analysis – the group analysis (Chapter 9, Table 9.5) showed weaker activations than the individual-subject results, probably because the individual activations were in different locations (BA1, BA2 and BA3) in different subjects.

Attention during the fMRI experiment is one of the important factors that affect the results and during this experiment subjects did not use the response button – this may reduce some of the attention of participants to the range of stimulus speed and so reduce the activation in the brain.

The lowest speed used was 2.9 cm s<sup>-1</sup> which may give some sensation of motion and hence may not provide an appropriate “zero speed” endpoint to the stimulus set – the experiment might be improved by using the Stationary stimulus from the first fMRI study (see 7.1 and figure 7.2 a) to provide more contrast in speed over the stimulus set.

## 10.5 Evaluation of the tactile display

The tactile display system has the ability to produce a wide variety of time-varying spatial patterns of touch stimulation on the fingertip. It easy to specify these patterns in software, and the system is easy to control and synchronise with other devices. These patterns are easy to detect and a wide range of touch sensations can be provided to the test subject. The sensation is “natural” and test subjects do not find the experience unpleasant. The present system provides stimulation at a preset amplitude and frequency in the range 25 to 200 Hz. Possible improvements would be:

- (1) the ability to change the stimulus amplitude and frequency under software control;
- (2) the ability to have different frequencies and amplitudes on the display at the same time, distributed over the different contactors;
- (3) the ability to use stimulation frequencies up to 500 Hz (the mechanism of the current stimulator does not operate well at frequencies above 200 Hz).

## 10.5 Future work

The brain activations observed in the two fMRI experiments were not as consistent as had been hoped. For example, in the first fMRI experiment, significant left-side SII activation for the Circle/Rest contrast was only observed in 6 subjects from 11 (Table 8.3), despite the fact that all subjects adequately performed the recognition task which presumably required involvement of SII. [Similarly, in the second fMRI experiment, no significant left-side SI or SII activation was found in 6 of the 12 subjects (Table 8.3).] It seems likely that this problem relates to the quality of the fMRI data rather than to the operation of the tactile display – use of a 3T imager, with much improved signal-to-noise ratio, would allow this idea to be tested (see below).

All subjects in the second fMRI experiment were right-handed (see table 9.2). However, one subject in the first fMRI experiment (see table 8.1) and one in the psychophysics experiment (see table 7.1) were left-handed. These left-handed subjects had to use their dominant hand to operate the response buttons, with stimulation on the non-dominant hand; it is possible that this resulted in different patterns of brain activation to right-handed subjects. For future experiments, it is recommended that all subjects should have the same handedness.

An additional possibility for the fMRI data analysis is to include the six movement variables as additional regressors in the SPM analysis – in principle this should improve the statistical significance of activations by reducing the residual variance in the data; however, observed movements in the present study were small (translations less than 3 mm and rotations less than 1.5 degrees).

The tactile display system offers many possibilities for psychophysics or functional imaging experiments. At present, for fMRI it has only been used in the 1.5 T MRI scanner at the Exeter MR Research Centre, and it is well known that fMRI experiments are easier to carry out in higher fields (e.g., 3 T) for which the signal-to-noise ratio is higher. Future work should include fMRI experiments similar to those in the present study, but at higher fields. Two identical tactile display systems have been constructed (see figure 9 in chapter 6), and it is hoped these can be used at other research sites. The availability of two displays also suggests the possibility of psychophysics or functional studies with stimulation of two fingers, to see how participants respond to different tactile patterns run simultaneously on two fingers, or one pattern moving between the two displays.

# Bibliography

## Bibliography

1. Wang, Z.X., et al., *Autologous nerve implantation into denervated monkey skin promotes regeneration of Meissner's corpuscle*. Medical science monitor: international medical journal of experimental and clinical research, 2011. **17**(12): p. BR377.
2. Vega, J.A., et al., *The Meissner and Pacinian sensory corpuscles revisited new data from the last decade*. Microscopy research and technique, 2009. **72**(4): p. 299-309.
3. Bruce, M. and D. Sinclair, *The relationship between tactile thresholds and histology in the human finger*. Journal of Neurology, Neurosurgery & Psychiatry, 1980. **43**(3): p. 235-242.
4. Toma, S. and Y. Nakajima, *Response characteristics of cutaneous mechanoreceptors to vibratory stimuli in human glabrous skin*. Neuroscience letters, 1995. **195**(1): p. 61-63.
5. Hamann, W., *Mammalian cutaneous mechanoreceptors*. Progress in biophysics and molecular biology, 1995. **64**(1): p. 81.
6. Bhat, G.M., et al., *Density And Structural Variations Of Meissner's Corpuscle At Different Sites In Human Glabrous Skin*. J. Anat. Soc. India, 2008. **57**(1): p. 30-33.
7. Cauna, N., *Structure and origin of the capsule of Meissner's corpuscle*. The Anatomical Record, 1956. **124**(1): p. 77-93.
8. Ogawa, H., *The Merkel cell as a possible mechanoreceptor cell*. Progress in neurobiology, 1996. **49**(4): p. 317-334.
9. Lucarz, A. and G. Brand, *Current considerations about Merkel cells*. European Journal of Cell Biology, 2007. **86**(5): p. 243-251.
10. Halata, Z., M. Grim, and K.I. Bauman, *Friedrich Sigmund Merkel and his "Merkel cell", morphology, development, and physiology: review and new results*. The Anatomical Record Part A: Discoveries in Molecular, Cellular, and Evolutionary Biology, 2003. **271**(1): p. 225-239.
11. Moll, I., et al., *Human Merkel cells-aspects of cell biology, distribution and functions*. European Journal of Cell Biology, 2005. **84**(2-3): p. 259-271.
12. Whitear, M. and E.B. Lane, *Fine structure of Merkel cells in lampreys*. Cell and Tissue Research, 1981. **220**(1): p. 139-151.
13. Haeberle, H. and E.A. Lumpkin, *Merkel cells in somatosensation*. Chemosensory perception, 2008. **1**(2): p. 110-118.
14. Leventhall, G., *Low Frequency Noise. What we know, what we do not know, and what we would like to know*. Low Frequency Noise, Vibration and Active Control, 2009. **28**(2): p. 79-104.
15. Paré, M., C. Behets, and O. Cornu, *Paucity of presumptive ruffini corpuscles in the index finger pad of humans*. The Journal of comparative neurology, 2003. **456**(3): p. 260-266.
16. Maeda, T., et al., *The Ruffini ending as the primary mechanoreceptor in the periodontal ligament: its morphology, cytochemical features, regeneration, and development*. Critical Reviews in Oral Biology & Medicine, 1999. **10**(3): p. 307-327.
17. Howe, R.D., *Tactile sensing and control of robotic manipulation*. Advanced Robotics, 1993. **8**(3): p. 245-261.
18. CHUANG, K.-H., et al., *IMAGE ANALYSIS OF FUNCTIONAL MAGNETIC RESONANCE IMAGING*. Biomedical Engineering: Applications, Basis and Communications, 2001. **13**(5): p. 248-255.
19. Halata, Z. and B.L. Munger, *Identification of the Ruffini corpuscle in human hairy skin*. Cell and Tissue Research, 1981. **219**(2): p. 437-440.
20. Hamann, W. and A. Iggo, *Ruffini corpuscle-a stretch receptor in the connective tissue of the skin and locomotion apparatus*. Transduction and cellular mechanisms in sensory receptors, 1988. **74**: p. 221.
21. Holmes, M.H. and J. Bell, *A model of a sensory mechanoreceptor derived from homogenization*. SIAM Journal on Applied Mathematics, 1990: p. 147-166.
22. Bentivoglio, M. and P. Pacini, *Filippo Pacini: a determined observer*. Brain research bulletin, 1995. **38**(2): p. 161-165.

23. Spencer, P.S. and H.H. Schaumburg, *An ultrastructural study of the inner core of the Pacinian corpuscle*. Journal of neurocytology, 1973. **2**(2): p. 217-235.
24. Bell, J., S. Bolanowski, and M.H. Holmes, *The structure and function of Pacinian corpuscles: A review*. Progress in neurobiology, 1994. **42**(1): p. 79-128.
25. Halata, Z., *The ultrastructure of the sensory nerve endings in the articular capsule of the knee joint of the domestic cat (Ruffini corpuscles and Pacinian corpuscles)*. Journal of anatomy, 1977. **124**(Pt 3): p. 717.
26. Cauna, N. and G. Mannan, *The structure of human digital Pacinian corpuscles (corpuscula lamellosa) and its functional significance*. Journal of anatomy, 1958. **92**(Pt 1): p. 1.
27. Pauling, L. and C.D. Coryell, *The magnetic properties and structure of hemoglobin, oxyhemoglobin and carbonmonoxyhemoglobin*. Proceedings of the National Academy of Sciences of the United States of America, 1936. **22**(4): p. 210.
28. Bolanowski Jr, S.J., et al., *Four channels mediate the mechanical aspects of touch*. The Journal of the Acoustical society of America, 1988. **84**: p. 1680.
29. Wu, G., et al., *Clustering of Pacinian corpuscle afferent fibres in the human median nerve*. Experimental brain research, 1999. **126**(3): p. 399-409.
30. Johansson, R.S., *Tactile sensibility in the human hand: receptive field characteristics of mechanoreceptive units in the glabrous skin area*. The Journal of physiology, 1978. **281**(1): p. 101-125.
31. Benarroch, E.E., *Basic neurosciences with clinical applications*2006: Butterworth-Heinemann.
32. Kandel, E.R., J.H. Schwartz, and T.M. Jessell, *Principles of neural science*. Vol. 4. 2000: McGraw-Hill New York.
33. Martin, J.H., *Neuroanatomy: text and atlas*2003: McGraw-Hill Medical.
34. Laming, P.R., et al., *Neuronal-glia interactions and behaviour*. Neuroscience & Biobehavioral Reviews, 2000. **24**(3): p. 295-340.
35. Choe, S., *Potassium channel structures*. Nature Reviews Neuroscience, 2002. **3**(2): p. 115-121.
36. Yellen, G., *The moving parts of voltage-gated ion channels*. Quarterly reviews of biophysics, 1998. **31**(3): p. 239-295.
37. HAAS, J.H., *Somatosensory System CH. 30*. The human nervous system, ed. G. Paxinos and J.K. Mai2004: Elsevier Academic Press London.
38. Peters, M., et al., *Unsolved problems in comparing brain sizes in Homo sapiens*. Brain and cognition, 1998. **37**(2): p. 254-285.
39. Fischl, B. and A.M. Dale, *Measuring the thickness of the human cerebral cortex from magnetic resonance images*. Proceedings of the National Academy of Sciences, 2000. **97**(20): p. 11050.
40. Kwong, K.K., et al., *Dynamic magnetic resonance imaging of human brain activity during primary sensory stimulation*. Proceedings of the National Academy of Sciences, 1992. **89**(12): p. 5675-5679.
41. Brodmann, K. and L. Garey, *Brodmann's Localisation in the cerebral cortex: the principles of comparative localisation in the cerebral cortex based on the cytoarchitectonics*2006: Springer Verlag.
42. Thottakara, P., et al., *Application of Brodmann's area templates for ROI selection in white matter tractography studies*. Neuroimage, 2006. **29**(3): p. 868-878.
43. Ploner, M., et al., *Differential organization of touch and pain in human primary somatosensory cortex*. Journal of neurophysiology, 2000. **83**(3): p. 1770-1776.
44. Geyer, S., A. Schleicher, and K. Zilles, *Areas 3a, 3b, and 1 of Human Primary Somatosensory Cortex:: 1. Microstructural Organization and Interindividual Variability*. Neuroimage, 1999. **10**(1): p. 63-83.
45. Eickhoff, S.B., et al., *The somatotopic organization of cytoarchitectonic areas on the human parietal operculum*. Cerebral Cortex, 2007. **17**(8): p. 1800-1811.



46. Eickhoff, S.B., et al., *The human parietal operculum. II. Stereotaxic maps and correlation with functional imaging results*. Cerebral Cortex, 2006. **16**(2): p. 268-279.
47. Eickhoff, S.B., et al., *The human parietal operculum. I. Cytoarchitectonic mapping of subdivisions*. Cerebral Cortex, 2006. **16**(2): p. 254-267.
48. Andersen, R.A. and C.A. Buneo, *Intentional maps in posterior parietal cortex*. Annual Review of Neuroscience, 2002. **25**(1): p. 189-220.
49. Andersen, R.A. and C.A. Buneo, *Sensorimotor integration in posterior parietal cortex*. Advances in neurology, 2003. **93**: p. 159.
50. Andersen, R.A., et al., *Multimodal representation of space in the posterior parietal cortex and its use in planning movements*. Annual Review of Neuroscience, 1997. **20**(1): p. 303-330.
51. Israr, A. and I. Poupyrev. *Tactile brush: Drawing on skin with a tactile grid display*. in *Proceedings of the 2011 annual conference on Human factors in computing systems*. 2011. ACM.
52. Gault, R.H., *"Hearing" through the sense organs of touch and vibration*. Journal of the Franklin Institute, 1927. **204**(3): p. 329-358.
53. Harrington, G.S., C.T. Wright, and J.H. Downs, *A new vibrotactile stimulator for functional MRI*. Human brain mapping, 2000. **10**(3): p. 140-145.
54. Briggs, R.W., et al., *A pneumatic vibrotactile stimulation device for fMRI*. Magnetic resonance in medicine, 2004. **51**(3): p. 640-643.
55. Killebrew, J.H., et al., *A dense array stimulator to generate arbitrary spatio-temporal tactile stimuli*. Journal of neuroscience methods, 2007. **161**(1): p. 62-74.
56. Summers, I.R. and C.M. Chanter, *A broadband tactile array on the fingertip*. The Journal of the Acoustical society of America, 2002. **112**: p. 2118.
57. Summers, I.R., et al. *Results from a Tactile Array on the Fingertip*. in *Proceedings of Eurohaptics 2001*. 2001. DTIC Document.
58. Summers, I.R., et al., *A functional-magnetic-resonance-imaging investigation of cortical activation from moving vibrotactile stimuli on the fingertip*. The Journal of the Acoustical society of America, 2009. **125**: p. 1033.
59. Chouvardas, V., A. Miliou, and M. Hatalis, *Tactile displays: Overview and recent advances*. Displays, 2008. **29**(3): p. 185-194.
60. Kajimoto, H., et al., *Smarttouch: Electric skin to touch the untouchable*. Computer Graphics and Applications, IEEE, 2004. **24**(1): p. 36-43.
61. Craig, J.C., *Identification of scanned and static tactile patterns*. Perception & psychophysics, 2002. **64**(1): p. 107-120.
62. Master, S., M. Larue, and F. Tremblay, *Characterization of human tactile pattern recognition performance at different ages*. Somatosensory & Motor Research, 2010. **27**(2): p. 60-67.
63. Johnson, K.O. and J.R. Phillips, *A rotating drum stimulator for scanning embossed patterns and textures across the skin*. Journal of neuroscience methods, 1988. **22**(3): p. 221-231.
64. Savini, N., et al., *Passive tactile recognition of geometrical shape in humans: An fMRI study*. Brain research bulletin, 2010. **83**(5): p. 223-231.
65. Reed, C.L., S. Shoham, and E. Halgren, *Neural substrates of tactile object recognition: An fMRI study*. Human brain mapping, 2004. **21**(4): p. 236-246.
66. Hao, Y., et al., *Novel MRI-compatible tactile stimulator for cortical mapping of foot sole pressure stimuli with fMRI*. Magnetic resonance in medicine, 2012.
67. Lozano, C.A., K.A. Kaczmarek, and M. Santello, *Electrotactile stimulation on the tongue: Intensity perception, discrimination, and cross-modality estimation*. Somatosensory & Motor Research, 2009. **26**(2-3): p. 50-63.
68. Kinoshita, H., et al., *Functional brain areas used for the lifting of objects using a precision grip: a PET study*. Brain research, 2000. **857**(1-2): p. 119.
69. Jousmäki, V. and R. Hari, *Somatosensory evoked fields to large-area vibrotactile stimuli*. Clinical neurophysiology, 1999. **110**(5): p. 905-909.

70. Bloch, F., W. Hansen, and M. Packard, *The nuclear induction experiment*. Physical Review, 1946. **70**(7-8): p. 474-485.
71. Purcell, E.M., H. Torrey, and R.V. Pound, *Resonance absorption by nuclear magnetic moments in a solid*. Physical Review, 1946. **69**(1-2): p. 37.
72. Gordon, R., *Magnets, molecules and medicine*. Physics in medicine and biology, 2000. **30**(8): p. 741.
73. Lauterbur, P.C., *Image formation by induced local interactions: examples employing nuclear magnetic resonance*. Nature, 1973. **242**(5394): p. 190-191.
74. Mansfield, P. and A. Maudsley, *Medical imaging by NMR*. British Journal of Radiology, 1977. **50**(591): p. 188-194.
75. Edelstein, W., et al., *Spin warp NMR imaging and applications to human whole-body imaging*. Physics in medicine and biology, 2000. **25**(4): p. 751.
76. Rodriguez, A., *Principles of magnetic resonance imaging*. Revista mexicana de física, 2004. **50**(003): p. 272–286.
77. Longmore, D., *The principles of magnetic resonance*. British medical bulletin, 1989. **45**(4): p. 848-880.
78. Gossuin, Y., et al., *Physics of magnetic resonance imaging: from spin to pixel*. J. Phys. D: Appl. Phys, 2010. **43**: p. 213001.
79. Lepage, M. and J. Gore. *Contrast mechanisms in magnetic resonance imaging*. in *Journal of Physics: Conference Series*. 2004. IOP Publishing.
80. Madhu, P. and A. Kumar, *Bloch equations revisited: New analytical solutions for the generalized Bloch equations*. Concepts in Magnetic Resonance, 1997. **9**(1): p. 1-12.
81. Hendee, W.R. and C.J. Morgan, *Magnetic Resonance Imaging Part I—Physical Principles*. Western Journal of Medicine, 1984. **141**(4): p. 491.
82. McRobbie, D.W., et al., *MRI from Picture to Proton*. second ed2007: Cambridge University Press.
83. Fullerton, G.D., *Basic concepts for nuclear magnetic resonance imaging*. Magnetic resonance imaging, 1982. **1**(1): p. 39-53.
84. Brown, M.A. and R.C. Semelka, *MRI: basic principles and applications*. third ed2003: Wiley and Sons.
85. Bernstein, M.A., K.F. King, and X.J. Zhou, *Handbook of MRI pulse sequences*2004: Academic Press.
86. Westbrook, C., C.K. Roth, and J. Talbot, *MRI in Practice*. third ed2005: Wiley-Blackwell.
87. Heeger, D.J. and D. Ress, *What does fMRI tell us about neuronal activity?* Nature Reviews Neuroscience, 2002. **3**(2): p. 142-151.
88. *fMRI Techniques and Protocols*. First ed., ed. M. Filippi2009, Humana Press.
89. Logothetis, N.K. and B.A. Wandell, *Interpreting the BOLD signal*. Annu. Rev. Physiol., 2004. **66**: p. 735-769.
90. by: Scott A. Huettel, Allen W. Song, and G. McCarthy, *Functional Magnetic Resonance Imaging*. first ed2004: Sinauer Associates, Inc.
91. Williams, D.S., et al., *Magnetic resonance imaging of perfusion using spin inversion of arterial water*. Proceedings of the National Academy of Sciences, 1992. **89**(1): p. 212-216.
92. Nair, D.G., *About being BOLD*. Brain Research Reviews, 2005. **50**(2): p. 229-243.
93. Thulborn, K.R., et al., *Oxygenation dependence of the transverse relaxation time of water protons in whole blood at high field*. Biochimica et Biophysica Acta (BBA)-General Subjects, 1982. **714**(2): p. 265-270.
94. Ogawa, S., et al., *Intrinsic signal changes accompanying sensory stimulation: functional brain mapping with magnetic resonance imaging*. Proceedings of the National Academy of Sciences, 1992. **89**(13): p. 5951-5955.

95. Buxton, R.B. and L.R. Frank, *A model for the coupling between cerebral blood flow and oxygen metabolism during neural stimulation*. Journal of Cerebral Blood Flow & Metabolism, 1997. **17**(1): p. 64-72.
96. Licht, J., et al., *Interactions between electrical activity and cortical microcirculation revealed by imaging spectroscopy: implications for functional brain mapping*. Science, 1996. **272**: p. 551.
97. Logothetis, N.K., *The underpinnings of the BOLD functional magnetic resonance imaging signal*. The Journal of Neuroscience, 2003. **23**(10): p. 3963-3971.
98. Buxton, R.B., *The elusive initial dip*. Neuroimage, 2001. **13**: p. 953-958.
99. PETER JEZZARD, PAUL M. MATTHEWS, and a.S.M. SMITH, eds. *Functional MRI: An Introduction to Methods*. First ed. 2001, University of Oxford, UK.
100. Buxton, R., et al. *BOLD signal dynamics: the balloon model with viscoelastic effects*. in *Sixth Meeting, International Society for Magnetic Resonance in Medicine, Sydney, Australia*. 1998.
101. van Zijl, P., J. Hua, and H. Lu, *The BOLD post-stimulus undershoot, one of the most debated issues in fMRI*. Neuroimage, 2012.
102. de Zwart, J.A., et al., *Application of sensitivity-encoded echo-planar imaging for blood oxygen level-dependent functional brain imaging†*. Magnetic resonance in medicine, 2002. **48**(6): p. 1011-1020.
103. Weishaupt, D., V.D. Köchli, and B. Marincek, *How does MRI work?: an introduction to the physics and function of magnetic resonance imaging*. second ed 2006: Springer.
104. Chee, M.W.L., et al., *Comparison of block and event-related fMRI designs in evaluating the word-frequency effect*. Human brain mapping, 2003. **18**(3): p. 186-193.
105. Poustchi-Amin, M., et al., *Principles and Applications of Echo-planar Imaging: A Review for the General Radiologist*. Radiographics, 2001. **21**(3): p. 767-779.
106. Erasmus, L., et al., *A short overview of MRI artefacts*. South African Journal of Radiology, 2009. **8**(2).
107. Hood, M.N., et al., *Chemical shift: the artifact and clinical tool revisited*. Radiographics, 1999. **19**(2): p. 357-371.
108. Buxton, R.B., *Introduction to functional magnetic resonance imaging: principles and techniques* 2002: Cambridge University Press.
109. Ashburner, J., *SPM: a history*. Neuroimage, 2012. **62**: p. 791-800.
110. Lindquist, M.A., *The statistical analysis of fMRI data*. Statistical Science, 2008. **23**(4): p. 439-464.
111. Oakes, T., et al., *Comparison of fMRI motion correction software tools*. Neuroimage, 2005. **28**(3): p. 529-543.
112. Khullar, S., et al., *ICA-fNORM: Spatial normalization of fMRI data using intrinsic group-ICA networks*. Frontiers in systems neuroscience, 2011. **5**.
113. Hammers, A., et al., *Implementation and application of a brain template for multiple volumes of interest*. Human brain mapping, 2002. **15**(3): p. 165-174.
114. Chau, W. and A.R. McIntosh, *The Talairach coordinate of a point in the MNI space: how to interpret it*. Neuroimage, 2005. **25**(2): p. 408.
115. Matthew Brett, Ingrid S. Johnsrude, and A.M. Owen, *The problem of functional localization in the human brain*. Nature Reviews Neuroscience, 2002. **3**: p. 243-249.
116. Poldrack, R.A., J.A. Mumford, and T.E. Nichols, *Handbook of functional mri data analysis*. first ed 2011: Cambridge University Press.
117. Carmack, P.S., et al., *Improved agreement between Talairach and MNI coordinate spaces in deep brain regions*. Neuroimage, 2004. **22**(1): p. 367-371.
118. Matsushashi, M., et al., *Multisensory convergence at human temporo-parietal junction—epicortical recording of evoked responses*. Clinical neurophysiology, 2004. **115**(5): p. 1145-1160.

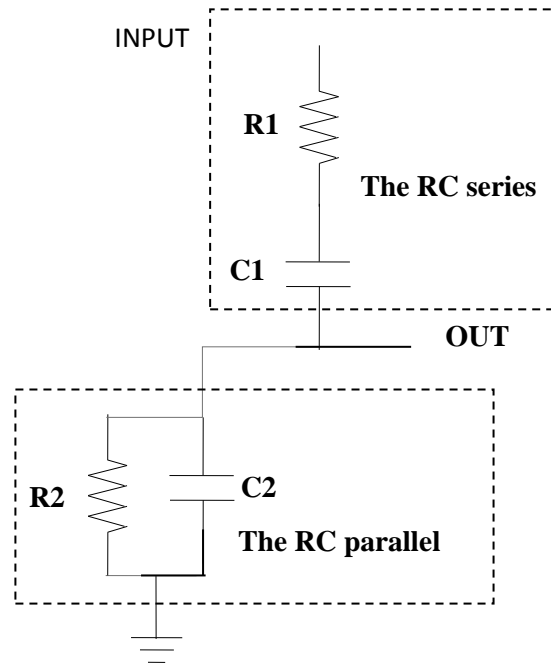
119. Yue, Y., J.M. Loh, and M.A. Lindquist, *Adaptive spatial smoothing of fMRI images*. *Statistics and its Interface*, 2010. **3**: p. 3-13.
120. Monti, M.M., *Statistical analysis of fMRI time-series: a critical review of the GLM approach*. *Frontiers in human neuroscience*, 2011. **5**(28): p. 1-13.
121. Mumford, J.A. and T. Nichols, *Modeling and inference of multisubject fMRI data*. *Engineering in Medicine and Biology Magazine, IEEE*, 2006. **25**(2): p. 42-51.
122. Büchel, C., et al., *Characterizing stimulus–response functions using nonlinear regressors in parametric fMRI experiments*. *Neuroimage*, 1998. **8**(2): p. 140-148.
123. Büchel, C., et al., *Non-linear regression in parametric activation studies*. *Neuroimage*, 1996. **3**(1): p. S53-S53.
124. Jones, L.A. and N.B. Sarter, *Tactile displays: Guidance for their design and application*. *Human Factors: The Journal of the Human Factors and Ergonomics Society*, 2008. **50**(1): p. 90-111.
125. Taylor, P., A. Hosseini-Sianaki, and C. Varley. *An electrorheological fluid-based tactile array for virtual environments*. 1996. IEEE.
126. Kaczmarek, K.A., M.E. Tyler, and P. Bach-y-Rita. *Pattern identification on a fingertip-scanned electro-tactile display*. 1997. *Proceedings - 19th International Conference - IEEE/EMBS Oct. 30 - Nov. 2, 1997*.
127. Kaczmarek, K.A. and M.E. Tyler. *Electrotactile haptic display on the fingertips: Preliminary results*. *Proc. 16th Annu. Int. Conf. IEEE Eng. Med. Biol. Soc.*, Nov 3–6, 1994, pp. 940-941.
128. Buchanan, J.P., *Handbook of piezoelectric crystals for radio equipment designers*, 1954, Philco Corp., Philadelphia.
129. Haertling, G.H., *Ferroelectric ceramics: history and technology*. *Journal of the American Ceramic Society*, 1999. **82**(4): p. 797-818.
130. Summers, I.R., et al. *Results from a Tactile Array on the Fingertip*. in *Eurohaptics 2001: Conference Proceedings*. July 2001.
131. Brady, A.C., I.R. Summers, and J.Q.C. Magnusson, *Discrimination of tactile rendering on virtual surfaces*. *ENACTIVE/06*, 2006: p. 107.
132. Palmer, R.M.a.R., *Op amps for everyone*. Ch. 15, ed. R. Mancini 2002: Texas Instruments Incorporated, Newnes.
133. Horowitz, P. and W. Hill, *The art of electronics*. Second ed 1989: Cambridge university press.
134. Carr, S., *Functional magnetic resonance imaging studies of the primary somatosensory cortex in relation to complex regional pain syndrome*, PhD thesis, in *School of Physics* 2009, University of Exeter.
135. Landis, J.R. and G.G. Koch, *The measurement of observer agreement for categorical data*. *biometrics*, 1977: p. 159-174.
136. Bodegård, A., et al., *Somatosensory areas in man activated by moving stimuli: cytoarchitectonic mapping and PET*. *Neuroreport*, 2000. **11**(1): p. 187-190.
137. Bodegård, A., et al., *Hierarchical processing of tactile shape in the human brain*. *Neuron*, 2001. **31**(2): p. 317-328.
138. Roland, P.E., B. O’Sullivan, and R. Kawashima, *Shape and roughness activate different somatosensory areas in the human brain*. *Proceedings of the National Academy of Sciences*, 1998. **95**(6): p. 3295-3300.
139. Schulz, M., et al., *An integrative MEG–fMRI study of the primary somatosensory cortex using cross-modal correspondence analysis*. *Neuroimage*, 2004. **22**(1): p. 120-133.
140. Mima, T., et al., *Human second somatosensory area: subdural and magnetoencephalographic recording of somatosensory evoked responses*. *Journal of Neurology, Neurosurgery & Psychiatry*, 1997. **63**(4): p. 501-505.
141. Polonara, G., et al., *Localization of the first and second somatosensory areas in the human cerebral cortex with functional MR imaging*. *American journal of neuroradiology*, 1999. **20**(2): p. 199-205.

142. Wacker, E., et al., *Tactile Motion and Pattern Processing Assessed with High-Field fMRI*. PLoS one, 2011. **6**(9): p. e24860.
143. Hegner, Y.L., et al., *BOLD adaptation in vibrotactile stimulation: neuronal networks involved in frequency discrimination*. Journal of neurophysiology, 2007. **97**(1): p. 264-271.
144. James, T.W., S. Kim, and J.S. Fisher, *The neural basis of haptic object processing*. Canadian Journal of Experimental Psychology, 2007. **61**(3): p. 219-229.
145. Chen, L.M., et al., *Fine-scale organization of SI (area 3b) in the squirrel monkey revealed with intrinsic optical imaging*. Journal of neurophysiology, 2001. **86**(6): p. 3011-3029.
146. Pei, Y.-C., et al., *Neural mechanisms of tactile motion integration in somatosensory cortex*. Neuron, 2011. **69**(3): p. 536-547.
147. Pei, Y.-C., et al., *Shape invariant coding of motion direction in somatosensory cortex*. PLoS biology, 2010. **8**(2): p. e1000305.
148. Bobich, L., et al., *Spatial localization of electrotactile stimuli on the fingertip in humans*. Somatosensory & Motor Research, 2007. **24**(6): p. 179-188.
149. Harrington, G.S. and H. Downs III, *fMRI mapping of the somatosensory cortex with vibratory stimuli: Is there a dependency on stimulus frequency?* Brain research, 2001. **897**(1): p. 188-192.
150. Burton, H. and R.J. Sinclair, *Second somatosensory cortical area in macaque monkeys: 2. Neuronal responses to punctate vibrotactile stimulation of glabrous skin on the hand*. Brain research, 1991. **538**(1): p. 127-135.
151. Roland, P.E. and E. Mortensen, *Somatosensory detection of microgeometry, macrogeometry and kinesthesia in man*. Brain Research Reviews, 1987.
152. Kakei, S., D.S. Hoffman, and P.L. Strick, *Muscle and movement representations in the primary motor cortex*. Science, 1999. **285**(5436): p. 2136-2139.
153. Mima, T., et al., *Brain structures related to active and passive finger movements in man*. Brain, 1999. **122**(10): p. 1989-1997.
154. Onishi, H., et al., *Neuromagnetic activation following active and passive finger movements*. Brain and Behavior, 2013.
155. Weiller, C., et al., *Brain representation of active and passive movements*. Neuroimage, 1996. **4**(2): p. 105-110.
156. Petrides, M., G. Cadoret, and S. Mackey, *Orofacial somatomotor responses in the macaque monkey homologue of Broca's area*. Nature, 2005. **435**(7046): p. 1235-1238.
157. Nishitani, N., et al., *Broca's region: from action to language*. Physiology, 2005. **20**(1): p. 60-69.
158. Amunts, K., et al., *Broca's region revisited: cytoarchitecture and intersubject variability*. Journal of Comparative Neurology, 1999. **412**(2): p. 319-341.
159. Bookheimer, S., *Functional MRI of language: new approaches to understanding the cortical organization of semantic processing*. Annual Review of Neuroscience, 2002. **25**(1): p. 151-188.
160. Min Guo, Y.Y., Araki Yuta ,Jiajia Yang, Jinglong WuYinghua Yu, Araki Yuta ,Jiajia Yang and Jinglong Wu. *Development and Evaluation of a tactile speed stimulator for MRI environment*. in *International Conference on Complex Medical Engineering (ICME)*. 2012. Harbin Heilongjiang.
161. Dépeault, A., E.-M. Meftah, and C.E. Chapman, *Tactile speed scaling: contributions of time and space*. Journal of neurophysiology, 2008. **99**(3): p. 1422-1434.
162. Basso, D., et al., *Touching Motion: rTMS on the Human Middle Temporal Complex Interferes with Tactile Speed Perception*. Brain topography, 2012. **25**(4): p. 389-398.
163. Ricciardi, E., et al., *Functional inhibition of the human middle temporal cortex affects non-visual motion perception: a repetitive transcranial magnetic stimulation study during tactile speed discrimination*. Experimental Biology and Medicine, 2011. **236**(2): p. 138-144.

164. DiCarlo, J.J. and K.O. Johnson, *Velocity invariance of receptive field structure in somatosensory cortical area 3b of the alert monkey*. The Journal of Neuroscience, 1999. **19**(1): p. 401-419.
165. Sinclair, R. and H. Burton, *Neuronal activity in the second somatosensory cortex of monkeys (Macaca mulatta) during active touch of gratings*. Journal of neurophysiology, 1993. **70**(1): p. 331-350.
166. Chung, Y.G., et al., *Frequency-dependent patterns of somatosensory cortical responses to vibrotactile stimulation in humans: A fMRI study*. Brain research, 2013.
167. Onishi, H., et al., *Neuromagnetic activation of primary and secondary somatosensory cortex following tactile-on and tactile-off stimulation*. Clinical neurophysiology, 2010. **121**(4): p. 588-593.
168. Francis, S., et al., *fMRI of the responses to vibratory stimulation of digit tips*. Neuroimage, 2000. **11**(3): p. 188-202.

## Appendix A

The easy method of the analysing the Wien-bridge oscillator is to consider the series and parallel RC components and ignore the rest components as show in the below figure.



The analysis circuit of the Wien bridge oscillator.

The impedance of series RC circuit is

$$Z1 = R1 + \frac{1}{j\omega C1}$$

where  $\omega$  is the frequency ( $\omega = 2\pi f$ ),  $\frac{1}{j\omega C1}$  the impedance of the capacitor ,

$j$  a phase shift,  $R$  the resistor and  $C$  the capacitor.

Then by multiplying the top and bottom of the equation  $Z1$  by  $j\omega C1$  gives:

$$Z1 = \frac{1 + j\omega C1 R1}{j\omega C1}$$

In the same way for the impedances of the parallel RC

$$Z_2 = \frac{\left(\frac{R_2}{j\omega C_2}\right)}{R + \frac{1}{j\omega C_2}}$$

by multiplying top and bottom of the equation  $Z_2$  by  $j\omega C_2$  we get

$$Z_2 = \frac{R_2}{1 + j\omega C_2 R_2}$$

The transfer function of the Wien bridge oscillator becomes:

$$\frac{Z_2}{Z_2 + Z_1}$$

and by substituting of  $Z_1$  and  $Z_2$  we obtain :

$$= \frac{\frac{R_2}{1 + j\omega C_2 R_2}}{\frac{R_2}{1 + j\omega C_2 R_2} + \frac{1 + j\omega C_1 R_1}{j\omega C_1}}$$

now to keep the maths simple we assume:

$$C_1 = C_2 = C$$

and

$$R_1 = R_2 = R$$

and by doing some simple mathematic on the above equation we get:

$$= \frac{j\omega CR}{-(\omega^2)C^2R^2 + 3j\omega CR + 1}$$

The necessary condition to have phase shift of zero is:

$$1 - \omega^2 C^2 R^2 = 0$$

From this condition we can get:



$$\omega = \frac{1}{RC}$$

or

$$f = \frac{1}{2\pi RC}$$

## Appendix B

The program used in the first fMRI study.

10 dim data

20 dim c

30 dim pulse as pin re6 for digital input

40 dim led[1] as pin rd8 for digital output

50 dim led[2] as pin rd9 for digital output

60 dim led[3] as pin rd10 for digital output

70 dim led[4] as pin rd11 for digital output

80 dim led[5] as pin rd0 for digital output

90 dim led[6] as pin rc13 for digital output

100 dim led[7] as pin rc14 for digital output

110 dim led[8] as pin rd1 for digital output

120 dim led[9] as pin rd2 for digital output

130 dim led[10] as pin rd3 for digital output

140 dim led[11] as pin rd12 for digital output

150 dim led[12] as pin rd13 for digital output

160 dim led[13] as pin rd4 for digital output

170 dim led[14] as pin rd5 for digital output

180 dim led[15] as pin rd6 for digital output

190 dim led[16] as pin rd7 for digital output

200 dim led[17] as pin rf0 for digital output

210 dim led[18] as pin rf1 for digital output

220 dim led[19] as pin rg1 for digital output

230 dim led[20] as pin rg0 for digital output

240 dim led[21] as pin rg14 for digital output

250 dim led[22] as pin rg12 for digital output

260 dim led[23] as pin rg13 for digital output

270 dim led[24] as pin re3 for digital output

```

280 dim led[25] as pin re4 for digital output
290 dim i,j,start1,start2,start3,start4,start5,start6,start7,start8
300 dim delay,delays[54],stim,stims[54]
310 for delay=0 to 53
320 read delays[delay]
330 next
340 data 5,0,6,3,1,4,2,4,2,5,0,6,3,1,4,2,6,0,3,5,1,4,1,6,0,5,2
350 data 3,2,1,6,0,5,3,4,6,4,0,3,1,2,5,4,6,2,5,0,3,1,2,6,1,0,5
360 for stim=0 to 53
370 read stims[stim]
380 next
390 data 4,0,5,18,3,9,10,1,14,8,7,2,1,6,0,5,10,16,8,9,2,7,16,3,9,4,0
400 data 1,8,14,5,10,6,8,18,7,2,0,1,6,5,10,4,7,3,14,9,8,16,10,9,18,8,1
410 let delay=0
420 let stim=0
430 while 1 do
440 while !pulse do
450 endwhile
460 sleep delays[delay]s
470 let delay=(delay+1)%54
480 if stims[stim]==0 then
490 gosub circle start1
500 endif
510 if stims[stim]==2 then
520 gosub station1 start2
530 endif
540 if stims[stim]==3 then
550 gosub circle start1
560 endif

```

```
570 if stims[stim]==8 then
580 gosub circle start1
590 endif
600 if stims[stim]==1 then
610 gosub random start3
620 endif
630 if stims[stim]==4 then
640 gosub station2 start4
650 endif
660 if stims[stim]==6 then
670 gosub station3 start5
680 endif
690 if stims[stim]==14 then
700 gosub station4 start6
710 endif
720 if stims[stim]==16 then
730 gosub station5 start7
740 endif
750 if stims[stim]==18 then
760 gosub station6 start8
770 endif
780 if stims[stim]==10 then
790 gosub circle start1
800 endif
810 if stims[stim]==5 then
820 gosub random start3
830 endif
840 if stims[stim]==7 then
850 gosub random start3
```

```
860 endif
870 if stims[stim]==9 then
880 gosub random start3
890 endif
900 let stim=(stim+1)%54
910 endwhile
920 end
930 sub circle start1
940 let start1=seconds
950 while seconds<start1+9 do
960 if stims[stim]==0 then
970 restore first
980 endif
990 if stims[stim]==10 then
1000 restore ten
1010 endif
1020 if stims[stim]==3 then
1030 restore fourteen
1040 endif
1050 if stims[stim]==8 then
1060 restore fifteen
1070 endif
1080 for j=1 to 12
1090 read data
1100 for i=1 to 25
1110 let led[i] = data & (1<<(25-i))
1120 label first
1130 data 0x880000
1140 data 0x84000
```

1150 data 0x4200  
1160 label ten  
1170 data 0x208  
1180 data 0xc  
1190 data 0x6  
1200 label fourteen  
1210 data 0x22  
1220 data 0x420  
1230 data 0x8400  
1240 label fifteen  
1250 data 0x208000  
1260 data 0x600000  
1270 data 0xc00000  
1280 label ten  
1290 data 0x880000  
1300 data 0x84000  
1310 data 0x4200  
1320 label fourteen  
1330 data 0x208  
1340 data 0xc  
1350 data 0x6  
1360 label fifteen  
1370 data 0x22  
1380 data 0x420  
1390 data 0x8400  
1400 next  
1410 sleep 47 ms  
1420 next  
1430 for i=1 to 25



```
1730 if stims[stim]==1 then
1740 restore third
1750 endif
1760 if stims[stim]==5 then
1770 restore twelve
1780 endif
1790 if stims[stim]==7 then
1800 restore sixteen
1810 endif
1820 if stims[stim]==9 then
1830 restore seventeen
1840 endif
1850 for j=1 to 36
1860 read data
1870 for i=1 to 25
1880 let led[i]=data & (1<<(25-i))
1890 label third
1900 data 0x880000
1910 data 0x42
1920 data 0x108
1930 data 0x60
1940 label twelve
1950 data 0x208
1960 data 0x84
1970 data 0x300000
1980 data 0x84
1990 label sixteen
2000 data 0x22
2010 data 0x18
```



2020 data 0xc0  
2030 data 0x10800  
2040 label seventeen  
2050 data 0x208000  
2060 data 0xc00  
2070 data 0xc00000  
2080 data 0x42000  
2090 data 0xc  
2100 data 0x108000  
2110 data 0x210  
2120 data 0xc00  
2130 data 0x108  
2140 data 0xc  
2150 data 0x180  
2160 data 0x42000  
2170 data 0x420  
2180 data 0x180  
2190 data 0xc  
2200 data 0x18  
2210 data 0x18000  
2220 data 0x21000  
2230 data 0x180  
2240 data 0xc  
2250 data 0x42  
2260 data 0xc00000  
2270 data 0x84000  
2280 data 0x60  
2290 label twelve  
2300 data 0x880000









3460 next

3470 endwhile

3480 endsub

## Appendix C

The program used in the second fMRI study.

10 dim data

20 dim c

30 dim pulse as pin re6 for digital input

40 dim led[1] as pin rd8 for digital output

50 dim led[2] as pin rd9 for digital output

60 dim led[3] as pin rd10 for digital output

70 dim led[4] as pin rd11 for digital output

80 dim led[5] as pin rd0 for digital output

90 dim led[6] as pin rc13 for digital output

100 dim led[7] as pin rc14 for digital output

110 dim led[8] as pin rd1 for digital output

120 dim led[9] as pin rd2 for digital output

130 dim led[10] as pin rd3 for digital output

140 dim led[11] as pin rd12 for digital output

150 dim led[12] as pin rd13 for digital output

160 dim led[13] as pin rd4 for digital output

170 dim led[14] as pin rd5 for digital output

180 dim led[15] as pin rd6 for digital output

190 dim led[16] as pin rd7 for digital output

200 dim led[17] as pin rf0 for digital output

210 dim led[18] as pin rf1 for digital output

220 dim led[19] as pin rg1 for digital output

230 dim led[20] as pin rg0 for digital output

240 dim led[21] as pin rg14 for digital output

250 dim led[22] as pin rg12 for digital output

```

260 dim led[23] as pin rg13 for digital output
270 dim led[24] as pin re3 for digital output
280 dim led[25] as pin re4 for digital output
290 dim i,j,start1,start2,start3,start4
300 dim delay,delay[36],stim,stims[36]
310 for delay=0 to 35
320 read delays[delay]
330 next
340 data 5,0,6,3,1,4,2,4,2,5,0,6,3,1,4,2,6,0
350 data 3,2,1,6,0,5,3,4,6,4,0,3,1,2,5,4,6,2
360 for stim=0 to 35
370 read stims[stim]
380 next
390 data 6,4,0,2,6,2,0,4,2,6,4,0,2,0,4,6,6,4
400 data 0,2,6,4,0,2,6,4,2,0,2,4,0,6,2,4,0,6
410 let delay=0
420 let stim=0
430 while 1 do
440 while !pulse do
450 endwhile
460 sleep delays[delay]s
470 let delay=(delay+1)%36
480 if stims[stim]==0 then
490 gosub circle1 start1
500 endif
510 if stims[stim]==2 then
520 gosub circle2 start2

```



```
530 endif
540 if stims[stim]==4 then
550 gosub circle3 start3
560 endif
570 if stims[stim]==6 then
580 gosub circle4 start4
590 endif
600 let stim=(stim+1)%36
610 endwhile
620 end
630 sub circle1 start1
640 let start1=seconds
650 while seconds<start1+9 do
660 restore first
670 for j=1 to 12
680 read data
690 for i=1 to 25
700 let led[i] = data & (1<<(25-i))
710 label first
720 data 0x880000
730 data 0x84000
740 data 0x4200
750 data 0x208
760 data 0xc
770 data 0x6
780 data 0x22
790 data 0x420
```







```
1620 while seconds<start4+9 do
1630 restore seven
1640 for j=1 to 12
1650 read data
1660 for i=1 to 25
1670 let led[i] = data & (1<<(25-i))
1680 label seven
1690 data 0x880000
1700 data 0x84000
1710 data 0x4200
1780 data 0x208
1790 data 0xc
1800 data 0x6
1810 data 0x22
1820 data 0x420
1830 data 0x8400
1840 data 0x208000
1850 data 0x600000
1860 data 0xc00000
1870 next
1880 sleep 737 ms
1890 next
1900 endwhile
1910 for i=1 to 25
1920 restore eight
1930 read led[i]
1940 label eight
```



## Appendix D

### 1.1 Magnetic resonance imaging

#### Information sheet (1)

#### Magnetic resonance imaging

Magnetic resonance imaging (MRI) is a system for producing pictures of the human body and does not use x-rays or other harmful radiation. It is a very safe technique and may be used on the majority of subjects.

The technique relies on a powerful magnet which you will lie inside. The strong magnetic field allows the system to detect the amount and the location of water within the body. Using this information, pictures of the soft tissues within the body are produced. If you suffer from claustrophobia you might find the environment uncomfortable—please discuss this with the operator before entering the scanner suite.

During the scan, the system is quite noisy and you will be provided with protective headphones. The magnetic field will strongly attract metal objects. As a result of the high magnetic field no metal objects may be taken in to the scanning room itself; this includes coins, keys, pens, etc. All jewellery should be removed. Also, as we are imaging the head, we would ask you not to wear makeup as some of the pigments used contain iron and will prevent a good image being taken.



An MRI image of the brain



The MRI scanner

This project has been reviewed and approved by the Local Research Ethics Committee.

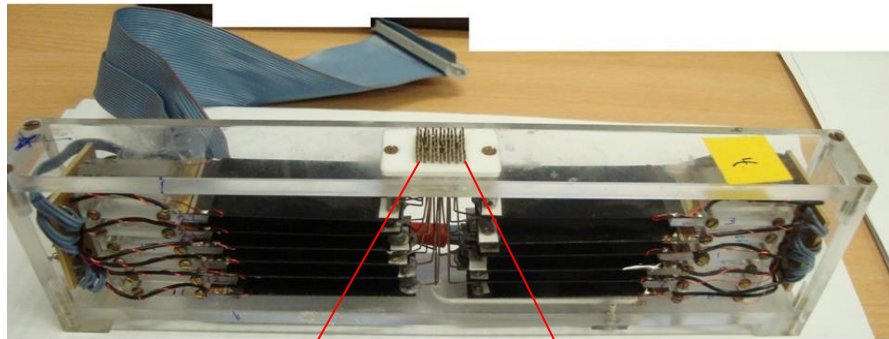
## 1.2 The touch stimulator

### Information sheet (2)

#### The touch stimulator

The touch stimulator consists of 25 pins arranged in a 5×5 array (see the image below). During the experiment the pins will vibrate in a certain way. The sensation should be comfortable.

The touch stimulator



The 25 pins



This project has been reviewed and approved by the Local Research Ethics Committee.



## 1.3 Tactile experiment invitation

### Invitation

We will be so grateful to you if you accept our invitation to take part in this research study. Before you decide you need to understand why the research is being done and what it would involve for you. Please take the time that you need to read the following information and talk to others about the study if you wish. Ask us if there is anything that you want more information about or is not clear to you. Take time to decide whether or not you wish to take part.

### The purpose of the study

The touch sense is one of the important senses in our body and we use it to get information about the shape and texture of different object, which is then interpreted by the brain. The aim of this study is to find out more information about touch perception when the skin receives mechanical deformation using touch stimulation. The experiment will be carried out in Physics Building, Exeter University. Also to find out if we use deferent type of paradigm of vibration (stationary/moving) of the pin will effect on the sense of the touch.

### Why have I been invited to take part?

The people who will take part in the study will be in good health and aged between 18-50. We believe you are appropriate to participate.

### What will happen to me if I take part?

This study uses touch stimulation to provide the skin with mechanical stimulation (touch stimulator (Please see the sheet (2))). One of your fingertips will be resting lightly over touch stimulator which will periodically vibrate in a non-painful and non-invasive way. The duration of the experiment will be 30 minutes. During the experiment the participant will ask to recognize the type of the stimulation, it is stationary or moving over the fingertip.

If you decide to be a participant in the study there are some forms you will ask to fill in before we start the experiment. These forms are registration form (to record your details) and the consent form (you agree to be part in this study).

What will happen to the results of the research study?

The results from this study will be published in the form of papers submitted to scientific journals and also presentations at relevant scientific conferences. You will be sent a summary of the findings of the study. You will not be identified in any report or publication.

**What if I have any questions?**

If you have any question at any time, Please feel free to contact Amer Alhussain on 07404262889 or Email: [aqma201@exeter.ac.uk](mailto:aqma201@exeter.ac.uk)

**Can I change my mind?**

You can stop being part in the study at any time without giving a reason and there will be no problem with this.

Amer Alhussain

PhD Researcher

This project has been reviewed and approved by the Local Research Ethics Committee

## 1.4 FMRI experiment Invitation

### Invitation

We will be so grateful to you if you accept our invitation to take part in this research study. Before you decide you need to understand why the research is being done and what it would involve for you. Please take the time that you need to read the following information and talk to others about the study if you wish. Ask us if there is anything that you want more information about or is not clear to you. Take time to decide whether or not you wish to take part.

### The purpose of the study

The touch sense is one of the important senses in our body and we use it to get information about the shape and texture of different object, which is then interpreted by the brain. The aim of this study is to find the active areas in the brain when the skin receives mechanical deformation that is felt as a touch sensation and also to find out about a group of subjects as a whole not to compare one individual with another.

### Why have I been invited to take part?

The people who will take part in the study will be in good health and aged between 18-50. We believe you are appropriate to participate.

### What will happen to me if I take part?

This study uses magnetic resonance imaging (MRI) (please see sheet (1)) to image your brain. The study will require one visit to the Magnetic Resonance Imaging Centre at the University of Exeter, St. Lukes Campus, Heavitree Road. In this visit there will be two sessions of imaging each of 45 minutes. During imaging a helmet-like device will be placed over your head to help the scanner produce clearer pictures. One of your fingertips will be resting lightly over some equipment (tactile stimulator (Please see the sheet (2))) which will periodically vibrate in a non-painful and non-invasive way. You will be able to rest outside of the scanner room between sessions.

Once you are in the system, the operators will be in constant contact with you. If at any time you feel uncomfortable or wish to end the scanning process you will be able to do so by squeezing a device that will stop the scan and alert the operator.

Images taken for research purposes are not intended for diagnosis of any illness. In addition, the researcher is not trained to make a diagnosis.

If you decide to be a participant in the study, there are some forms you will be asked to fill in before we start the experiment. These forms are the safety checklist (to know if you are fit to enter the scanner room), registration form (to record your details) and the consent form (you agree to be part of this study).

What will happen to the results of the research study?

The results from this study will be published in the form of papers submitted to scientific journals and also presentations at relevant scientific conferences. You will be sent a summary of the findings of the study. You will not be identified in any report or publication.

What if I have any questions?

If you have any question at any time, please feel free to contact Amer Alhussain on 07404262889 or Email: [aqma201@exeter.ac.uk](mailto:aqma201@exeter.ac.uk)

Can I change my mind?

You can stop being part of the study at any time without giving a reason and there will be no problem with this.

Amer Alhussain

PhD Researcher

This project has been reviewed and approved by the Local Research Ethics Committee

## 1.5 MRI Safety Checklist

### Participant Safety Checklist

Name: .....

Date of Birth: .....

Weight: .....

Study Name/Volunteer Number: .....

*Please check the following list carefully, answering all appropriate questions.*

*Please do not hesitate to ask staff, if you have any queries regarding these questions.*

1. Do you have a pacemaker, artificial heart valve or coronary stent? Yes  No

2. Have you ever had major surgery?  
If yes, please give brief details: Yes  No

3. Do you have any aneurysm clips  
(clips put around blood vessels during surgery)? Yes  No

4. Do you have any implants in your body?

Yes  No  Joint replacements, pins or wires

Yes  No  Implanted cardioverter defibrillator (ICD)

Yes  No  Electronic implant or device

Yes  No  Magnetically-activated implant or device

Yes  No  Neurostimulation system

Yes  No  Spinal cord stimulator

Yes  No  Insulin or infusion pump

Yes  No  Implanted drug infusion pump

Yes  No  Internal electrodes or wires

Yes  No  Bone growth/bone fusion stimulator

Yes  No  Any type of prosthesis

Yes  No  Heart valve prosthesis

Yes  No  Eyelid spring or wire

Yes  No  Metallic stent, filter or coil

Yes  No  Shunt (spinal or intraventricular)

Yes  No  Vascular access port and/or catheter

Yes  No  Wire mesh implant

Yes  No  Bone/joint pin, screw, nail, wire, plate etc.

Yes  No  Other Implant .....

5. Do you have an artificial limb, calliper or surgical corset? Yes  No

6. Do you have any shrapnel or metal fragments, for example from working in a machine tool shop? Yes  No

7. Do you have a cochlear implant? Yes  No

8. Do you wear dentures, plate or a hearing aid? Yes  No

9. Are you wearing a skin patch (e.g. anti-smoking medication), have any tattoos, body piercing, permanent makeup or coloured contact lenses? Yes  No

10. Are you aware of any metal objects present within or about your body, other than those described above? Yes  No

11. Are you susceptible to claustrophobia? Yes  No

12. Do you suffer from blackout, diabetes, epilepsy or fits? Yes  No

**For women:**

13. Are you pregnant or experiencing a late menstrual period? Yes  No

14. Do you have an intra-uterine contraceptive device fitted? Yes  No

15. Are you taking any type of fertility medication or having fertility treatment? Yes  No

## **Important Instructions**

**Remove all metallic objects before entering the scanner room including hearing aids, mobile phones, keys, glasses, hair pins, jewellery, watches, safety pins, paperclips, credit cards, magnetic strip cards, coins, pens, pocket knives, nail clippers, steel-toed boots/shoes and all tools. Loose metallic objects are especially prohibited within the MR environment.**

**I have understood the above questions and have marked the answers correctly.**

Signature .....

Date .....

(Participant/Parent/Guardian)

MR Centre Staff Signature .....

## Appendix E 1.1

### 1. Result of contrast between Circle and Rest (Subjects 2 to 11) first fMRI experiment.

Left

Right



Fig. 1: Glass-brain views (upper panels) and rendered-brain views (lower panels) of activation for the contrast between Circle and Rest for subject 2 in areas SI and SII. Threshold uncorrected,  $p$  value of  $\leq 0.001$ . No activations were observed in right side SII ( $p \leq 0.009$ , uncorrected).



Left

Right

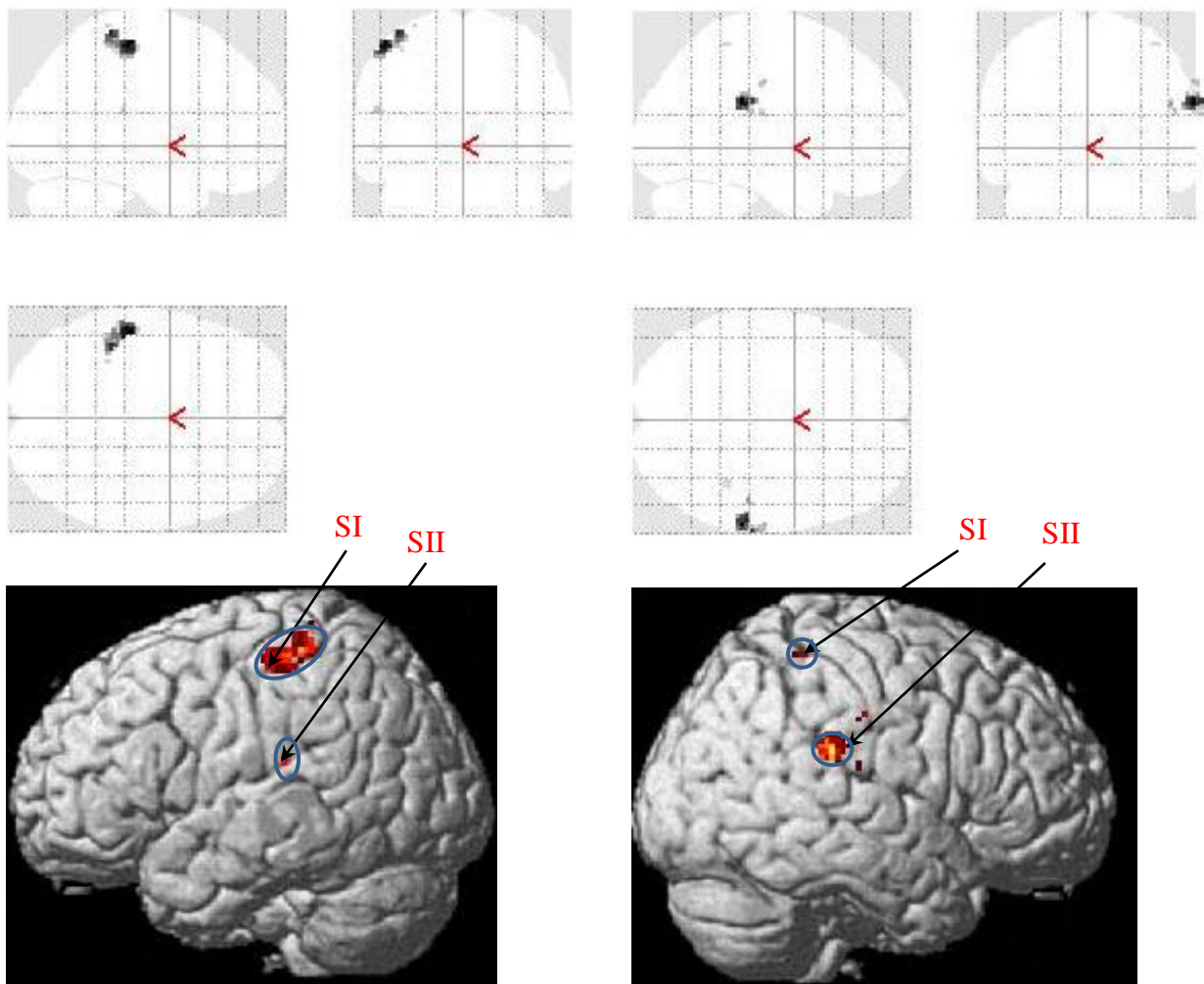


Fig. 2: Glass-brain views (upper panels) and rendered-brain (lower panels) of activation views for the contrast between Circle and Rest for subject 3 in areas SI and SII. Threshold uncorrected,  $p$  value of  $\leq 0.001$ ..

Left

Right

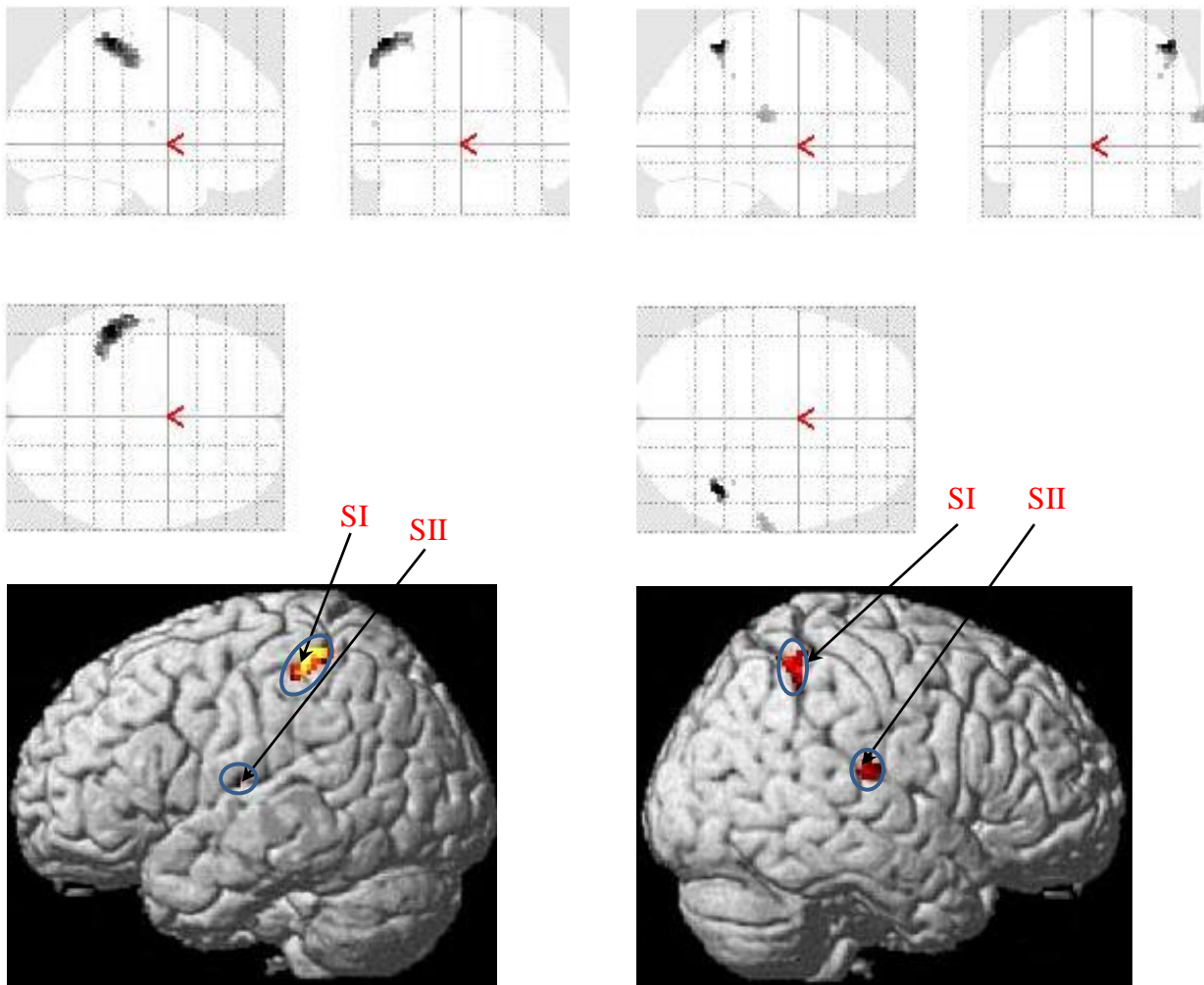


Fig. 3: Glass-brain views (upper panels) and rendered-brain views (lower panels) of activation for the contrast between Circle and Rest for subject 4 in areas SI and SII. Threshold corrected,  $p$  value of  $\leq 0.05$ .

Left

Right

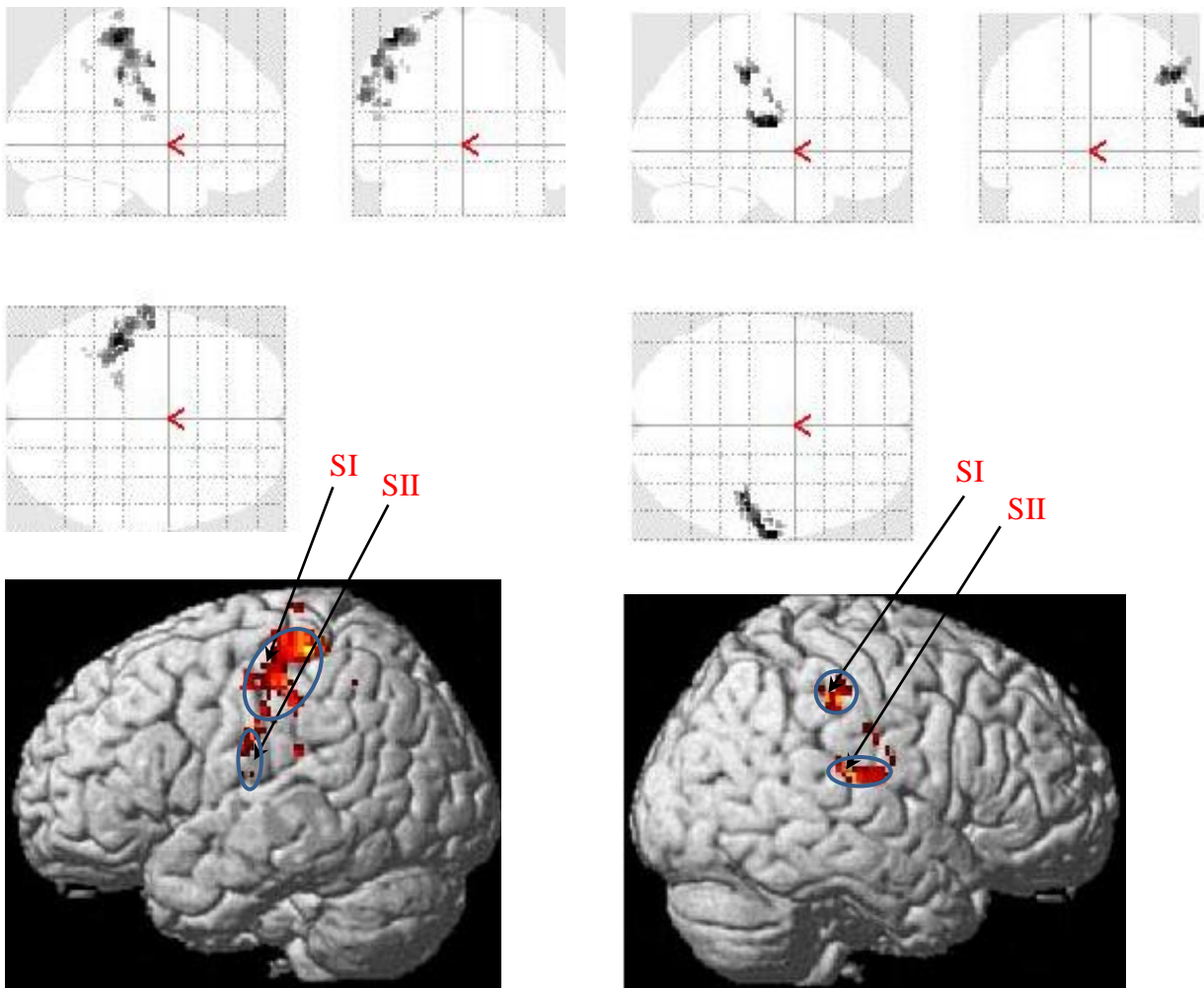


Fig. 4: Glass-brain views (upper panels) and rendered-brain views (lower panels) of activation for the contrast between Circle and Rest for subject 5 in areas SI and SII. Threshold corrected,  $p$  value of  $\leq 0.05$ .

Left

Right

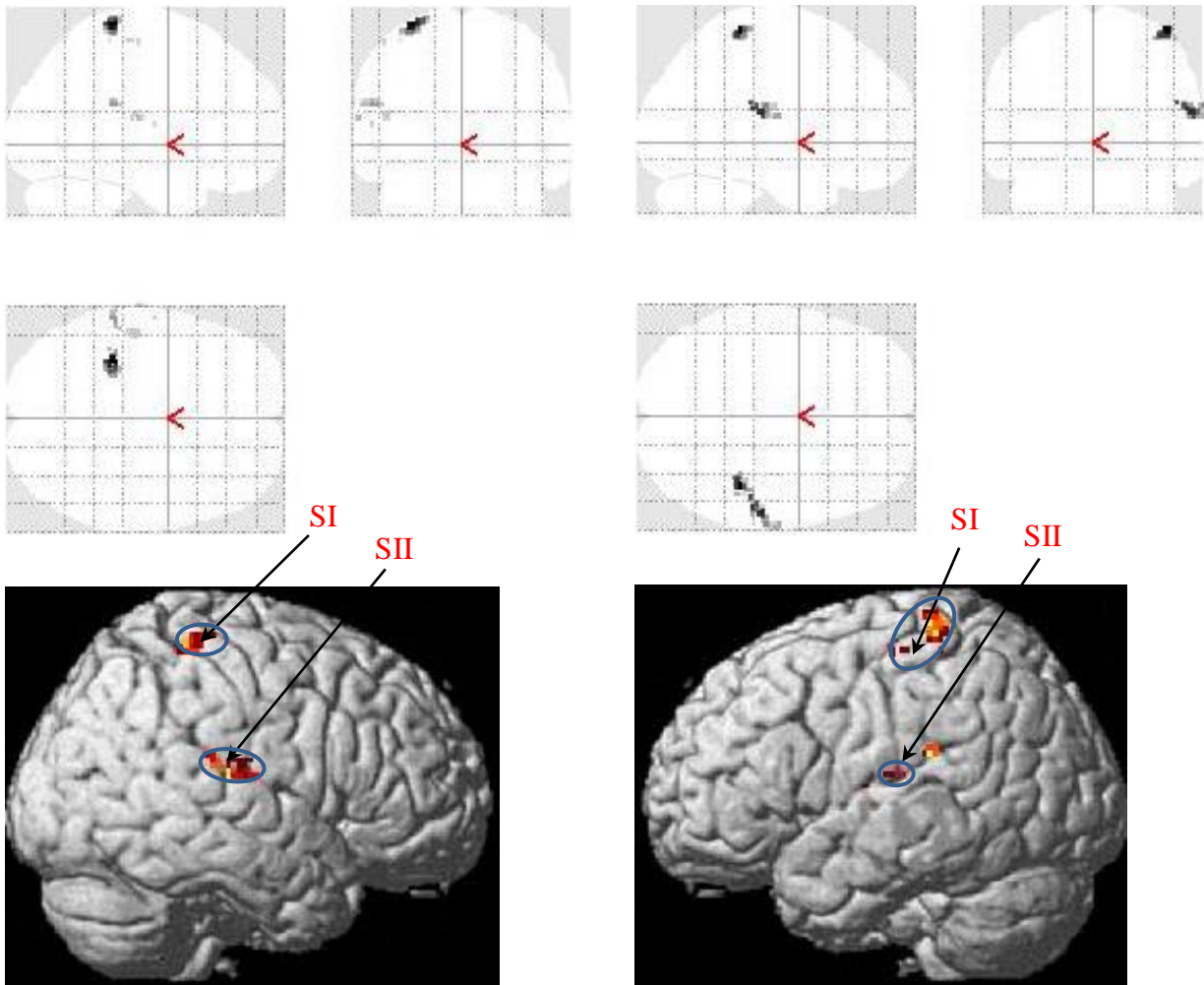


Fig. 5: Glass-brain views (upper panels) and rendered-brain views (lower panels) of activation for the contrast between Circle and Rest for subject 6 in areas SI and SII. Threshold uncorrected,  $p$  value  $\leq 0.001$ .

Left

Right

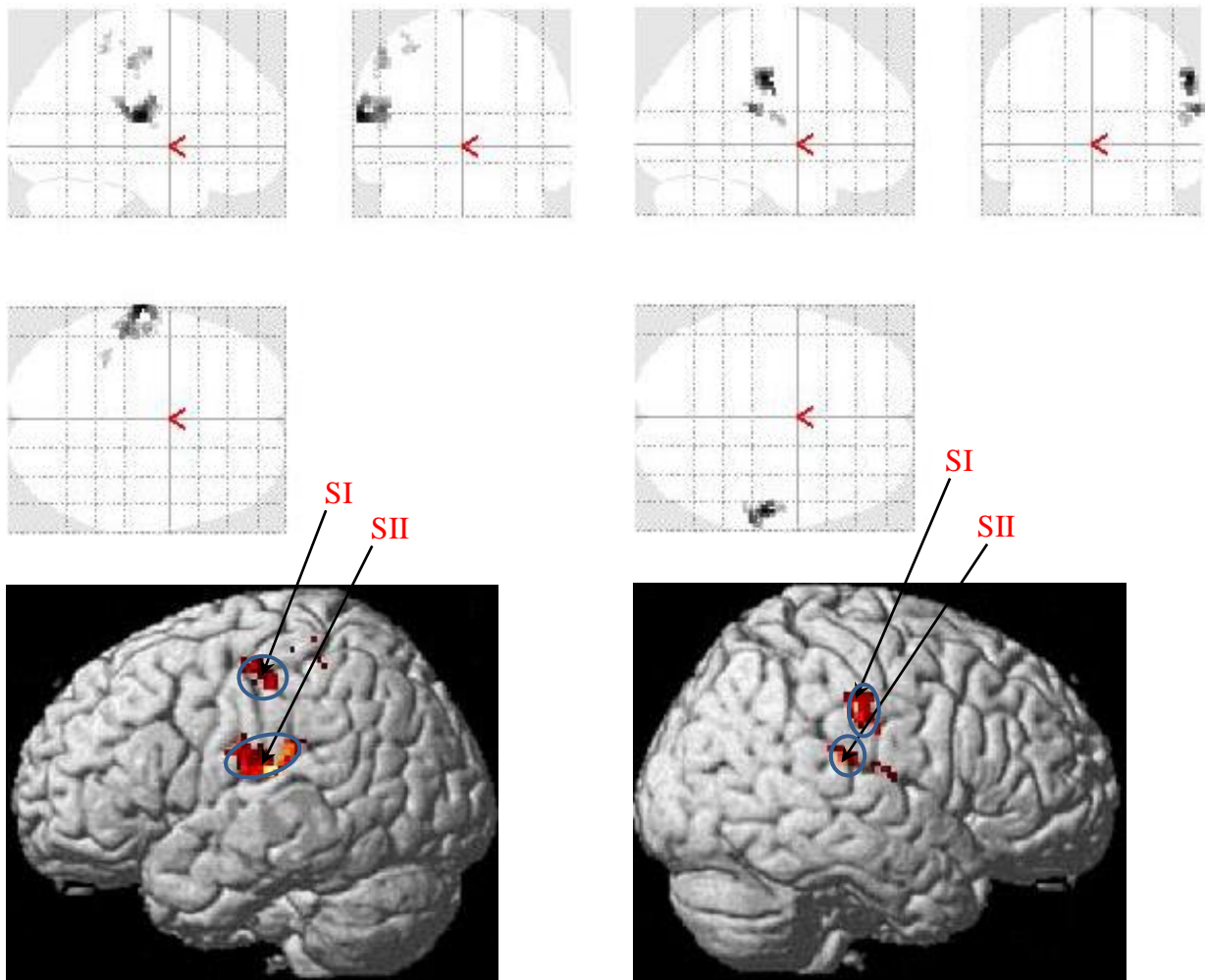


Fig. 6: Glass-brain views (upper panels) and rendered-brain views (lower panels) of activation for the contrast between Circle and Rest for subject 7 in areas SI and SII. Threshold corrected,  $p$  value of  $\leq 0.05$ .



Left

Right

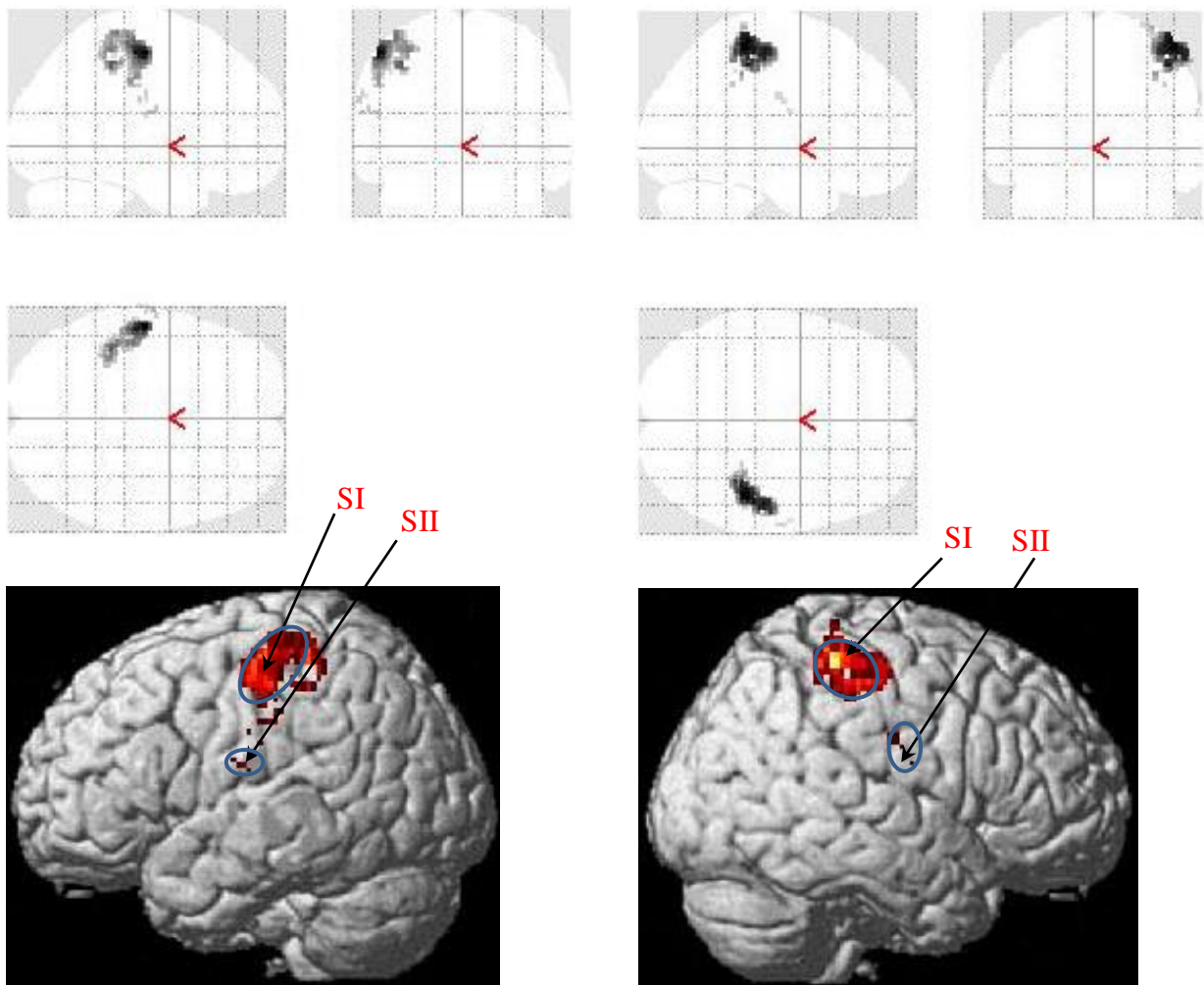


Fig. 7: Glass-brain views (upper panels) and rendered-brain views (lower panels) of activation for the contrast between Circle and Rest for subject 8 in areas SI and SII. Threshold corrected,  $p$  value of  $\leq 0.05$ .

Left

Right

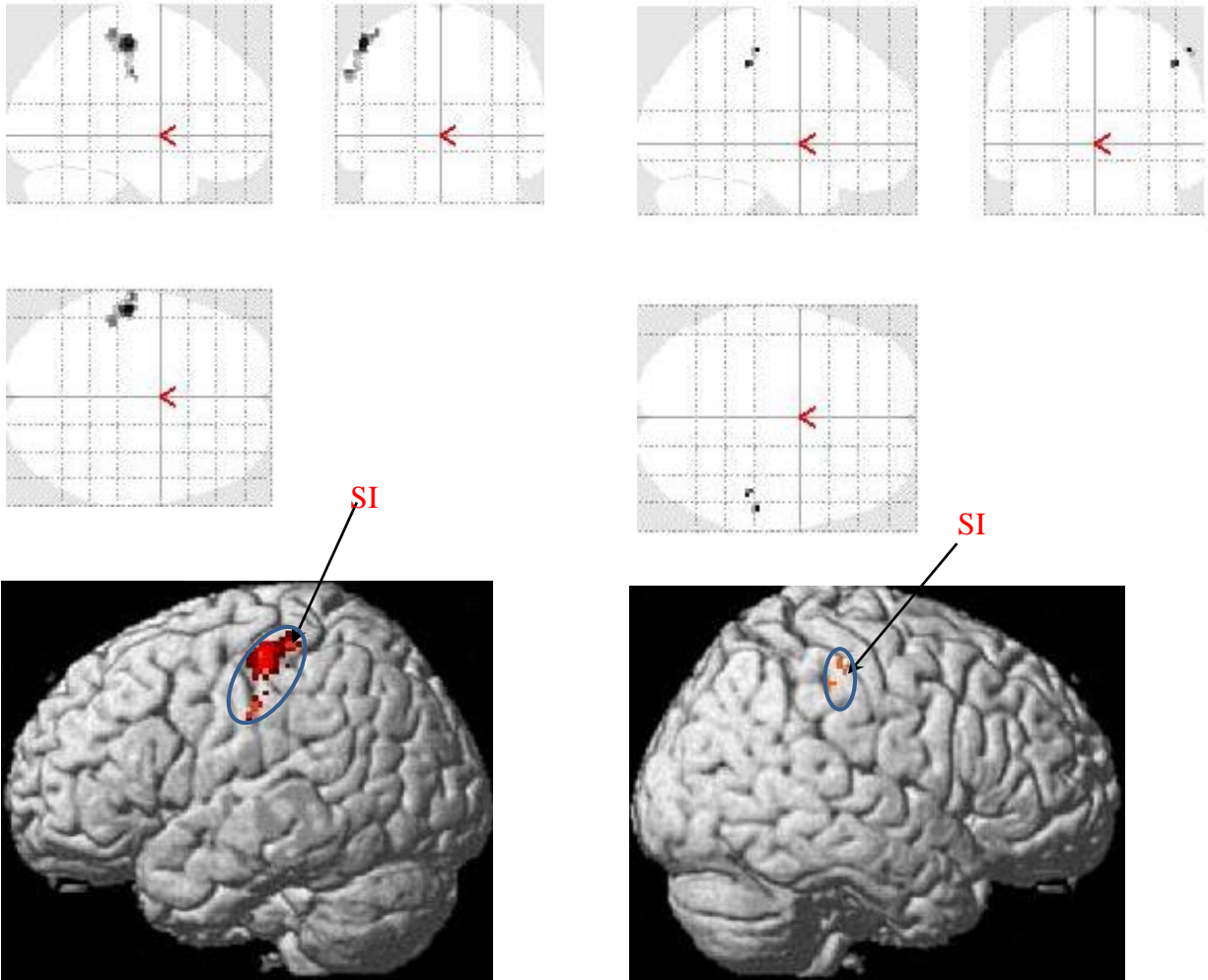


Fig.8: Glass-brain views (upper panels) and rendered-brain views (lower panels) of activation for the contrast between Circle and Rest for subject 9 in areas SI and SII. Threshold uncorrected,  $p$  value of  $\leq 0.001$ .

Left

Right

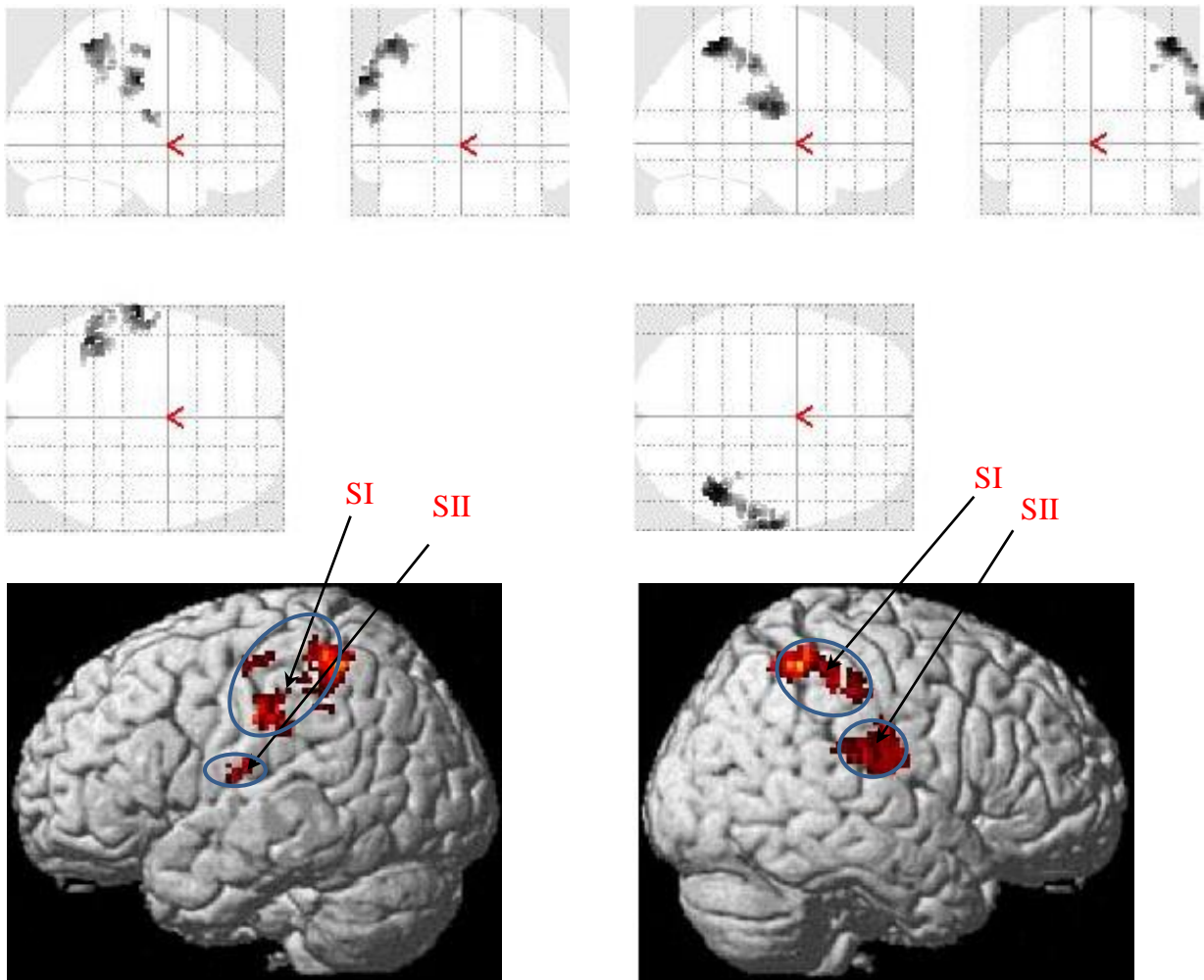


Fig. 9: Glass-brain views (upper panels) and rendered-brain views (lower panels) of activation for the contrast between Circle and Rest for subject 10 in areas SI and SII. Threshold corrected,  $p$  value of  $\leq 0.05$ .



Right

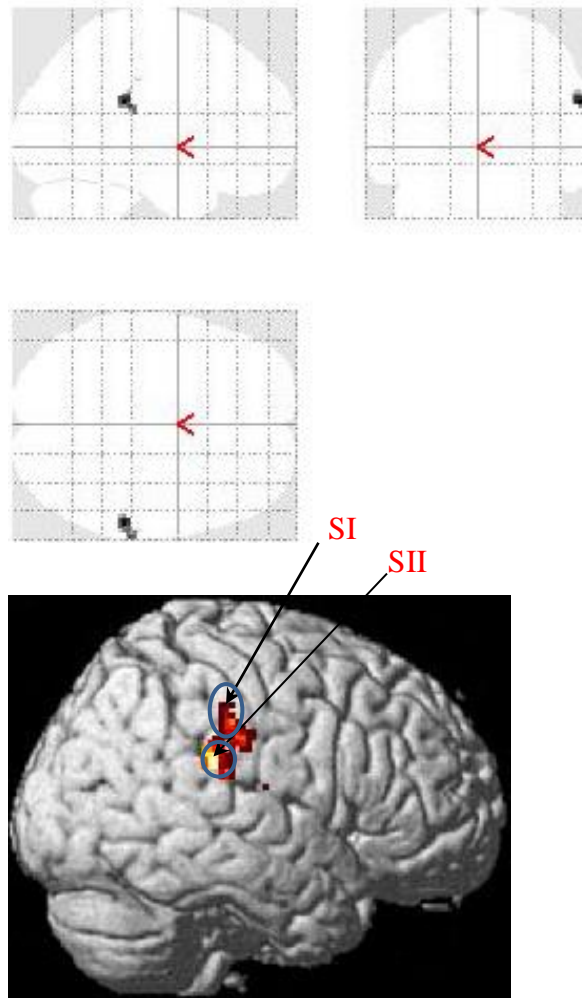


Fig. 10: Glass-brain views (upper panel) and rendered-brain views (lower panel) of activation for the contrast between Circle and Rest for subject 11 in areas SI and SII. Threshold uncorrected,  $p$  value of  $\leq 0.001$ . No activations were observed in left side SI and SII ( $p \leq 0.009$ , uncorrected).

## Appendix E 1.2

### 2. Results of contrast between Random and Rest (Subjects 2 to 11) first fMRI experiment.

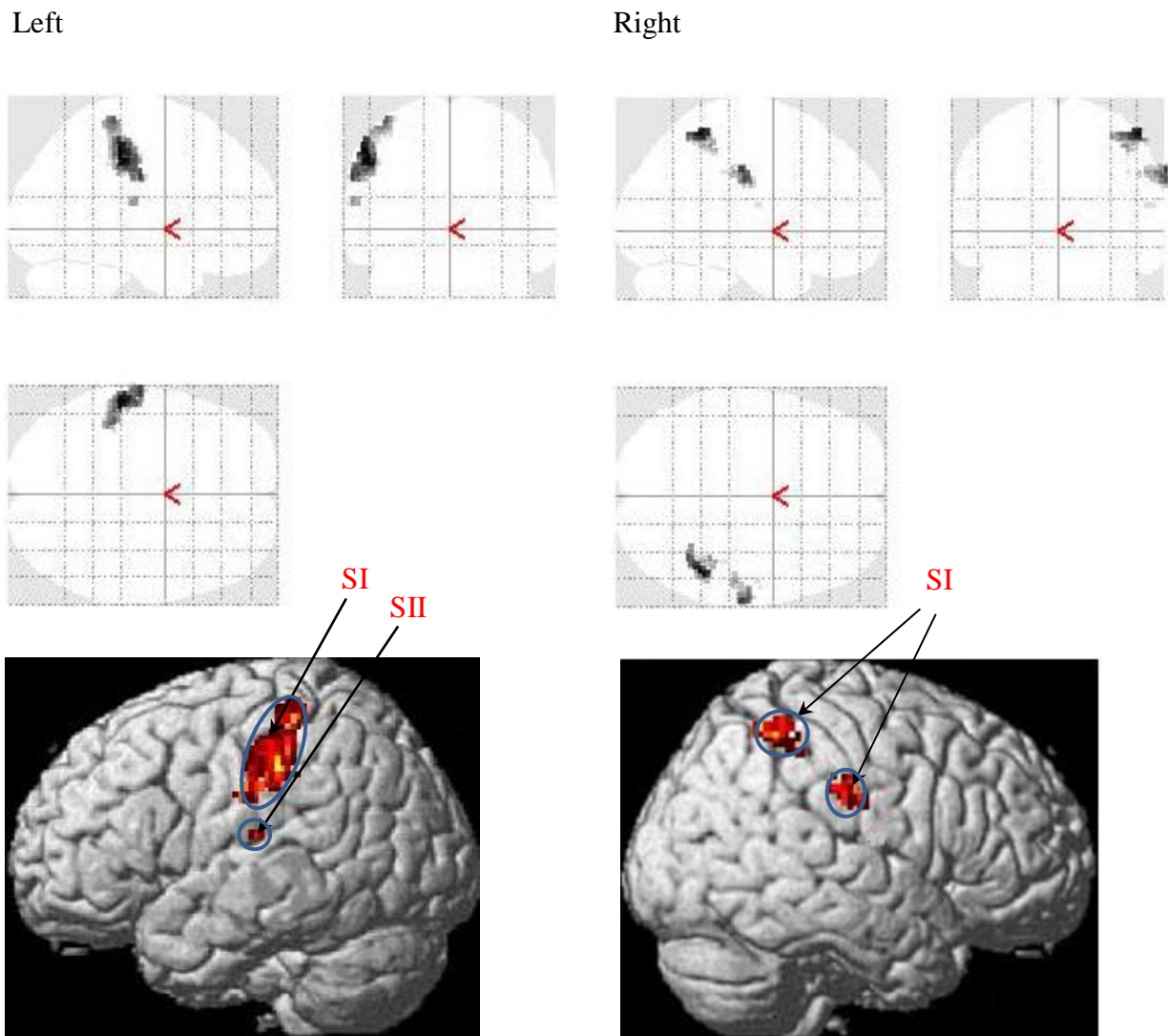


Fig. 1: Glass-brain views (upper panels) and rendered-brain views (lower panels) of activation for the contrast between Random and Rest for subject 2 in areas SI and SII. Threshold uncorrected,  $p$  value of  $\leq 0.001$ .

Left

Right

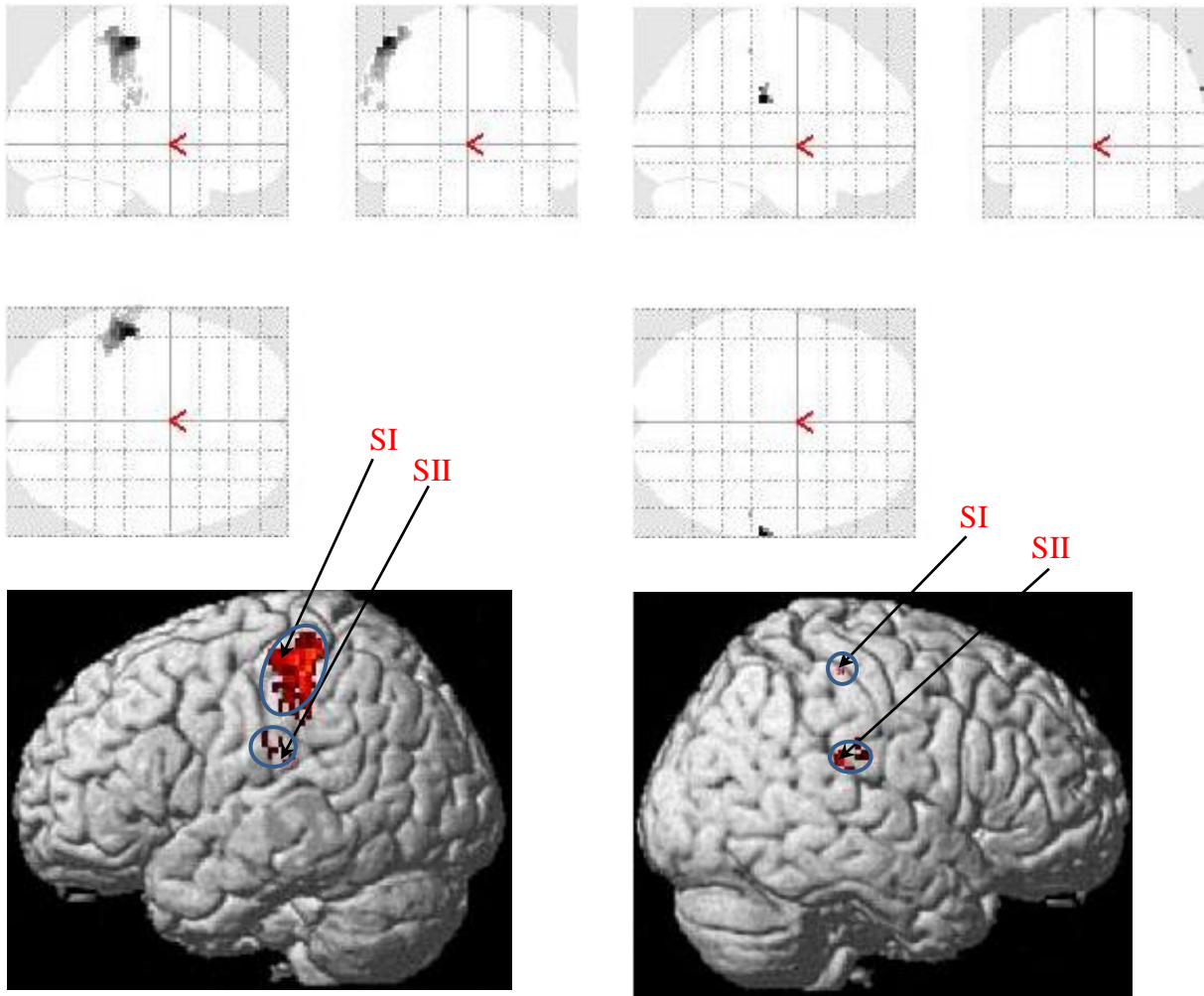


Fig. 2: Glass-brain views (upper panels and rendered-brain views (lower panels) of activation for the contrast between Random and Rest for subject 3 in areas SI and SII. Threshold corrected,  $p$  value of  $\leq 0.05$ .

Left

Right

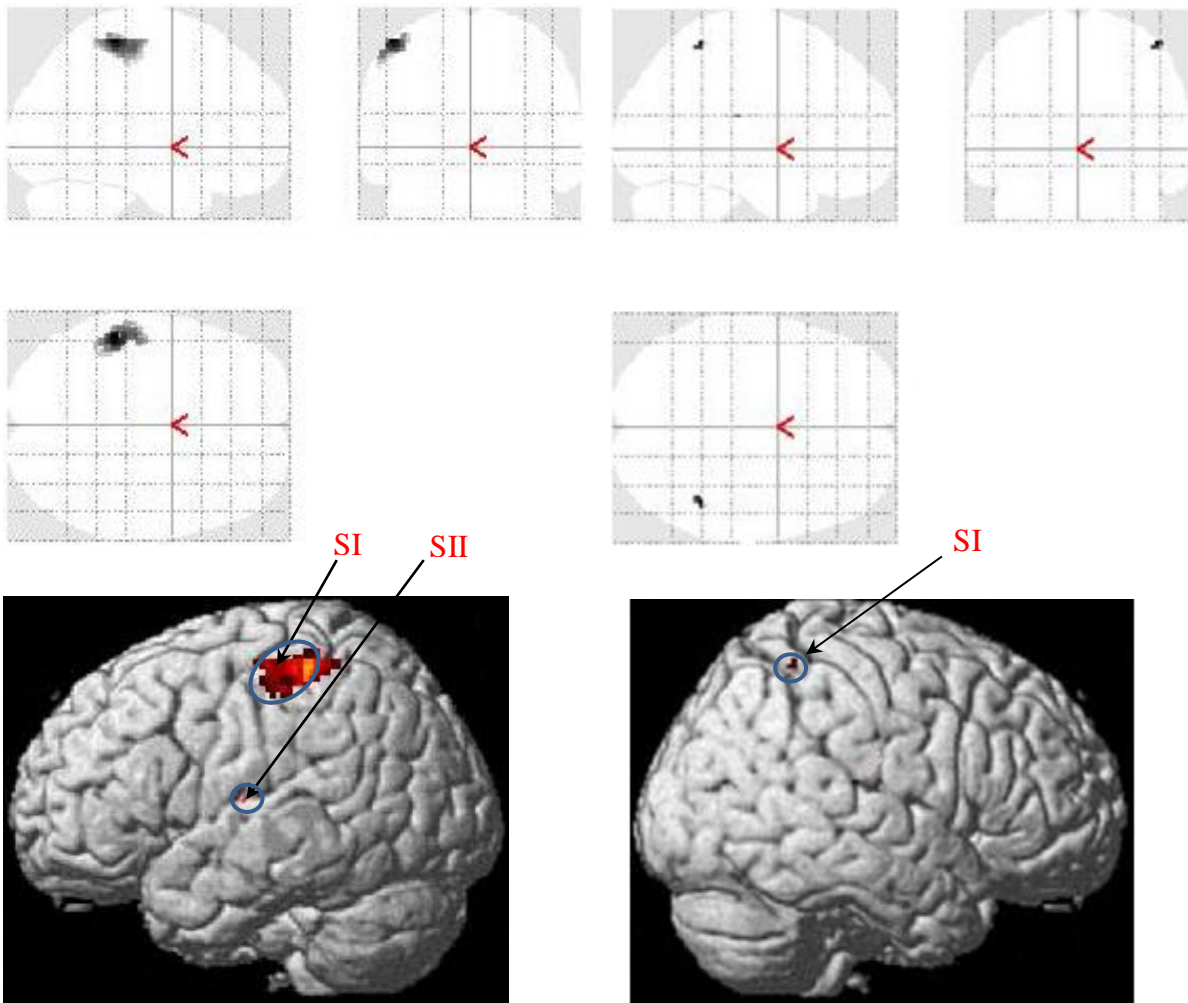


Fig. 3: Glass-brain views (upper panels) and rendered-brain views (lower panels) of activation for the contrast between Random and Rest for subject 4 in areas SI and SII. Threshold uncorrected,  $p$  value of  $\leq 0.001$ .

Left

Right

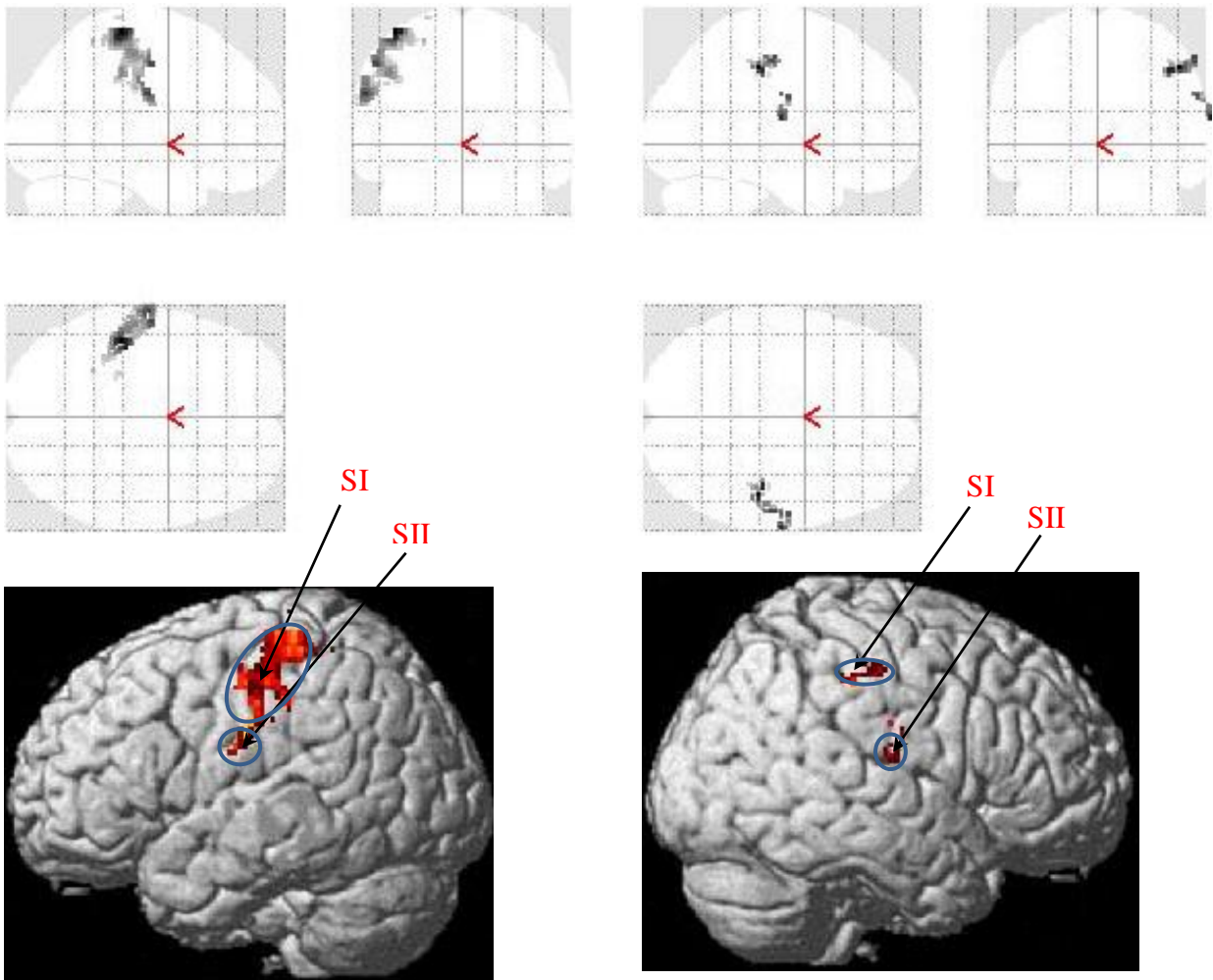


Fig. 4: Glass-brain views (upper panels) and rendered-brain views (lower panels) of activation for the contrast between Random and Rest for subject 5 in areas SI and SII. Threshold corrected,  $p$  value of  $\leq 0.05$ .

Left

Right

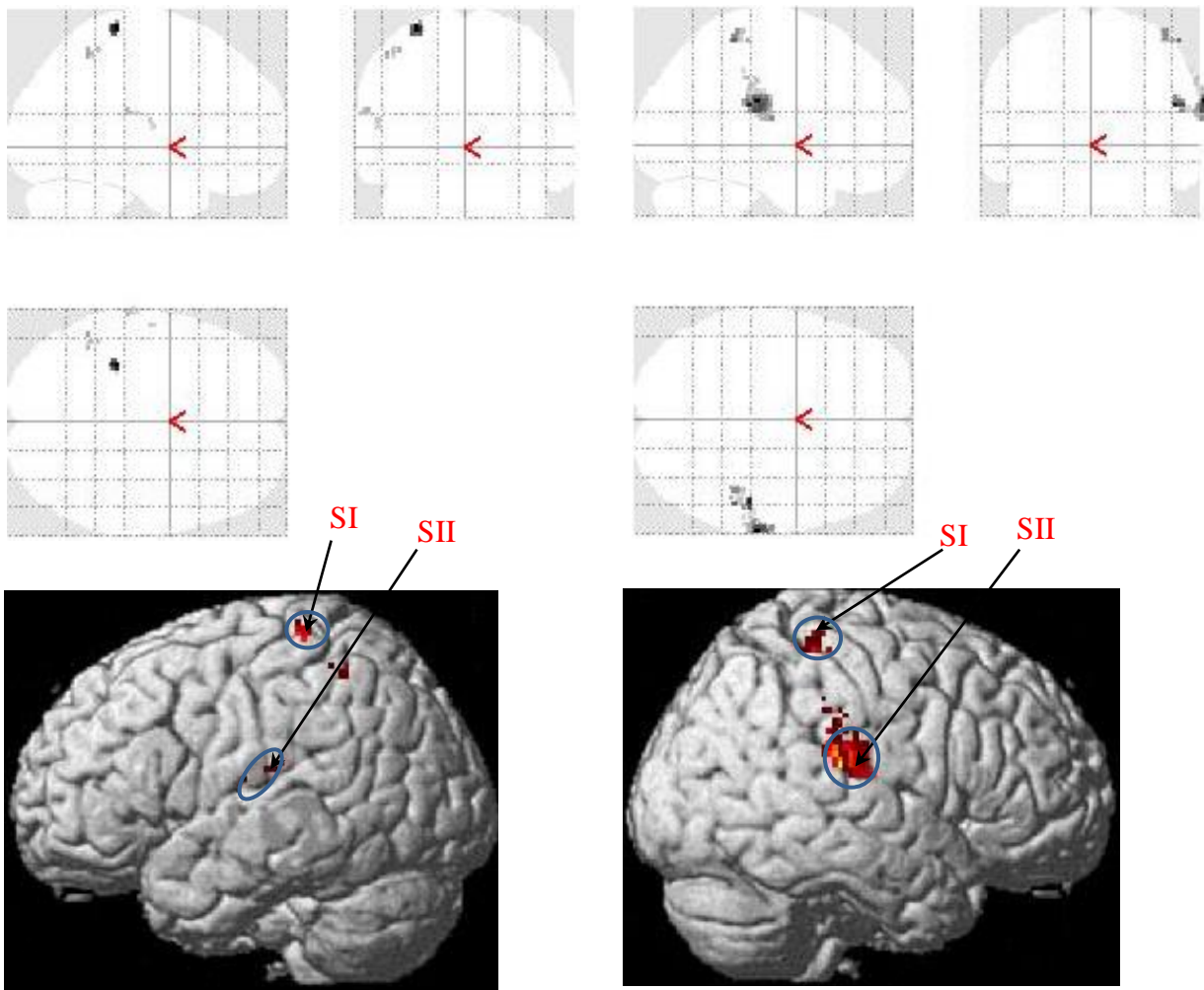


Fig. 5: Glass-brain views (upper panels) and rendered-brain views (lower panels) of activation for the contrast between Random and Rest for subject 6 in areas SI and SII. Threshold uncorrected,  $p$  value of  $\leq 0.001$ .



Left

Right

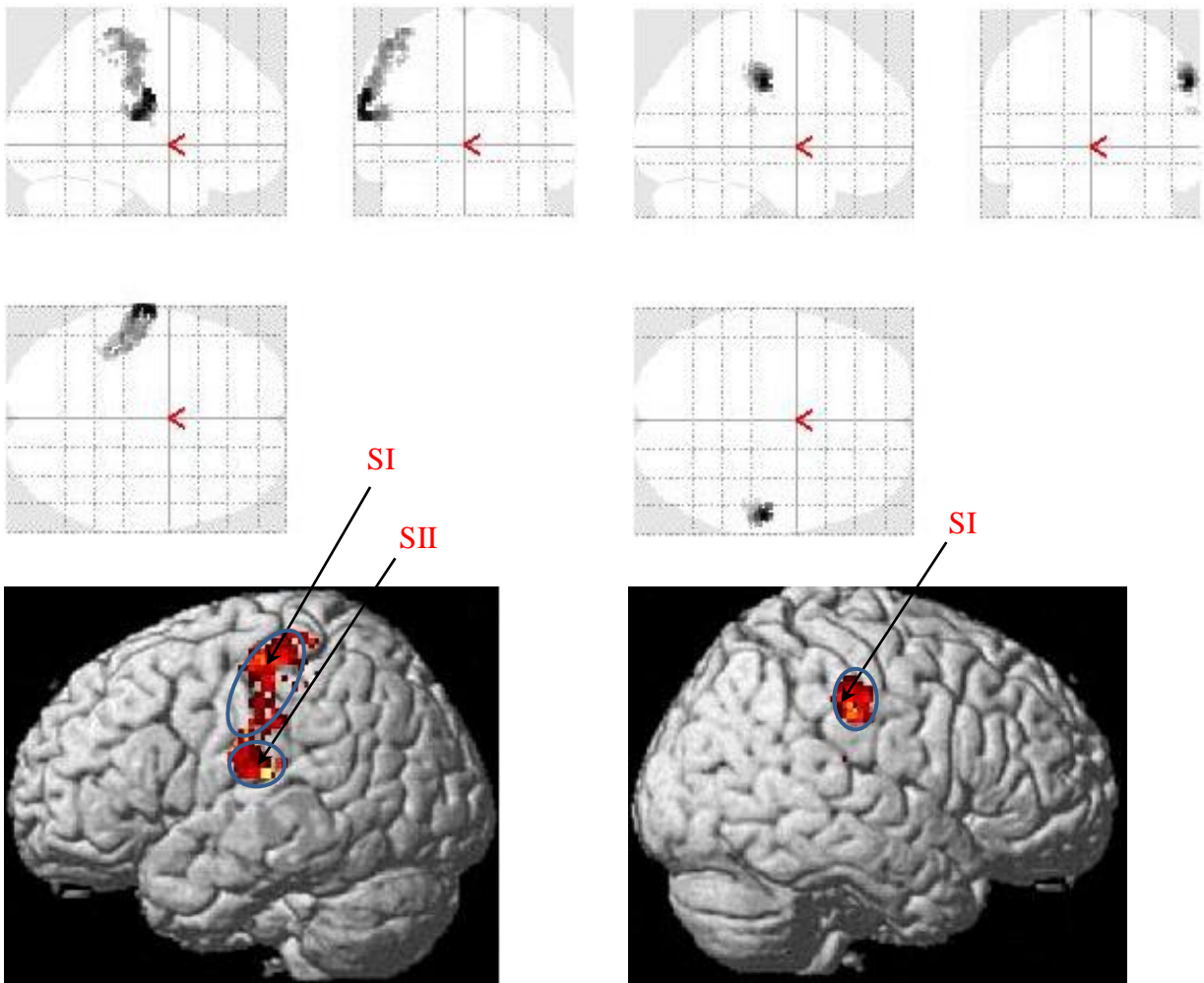


Fig. 6: Glass-brain views (upper panels) and rendered-brain views (lower panels) of activation for the contrast between Random and Rest for subject 7 in areas SI and SII. Threshold corrected,  $p$  value of  $\leq 0.05$ .

Left

Right

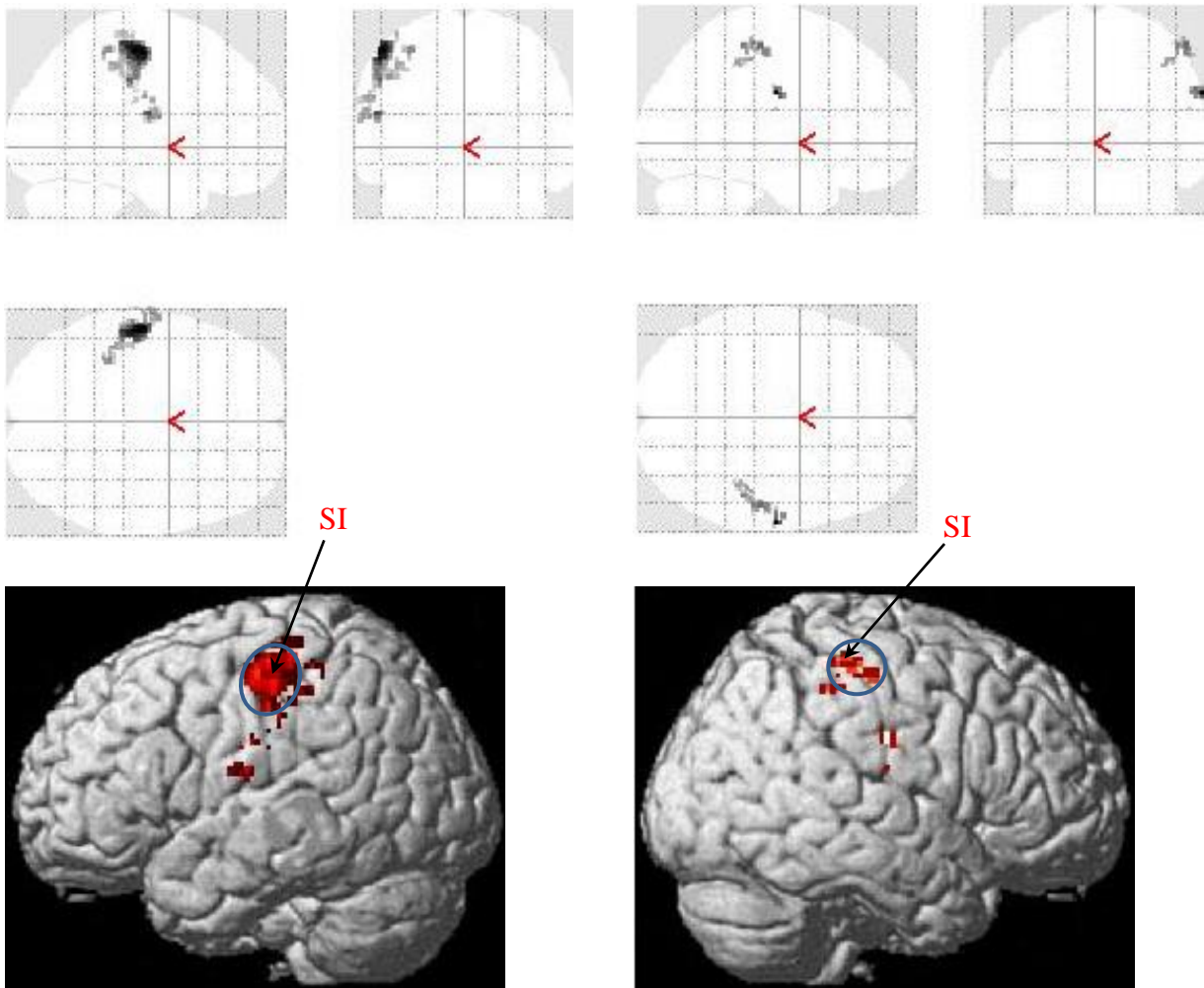
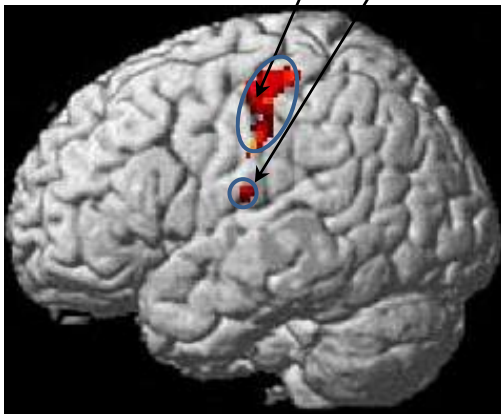
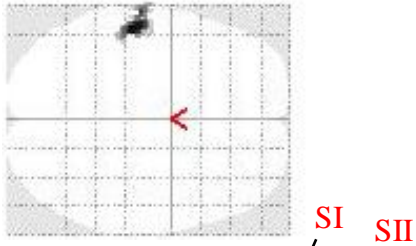
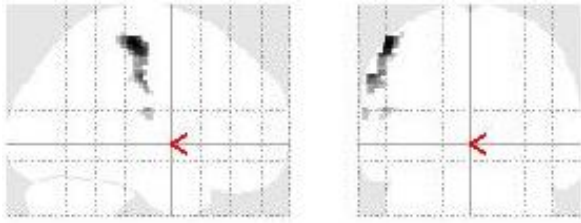


Fig. 7: Glass-brain views (upper panels) and rendered-brain views (lower panels) of activation for the contrast between Random and Rest for subject 8 in areas SI. Threshold corrected,  $p$  value of  $\leq 0.05$ .



Left



Right

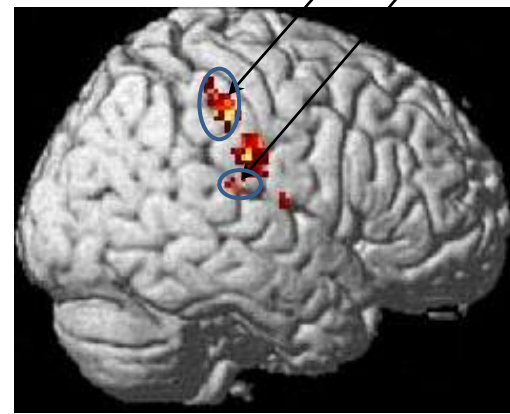
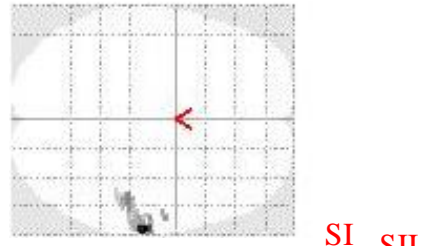
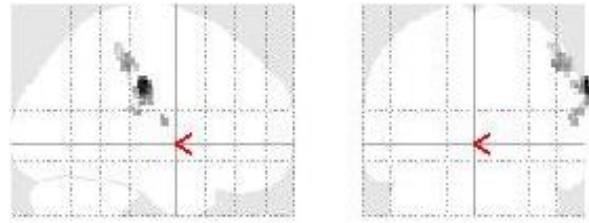


Fig. 8: Glass-brain views (upper panels) and rendered-brain views (lower panels) of activation for the contrast between Random and Rest for subject 9 in areas SI and SII. Threshold uncorrected,  $p$  value of  $\leq 0.001$ .

Left

Right

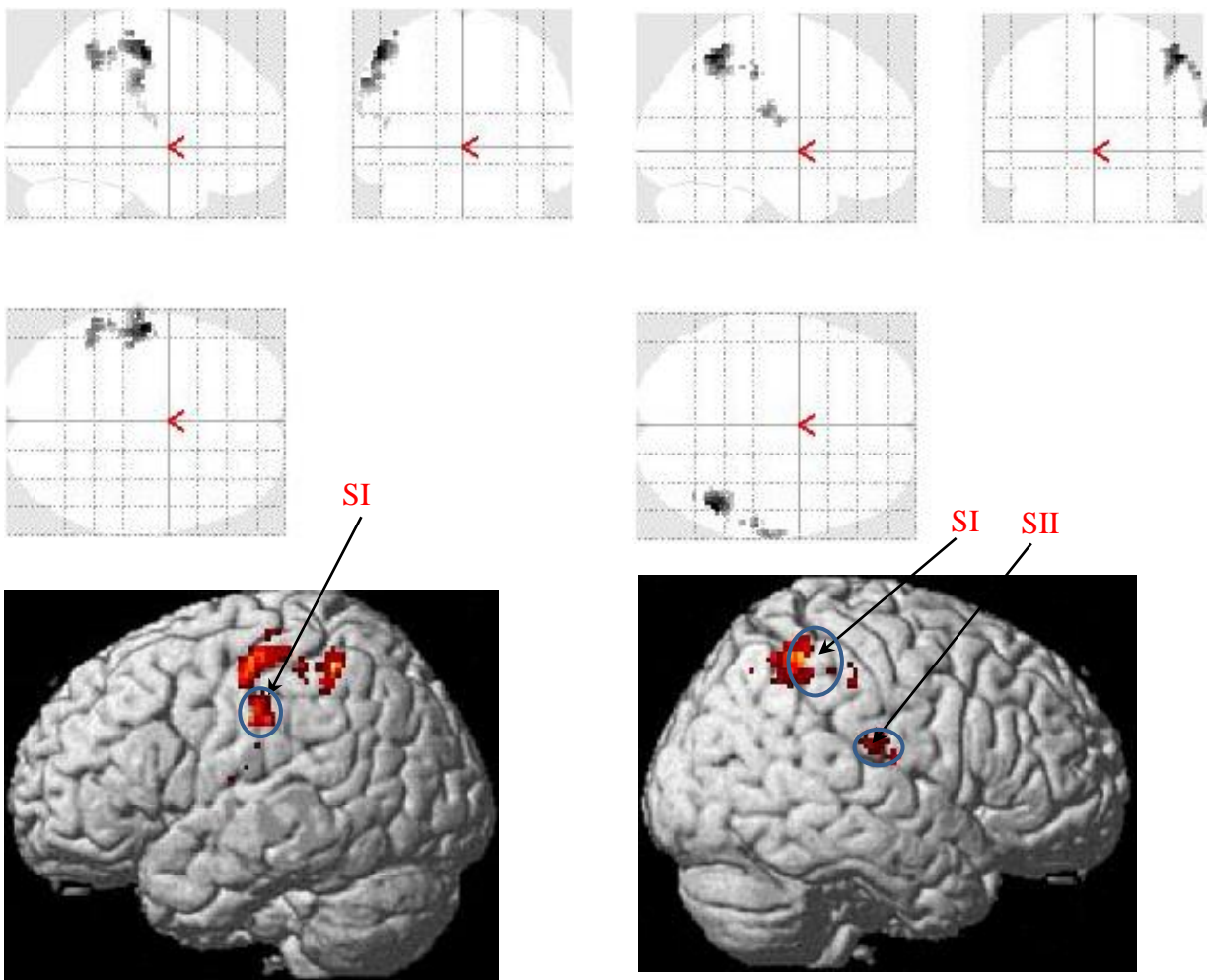


Fig. 9: Glass-brain views (upper panels) and rendered-brain views (lower panels) of activation for the contrast between Random and Rest for subject 10 in areas SI and SII. Threshold corrected,  $p$  value of  $\leq 0.05$ .

Left

Right

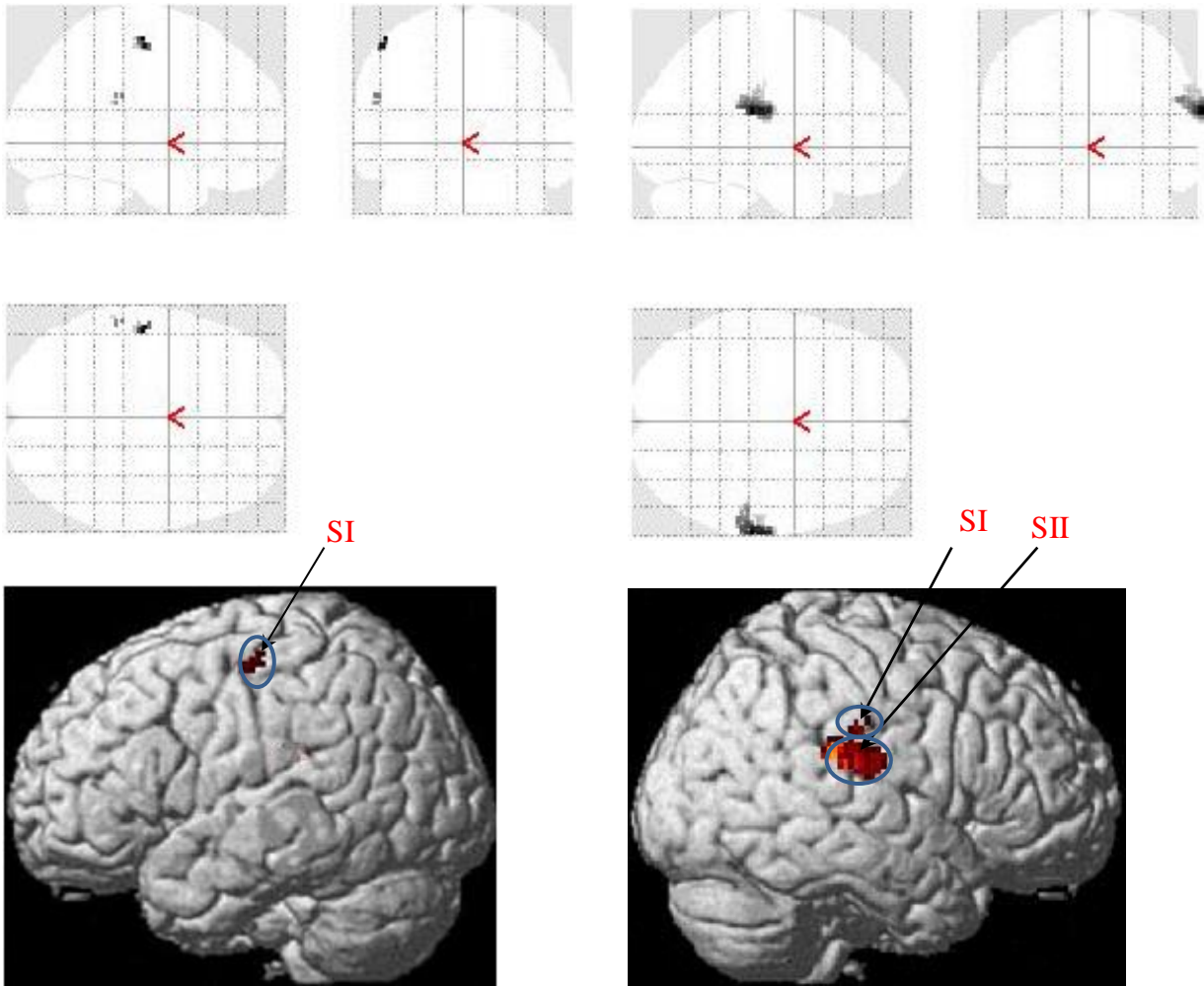
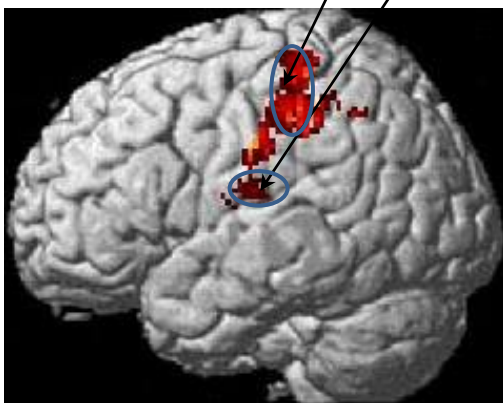
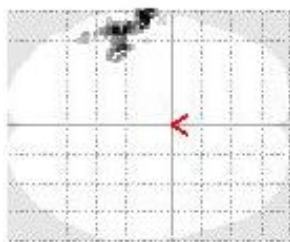
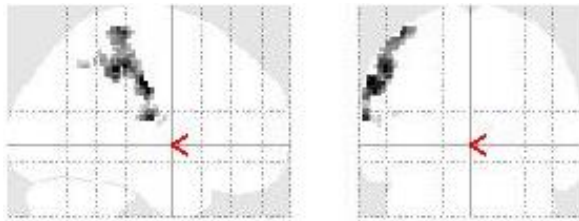


Fig. 10: Glass-brain views (upper panels) and rendered-brain (lower panels) of activation views for the contrast between Random and Rest for subject 11 in areas SI and SII. Threshold uncorrected,  $p$  value of  $\leq 0.009$ .

## Appendix E 1.3

### 3. Results of contrast between Stationary and Rest (Subjects 3 and 11) first fMRI experiment.

Left



Right

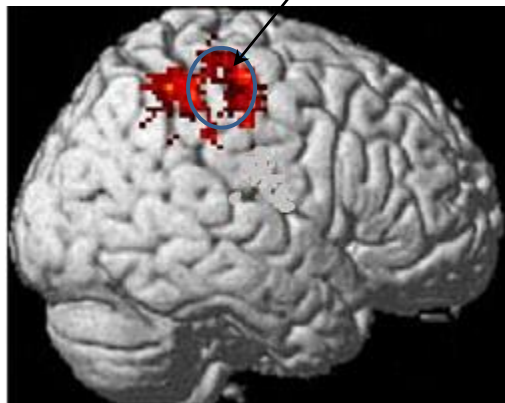
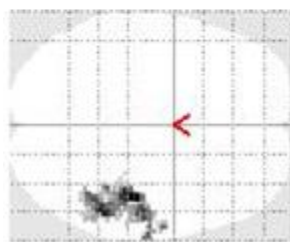
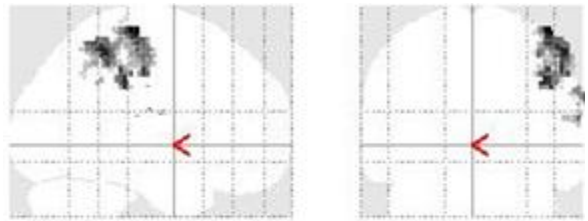


Fig. 1: Glass-brain views (upper panels) and rendered-brain views (lower panels) of activation for the contrast between Stationary and Rest for subject 2 in areas SI and SII. Threshold uncorrected,  $p$  value of  $\leq 0.009$ .

Left

Right

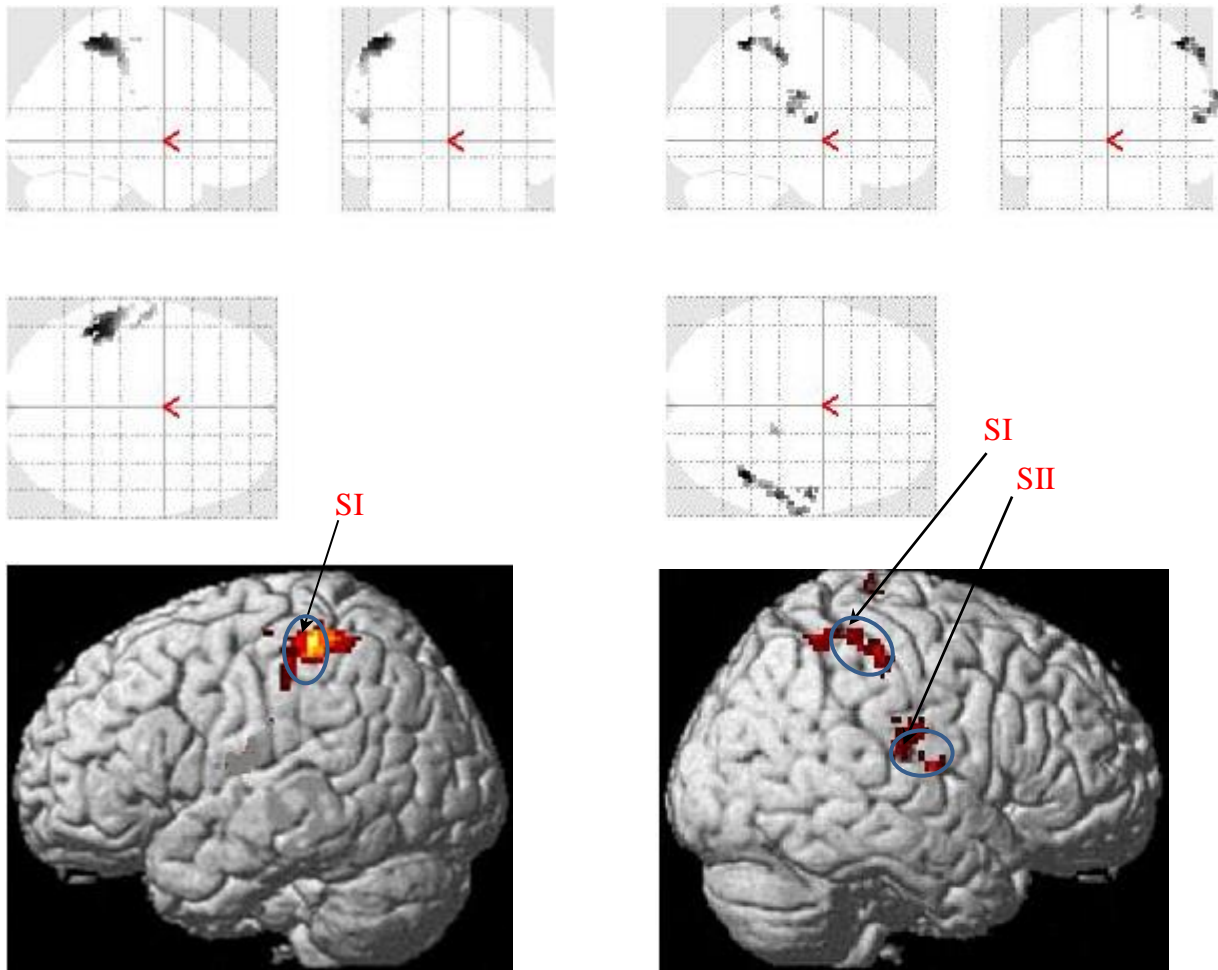


Fig. 2: Glass-brain views (upper panels) and rendered-brain views (lower panels) of activation for the contrast between Stationary and Rest for subject 4 in areas SI and SII. Threshold uncorrected,  $p$  value of  $\leq 0.009$ .

Left

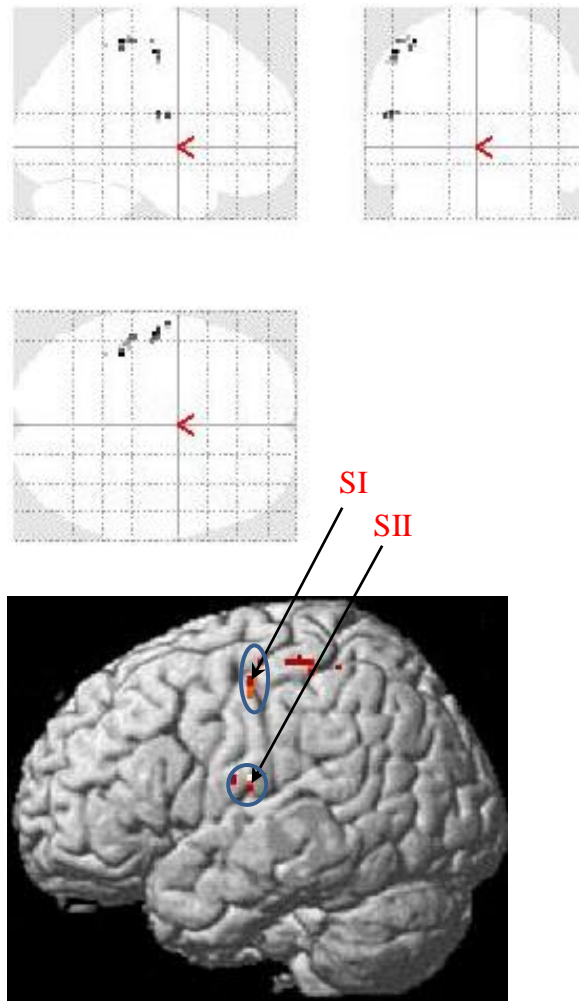


Fig. 3: Glass-brain views (upper panel) and rendered-brain views (lower panel) of activation for the contrast between Stationary and Rest for subject 5 in areas SI and SII. Threshold uncorrected,  $p$  value of  $\leq 0.009$ . No activations were observed on the right side of the brain ( $p \leq 0.009$ , uncorrected).



Left

Right

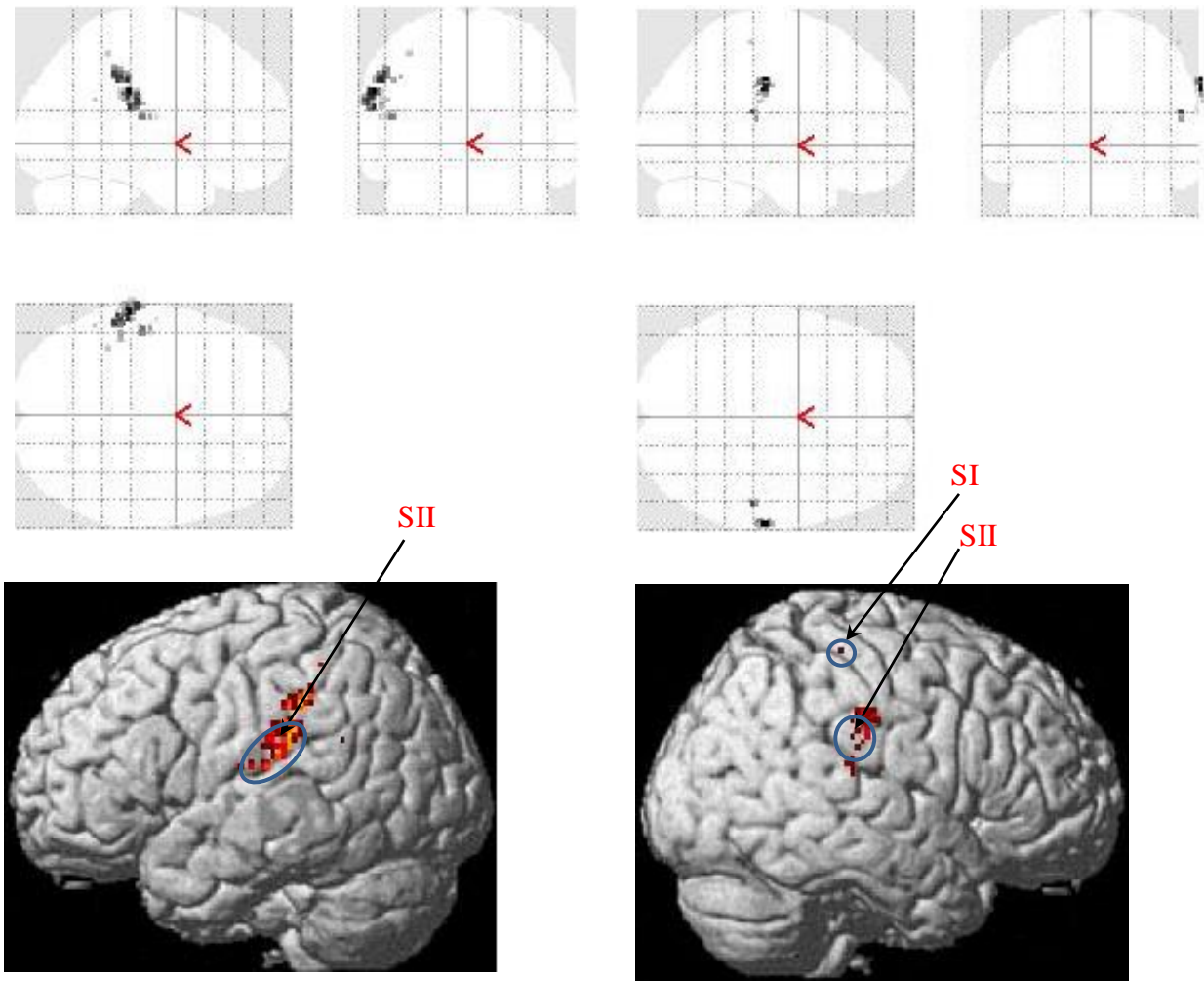


Fig. 4: Glass-brain views (upper panels) and rendered-brain views (lower panels) of activation for the contrast between Stationary and Rest for subject 6 in areas SI and SII. Threshold uncorrected,  $p$  value of  $\leq 0.001$ .

Left

Right

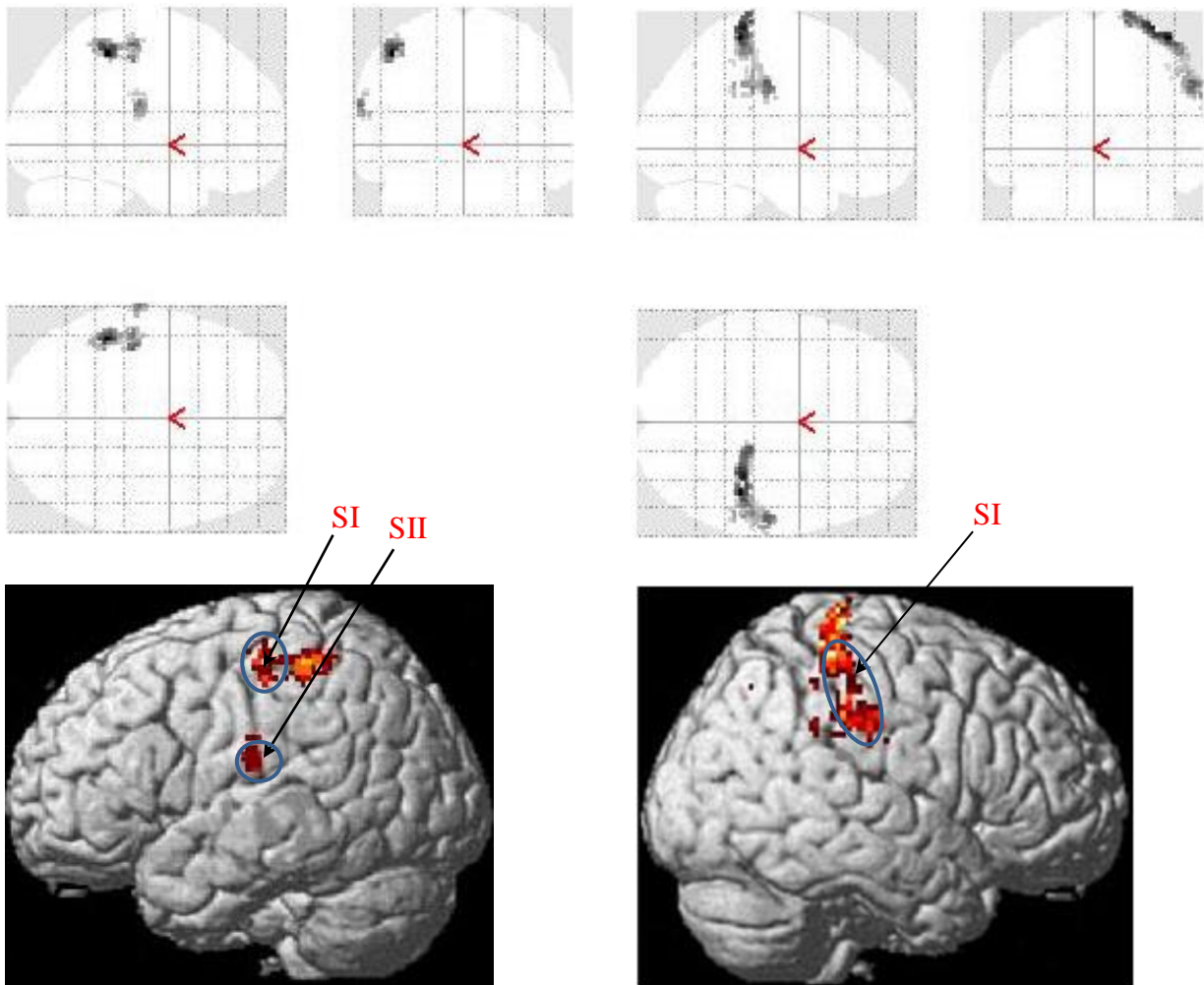


Fig. 5: Glass-brain views (upper panels) and rendered-brain views (lower panels) of activation for the contrast between Stationary and Rest for subject 7 in areas SI and SII. Threshold uncorrected,  $p$  value of  $\leq 0.001$ .



Left

Right

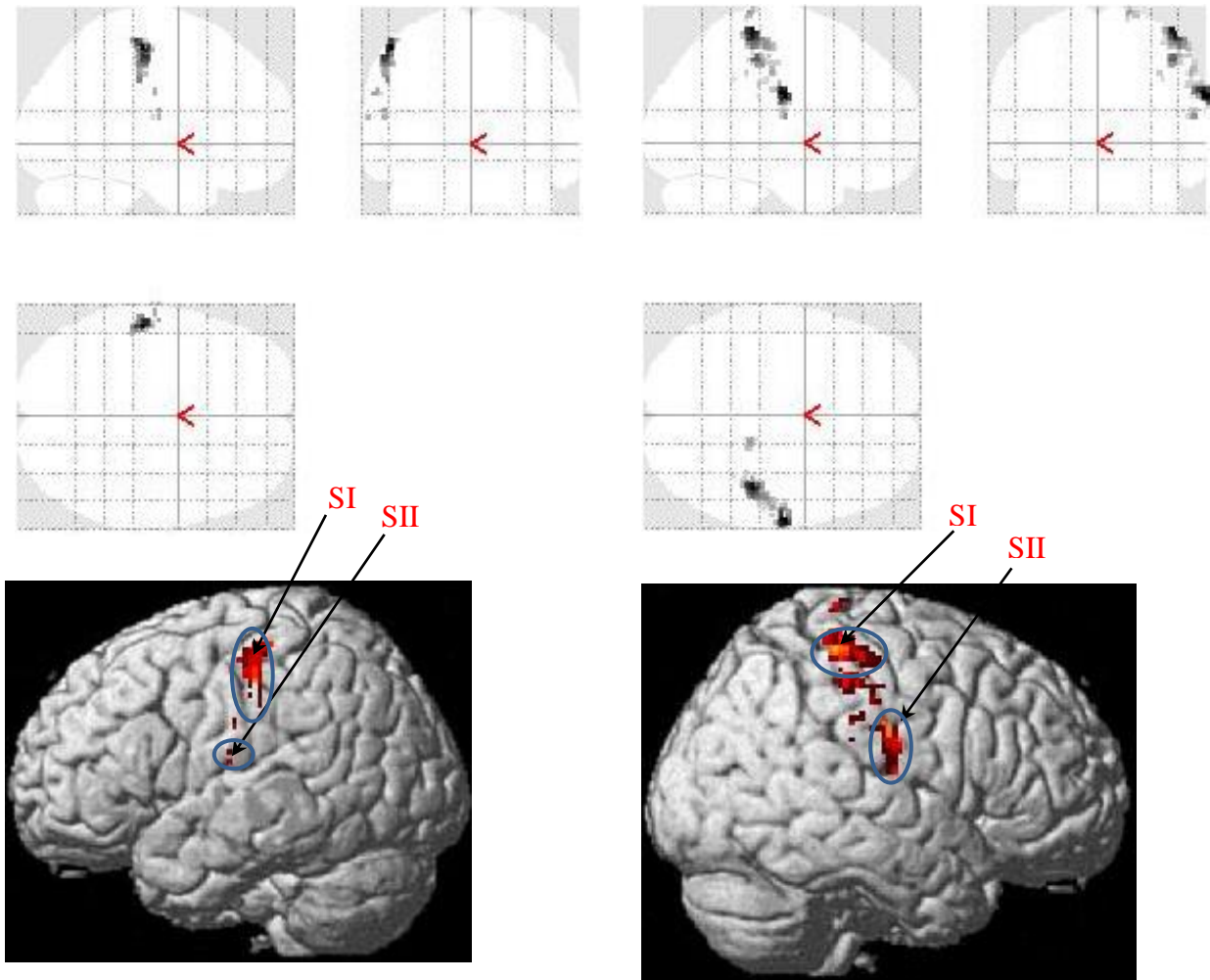


Fig. 6: Glass-brain views (upper panels) and rendered-brain views (lower panels) of activation for the contrast between Stationary and Rest for subject 8 in areas SI and SII. Threshold uncorrected,  $p$  value of  $\leq 0.001$

Left

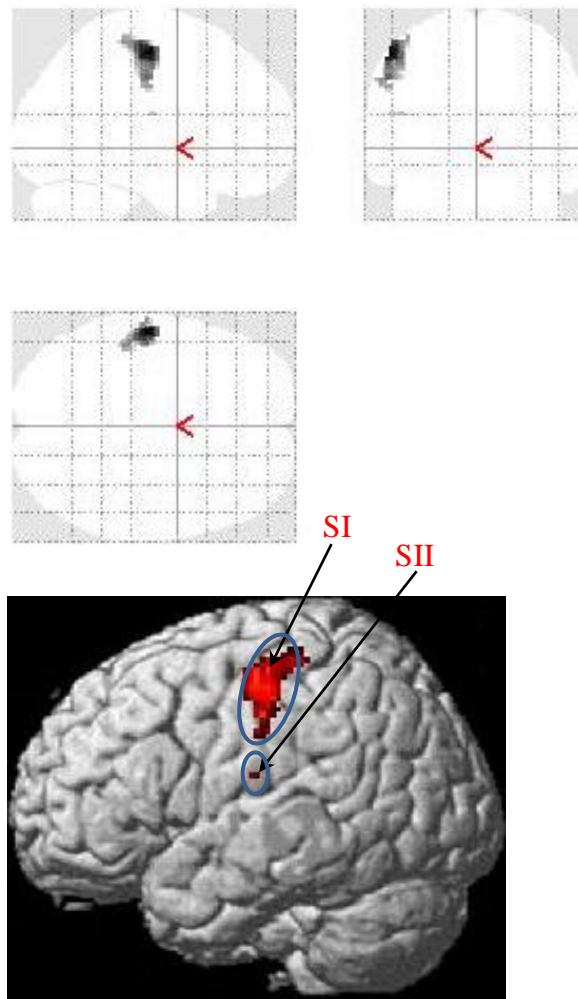


Fig. 7: Glass-brain views (upper panel) and rendered-brain views (lower panel) of activation for the contrast between Stationary and Rest for subject 9 in areas SI and SII. Threshold uncorrected,  $p$  value of  $\leq 0.009$ . No activations were observed on the right side of the brain ( $p \leq 0.009$ , uncorrected).

# Appendix F

## Result of second fMRI experiment

Left

Right

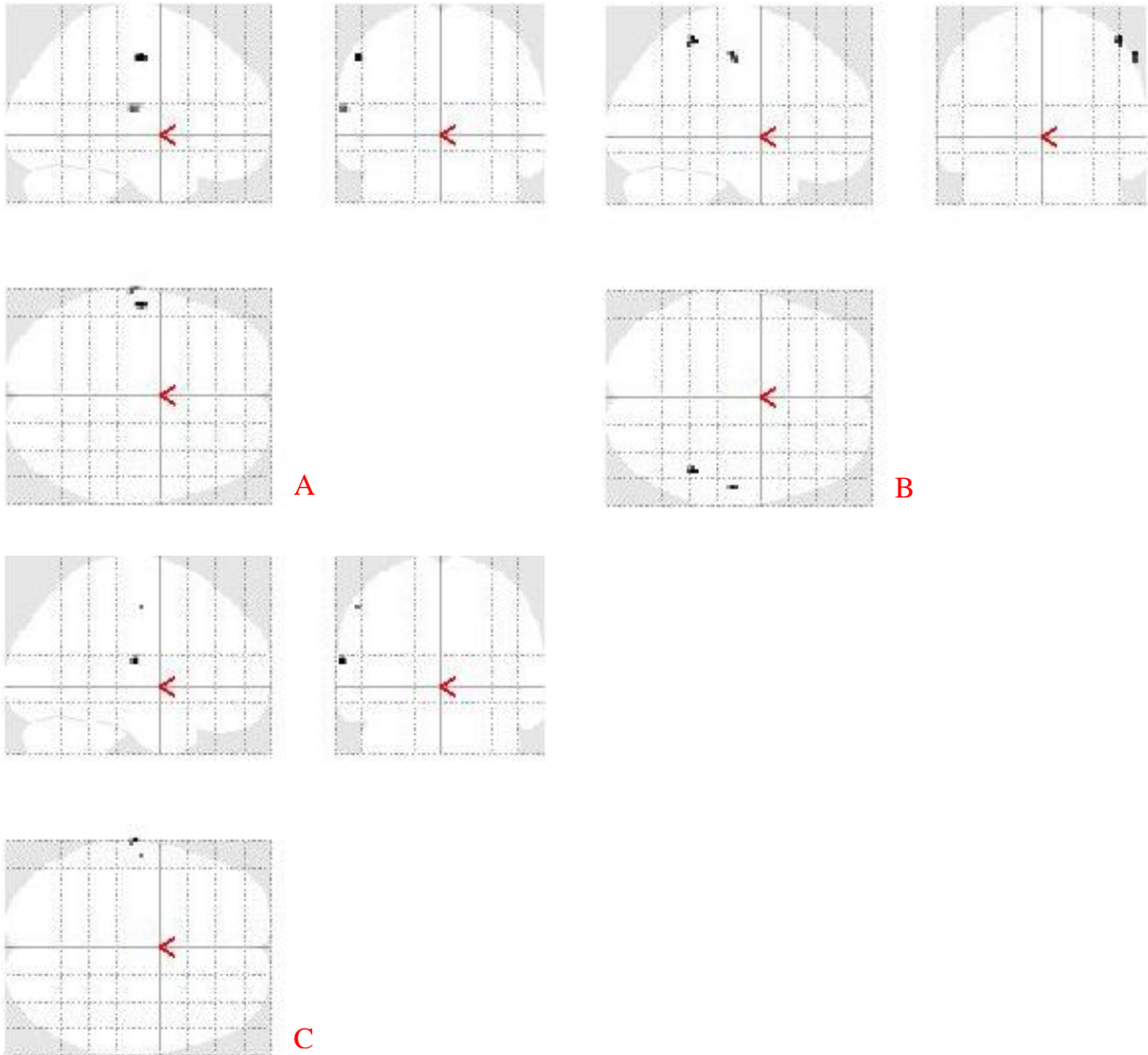


Fig. 1: (A, B) Activations in SI and SII for the contrast between stimulus (all speeds) and rest for subject 2; threshold corrected with  $p$  value of  $\leq 0.05$ ; (C) area showing a linear relation between activation and speed; threshold corrected with  $p$  value of  $\leq 0.05$ .

Left

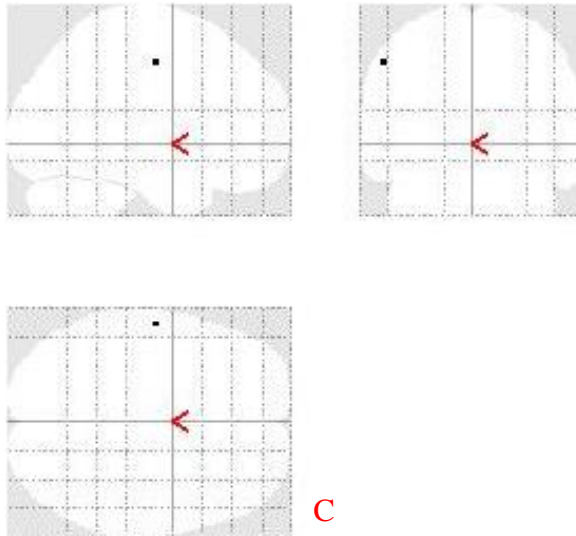


Fig. 2: (C) Subject 3, area showing a linear relation between activation and speed; threshold uncorrected with  $p$  value of  $\leq 0.001$ .

Left

Right

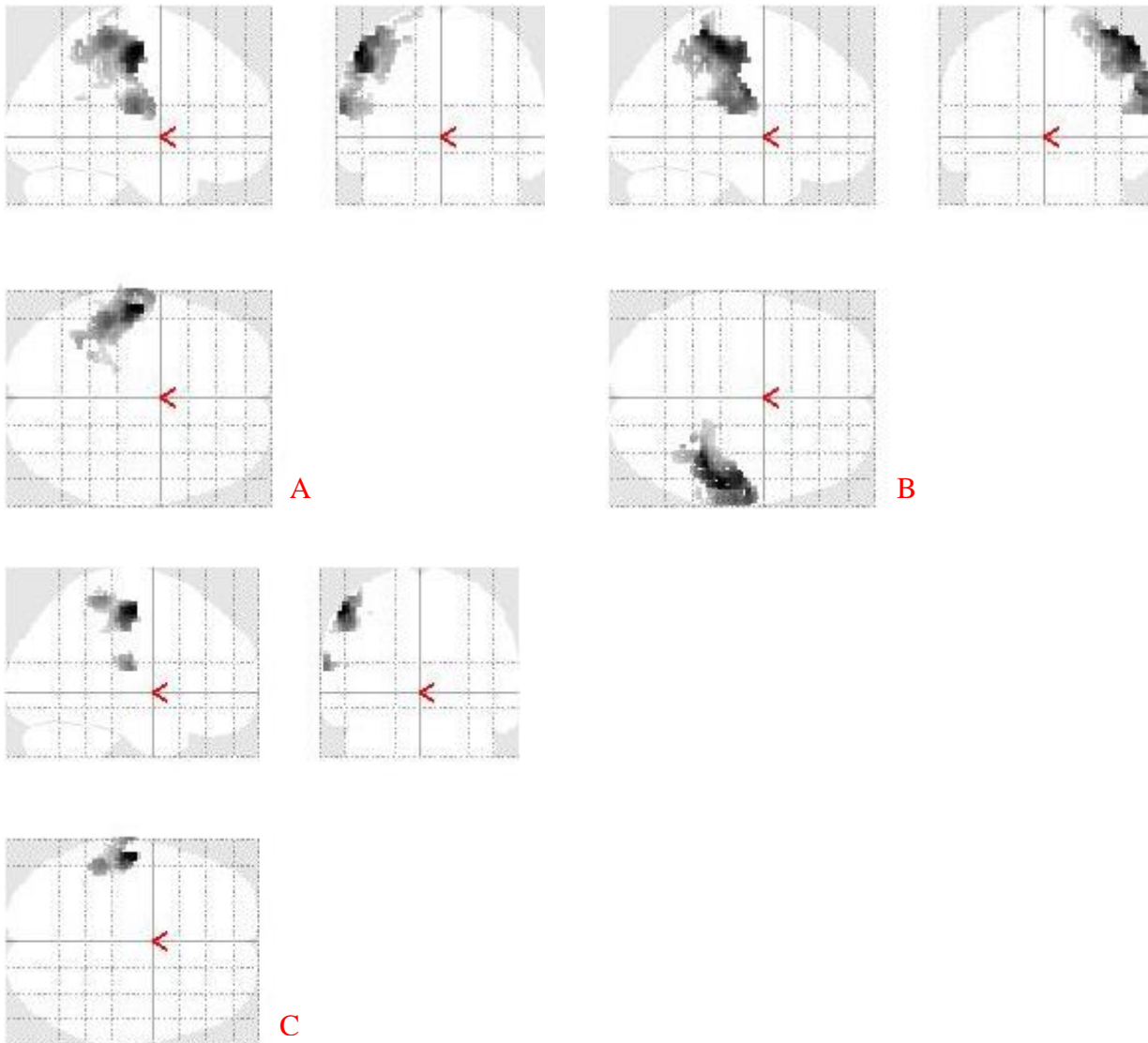


Fig. 3: (A, B) Activations in SI and SII for the contrast between stimulus (all speeds) and rest for subject 4; threshold corrected with  $p$  value of  $\leq 0.05$ ; (C) area showing a linear relation between activation and speed; threshold corrected with  $p$  value of  $\leq 0.05$ .

Left

Right

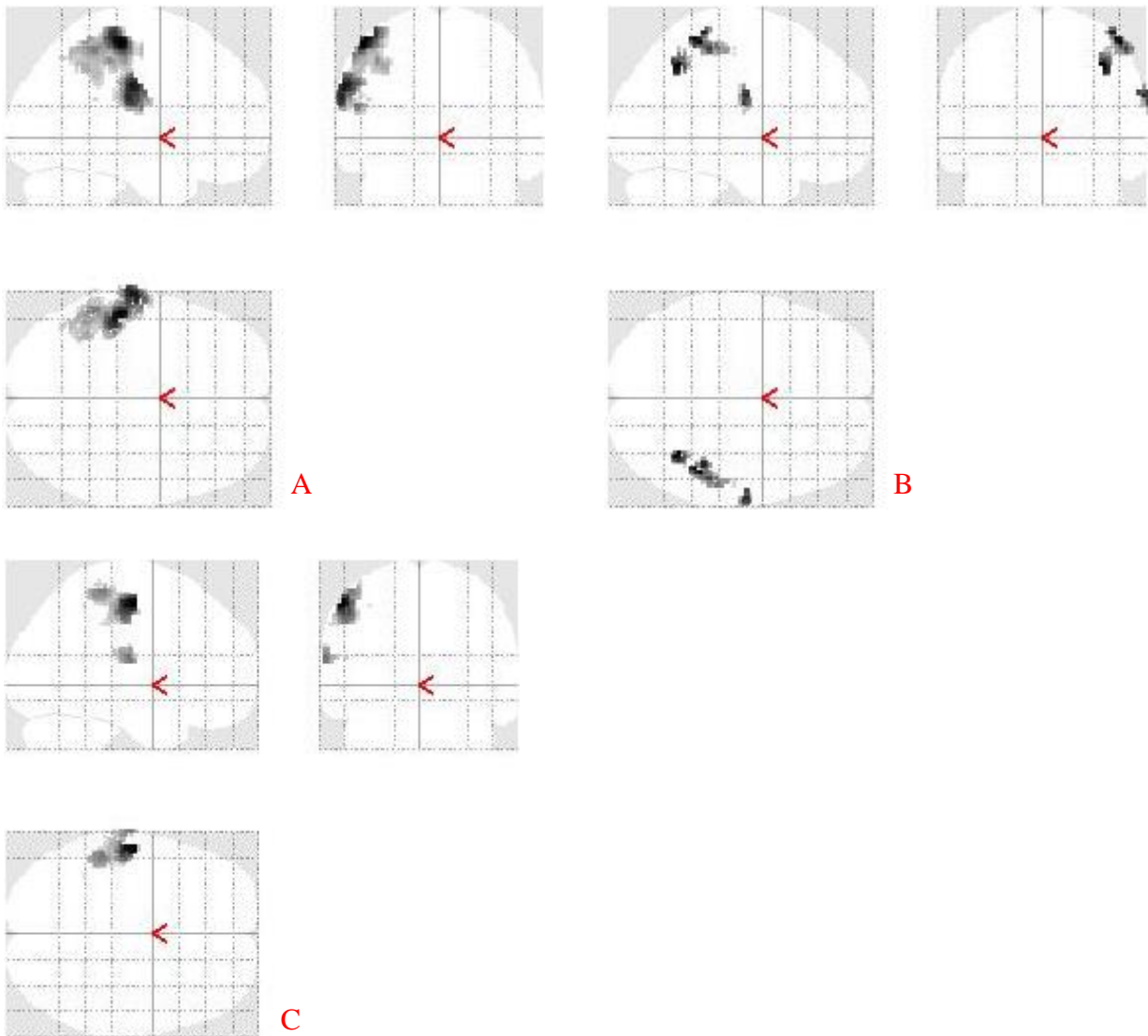


Fig. 4: (A, B) Activations in SI and SII for the contrast between stimulus (all speeds) and rest for subject 5; threshold corrected with  $p$  value of  $\leq 0.05$ ; (C) area showing a linear relation between activation and speed; threshold corrected with  $p$  value of  $\leq 0.05$ .

Left

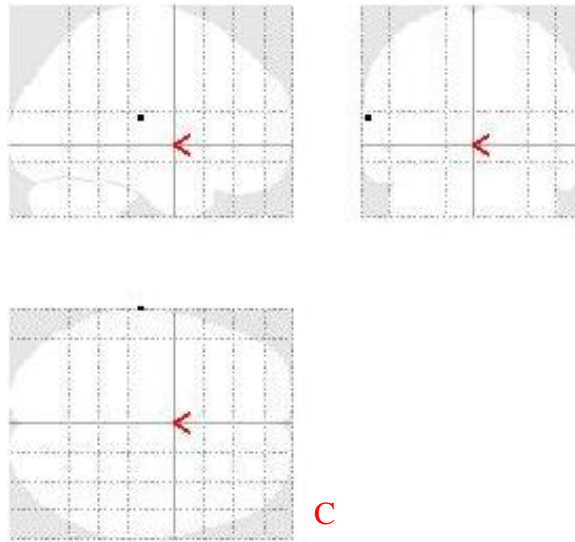


Fig. 5: (C) Subject 7, area showing a linear relation between activation and speed; threshold uncorrected with  $p$  value of  $\leq 0.001$ .

Left

Right

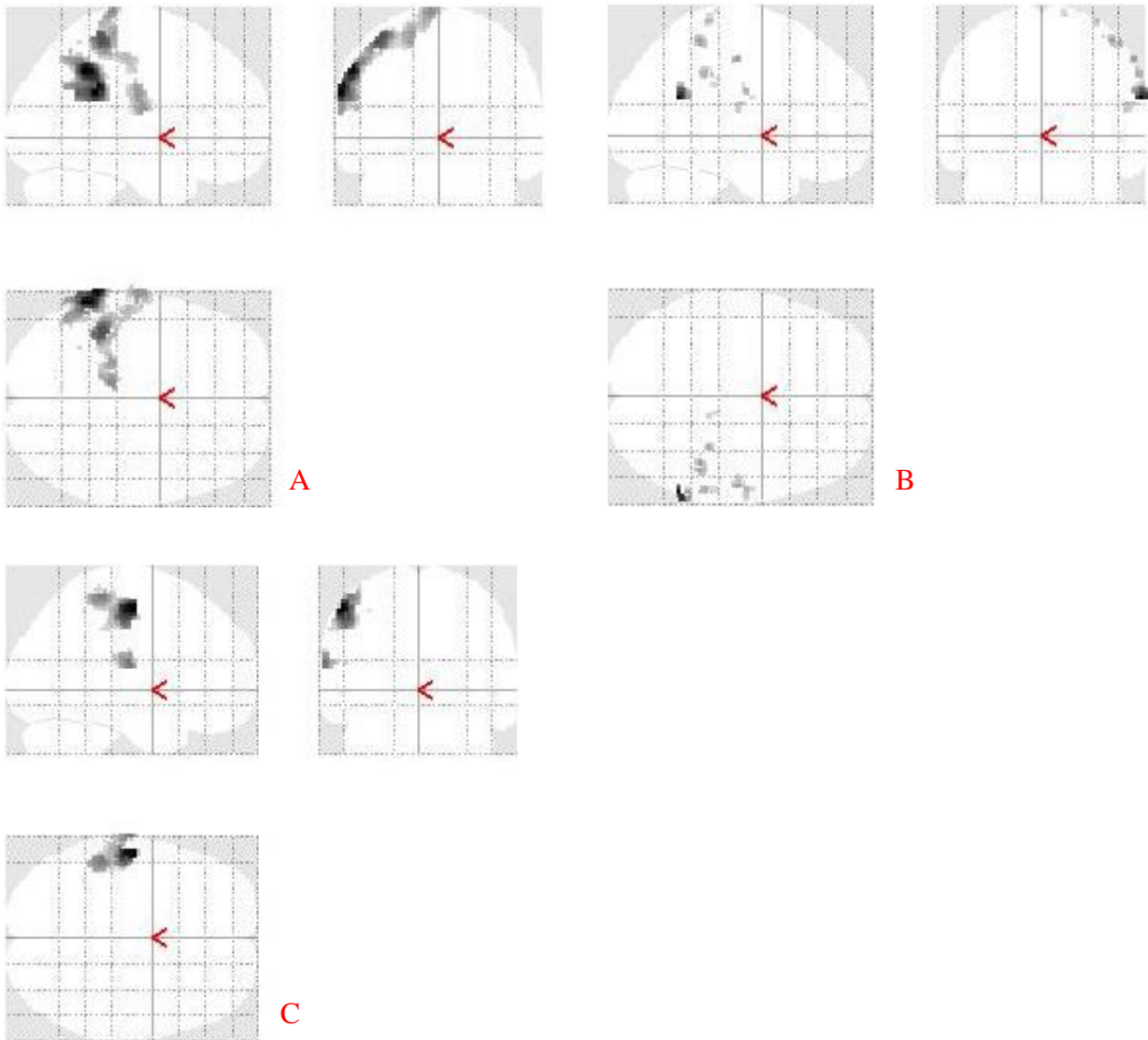


Fig. 6: (A, B) Activations in SI and SII for the contrast between stimulus (all speeds) and rest for subject 8; threshold corrected with  $p$  value of  $\leq 0.05$ ; (C) area showing a linear relation between activation and speed; threshold corrected with  $p$  value of  $\leq 0.05$ .



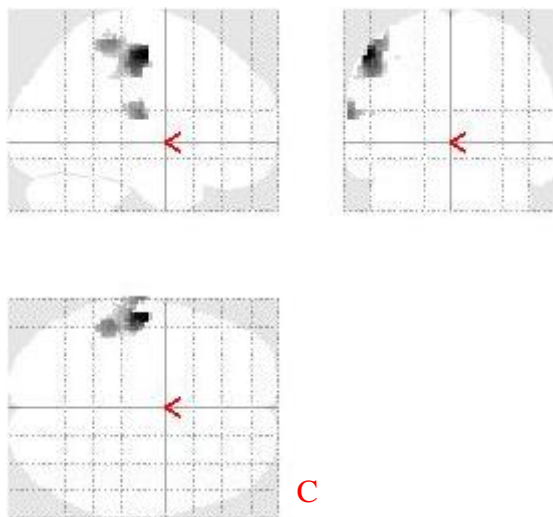


Fig. 7: C area showing a linear relation between activation and speed; threshold corrected with  $p$  value of  $\leq 0.05$ .

Left

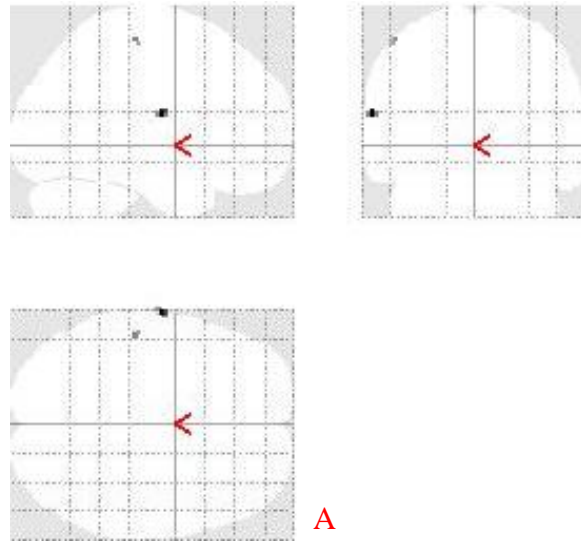


Fig. 8: (A) Activations in SI and SII for the contrast between stimulus (all speeds) and rest for subject 10; threshold uncorrected with  $p$  value of  $\leq 0.001$ .

Left

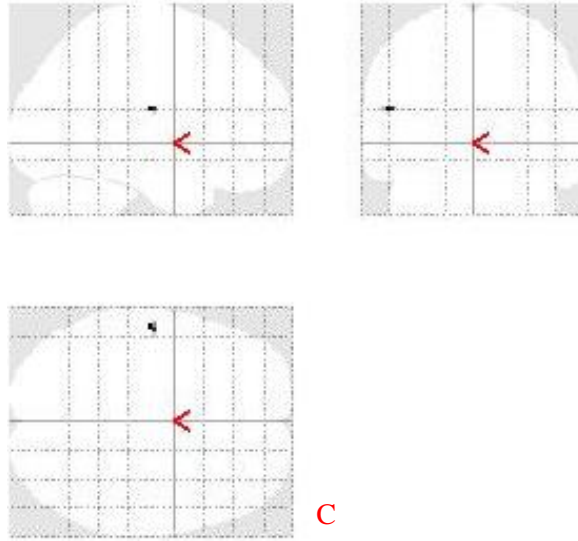


Fig. 9: (C) Subject 11, area showing a linear relation between activation and speed; threshold uncorrected with  $p$  value of  $\leq 0.001$ .

Left

Right

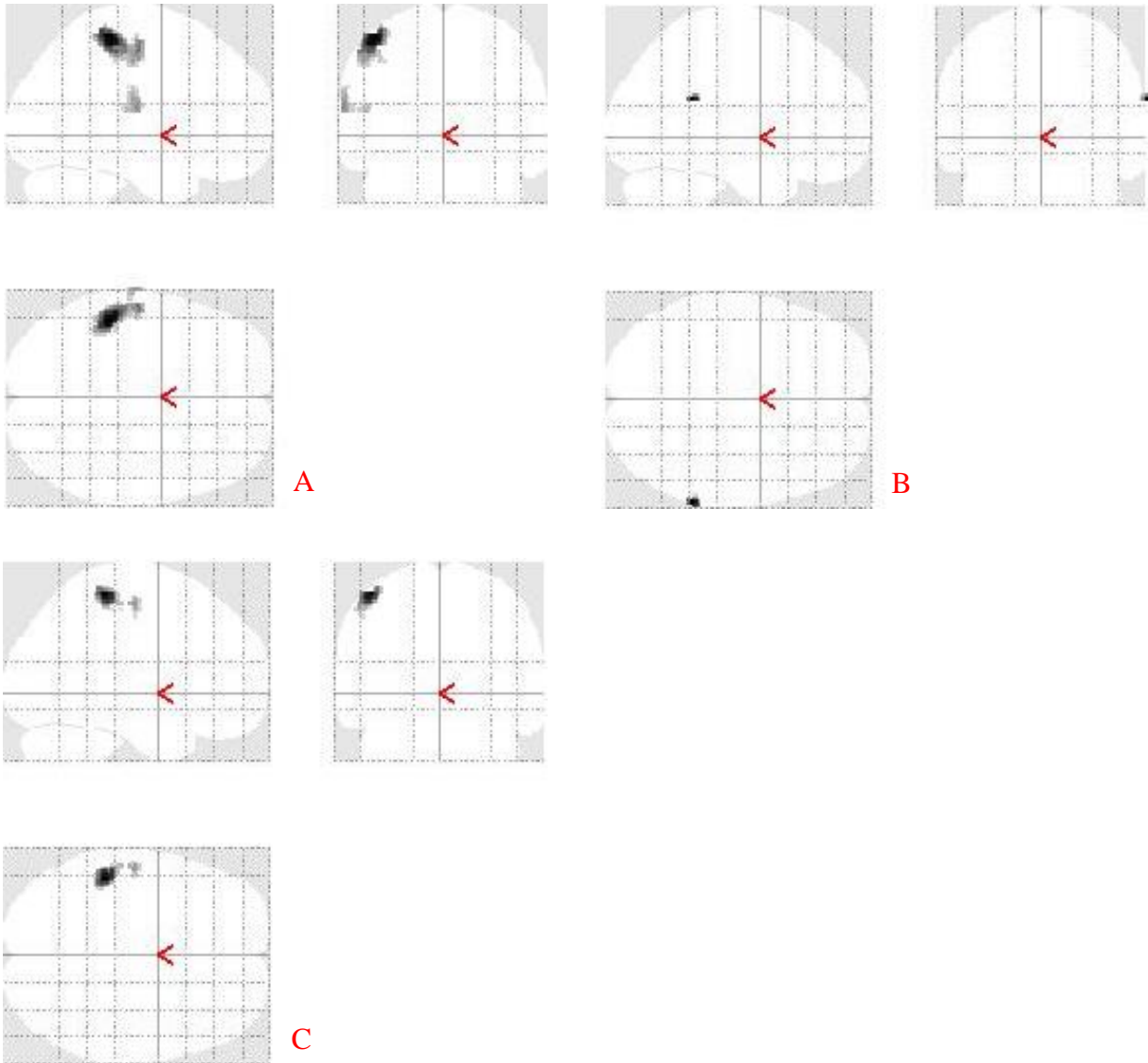



Fig. 10: (A, B) Activations in SI and SII for the contrast between stimulus (all speeds) and rest for subject 12; threshold corrected with  $p$  value of  $\leq 0.05$ ; (C) area showing a linear relation between activation and speed; threshold corrected with  $p$  value of  $\leq 0.05$ .

# Appendix G

Poster Published In Proceedings of the 29th Annual Scientific Meeting of the ESMRMB, Lisbon/PT, October 2012.



## Discrimination of tactile trajectories on the fingertip: an fMRI study

Alhussain, AQ<sup>1</sup>, Benattayallah A, Fulford J, Summers IR  
Peninsula MR Research Centre, University of Exeter, UK

**Introduction**

Previous studies (e.g., [1, 2]) have identified brain regions associated with tactile movement. The present study investigates whether cortical activation depends on the nature of the movement, using stimuli moving in two dimensions over the fingertip (as opposed to the one-dimensional movement over the tongue investigated by Matteau et al. [3]).

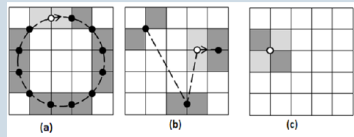


Fig. 1. Stimuli as a sequence of timeframes over the array (dots indicate apparent stimulus): (a) circle, (b) random (part of), (c) stationary.

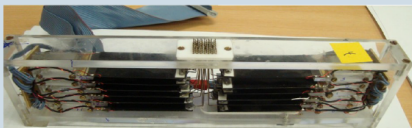


Fig. 2. The tactile display (contactors in centre of upper surface)

**Subjects and Methods**

Eleven volunteers participated (excluding those with recognition scores < 66.7%), all male, 24-40 years. Images (EPI BOLD, TR = 3 s, TE = 45 ms, 39 slices of 3 mm thickness, in-plane resolution 3 mm) were acquired over 32.4 minutes, during which repeated blocks were presented: 9-s tactile stimulus followed by 9-s rest period, 5-s response period and further rest (21-33 s, variable). Stimuli were of three types (Figure 1). Within the 9-s stimulus period, "circle" stimuli followed 9 rotations around the fingertip, "random" stimuli followed a path of no obvious shape, and "stationary" stimuli involved alternating diagonals of a 2 × 2 square (giving sufficient modulation to minimise adaptation). Figure 2 shows the tactile display, which has 25 contactors at 2 mm spacing in a 5 × 5 array on the fingertip, driven by piezoelectric mechanisms which can operate in a high magnetic field. The 40 Hz vibrotactile stimulation was at a comfortable level. Subjects were required to identify the stimulus type via three buttons .

Response Stimulation	Circle	Random	Stationary
Circle	144	45	9
Random	38	158	2
Stationary		5	193

Fig. 3. Confusion matrix for the identification scores.

**Results**

Figure 3 shows a confusion matrix of identification scores for subjects included in the analysis. The overall mean score is 83%; there is some confusion between the circle and random stimuli. Functional MRI data were analysed using SPM8 software (www.fil.ion.ucl.ac.uk/spm). Results show a significant increase in BOLD signal in brain regions responsible for low-level and high-level aspects of tactile shape discrimination. Both the primary and secondary somatosensory cortices show a significant increase in BOLD signal during tactile stimulation, compared to rest (for all stimulus types: circle, random and stationary), as shown in figure 4. In brain areas BA40 and BA37, thought to be involved in high-level aspects of tactile perception [3,4], there is significant increase in BOLD signal during stimulation with moving stimuli (circle, random), compared to stationary stimuli ( Figure 5).

**Conclusions and future work**

- ◇ Using fMRI during a discrimination task for tactile trajectories on the fingertip, activation was observed in brain areas SI, SII, BA40 and BA37.
- ◇ Brain areas associated with the circle/random contrast were not identified.
- ◇ There remains the interesting possibility of analysing the fMRI data according to the subject's response, rather than stimulus type.
- ◇ The tactile display is easy to program and can produce many types of tactile stimuli (moving or stationary). Planned future studies include an investigation of the effect of movement speed.

**Acknowledgment:** We are grateful to Philips Healthcare for scientific support

**References**

[1] Vanello N et al. (2004) Proc. HBM 2004, TU323; [2] Summers IR et al. (2009) J. Acoust. Soc. Amer. 125, 1033-39; [3] Matteau I et al. (2010) Brain Res. Bull. 82, 264-70. [4] N Savini et al (2010) Brain Res. Bull. 83, 223-231.




Fig. 4. SI and SII activations for contrast between stimulation and rest (group analysis, p < 0.001 uncorrected).

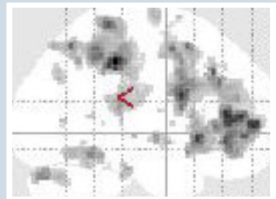


Fig. 5. Activation in Brodmann area 40 for contrast between moving (circle, random) and stationary stimuli (group analysis, p < 0.001 uncorrected)

203